Circulating miRNA and microbiome biomarkers for early diagnosis of atherosclerosis using the Wisconsin Miniature Swine™ Model of Familial Hypercholesterolemia

by

Hadjer Namous

A dissertation submitted in partial fulfillment of

the requirements for the degree of

Doctor of Philosophy

(Animal Sciences)

at the

UNIVERSITY OF WISCONSIN-MADISON

2023

Date of final oral examination: 12/16/2022

The dissertation is approved by the following members of the Final Oral Committee:

Hasan Khatib, Professor, Animal and Dairy Sciences
Jess Reed, Emeritus Professor, Animal and Dairy Sciences
Brian Kirkpatrick, Professor, Animal and Dairy Sciences
Tom Crenshaw, Professor, Animal and Dairy Sciences
Judith Simcox, Assistant Professor, Biochemistry

DEDICATION

To my parents, my husband, and my son.

ACKNOWLEDGMENTS

First, I sincerely thank my major advisor, Dr. Hasan Khatib, for his guidance and useful critiques, comments, and evaluations over the past years. They helped me shape my identity as a scientist. Second, I want to thank my co-advisor, Dr. Jess Reed, for his guidance, discussions, suggestions and for funding this Ph.D.

My thanks are also extended to Dr. Brian Kirkpatrick, Dr. Judith Simcox, and Dr. Tom Crenshaw for serving as committee members and for their valuable recommendations.

Also, a special thank you to Dr. Tom Crenshaw for spending time chatting with me and discussing science and other subjects. Thank you also for helping me navigate difficult situations and advising me throughout the past four years.

I want to thank Christian Krueger for his advice, discussions, suggestions that helped me progress with my Ph.D. as well as his contributions to this work. I also want to thank our collaborators from the Cardiovascular Research Foundation for their contributions and funding the project. Specifically, I want to thank Dr. Juan Granada for his unconditional support and guidance in navigating my project's medical aspects and interpreting the findings. Thank you also for believing in me.

To my friends and fellows Beth Lett, Allison Quick, and Jessica Townsend thank you for your support, kind words, and camaraderie over the years. Special thanks to Yiding Wang, my lab-adopted daughter, who was there with me and helped me beyond expectations. My thanks extend to my former lab colleague Camila Braz for her assistance with bioinformatic analysis and the time we spent talking about science, food, and life.

To STRC staff, Jamie Reichert, Jennifer Frank, Keri Graff, and Justin, I am truly grateful to have worked with you and learned from you. Thank you immensely for all the help you have given me, especially with the blood collections. You guys are amazing.

My deepest gratitude goes to Sandy Bertics, Faye Nashold, Steve Switzer, and Megan Sippel. These people have been very kind and helpful throughout my Ph.D. They are truly amazing people to have. Thank you all for checking on me during the tough periods of my pregnancy and ensuring that I feel safe during the COVID pandemic. I will forever remember you.

I also thank Devin Wixon, associate director of the DELTA program, and Anna Kowalkowski , Biocore 181 instructor, for guiding me throughout my DETLA internship and helping me hone my teaching skills.

I want to thank my parents and my husband for their unconditional support and continuous encouragement. Finally, thank you, my son, for being a strong little guy without mommy around most of the day, every day for the past two years.

ABSTRACT

This thesis is focused on the discovery of biomarkers for early diagnosis of atherosclerosis using the Wisconsin Miniature Swine™ Model of Familial hypercholesterolemia (WMS-FH). The three main chapters explore the transcriptomic profile of atherosclerosis lesions in WMS-FH and circulating molecular (miRNA and microbiome) signatures in the early life of WMS-FH associated with later-life disease development. The first chapter assessed the transcriptome profile of aortic tissues with fibroatheromatous lesions. Distinct gene expression patterns were identified, and captured genes were mostly enriched in inflammatory processes common to human atherosclerosis. Ten specific genes were identified as central to the pathophysiology of fibroatheroma and represent promising therapeutic targets. The second chapter aimed to identify circulating miRNA biomarkers for early diagnosis of atherosclerosis in WMS-FH pigs. Circulating miRNA signatures were captured at months 3, 6, and 9 of age before atherosclerosis is known to occur in WMS-FH. These miRNAs and their target genes participate in biological processes known to drive disease development, specifically inflammatory processes, and cholesterol homeostasis. Imaging pigs' vascular systems around 1-year old using Optical Coherent Tomography (OCT) revealed that atherosclerosis is exclusively present in the coronary arteries. Receiver Operating Characteristic Curve analysis showed that miRNAs with strong discriminatory power for atherosclerosis were captured at months 3 and 9. The identified miRNAs represent promising biomarkers for early diagnosis of coronary artery atherosclerosis. For the first time, the last chapter identified circulating microbiome signatures that correlate with atherosclerosis development. We captured taxa with strong discriminatory power for coronary artery atherosclerosis. Similar to miRNA potential, the identified taxa present a promising biomarker category for early disease diagnosis.

In conclusion, this work demonstrated that WMS-FH mimics human atherosclerosis at the molecular level. Additionally, plasma miRNA and microbiome signatures specific to atherosclerosis can be detected in the early life of animals before disease development. Future work should focus on understanding the mechanisms of action for each category of biomarkers. Also, investigating possible interactions between miRNAs and the microbiome will give further insights into more complex mechanisms that are potentially governing disease development.

TABLE OF CONTENTS

LIST OF TABLES

CHAPTER TWO: HUB-GENES INFLUENCE CELLULAR-MEDIATED RESPONSES AND MYOFIBROBLAST KINETICS IN FIBRO-ATHEROMA DEVELOPMENT IN AN ATHEROSCLEROSIS SWINE MODEL

CHAPTER THREE: CIRCULATING MIRNA DYNAMICS IN WISCONSIN MINIATURE SWINE™ OF FAMILIAL HYPERCHOLESTEROLEMIA: POTENTIAL BIOMARKERS FOR EARLY DIAGNOSIS OF CORONARY ARTERY DISEASE

CHAPTER FOUR: PLASMA MICROBIOME SIGNATURES IN FAMILIAL HYPERCHOLESTEROLEMIC WISCONSIN MINIATURE SWINE™ MODEL OF ATHEROSCLEROSIS

LIST OF FIGURES

CHAPTER ONE: LITERATUE REVIEW

CHAPTER TWO: HUB-GENES INFLUENCE CELLULAR-MEDIATED RESPONSES AND MYOFIBROBLAST KINETICS IN FIBRO-ATHEROMA DEVELOPMENT IN AN ATHEROSCLEROSIS SWINE MODE

CHAPTER THREE: CIRCULATING MIRNA DYNAMICS IN WISCONSIN MINIATURE SWINE™ OF FAMILIAL HYPERCHOLESTEROLEMIA: POTENTIAL BIOMARKERS FOR EARLY DIAGNOSIS OF CORONARY ARTERY DISEASE

LIST OF ABBREVIATIONS

ABCA1	ATP-Binding Cassette Transporter A 1
ABCG1	ATP-Binding Cassette Transporter G 1
ACTA2	Actin Alpha 2, Smooth Muscle
ACTC1	Actin Alpha Cardiac Muscle 1
AIF1	Allograft Inflammatory Factor 1
APoA1	Apolipoprotein A 1
APOB	Apolipoprotein B
APOE	Apolipoprotein E
AUC	Area Under the Curve
BP	Biological Processes
C1QA	Complement Component 1, Q subcomponent, A Chain
C1QC	Complement Component 1, Q subcomponent, C Chain
C3	Complement C 3
C5AR1	Complement C5a Receptor 1
CACS	Coronary Artery Calcium Score
CCL5	C-C Motif Chemokine Ligand 5
CD36	Glycoprotein IIIb
CD68	CD68 Molecule
CILP2	Cartilage Intermediate Layer Protein 2
cIMT	Carotid Intima-Media Thickness
CNN1	Calponin 1
COL1A2	Collagen Type I Alpha 2 Chain

COMP	Cartilage Oligomeric Matrix Protein
CRP	C-Reactive Protein
CSF1R	Colony Stimulating Factor 1 Receptor
CSF2RB	Colony Stimulating Factor 2 Receptor Subunit Beta
CTSS	Cathepsin S
CVDs	Cardiovascular Diseases
CXCL1	C-X-C Chemokine Ligand 1
CXCL12	C-X-C Motif Chemokine Ligand 12
CXCL14	C-X-C Motif Chemokine Ligand 14
CXCL2	C-X-C Chemokine Ligand 2
CXCL4	C-X-C Chemokine Ligand 4
CXCL8	C-X-C Chemokine Ligand 8
CXCR4	C-X-C Chemokine Receptor 4
CYP2B22	Cytochrome P450 family 2 subfamily B member 6B
DE	Differentially Expressed
DEGs	Differentially Expressed Genes
DES	Desmin
DNMT1	DNA Methyltransferase 1
DNMT3A	DNA Methyltransferase 3 A
DU	Differentially Abundant
ECMs	Extracellular Matrix Proteins
ECs	Endothelial Cells
eNOS	endothelial Nitric Oxide Synthase

ET	Elastin Trichrome
FCER1G	Fc Epsilon Receptor Ig
FGF	Fibroblast Growth Factor
GO	Gene Ontology
H&E	Hematoxylin and Eosin
HAT1	Histone Acetyltransferase 1
HDL	High Density Lipoprotein
ICAM1	Intercellular Adhesion Molecule 1
IEL	Internal Elastic Lamina
IFN-ɣ	Interferon Gamma
IL-1	Interleukin 1
IL-10	Interleukin 10
IL-18	Interleukin 18
IL-6	Interleukin 6
ITGA5	Integrin Subunit Alpha 5
ITGA6	Integrin Subunit Alpha 6
ITGAL	Integrin Subunit Alpha L
ITGB1	Integrin Subunit beta 1
ITGB2	Integrin Subunit beta 2
ITGB4	Integrin Subunit beta 4
KEGG	Kyoto Encyclopedia of Genes and Genomes
KLF5	KLF Transcription Factor 5
LCP1	Lymphocyte Cytosolic Protein 1

LCP2	Lymphocyte Cytosolic Protein 2
LDL	Low Density Lipoprotein
LDLR	Low Density Lipoprotein Receptor
LOX-1	Oxidized Low Density Lipoprotein Receptor
Lp-PLA2	Lipoprotein-associated Phospholipase -A2
LPS	Lipopolysaccharides
LRP1	LDLR Related Protein 1
LRP6	LDL Receptor Related Protein 6
MCP1	Monocyte Chemotactic Protein 1
M-CSF	Monocyte Colony Stimulating Factor
MECP2	Methyl-CpG Binding Protein 2
MerTK	Mer Tyrosine Kinase
MGP	Matrix Gla-Protein
MMP-10	Matrix Metalloproteinase 10
MMP13	Matrix Metalloproteinase 13
MMP-3	Matrix Metalloproteinase 3
MMP7	Matrix Metalloproteinase 7
MMP-9	Matrix Metalloproteinase 9
MMPs	Matrix Metalloproteinases
MPEG1	Macrophage Expressed 1
MPO	Myeloperoxidase
MTHFR	Methylenetetrahydrofolate Reductase
MYH11	Smooth Muscle Myosin Heavy Chain

NADPH	Nicotinamide Adenine Dinucleotide Phosphate
NF-kB	Nuclear Factor Kappa B
NO	Nitric Oxide
NOS3	Nitric Oxide Synthase 3
OCT	Optical Coherence Tomography
OPN	Osteopontin
oxLDL	Oxidized Low Density Lipoprotein Receptor
PAECs	Porcine Aortic Endothelial Cells
PCSK9	Proprotein Convertase Subtilisin/Kexin Type 9
PDGF	Platelet-Derived Growth Factor
PPAR	Peroxisome Proliferator Activated Receptor
PPARG	Peroxisome Proliferator Activated Receptor Gamma
PPI	Protein-Protein Interaction
ROC	Receiver Operating Characteristics
RT-qPCR	Real Time quantitative Polymerase Chain Reaction
S100A1	S100 Calcium Binding Protein A1
S100A4	S100 Calcium Binding Protein A4
S100A8	S100 Calcium Binding Protein A8
S100A9	S100 Calcium Binding Protein A9
SAA	Serum Amyloid A
SIRT	Sirtuin
SIRT1	Sirtuin 1
SNPs	Single Nucleotide Polymorphisms

SOX2	SRY-Box Transcription Factor 2
SOX4	SRY-Box Transcription Factor 4
SOX9	SRY-Box Transcription Factor 9
SP1	Sp1 Transcription Factor
SPI1	Hematopoietic Transcription Factor PU.1
SRA-1	Scavenger Receptor A 1
SRB-1	Scavenger Receptor B 1
STK11	Serine/Threonine Kinase 11
TLR 4	Toll Like Receptor 4
TLR 6	Toll Like Receptor 6
TLR 2	Toll Like Receptor 2
TLRs	Toll Like Receptors
TMAO	Trimethylamine N-Oxide
TNF-α	Tumor Necrosis Factor α
TR4	Orphan Nuclear Receptor 4
TRAF6	TNF Receptor Associated Factor 6
VCAM1	Vascular Cell Adhesion Molecule 1
VEGFA	Vascular Endothelial Growth Factor A
VLDL	Very low-density lipoprotein
VSMCs	Vascular Smooth Muscle Cells
WHHL	Watanabe Heritable Hyper Lipidemia
WMS	Wisconsin Miniature Swine
WMS-FH	Wisconsin Miniature Swine of Familial Hypercholesterolemia

WMS-N	Wisconsin Miniature Swine normochlesterolemic
YY1	YY1 Transcription Factor

CHAPTER ONE: LITERATUE REVIEW

I. Introduction

For the past two decades, cardiovascular diseases (CVDs) have been the top causes of mortality worldwide (1,2,3). Atherosclerosis is a slow and progressive disease that involves genetic and environmental factors and is the major cause of CVDs.

Our understanding of atherosclerosis has improved over the last decade of research; however, due to the complexity of the disease and intertwined pathways involving all layers of the blood vessel, there is still more to learn to improve prevention and therapeutic strategies. Specifically, the central molecular and cellular mechanisms that are unique to the early stages of atherosclerosis and are at the core of the pathophysiology need more focused research to be fully deciphered.

Most cases of atherosclerosis remain asymptomatic for decades (1,4). Diagnosis can be made only when clinical symptoms arise, such as reduced blood flow, blood clotting, and stroke. When a diagnosis occurs, atherosclerosis is in its advanced stages (4). Unfortunately, in advanced stages, the blood vessel wall becomes altered (5), and reversing the altered tissue to its normal state is impossible, given our current knowledge and the available technologies and therapies. Hence, early atherosclerosis diagnosis is critical to disease prevention and treatment.

The scope of the present work aims to identify molecular signatures in the circulation that can be useful biomarkers and potential therapeutic targets at early time points before the manifestation of atherosclerosis.

II. Atherosclerosis pathophysiology

II.1 Composition of the vessel wall

A normal blood vessel is composed of three different layers (Figure 1). The innermost layer is the closest to the arterial lumen and is called the tunica intima. The tunica intima is comprised of a monolayer of endothelial cells (ECs) that are in direct contact with blood. ECs at this layer reside on a membrane of non-fibrillar collagen and other extracellular molecules (5,6). The middle layer is known as tunica media. The tunica media is the thickest of all layers and is under the intima. The media contains layers of vascular smooth muscle cells (VSMCs) and an elastin-rich extracellular matrix (7). The external layer of the blood vessel is the tunica externa (also referred to as adventitia). This layer consists mainly of connective tissues (e.g., collagen fibrils) and contains blood vessels, nerve endings and lymphatics, fibroblasts, different types of leukocytes, and progenitor/stem cells (5,8,9).

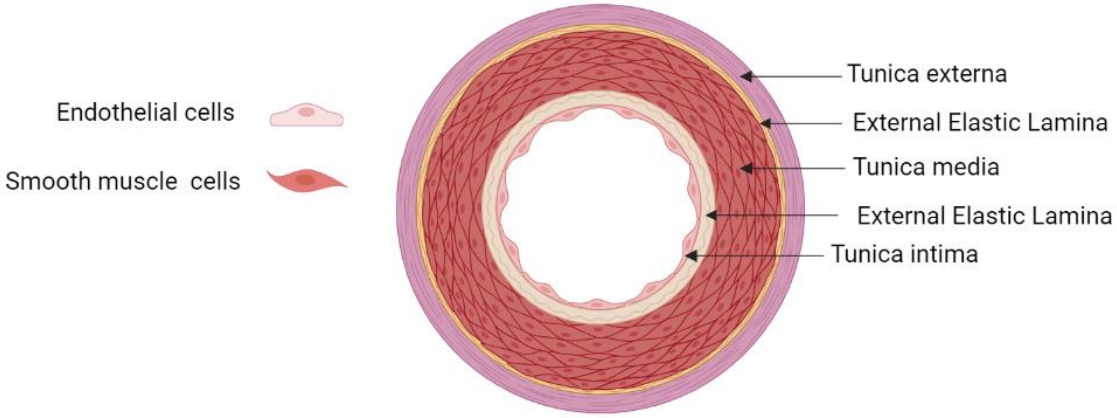

Figure 1. Cross section of a healthy aorta. Created with BioRender.com.

II.2 Features of atherosclerosis

Atherosclerosis is composed of two Greek words,"athere-" meaning gruel or paste, and "sklerosis," meaning hardening, referring to lipid buildup and hardening of the arterial wall.

Atherosclerosis plaques form through the accumulation of lipids, inflammatory cells, and extracellular matrix deposition in the arterial subintima. All three layers composing the vessel wall are involved, each contributing through different biological processes and mechanisms (10, 11). Throughout the stages of the disease, the arterial beds undergo major histological and molecular changes. A fatty streak is the earliest stage, which then progresses to a fibroatheromatous plaque (12). In the disease's later stages, lesions calcify and rupture (13,14). Each of these modifications/stages occurs in different locations of the vasculature and is mediated by different types of cells ranging from innate and adaptive immune cells to vascular endothelial and smooth muscle cells (15–18). Additionally, local hemodynamics determine the focality of lesion development (19).

The features of the atherosclerotic plaque depend on the stage of the lesion (Figure 2). The earliest manifestation of a lesion is a fatty streak, also referred to as intimal xanthomas. Xanthomas are presented as minimally raised yellowish discoloration due to high low-density lipoprotein cholesterol levels (LDL-C). LDL-C has been shown to fuel atherosclerosis (21,21). Fatty streaks can be observed in fetuses and early childhood (22–24). The streaks do not cause any symptoms and can regress over time. With the entrapment and accumulation of lipids and cells, the lesion grows. When VSMCs get involved, fibroatheroma develops. These cells migrate to the subintimal space and produce the extracellular matrix resulting in the entrapment of lipoproteins and other inflammatory cells (25–27). Fibroatheroma has a thick cap that entraps lipids and foam cells and keeps the lesion content in the subintimal space. Over time, this fibrous cap thins which renders the plaque unstable and increases the risk of rupture (14,28). At thin fibrous caps, small spots of calcification occur. When these freckled calcifications spread within lesions, the plaque becomes

calcified (13). Thinned caps eventually rupture and release the necrotic core to the circulation, activating coagulation pathways (14,28) that can lead to thrombosis and stroke.

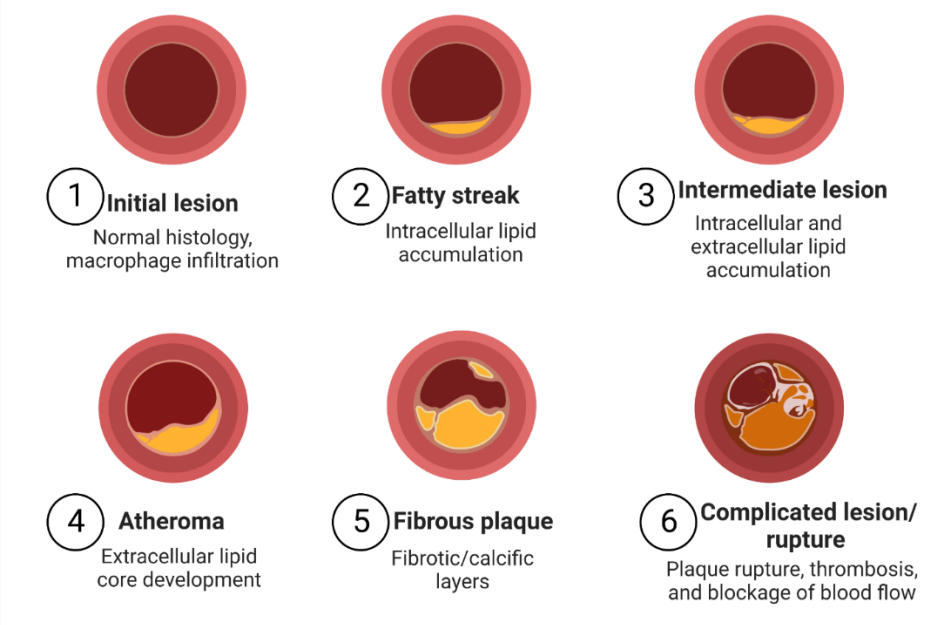

Figure 2. The different stages of atherosclerosis progression. Created with BioRender.com

II. 3 Mechanisms of atherosclerosis

Mechanisms behind the different phenotypic features of atherosclerosis have been studied extensively. These mechanisms include endothelial dysfunction, lipid infiltration and modifications, leukocyte recruitment and foam cell formation, VSMCs involvement and fibrous cap formation, necrotic core development, calcification, fibrous cap thinning, and rupture.

II.3.1 Endothelial dysfunction

Endothelial cells are present as a continuous layer – the endothelium – in direct contact with blood. The endothelium offers an uninterrupted barrier between blood and tissues. It works as a sensor for changes in circulation and a signal transducer to the other layers of the vessel wall.

A healthy endothelium confers tight control and regulation of molecules and cell permeability (6) through vasodilation, anti-inflammatory, and anti-proliferative properties (15,16). Once dysregulated, the endothelium increases proliferation and is pro-inflammatory. Factors that can lead to endothelial dysfunction include hypercholesterolemia, hypertension, smoking, air pollutants, and low and highly oscillatory shear stresses (15,17,29 –38).

A hallmark of endothelial dysfunction is the decreased availability of Nitric oxide (NO) (39). NO is a relaxing factor and the main vasodilator produced by endothelial cells via endothelial NO synthase (eNOS) (40,41). Under normal physiological conditions, NO inhibits platelet aggregation and inflammation and is atheroprotective (40,42,43). In contrast, oxidative stress increases and leads to decreased NO production in the presence of risk factors such as hyperlipidemia, hypertension, and smoking (41). Furthermore, oxidative stress promotes atherogenesis by increasing inflammatory molecules production, such as cytokines (tumor necrosis factor α (TNF- α), interleukins -1 and -6 (IL1, and IL-6)), adhesion molecules (vascular cell adhesion molecule 1 (VCAM1) and intercellular adhesion molecule 1 (ICAM1)), and chemokines (44–46). These molecules inhibit the activity of eNOS and, consequently, NO production (47–49). Additionally, single nucleotide polymorphisms (SNPs) in eNOS synthase were found to associate with coronary heart disease and hypertension (41).

Damaged endothelium is overly permeable, leading to the uptake of lipoproteins and other toxic substances and the trafficking of cells from the blood to the subintimal compartment of the vessel wall.

II.3.2 Lipid infiltration and modification

Increased permeability of ECs allows the transport of other molecules and cells from the blood. Increased levels of lipoprotein particles in the plasma favor their infiltration. Low-density

lipoprotein (LDL) particles are known to drive atherogenesis (21). Lipoprotein particles cross the endothelium by diffusion or paracellularly and via transcytosis (50–53). Additionally, turbulent blood flow increases the concentration of plasma LDL adjacent to the lumen surface. As a result, there is an increased transport of LDL particles into the wall (31,54). Other possible transport mechanisms include glycocalyx (55,56) and pericytes (57).

When LDL particles enter the subintimal space, they are exposed to chemical modifications such as oxidation. Oxidation of LDL occurs due to the interaction between lipoproteins and reactive oxygen species (ROS), oxidative and lipid oxygenases, and other enzymes (58,59). This chemical modification occurs in the early stages of the disease. It contributes to the inflammatory mechanisms initiated by endothelial dysfunction, and they continue so throughout the life span of the plaque (30,60,61). The extensive modification of LDL particles affects their recognition and binding by LDL-receptor (LDLR) and instead are recognized by scavenger receptors (62–64). Oxidized LDL (ox-LDL) activates and stimulates ECs to express leukocyte adhesion molecules on the surface of cells (60). Leukocytes are then recruited to the subintimal space.

Other LDL modifications (e.g., glycosylation, acetylation, and aggregation) also contribute to atherosclerosis development (65–67).

II.3.3 Leukocyte recruitment

In early atherosclerosis, when endothelium dysfunction takes place, leukocytes are recruited and migrate to the subendothelial space. Contrary to its normal state, the damaged endothelium barrier overexpresses adhesion molecules (e.g., VCAM1, ICAM1, P- and E-Selectins), which then bind to their corresponding ligands (e.g., integrins) present on leukocyte cell surfaces. Activated ECs also excrete cytokines and chemokines (e.g., TNF-α, c-c motif

chemokine ligand (CCL5), monocyte chemotactic protein 1 (MCP-1)) that attract and activate the inflammatory cells (68–76). Adhered leukocytes then migrate past endothelium junctions and penetrate through transcytosis into the subintima sites of lipid accumulation (72,77,78). Several leukocytes are recruited, including monocytes, neutrophils, and lymphocytes (78).

Recruitment of monocytes is initiated by tethering to activated ECs via Selectin-dependent adhesion molecules such as E- and P selectins (77–80). Tethered monocytes roll slowly on the endothelium and become tightly adhered via the binding of integrins (e.g., integrin subunit α L (ITGAL), and integrin subunit β 2 (ITGB2)) and EC adhesion molecules (e.g., VCAM1, ICAM1) (78,81–84). Monocyte adhesiveness increases with endothelial chemokines such as c-x-c motif chemokine ligands -1, -2, -4 (CXCL1, CXCL2, CXCL4) and CCL5 (84,85). Finally, monocytes traverse the endothelium via disrupted EC junctions (72). Once in the subintimal space, monocytes undergo differentiation to macrophages which can be pro- or anti-inflammatory.

II.3.4 Foam cell formation

Monocytes are trafficked to sites of lipid accumulation. Once in the subintimal space, monocytes differentiate into macrophages under the influence of monocyte–colony stimulating factor (M-CSF) (86,87). Resulting macrophages polarize to pro-inflammatory (M1) or anti-inflammatory (M2) phenotypes (85). Macrophages are scavenger cells with high plasticity allowing them to exhibit various responses based on the cues within the surrounding environment. In atherosclerosis, macrophages engulf modified LDL particles via scavenger receptors like glycoprotein IIlb (CD36), ox-LDL receptor (LOX-1), and scavenger receptor A-1 (SRA-1) (62,63). Captured LDL particles are processed in lysosomes and degraded (88–90). With high amounts of sequestered LDL, the cholesterol efflux mechanism is activated in macrophages to

excrete free cholesterol using cell membrane transporters, like ATP-binding cassette transporter A1 (ABCA1), ATP-binding cassette transporter G1 (ABCG1) and scavenger receptor B1 (SRB1) (91). Released cholesterol is then captured by high-density lipoprotein (HDL) and apolipoprotein A1 (ApoA1) and taken to the liver for reverse cholesterol transport (64). However, excessive and prolonged accumulation of cholesterol induces cholesterol crystal formation in lysosomes and subsequently activates the inflammasome and Toll-Like receptor 4 (TLR4) signaling (92–96). Consequently, the nuclear factor-kB (NF-kB) is activated, and proinflammatory cytokines and chemokines are produced (97). The unrestrained uptake of LDL by macrophages eventually affects lysosomal function resulting in the accumulation of unprocessed lipids inside cells, although the exact mechanisms are not clear. These lipid-laden cells become foam cells. With foam cell formation, more cytokines are released, leading to the proliferation of VSMCs (27,98,99), further promoting atherosclerosis.

In addition to macrophages, VSMCs exhibit macrophage-like phenotype and can uptake LDL (27,100–102); therefore, they contribute to foam cell formation.

II.3.5 Vascular smooth muscle cell migration and fibrous cap formation.

With the accumulation of lipids within foam cells and secretion of cytokines such as TNF, VSMCs proliferate and migrate along with fibroblasts leading to intimal thickening and fibrous cap formation. The fibrous cap forms a barrier between the foam cells and thickened intima and lumen. Its role is to confer structural support and avoid triggering thrombosis via exposure of the lesion core (14,28). Fibroatheroma is a hallmark of advanced atherosclerosis. At this advanced stage, plaque regression is unlikely to occur (103,104). Under normal physiological conditions, VSMCs show a contractile phenotype that governs blood vessel diameter and blood flow (25–27).

However, upon injury, these cells switch to a synthetic phenotype where they are migratory and proliferative (25,26,105,106). In response to growth factors and cytokines produced by foam cells and activated ECs, VSMCs migrate from the media to the intima (98,106–108), where VSMCs differentiation genes such as smooth muscle alpha-actin (ACTA2) and smooth muscle myosin heavy chain (MYH11) are downregulated (16). Also, the presence of LDL enhances platelet-derived growth factor (PDGF) expression VSMCs and, subsequently, their proliferation (109–111). In addition to stimulating VSMCs proliferation, TNF-α, IL-1, and fibroblast growth factor (FGF), also promote the synthesis and secretion of arterial modeling and plaque stabilization molecules such as extracellular matrix proteins (ECMs) and proteoglycans (14,110–113). The proliferating VSMCs paired with ECMs generate the fibrous cap surrounding the lesion. The thickness and collagen content of the fibrous cap are important features of a stable plaque (114).

II.3.6 Necrotic core formation

A necrotic core forms as a result of cell death (apoptosis) within the caped lesion and consists of a lipid-laden region with reduced supporting collagen (115,116). The necrotic core becomes larger with more cell death and the accumulation of dead cells.

Foam cells undergo apoptosis in early atherosclerosis, which continues throughout plaque progression. Factors triggering and influencing cell apoptosis in lesions include accumulation of cholesterol, LDL particles, oxidative stress, elevated levels of pro-inflammatory cytokines (e.g., TNF-α), and activation of the Fas death pathway (16,18,117). In early lesions, dead cells are discarded via efferocytosis (118). In contrast, dead cells' clearance is inefficient in advanced lesions due to impaired receptors mediating the process, such as mer-tyrosine kinase (MerTK), LDLR-related protein 1 (LRP1), CD36, and scavenger receptor B 1 (SR-B1) (117,118).

Furthermore, oxLDL hinders the recognition of apoptotic cells by efferocytotic receptors (119–121). Efferocytosis impairment also favors the accumulation of cholesterol crystals, which also increases lesion size (122). Also, the accumulation of cholesterol crystals within lysosomes in macrophages leads to the disruption of their membranes and the release of the content to the cytosol, eventually leading to more intense inflammation (123).

II.3.7 Calcification

Calcification of plaques results from calcium deposition in atherosclerotic lesions due to lipid accumulation and inflammation. It is another hallmark of advanced atherosclerosis.

Calcification is thought to be initiated by inflammatory cell apoptosis, release of vesicles from apoptotic cells, and induction of bone formation resulting from differentiation of pericytes and/or VSMCs (16,124–127). VSMCs switch from contractile to osteochondrogenic phenotype (128); hence, they can generate calcifying vesicles leading to calcium deposits. Calcification mechanisms are believed to be initiated by reduced levels of calcification inhibitors such as matrix gla-protein (MGP), osteopontin (OPN), and fetuin (129).

Microcalcifications are observed in the early lesion and evolve into larger calcifications. Microcalcifications, also known as spotty calcifications, are often associated with plaque rupture, while larger calcified areas are associated with stable plaque (13, 130).

II.3.8 Plaque rupture

As mentioned earlier, later stages of atherosclerosis are characterized by a fibrous cap that is the result of VSMCs migration and proliferation, extracellular matrix protein secretion, and collagen deposition. The formed cap entrapping the lipid and inflammatory cells along with other

secretions will thin over time due to cell apoptosis and released content from dead cells. Fibrous cap thinning, large necrotic core, and increased inflammatory responses are features of vulnerable plaque (130).

Thinning of the fibrous cap results from its degradation. The degradation of the cap is hypothesized to occur because of the loss of VSMCs (131). Also, proinflammatory cytokine interferon-gamma (IFN-ɣ) inhibits collagen type I gene (COL1A2) expression and, consequently, collagen production by VSMCs (132). Another hypothesis states that the continuous secretion of matrix metalloproteinases (MMPs) responsible for collagen matrices degradation reduces the collagen content, hence, weakening the cap structure (133–135). Inflammation mediators like IL-1 and TNF-α were shown to increase MMPs expression in VSMCs (136). Other cells also produce MMPs and further contribute to thinning of the cap (133). When exposed to hemodynamic forces, the thinned cap is susceptible to rupture (137).

Although extensive work was carried out to elucidate the mechanisms governing atherosclerosis progression at each stage, our knowledge is still lacking due to the interplay between the different layers of the aortic tissue, cells, and molecules involved, in addition to the complexity of the involved pathways. Further work is needed to investigate the mechanisms behind fatty streak regression, cholesterol efflux disturbances, lysosomal dysfunction, and lesion calcification.

III. Biomarkers for atherosclerosis diagnosis

Atherosclerosis is described as a slow and silent progressive disease spanning several decades. The slow progression of atherosclerosis grants a critical window of time to diagnose the disease in its early stages. As mentioned before, the earliest manifestation of the disease is a fatty

streak which can regress. Therefore, we are presented with an advantage to timely predict and diagnose the onset of atherosclerosis for early mitigation and therapeutic interventions.

Traditionally lipid biomarkers, such as LDL-cholesterol, were used to assess disease susceptibility (138,139); however, these markers cannot explain why cardiovascular events occur in individuals with normal cholesterol levels (140). In addition to traditional lipid markers, several biomarkers to diagnose atherosclerosis were proposed. These biomarkers include SNPs, inflammation and oxidative stress markers, quantitative imaging, and miRNAs (141–144). Recently, a new potential biomarkers category has emerged that focuses on the host microbiome and microbiota metabolites (145,146).

The sections below summarize the different categories of proposed biomarkers for atherosclerosis diagnosis.

III.1 Single nucleotide polymorphisms (SNPs) biomarkers

Genetic mutations contribute to atherosclerosis pathogenesis and CVDs predisposition. Some identified SNPs are located in genes with known functions in inflammation, oxidative stress, lipid transportation, and endothelial dysfunction, which are pathogenic processes in atherosclerosis (144). Among these, mutations in the low-density lipoprotein receptor (LDLR), apolipoprotein B (APOB), and proprotein convertase subtilisin/kexin type 9 (PCSK9) genes (147) associate with familial hypercholesterolemia, a well-established risk factor for atherosclerosis of the arteries. These mutations affect cholesterol transport and clearance from circulation (148–150). Other SNPs also correlate with atherosclerosis and its clinical manifestations. For instance, MMP-3 and MMP-9 SNPs correlate with CVD events such as myocardial infarction and ischemic stroke (151). Another example is that of C-reactive protein (CRP). Two sets of haplotypes of the CRP gene, an

inflammation marker, are associated with stroke in Chinese Han (152). Other SNPs in this gene also associate with CVDs risk (153). Similarly, SNPs in nitric oxide synthase 3 (NOS3) and methylenetetrahydrofolate reductase (MTHFR) showed a significant association with coronary atherosclerosis in Iranians (41,154). Conversely, P-Selectin SNPs are associated with a lower risk of coronary artery disease in Mexicans (155). Whether these SNPs are consistent across ethnicities is unknown. Additionally, identified SNPs, regardless of whether they have a known function or not, contribute ~13% to CVD heritability when combined (144); hence, SNPs alone are not enough to estimate and diagnose atherosclerosis and cardiovascular risk.

III.2 Inflammation biomarkers

Inflammation is an ongoing process from the early to later stages of atherosclerosis. Several inflammation markers, such as CRP and TNF-α, can be found in the circulation and have been proposed as diagnostic markers for atherosclerosis (156–158). In a population-based study, CRP and TNFα significantly associated with CVDs and predicted CVD events and mortality in males but not females (157). Similar to CRP and TNF-α, serum amyloid A (SAA) was also shown to associate with CVDs and early mortality (159,160). SAA induces endothelial dysfunction in early atherosclerosis (161).

Cytokines, specifically interleukins, such as IL-6, and MCP-1, drive the early inflammatory processes in atherosclerosis (143). IL-6 was reported to be higher in patients with atherosclerosis and cardiac events like stroke and heart failure (157,158,162). TNF-α, another cytokine involved in several stages of atherogenesis, was shown to be independently associated with atherosclerosis severity and predict CVD events (157,163).

III.3 Oxidative stress biomarkers

Oxidative stress also plays a role in atherogenesis by increasing free radical production in the vessel wall (164,165). This biomarkers' category includes myeloperoxidase (MPO), MMPs, and nicotinamide adenine dinucleotide phosphate (NADPH) oxidase.

MPO is excreted by inflammatory cells, induces LDL oxidation, and catalyzes the formation of several reactive species, thus contributing to oxidative stress (166). MPO levels were higher in CVD patients (167) and predicted increased risk for cardiovascular events and atherosclerosis progression (168–169). MMPs promote plaque vulnerability by degrading ECM, causing thinning of the fibrous cap. In addition, these molecules are activated by MPO (166). For example, MMP-9 can predict CVD mortality and was also found to be associated with initial CVD events in patients (170,171). Moreover, MMP-3 and MMP-10 were also reported as possible biomarkers for subclinical atherosclerosis (172,173).

III.4 MicroRNA biomarkers

MicroRNAs, a short class of non-coding RNAs, can be found in cells and in circulation in blood bound to lipoproteins (174), encapsulated in exosomes and microvesicles (175). They make very promising biomarkers because of their role in gene expression regulation and cell-to-cell communications (176). Several studies have demonstrated an association between miRNA profiles and atherosclerosis and its clinical manifestations. For example, miR-574-3p was found to negatively correlate with stroke in participants of the Framingham Heart Study (177). In a multi-ethnic Chinese study, miR-130a, miR-155, and miR-221 negatively correlated with atherosclerosis severity measured by angiography (178). Similarly, a different study found that miR-221 was downregulated in the serum of patients with atherosclerosis (179). Moreover, miR-130a, miR-27b,

and miR-210 serum levels were higher in patients with periphery artery atherosclerosis (180). In contrast, levels of miR-126, miR-17, miR-145, and miR-155 were lower in patients with the disease (181). Dysregulated levels of circulating miRNAs in atherosclerosis were also reported in several other studies (182–186)

Circulating miRNA profiles differed based on lesion location, as reported in a systematic review (187). Likewise, a study of extracellular vesicles captured miRNA signatures of atherosclerosis that are location specific (188).

III.5 Microbiome and microbiota-metabolite biomarkers

Microbiota is recognized as an essential player in human health. Current knowledge suggests that the gut microbiome regulates the host immune system and metabolism (189–191). For example, bacterial lipopolysaccharides (LPS) induce polarization of macrophages to a pro-inflammatory state (M1) (192,193) via Toll-Like Receptors (TLRs), leading to cytokines production and promoting atherosclerosis (193,194). In addition, gut microbiota was reported to metabolize host cholesterol, thus, reducing total cholesterol levels in circulation (195,196), which minimizes the risk of developing atherosclerosis. Mechanisms by which the gut microbiome regulates cholesterol metabolism include regulating the expression of cholesterol efflux genes, such as ABCA1 and ABCG1 (197). Also, trimethylamine N-oxide (TMOA) synthesis by gut microbes is linked to an increased risk of cardiovascular diseases (146). Although microbiome studies in the context of CVDs are scarce, there is evidence of the dysbiosis of the microflora in the gut, atherosclerosis plaque (198, 199), and in the blood (200). Therefore, the observed dysbiosis can be used as a marker for disease diagnosis. For example, a recent study showed that patients with CVD presented higher ratios of Firmicutes/Bacteroidetes DNA compared to healthy

individuals (201). In addition to microbial DNA, microbiome-derived metabolites such as TMAO, indole- and phenyl-derived metabolites are promising biomarkers and have been associated with atherosclerosis (145,202–205).

III.6 Imaging markers

Current imaging techniques for atherosclerosis diagnosis can detect anatomical and physiological changes in lesions (142,206,207). Some of the measurements these techniques capture are summarized below, including coronary artery calcium score (CACS), carotid intima-media thickness (cIMT), and arterial stiffness.

a. Coronary Artery Calcium Score (CACS)

As mentioned in earlier sections, calcification plays an important role in atherosclerosis. Coronary Artery Calcium Score (CACS) measures the amount of calcium in coronary arteries and provides a noninvasive measure of the total atherosclerosis burden. This measurement is a well-established predictor of the disease (208) and has been proposed as a marker for atherosclerosis risk assessment (206,209). A low CACS was associated with a lower risk of CVD events (210). Additionally, CACS independently predicted mortality due to coronary atherosclerosis in asymptomatic individuals (211).

b. Carotid Intima-Media Thickness (cIMT)

Carotid Intima-Media Thickness (cIMT) measures the distance between the lumen intima and adventitia-media borders. cIMT correlated with CVD and stroke and was shown to be a strong predictor of atherosclerosis and CVD events (212–214). In contrast, cIMT showed no significant

benefit in risk prediction (215). Therefore, cIMT measurement usefulness in detecting subclinical atherosclerosis in clinical practice is not well-established (216).

c. Arterial Stiffness

Arterial stiffness measurement is not currently used as a biomarker for atherosclerosis in clinical trials due to the various imaging techniques and calculation methods employed (217). However, the correlation between arterial stiffness and cardiovascular events has been shown (218). For example, Oberoi et al. demonstrated that aortic stiffness positively correlates with coronary atherosclerosis (219). Moreover, Zureik et al. demonstrated that arterial stiffness is associated with fibrous or calcified plaque (220,221). Also, aortic and carotid artery stiffness was strongly associated with cIMT and the severity of the plaque (222).

IV. Animal models to study atherosclerosis

Currently, different animal models and in vitro systems are used to study atherosclerosis at phenotypic and molecular levels. In-vitro models are important because they allow investigation of the mechanisms of action at the molecular level. However, animal models are better suited to study the disease complexity and are of particular value in preclinical testing of therapeutics and biomarker discovery; hence, in the section below, we will focus on animal models.

Among the present animal models to study atherosclerosis are mice, rabbits, non-human primates, and swine models.

Mice models of atherosclerosis are the most frequently used models to study the disease mainly due to the presence of various wild-type strains, different genetically modified versions, rapid reproduction, short-time for disease development, and ease of genetic modification (223–

225). Examples of these models include $APOE^{-/-}$, $LDLR^{-/-}$, $APOE^{-/-}LDLR^{-/-}$, and PSCK-AAV (226,227). However, these models present certain disadvantages. For example, $APOE^{-/-}$ mice VLDL is the most abundant lipoprotein, whereas LDL is the most abundant in humans (228). Also, plaque rupture events are rare (229,230). Similarly, $LDLR^{-/-}$ mice lack spontaneous plaque rupture and thrombosis complications. $LDLR^{-/-}$ mice present a more human-like lipoprotein profile. However, the animals need a high-fat diet to develop atherosclerosis (231). Like LDL-/- mice, PSCK9-AAV mice require high-fat diet to develop atherosclerosis and do not have spontaneous plaque rupture (227).

Rabbits are very sensitive to high-fat diets and have been widely used to study atherosclerosis (224). Rabbit models include Watanabe heritable hyperlipidemic rabbits (WHHL), New Zealand White rabbits, and $ApoE^{-/-}$ rabbits (232–235). Additionally, rabbits are easy to handle and relatively inexpensive (224). However, their lesions are largely foamy and hepatic lipase deficient, and V-LDL is the primary lipoprotein, making their lipid metabolism and lipoprotein profile not similar to humans (233).

While mice and rabbit models helped elucidate many mechanisms in atherosclerosis, and they continue to do so, the small size of the animals presents disadvantages due to the low complexity of the disease. In addition, these small arteries prevent the use of imaging techniques and the lack of tissue for extensive and high-throughput multi-omics studies. Therefore, large animals are needed to address the shortcoming of small animal models.

Non-human primates are large animals and are similar to humans in terms of their lipoprotein profile, hemodynamics, heart rate, and atherosclerotic lesions (224,236). However, non-human primates are not as employed in atherosclerosis studies due to ethical, regulatory, and

financial reasons. In addition, the long time frame for lesion development in non-human primates is another disadvantage to employing this animal model in atherosclerosis studies.

Swine are another large animal that has been frequently used in studying atherosclerosis. Like non-human primates, swine have a lipoprotein profile and lesion characteristics similar to humans (237–241). Swine also have similar cardiovascular system anatomy and can be imaged noninvasively (241–245). Moreover, swine models with specific genetics continue to emerge with advances in gene editing technologies. For example, the swine model of familial hypercholesterolemia, which harbors a mutation in the LDLR gene, was first reported by Rapacz et al. (246). Another example is that of genetically modified pigs, the D374Y-PCSK9 transgenic Yucatan pigs (247). Other swine models of atherosclerosis exist, such as the Ossabow and the genetically modified Ossabow pigs (248,249)

Despite the burgeoning of studies proposing potential biomarkers for atherosclerosis, effective biomarkers for disease diagnosis are lacking. Some of the biomarkers showed no significant association with atherosclerosis plaque (e.g., MCP-1 and IL-6) (250), are sex-specific (e.g., CRP) (157), and were found to correlate with the disease in certain ethnicities and not all (CRP, MTHFR, and SELP) (152,154). In addition, some of these biomarkers showed contradictory results (e.g., cIMT) (215). Other proposed biomarkers require more work to elucidate the mechanisms underlying their participation in atherosclerosis. Moreover, the inherent difference in the assays/methods used to measure these markers weakens their usefulness in disease diagnosis.

Additionally, the biggest hurdle of the proposed biomarkers stems from the fact that human studies focus on one time-point analysis, which often is linked to clinical manifestations of atherosclerosis (173,184,186,208,210,215,251). Therefore, these studies limit the diagnosis to

later stages when pathological manifestations appear. However, diagnosis in later stages is problematic because of the limited success of mitigation and therapeutic strategies to reduce the risk of cardiac events. Thus, it is best to approach the discovery of diagnosis biomarkers for atherosclerosis in the early stages by performing longitudinal studies at the earliest points possible before disease manifestation. However, longitudinal human studies are challenging due to difficulties in recruiting children and young individuals, expenses, and regulatory requirements.

To address the limitations above, we designed the present study in which we used the following:

1- A swine translational model of atherosclerosis, the Wisconsin Miniature Swine™ of Familial Hypercholesterolemia (WMS-FH). WMS-FH develops atherosclerosis spontaneously and displays complex lesions similar to humans and in different arterial beds (252, 241,246); hence, this model is well suited to study atherosclerosis.

2- A longitudinal approach to monitor the dynamics of circulating miRNAs and microbiome in earlier stages of life before the onset of early atherosclerosis lesions.

3- Different categories of biomarkers, including circulating miRNAs and bacterial DNA (microbiome) for early diagnosis of atherosclerosis.

We hypothesize that circulating miRNA and microbiome signatures of atherosclerosis development can be detected in the early stages of life.

V. Research approach

V.1 Assess aortic tissue mRNA expression differences between WMS FH and WMS-N (Aim 1)

a. Rationale

The aortic tissue is a complex environment composed of different cell populations, ECs, SMCs, resident leukocytes, fibroblasts, stem cells, and others (8). When atherosclerosis develops in the arteries, the tissue structure loses elasticity and hardens. This change in the phenotype results from perturbations in mRNA expression patterns of the different cells comprising the tissue and recruitment of other cells from the bloodstream. In humans, studies demonstrated differences in mRNA expression between normal aortic tissues and those with atherosclerotic lesions (253-255). Our proposed research uses a well-suited swine model (WMS-FH) to study atherosclerosis. Our animals (WMS-FH) are derived from "Rapacz swine." These pigs are homozygous for a single point mutation in the low-density lipoprotein receptor (LDLR) (246) which hinders cholesterol clearance from the blood. Because of their hypercholesterolemia, WMS-FH develops human-like complex lesions in different arterial beds (coronary, femoral, and brachial) starting at 12 months (245,256–258). The natural history of disease progression and response to interventional vascular therapies in this animal model has been previously documented in the literature (243,244,259,260). In contrast, the WMS-N are normocholesterolemic and do not have the LDLR gene mutation but are from the same genetic background. Figure 3 illustrates the LDLR pathway and the dysregulations that cause familial hypercholesterolemia (FH). In this study, we aimed to identify differentially expressed genes between abdominal aortic tissues of WMS-FH and WMS-N. We also aimed to determine key pathways and hub genes central to the pathophysiology of atherosclerosis, which will also present us with possible targeted therapeutic strategies. The

abdominal aortic tissue region was chosen because this is the first location where WMS-FH pigs display fibroatheromatous plaque.

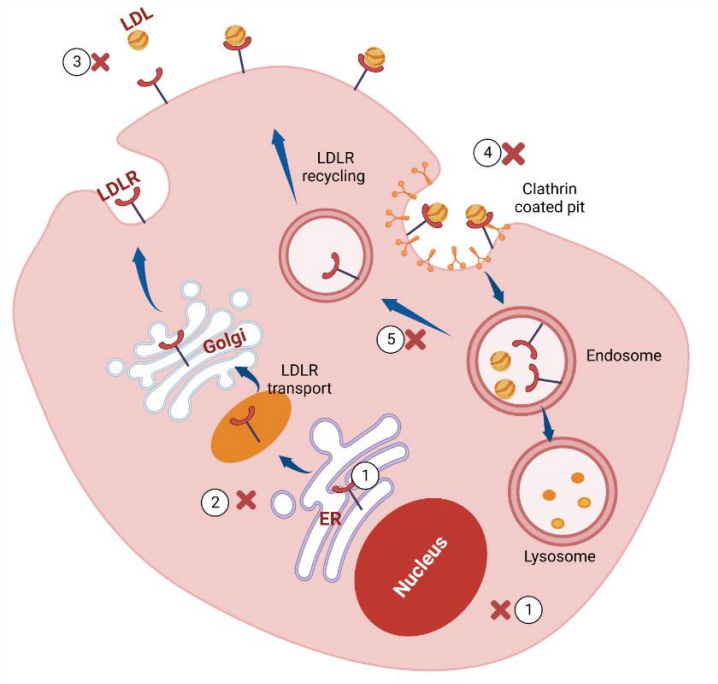

Figure 3. Low-density lipoprotein receptor (LDLR) pathway and dysregulation.1) Class1: null allele, 2) Class 2: Endoplasmic reticulum (ER) retention. 3) Class 3: Deficient low-density lipoprotein (LDL) binding. 4) Class 4: Impaired endocytosis. 5) Class 5: Impaired recycling. **Class 3 is the main mechanism by which WMS-FH pigs are hypercholesterolemic.** Created with BioRender.com.

V. 2 Assess circulating miRNAs changes in early life of WMS-FH and determine the diagnostic power of identified miRNAs (Aim2)

b. Rationale

Given the silent nature of atherosclerosis in the early stages, early detection is imperative. Biomarkers, specifically miRNAs, have been proposed as diagnostic tools for atherosclerosis (179,250,261). Nonetheless, circulating miRNA profile assessment is mostly paired with existing

clinical manifestations of the disease, such as stroke and the presence of lesions (179,251,262). Clinical manifestations occur when atherosclerosis is in advanced stages. Furthermore, human longitudinal studies before disease development are difficult to conduct and are rare, if present. Here we aimed to investigate the dynamic changes in circulating miRNA expression within individuals and between WMS-FH and WMS-N pigs for months 3, 6, and 9. The three-time points represent animal age at the time of blood collection, which was selected based on the cholesterol profiles in WMS FH animals. Month 3 was selected as an early time point before serum total cholesterol levels peak. Serum total cholesterol levels peak around month 6 and stabilize around month 9. The presence of the disease in animals was determined via Optical Coherence Tomography (OTC) at the Cardiovascular Research Foundation (NY, USA). The diagnostic power of identified miRNAs was determined following a discriminatory power analysis using the Receiver Operating Characteristic Curve (ROC).

V.3 Identify circulating microbiome signatures in WMS FH and identify the diagnostic power of identified taxa (Aim 3)

c. Rationale

Microbiota disturbances are associated with diseases (145,263,264). Indeed, bacterial presence was confirmed in atherosclerotic plaque (265,266). Additionally, microbiota contributes to the immune system (267,268), and cholesterol metabolism (195,196), two key players in atherosclerosis development and progression. Blood has long been considered a sterile environment and to only harbor microorganisms in cases of sepsis. However, bacterial DNA was found in the circulation of healthy individuals.

Moreover, very few studies have demonstrated the presence of microbial DNA in the blood of patients with CVDs (200,269). Blood microbiome also correlated with LDL levels (200). Therefore, circulating microbiome signatures are candidate diagnosis biomarkers. Here we aimed to identify microbiome (Bacterial DNA) signatures in the plasma of WMS FH. Similar to miRNA signatures, we profiled WMS-FH and WMS-N animals at months 3, 6, and 9 for differences in bacterial DNA using 16S rRNA gene full-length sequencing. The diagnostic power was determined using the same approach in Aim 2.

Visual abstract of the research approach (Created with BioRender.com)

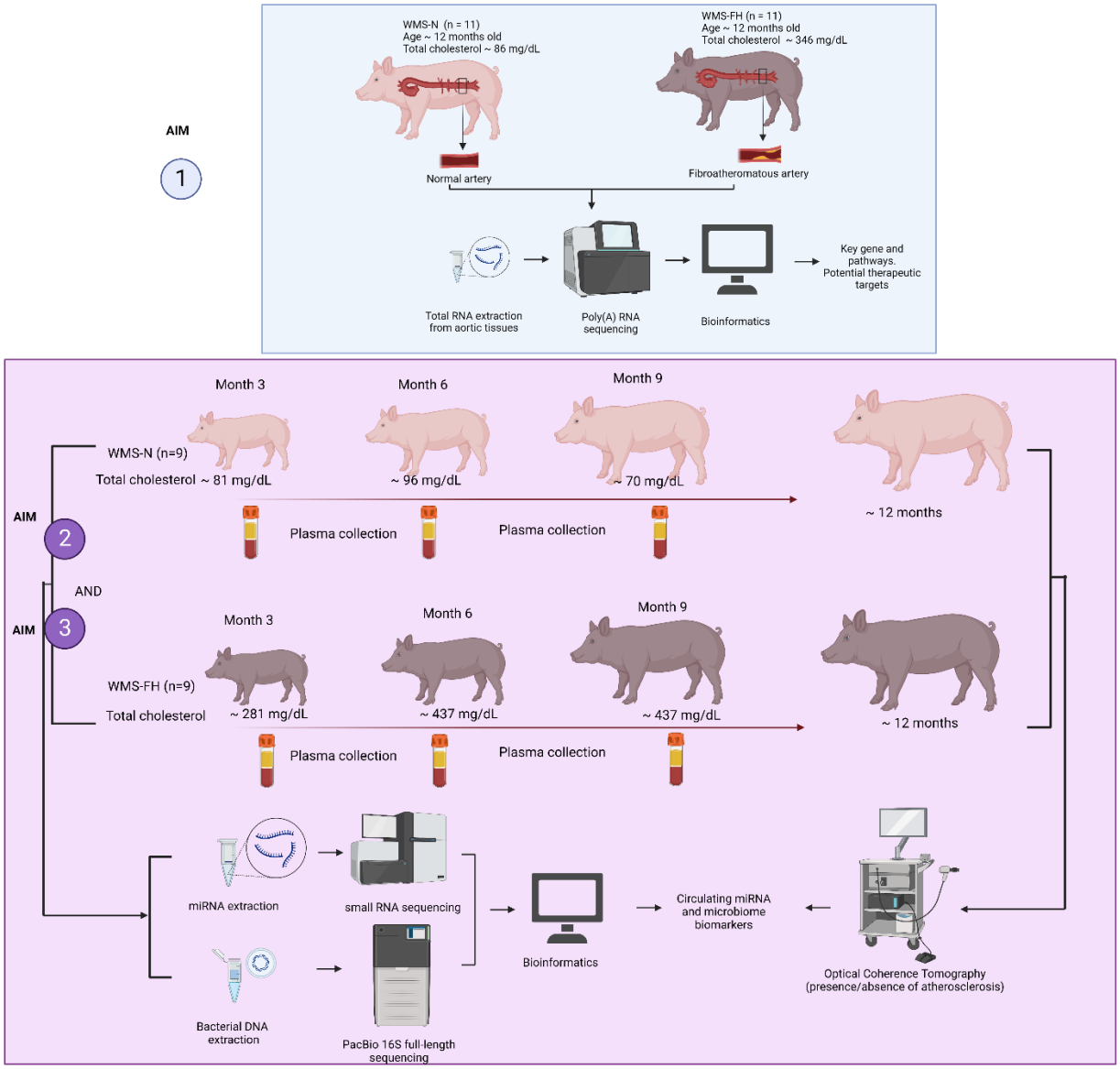

Aim 1: Assess aortic tissue mRNA expression differences between WMS FH & WMS-N.

Aim2 : Assess circulating miRNA changes in the ealry life of WMS-FH and determine the diagnostic power of identified miRNAs.

Aim 3: Identify circulating microbiome signatures in WMS FH and determine the diagnostic power of identified taxa.

References

1. Benjamin EJ., Muntner P., Alonso A., et al. Heart Disease and Stroke Statistics—2019 Update: A Report From the American Heart Association. Circulation 2019;139(10):e56–528. Doi: 10.1161/CIR.0000000000000659.
2. Heron M. Deaths: Leading causes for 2017. National Vital Statistics Reports; vol 68 no 6. Hyattsville, MD: National Center for Health Statistics. 2019. https://www.cdc.gov/nchs/products/index.htm. (Accessed on 18/01/2020).
3. Xu JQ, Murphy SL, Kochanek KD, Arias E. Mortality in the United States, 2018. NCHS Data Brief, no 355. Hyattsville, MD: National Center for Health Statistics. 2020. https://www.cdc.gov/nchs/data/databriefs/db355_tables-508.pdf#1. (Accessed on 29/12/2020)
4. Toth PP. Subclinical atherosclerosis: what it is, what it means and what we can do about it. Int J Clin Pract 2008;62(8):1246–54. Doi: 10.1111/j.1742-1241.2008.01804.x.
5. Tucker WD, Arora Y, Mahajan K. Anatomy, Blood Vessels. 2022 Aug 8. In: StatPearls [Internet]. Treasure Island (FL): StatPearls Publishing; 2022 Jan–. PMID: 29262226.
6. Kerr P., Tan R., Plane F. Endothelium. In: Fitridge R, and Thompson M, editors. Mechanisms of Vascular Disease: A Reference Book for Vascular Specialists. University of Adelaide Press: JSTOR; 2011. p. 1–12. Doi: 0.20851/j.ctt1sq5w94.5.
7. Wilson DP. Vascular Smooth Muscle Structure and Function. In: Fitridge R, and Thompson M, editors. Mechanisms of Vascular Disease Book Subtitle: A Reference Book for Vascular Specialists. University of Adelaide Press, JSTOR; 2011. p. 1–13. Doi: 10.1017/UPO9781922064004.003

8. Fernando S., Bursill CA., Nicholls SJ., Psaltis PJ. Mechanisms of Vascular Disease. Mechanisms of Vascular Disease 2020:19–45. Doi: 10.1007/978-3-030-43683-4.

9. Tinajero MG., Gotlieb AI. Recent Developments in Vascular Adventitial Pathobiology: The Dynamic Adventitia as a Complex Regulator of Vascular Disease. American Journal of Pathology 2020:520–34. Doi: 10.1016/j.ajpath.2019.10.021.

10. Cockerill G., Xu Q. Atherosclerosis. In: Fitridge R, and Thompson M, editors. Mechanisms of Vascular Disease: A Reference Book for Vascular Specialists. University of Adelaide Press, JSTOR; 2011. p. 1–19. Doi: 10.20851/j.ctt1sq5w94.7.

11. Lu H., Daugherty A. Atherosclerosis. Arterioscler Thromb Vasc Biol 2015;35(3):485–91. Doi: 10.1161/ATVBAHA.115.305380.

12. Rafieian-Kopaei M., Setorki M., Doudi M., Baradaran A., Nasri H. Atherosclerosis: Process, Indicators, Risk Factors and New Hopes. Int J Prev Med 2014;5(8).

13. Shi X., Gao J., Lv Q., et al. Calcification in Atherosclerotic Plaque Vulnerability: Friend or Foe? Front Physiol 2020;11. Doi: 10.3389/fphys.2020.00056.

14. Bentzon JF., Otsuka F., Virmani R., Falk E. Mechanisms of Plaque Formation and Rupture. Circ Res 2014;114(12):1852–66. Doi: 10.1161/CIRCRESAHA.114.302721.

15. Seidman MA., Mitchell RN., Stone JR. Pathophysiology of Atherosclerosis. Cellular and Molecular Pathobiology of Cardiovascular Disease. Elsevier Inc.; 2014. p. 221–37. Doi: 10.1016/B978-0-12-405206-2.00012-0.

16. Fernando S., Bursill CA., Nicholls SJ., Psaltis PJ. Pathophysiology of atherosclerosis. Mechanisms of Vascular Disease. Springer Nature Switzerland; 2020. p. 19–45. Doi: 10.1007/978-3-030-43683-4_2.

17. Sakakura K., Nakano M., Otsuka F., Ladich E., Kolodgie FD., Virmani R. Pathophysiology of Atherosclerosis Plaque Progression. Heart Lung Circ 2013;22(6):399–411. Doi: 10.1016/j.hlc.2013.03.001.

18. Sakakura K., Nakano M., Otsuka F., Ladich E., Kolodgie FD., Virmani R. Pathophysiology of Atherosclerosis Plaque Progression. Heart Lung Circ 2013;22(6):399–411. Doi: 10.1016/j.hlc.2013.03.001.

19. Lawrence-Brown MM., Liffman K., Semmens JB., Sutalo Book ID., Fitridge R., Thompson M. Vascular Arterial Hemodynamics. In: Fitridge R, and Thompson M, editors. Mechanisms of Vascular Disease Book Subtitle: A Reference Book for Vascular Specialists. University of Adelaide Press, JSTOR; 2011. p. 1–25. Doi: 10.20851/j.ctt1sq5w94.12.

20. Zhang X., Fernández-Hernando C. Transport of LDLs into the arterial wall: impact in atherosclerosis. Curr Opin Lipidol n.d. Doi: 10.1097/mol.0000000000000701.

21. Tomkin GH., Owens D. LDL as a Cause of Atherosclerosis. The Open Atherosclerosis & Thrombosis Journal 2012;5(1):13–21. Doi: 10.2174/1876506801205010013.

22. Palinski W., Napoli C. The fetal origins of atherosclerosis: Maternal hypercholesterolemia, and cholesterol-lowering or antioxidant treatment during pregnancy influence in utero programming and postnatal susceptibility to atherogenesis. FASEB Journal 2002;16(11):1348–60. Doi: 10.1096/fj.02-0226rev.

23. McGill J., McMahan CA., Herderick EE., Malcom GT., Tracy RE., Jack P. Origin of atherosclerosis in childhood and adolescence. American Journal of Clinical Nutrition 2000;72(5 SUPPL.): 1307S–15S. Doi: https://doi.org/10.1093/ajcn/72.5.1307s

24. Napoli C., Armiento FPD., Mancini FP., Postiglione A., Witztum JL. Fatty Streak Formation Occurs in Human Fetal Aortas and is Greatly Enhanced by Maternal Hypercholesterolemia 1997;100(11):1–11. Doi: 10.1172/JCI119813.

25. Wilson D. Vascular smooth muscle structure and function. Mechanisms of Vascular Disease: A Reference Book for Vascular Specialists 2011:13–24. Doi: 10.1017/UPO9781922064004.003.

26. Michel J-B., Li Z., Lacolley P. Smooth muscle cells and vascular diseases. Cardiovasc Res 2012;95(2):135–7. Doi: 10.1093/cvr/cvs172.

27. Bennett MR., Sinha S., Owens GK. Vascular Smooth Muscle Cells in Atherosclerosis. Circ Res 2016;118(4):692–702. Doi: 10.1161/CIRCRESAHA.115.306361.

28. Loftus I. Mechanisms of Plaque Rupture. In: Fitridge R, and Thompson M, editors. Mechanisms of Vascular disease: A reference Book for Vascular Specialists. Adelaide: University of Adelaide Press; 2011. p. 1–37. Doi: 0.20851/j.ctt1sq5w94.8.

29. di Pietro N., Formoso G., Pandolfi A. Physiology and pathophysiology of oxLDL uptake by vascular wall cells in atherosclerosis. Vascul Pharmacol 2016;84:1–7. Doi: 10.1016/j.vph.2016.05.013.

30. Dhawan SS., Nanjundappa RPA., Branch JR., et al. Shear stress and plaque development. Expert Rev Cardiovasc Ther 2010:545–56. Doi: 10.1586/erc.10.28.

31. Tarbell JM. Shear stress and the endothelial transport barrier. Cardiovasc Res 2010;87(2):320–30. Doi: 10.1093/cvr/cvq146.

32. Brands PJ., Hoeks APGG., Hofstra L., et al. Wall shear stress and early atherosclerosis: a review. Stroke 2004. Doi: 10.1016/S0301-5629(97)00044-6.

33. Cunningham KS., Gotlieb AI. The role of shear stress in the pathogenesis of atherosclerosis 2005:9–23. Doi: 10.1038/labinvest.3700215.

34. Siasos G., Sara JD., Zaromytidou M., et al. Local Low Shear Stress and Endothelial Dysfunction in Patients With Nonobstructive Coronary Atherosclerosis 2018;71(19). Doi: 10.1016/j.jacc.2018.02.073.

35. Souilhol C., Serbanovic-Canic J., Fragiadaki M., et al. Endothelial responses to shear stress in atherosclerosis: a novel role for developmental genes. Nat Rev Cardiol 2020:52–63. Doi: 10.1038/s41569-019-0239-5.

36. Conklin BS., Vito RP., Chen C. Effect of low shear stress on permeability and occludin expression in porcine artery endothelial cells. World J Surg 2007;31(4):733–43. Doi: 10.1007/s00268-006-0735-8.

37. Xie X., Wang F., Zhu L., et al. Low shear stress induces endothelial cell apoptosis and monocyte adhesion by upregulating PECAM-1 expression. Mol Med Rep 2020:2580–8. Doi: 10.3892/mmr.2020.11060.

38. Peiffer V., Sherwin SJ., Weinberg PD. Does low and oscillatory wall shear stress correlate spatially with early atherosclerosis ? A systematic review 2013:242–50. Doi: 10.1093/cvr/cvt044.

39. Archer SL., Huang JM., Hampl V., Nelson DP., Shultz PJ., Weir EK. Nitric oxide and cGMP cause vasorelaxation by activation of a charybdotoxin-sensitive K channel by cGMP-dependent protein kinase. Proceedings of the National Academy of Sciences 1994;91(16):7583–7. Doi: 10.1073/pnas.91.16.7583.

40. Wang X-F., Ye Z-X., Chen J-Y., et al. Roles of Nitric Oxide Signaling Pathway in Atherosclerosis. Atheroscl. Open Access. 2018;3(1):1–10.

41. Levinsson A., Olin A., Björck L., Rosengren A., Nyberg F. Nitric Oxide Nitric oxide synthase (NOS) single nucleotide polymorphisms are associated with coronary heart disease and hypertension in the INTERGENE study. NITRIC OXIDE 2014;39:1–7. Doi: 10.1016/j.niox.2014.03.164.

42. Chen J., Ye Z., Wang X., et al. Nitric oxide bioavailability dysfunction involves in atherosclerosis. Biomedicine & Pharmacotherapy 2018;97:423–8. Doi: 10.1016/j.biopha.2017.10.122.

43. Cooke JP., Tsao PS. Is NO an endogenous antiatherogenic molecule? Arterioscler Thromb 1994;14(5):653–5. Doi: 10.1161/01.ATV.14.5.653.

44. Araujo JA., Nel AE. Particulate matter and atherosclerosis: Role of particle size, composition and oxidative stress. Part Fibre Toxicol 2009;6:1–19. Doi: 10.1186/1743-8977-6-24.

45. Lu Y., Sun Y., Jiang Z., et al. Guanxinshutong Alleviates Atherosclerosis by Suppressing Oxidative Stress and Proinflammation in ApoE−/− Mice. Evid Bas Comp and Alt Med 2020:1-13. Doi: 10.1155/2020/1219371.

46. Marchio P., Guerra-Ojeda S., Vila JM., Aldasoro M., Victor VM., Mauricio MD. Review Article Targeting Early Atherosclerosis: A Focus on Oxidative Stress and Inflammation. Oxi Med and Cell Long 2019, 1-32. Doi: 10.1155/2019/8563845.

47. Chen J., Ye Z., Wang X., et al. Nitric oxide bioavailability dysfunction involves in atherosclerosis. Biomed & Pharma 2018;97:423–8. Doi: 10.1016/j.biopha.2017.10.122.

48. Cyr AR., Huckaby L v., Shiva SS., Zuckerbraun BS. Nitric Oxide and Endothelial Dysfunction. Crit Care Clin 2020;36(2):307–21. Doi: 10.1016/j.ccc.2019.12.009.

49. Esper RJ., Nordaby RA., Vilariño JO., Paragano A., Cacharrón JL., Machado RA. Endothelial dysfunction: A comprehensive appraisal. Cardiovasc Diabetol 2006;5. Doi: 10.1186/1475-2840-5-4.

50. Pappenheimer JR., Renkin EM., Borrero LM. Filtration, Diffusion and Molecular Sieving Through Peripheral Capillary Membranes. American Journal of Physiology-Legacy Content 1951;167(1):13–46. Doi: 10.1152/ajplegacy.1951.167.1.13.

51. Michel CC. Transport of macromolecules through microvascular walls. Cardiovasc Res 1996;32(4):644–53.

52. Zhang X., Sessa WC., Fernández-Hernando C. Endothelial Transcytosis of Lipoproteins in Atherosclerosis. Front Cardiovasc Med 2018;5. Doi: 10.3389/fcvm.2018.00130.

53. Jang E., Robert J., Rohrer L., von Eckardstein A., Lee WL. Transendothelial transport of lipoproteins. Atherosclerosis 2020;315:111–25. Doi: 10.1016/j.atherosclerosis.2020.09.020.

54. Kang H., Cancel LM., Tarbell JM. Effect of shear stress on water and LDL transport through cultured endothelial cell monolayers. Atherosclerosis 2014;233(2):682–90. Doi: 10.1016/j.atherosclerosis.2014.01.056.

55. Alphonsus CS., Rodseth RN. The endothelial glycocalyx: a review of the vascular barrier. Anaesthesia 2014;69(7):777–84. Doi: 10.1111/anae.12661.

56. Yang Y., Schmidt EP. The endothelial glycocalyx. Tissue Barriers 2013;1(1):e23494. Doi: 10.4161/tisb.23494.

57. Summerhill, V., Orekhov, A. Pericytes in Atherosclerosis. In: Birbrair, A. (eds) Pericyte Biology in Disease 2019. Advances in Experimental Medicine and Biology, vol 1147. Springer, Cham. https://doi.org/10.1007/978-3-030-16908-4_13

58. Yoshida H., Kisugi R. Clinica Chimica Acta Mechanisms of LDL oxidation. Clinica Chimica Acta 2010;411(23–24):1875–82. Doi: 10.1016/j.cca.2010.08.038.

59. Jialal I., Devaraj S. The Role of Oxidized Low Density Lipoprotein in Atherogenesis. J Nutr 1996;126(suppl_4):1053S-1057S. Doi: 10.1093/jn/126.suppl_4.1053S.

60. Pirillo A., Norata GD., Catapano AL. LOX-1, OxLDL, and Atherosclerosis. Mediators Inflamm 2013;2013:1–12. Doi: 10.1155/2013/152786.

61. Sohrabi Y., Lagache SMM., Voges VC., et al. OxLDL-mediated immunologic memory in endothelial cells. J Mol Cell Cardiol 2020;146:121–32. Doi: 10.1016/j.yjmcc.2020.07.006.

62. Greaves DR., Gordon S. The macrophage scavenger receptor at 30 years of age: current knowledge and future challenges. J Lipid Res 2009;50:S282–6. Doi: 10.1194/jlr.R800066-JLR200.

63. Park YM. CD36, a scavenger receptor implicated in atherosclerosis. Exp Mol Med 2014. Doi: 10.1038/emm.2014.38.

64. Chistiakov DA., Bobryshev Y v., Orekhov AN. Macrophage-mediated cholesterol handling in atherosclerosis. J Cell Mol Med 2016;20(1):17–28. Doi: 10.1111/jcmm.12689.

65. Lu M., Gursky O. Aggregation and fusion of low-density lipoproteins in vivo and in vitro. Biomol Concepts 2013;4(5):501–18. Doi: 10.1515/bmc-2013-0016.

66. Lyons TJ. Glycation and oxidation: A role in the pathogenesis of atherosclerosis. Am J Cardiol 1993;71(6):B26–31. Doi: 10.1016/0002-9149(93)90142-Y.

67. Ling W., Lougheed M., Suzuki H., Buchan A., Kodama T., Steinbrecher UP. Oxidized or acetylated low density lipoproteins are rapidly cleared by the liver in mice with disruption of the scavenger receptor class A type I/II gene. Journal of Clinical Investigation 1997;100(2):244–52. Doi: 10.1172/JCI119528.

68. Li M., Qian M., Kyler K., Xu J. Endothelial–Vascular Smooth Muscle Cells Interactions in Atherosclerosis. Front Cardiovasc Med 2018. Doi: 10.3389/fcvm.2018.00151.

69. Berrou E., Breton M., Deudon E., Picard J. Effect of endothelial-cell-conditioned medium on proteoglycan synthesis in cultured smooth muscle cells from pig aorta. J Cell Physiol 1988;137(3):430–8. Doi: 10.1002/jcp.1041370306.

70. Sitia S., Tomasoni L., Atzeni F., et al. From endothelial dysfunction to atherosclerosis. Autoimmun Rev 2010:830–4. Doi: 10.1016/j.autrev.2010.07.016.

71. Davignon J., Ganz P. Role of endothelial dysfunction in atherosclerosis. Circulation 2004. Doi: 10.1161/01.CIR.0000131515.03336.f8.

72. Sluiter TJ., van Buul JD., Huveneers S., Quax PHA., de Vries MR. Endothelial barrier function and leukocyte transmigration in atherosclerosis. Biomedicines 2021;9(4). Doi: 10.3390/BIOMEDICINES9040328.

73. Sheppard D. Endothelial integrins and angiogenesis: not so simple anymore. Journal of Clinical Investigation 2002;110(7):913–4. Doi: 10.1172/jci16713.

74. Vanhoutte PM. Endothelial dysfunction - The first step toward coronary arteriosclerosis. Circulation Journal 2009;73(4):595–601. Doi: 10.1253/circj.CJ-08-1169.

75. Lomonaco MB., Lowenstein CJ., Ave E. Enhanced assay of endothelial exocytosis using extracellular matrix components. Anal Biochem 2014;452:19–24. Doi: 10.1016/j.ab.2014.02.015.

76. Straub AC., Lohman AW., Billaud M., et al. Endothelial cell expression of haemoglobin α regulates nitric oxide signalling. Nature 2012;491(7424):473–7. Doi: 10.1038/nature11626.

77. Olson TS., Ley K. Chemokines and chemokine receptors in leukocyte trafficking. American Journal of Physiology-Regulatory, Integrative and Comparative Physiology 2002;283(1):R7–28. Doi: 10.1152/ajpregu.00738.2001.

78. Gerhardt T., Ley K. Monocyte trafficking across the vessel wall. Cardiovasc Res 2015;107(3):321–30. Doi: 10.1093/cvr/cvv147.

79. Ley K., Laudanna C., Cybulsky MI., Nourshargh S. Getting to the site of inflammation: the leukocyte adhesion cascade updated. Nat Rev Immunol 2007;7(9):678–89. Doi: 10.1038/nri2156.

80. Ramos CL., Huo Y., Jung U., et al. Direct Demonstration of P-Selectin– and VCAM-1–Dependent Mononuclear Cell Rolling in Early Atherosclerotic Lesions of Apolipoprotein E–Deficient Mice. Circ Res 1999;84(11):1237–44. Doi: 10.1161/01.RES.84.11.1237.

81. Blankenberg S., Barbaux S., Tiret L. Adhesion molecules and atherosclerosis. Atherosclerosis 2003;170:191–203. Doi: 10.1016/S0021-9150(03)00097-2.

82. Tavares JC., Muscará MN. Adhesion Molecules and Endothelium. Endothelium and Cardiovascular Diseases: Vascular Biology and Clinical Syndromes 2018:189–201. Doi: 10.1016/B978-0-12-812348-5.00014-3.

83. Galkina E., Ley K. Vascular Adhesion Molecules in Atherosclerosis. Arterioscler Thromb Vasc Biol 2007;27(11):2292–301. Doi: 10.1161/ATVBAHA.107.149179.

84. Galkina E., Ley K. Immune and Inflammatory Mechanisms of Atherosclerosis. Annu Rev Immunol 2009. Doi: 10.1146/annurev.immunol.021908.132620.

85. Amengual J., Barrett TJ. Monocytes and macrophages in atherogenesis. Curr Opin Lipidol 2019;30(5):401–8. Doi: 10.1097/MOL.0000000000000634.

86. Fuhrman B., Partoush A., Volkova N., Aviram M. Ox-LDL induces monocyte-to-macrophage differentiation in vivo: Possible role for the macrophage colony stimulating factor receptor (M-CSF-R). Atherosclerosis 2008;196(2):598–607. Doi: 10.1016/j.atherosclerosis.2007.06.026.

87. Wang M., Subramanian M., Abramowicz S., et al. Interleukin-3/granulocyte macrophage colony-stimulating factor receptor promotes stem cell expansion, monocytosis, and atheroma macrophage burden in mice with hematopoietic ApoE deficiency. Arterioscler Thromb Vasc Biol 2014;34(5):976–84. Doi: 10.1161/ATVBAHA.113.303097.

88. Remmerie A., Scott CL. Macrophages and lipid metabolism. Cell Immunol 2018. Doi: 10.1016/j.cellimm.2018.01.020.

89. Flynn MC., Pernes G., Lee MKS., Nagareddy PR., Murphy AJ. Monocytes, macrophages, and metabolic disease in atherosclerosis. Front Pharmacol 2019. Doi: 10.3389/fphar.2019.00666.

90. Moore KJ., Sheedy FJ., Fisher EA. Macrophages in atherosclerosis: a dynamic balance. Nat Rev Immunol 2013;13(10):709–21. Doi: 10.1038/nri3520.

91. Rodrigues A., Burke MF., Jafri K., et al. Cholesterol Efflux Capacity, High-Density Lipoprotein Function, and Atherosclerosis 2011:127–35.

92. Baumer Y., McCurdy S., Weatherby TM., et al. Hyperlipidemia-induced cholesterol crystal production by endothelial cells promotes atherogenesis. Nat Commun 2017;8(1). Doi: 10.1038/s41467-017-01186-z.

93. Niyonzima N., Bakke SS., Gregersen I., et al. Cholesterol crystals use complement to increase NLRP3 signaling pathways in coronary and carotid atherosclerosis. EBioMedicine n.d. Doi: 10.1016/j.ebiom.2020.102985.

94. Hovland A., Jonasson L., Garred P., et al. The complement system and toll-like receptors as integrated players in the pathophysiology of atherosclerosis. Atherosclerosis 2015;241(2):480–94. Doi: 10.1016/j.atherosclerosis.2015.05.038.

95. Stewart CR., Stuart LM., Wilkinson K., et al. CD36 ligands promote sterile inflammation through assembly of a Toll-like receptor 4 and 6 heterodimer. Nat Immunol 2010;11(2):155–61. Doi: 10.1038/ni.1836.

96. Xu XH., Shah PK., Faure E., et al. Toll-Like Receptor-4 Is Expressed by Macrophages in Murine and Human Lipid-Rich Atherosclerotic Plaques and Upregulated by Oxidized LDL. Circulation 2001;104(25):3103–8. Doi: 10.1161/HC5001.100631.

97. de Winther MPJ., Kanters E., Kraal G., Hofker MH. Nuclear factor κB signaling in atherogenesis. Arterioscler Thromb Vasc Biol 2005;25(5):904–14. Doi: 10.1161/01.ATV.0000160340.72641.87.

98. Grootaert MOJ., Bennett MR. Vascular smooth muscle cells in atherosclerosis: Time for a re-assessment. Cardiovasc Res 2021:2326–39. Doi: 10.1093/cvr/cvab046.

99. Basatemur GL., Jørgensen HF., Clarke MCH., Bennett MR., Mallat Z. Vascular smooth muscle cells in atherosclerosis. Nat Rev Cardiol 2019;16(12):727–44. Doi: 10.1038/s41569-019-0227-9.

100. Aoyama T., Chen M., Fujiwara H., Masaki T., Sawamura T. LOX-1 mediates lysophosphatidylcholine-induced oxidized LDL uptake in smooth muscle cells. FEBS Lett 2000;467(2–3):217–20. Doi: 10.1016/S0014-5793(00)01154-6.

101. Mietus-Snyder M., Gowri MS., Pitas RE. Class A Scavenger Receptor Up-regulation in Smooth Muscle Cells by Oxidized Low Density Lipoprotein. Journal of Biological Chemistry 2000;275(23):17661–70. Doi: 10.1074/jbc.275.23.17661.

102. Li Y., Zhu H., Zhang Q., et al. Smooth muscle-derived macrophage-like cells contribute to multiple cell lineages in the atherosclerotic plaque. Cell Discov 2021. Doi: 10.1038/s41421-021-00328-4.

103. Puri R., Nissen SE., Ballantyne CM., et al. Factors underlying regression of coronary atheroma with potent statin therapy. Eur Heart J 2013;34(24):1818–25. Doi: 10.1093/eurheartj/eht084.

104. Khera A v., Cuchel M., de la Llera-Moya M., et al. Cholesterol Efflux Capacity, High-Density Lipoprotein Function, and Atherosclerosis. New England Journal of Medicine 2011;364(2):127–35. Doi: 10.1056/NEJMoa1001689.

105. Allahverdian S., Chaabane C., Boukais K., Francis GA., Bochaton-Piallat M-L. Smooth muscle cell fate and plasticity in atherosclerosis. Cardiovasc Res 2018;114(4):540–50. Doi: 10.1093/cvr/cvy022.

106. Chou EL., Lino Cardenas CL., Chaffin M., et al. Vascular smooth muscle cell phenotype switching in carotid atherosclerosis. JVS Vasc Sci 2022;3:41–7. Doi: 10.1016/j.jvssci.2021.11.002.

107. Yurdagul A. Crosstalk Between Macrophages and Vascular Smooth Muscle Cells in Atherosclerotic Plaque Stability. Arterioscler Thromb Vasc Biol 2022:ATVBAHA121316233. Doi: 10.1161/ATVBAHA.121.316233.

108. Doran AC., Meller N., McNamara CA. Role of smooth muscle cells in the initiation and early progression of atherosclerosis. Arterioscler Thromb Vasc Biol 2008;28(5):812–9. Doi: 10.1161/ATVBAHA.107.159327.

109. Stiko-Rahm A., Hultgårdh-Nilsson A., Regnström J., Hamsten A., Nilsson J. Native and oxidized LDL enhances production of PDGF AA and the surface expression of PDGF receptors in cultured human smooth muscle cells. Arterioscler Thromb 1992;12(9):1099–109. Doi: 10.1161/01.ATV.12.9.1099.

110. Forsyth EA., Aly HM., Neville RF., Sidawy AN. Proliferation and extracellular matrix production by human infragenicular smooth muscle cells in response to interleukin-1β. J Vasc Surg 1997;26(6):1002–8. Doi: 10.1016/S0741-5214(97)70013-2.

111. Raines EW., Dower SK., Ross R. Interleukin-1 Mitogenic Activity for Fibroblasts and Smooth Muscle Cells Is Due to PDGF-AA. Science (1979) 1989;243(4889):393–6. Doi: 10.1126/science.2783498.

112. Badimon L., Padró T., Vilahur G. Atherosclerosis, platelets and thrombosis in acute ischaemic heart disease. Eur Heart J Acute Cardiovasc Care 2012;1(1):60–74. Doi: 10.1177/2048872612441582.

113. Shen C-M., Mao SJT., Huang GS., Yang P-C., Chu R-M. Stimulation of smooth muscle cell proliferation by ox-LDL- and acetyl LDL-induced macrophage-derived foam cells. Life Sci 2001;70(4):443–52. Doi: 10.1016/S0024-3205(01)01428-X.

114. Li Z-Y., Howarth SPS., Tang T., Gillard JH. How Critical Is Fibrous Cap Thickness to Carotid Plaque Stability? Stroke 2006;37(5):1195–9. Doi: 10.1161/01.STR.0000217331.61083.3b.

115. Motoyama S., Sarai M., Harigaya H., et al. Computed Tomographic Angiography Characteristics of Atherosclerotic Plaques Subsequently Resulting in Acute Coronary Syndrome. J Am Coll Cardiol 2009;54(1):49–57. Doi: 10.1016/j.jacc.2009.02.068.

116. Thim T., Hagensen MK., Bentzon JF., Falk E. From vulnerable plaque to atherothrombosis. J Intern Med 2008;263(5):506–16. Doi: 10.1111/j.1365-2796.2008.01947.x.

117. Gonzalez L., Trigatti BL. Macrophage Apoptosis and Necrotic Core Development in Atherosclerosis: A Rapidly Advancing Field with Clinical Relevance to Imaging and Therapy. Canadian Journal of Cardiology 2017:303–12. Doi: 10.1016/j.cjca.2016.12.010.

118. Cabrera JTO., Makino A. Efferocytosis of vascular cells in cardiovascular disease. Pharmacol Ther 2022;229:107919. Doi: 10.1016/j.pharmthera.2021.107919.

119. Schrijvers DM., de Meyer GRY., Herman AG., Martinet W. Phagocytosis in atherosclerosis: Molecular mechanisms and implications for plaque progression and stability. Cardiovasc Res 2007:470–80. Doi: 10.1016/j.cardiores.2006.09.005.

120. Shaw PX., Hörkkö S., Tsimikas S., et al. Human-Derived Anti-Oxidized LDL Autoantibody Blocks Uptake of Oxidized LDL by Macrophages and Localizes to

Atherosclerotic Lesions In Vivo. Arterioscler Thromb Vasc Biol 2001;21(8):1333–9. Doi: 10.1161/hq0801.093587.

121. Schrijvers DM., de Meyer GRY., Kockx MM., Herman AG., Martinet W. Phagocytosis of apoptotic cells by macrophages is impaired in atherosclerosis. Arterioscler Thromb Vasc Biol 2005;25(6):1256–61. Doi: 10.1161/01.ATV.0000166517.18801.a7.

122. Mulay SR., Anders H-J. Crystallopathies. New England Journal of Medicine 2016;374(25):2465–76. Doi: 10.1056/NEJMra1601611.

123. Nidorf SM., Fiolet A., Abela GS. Viewing atherosclerosis through a crystal lens: How the evolving structure of cholesterol crystals in atherosclerotic plaque alters its stability. J Clin Lipidol 2020;14(5):619–30. Doi: 10.1016/j.jacl.2020.07.003.

124. Pugliese G., Iacobini C., Fantauzzi CB., Menini S. The dark and bright side of atherosclerotic calcification. Atherosclerosis 2015;238(2):220–30. Doi: 10.1016/j.atherosclerosis.2014.12.011.

125. Lomashvili KA. Phosphate-Induced Vascular Calcification: Role of Pyrophosphate and Osteopontin. Journal of the American Society of Nephrology 2004;15(6):1392–401. Doi: 10.1097/01.ASN.0000128955.83129.9C.

126. Shanahan CM. Inflammation Ushers in Calcification. Circulation 2007;116(24):2782–5. Doi: 10.1161/CIRCULATIONAHA.107.749655.

127. Canfield AE., Sutton AB., Hoyland JA., Schor AM. Association of thrombospondin-1 with osteogenic differentiation of retinal pericytes in vitro. J Cell Sci 1996;109(2):343–53. Doi: 10.1242/jcs.109.2.343.

128. Durham AL., Speer MY., Scatena M., Giachelli CM., Shanahan CM. Role of smooth muscle cells in vascular calcification: implications in atherosclerosis and arterial stiffness. Cardiovasc Res 2018;114(4):590–600. Doi: 10.1093/cvr/cvy010.

129. Nakahara T., Dweck MR., Narula N., Pisapia D., Narula J., Strauss HW. Coronary Artery Calcification. JACC Cardiovasc Imaging 2017;10(5):582–93. Doi: 10.1016/j.jcmg.2017.03.005.

130. Stefanadis C., Antoniou C., Tsiachris D., Pietri P. Coronary Atherosclerotic Vulnerable Plaque: Current Perspectives. J Am Heart Assoc 2017;6(3). Doi: 10.1161/JAHA.117.005543.

131. Grootaert MOJ., Moulis M., Roth L., et al. Vascular smooth muscle cell death, autophagy and senescence in atherosclerosis. Cardiovasc Res 2018;114(4):622–34. Doi: 10.1093/cvr/cvy007.

132. Weng X., Cheng X., Wu X., Xu H., Fang M., Xu Y. Sin3B mediates collagen type I gene repression by interferon gamma in vascular smooth muscle cells. Biochem Biophys Res Commun 2014;447(2):263–70. Doi: 10.1016/j.bbrc.2014.03.140.

133. Newby AC. Dual role of matrix metalloproteinases (matrixins) in intimal thickening and atherosclerotic plaque rupture. Physiol Rev 2005;85(1):1–31. Doi: 10.1152/physrev.00048.2003.

134. Galis ZS., Sukhova GK., Lark MW., Libby P. Increased expression of matrix metalloproteinases and matrix degrading activity in vulnerable regions of human atherosclerotic plaques. Journal of Clinical Investigation 1994;94(6):2493. Doi: 10.1172/JCI117619.

135. Jager NA., Vries BMW de., Hillebrands J., et al. Distribution of Matrix Metalloproteinases in Human Atherosclerotic Carotid Plaques and Their Production by Smooth Muscle Cells and Macrophage Subsets 2016;(September 2015):283–91. Doi: 10.1007/s11307-015-0882-0.

136. P Sarén, H G Welgus, P T Kovanen; TNF-alpha and IL-1beta selectively induce expression of 92-kDa gelatinase by human macrophages. J Immunol 1 November 1996; 157 (9): 4159–4165. Doi: https://doi.org/10.4049/jimmunol.157.9.4159

137. Slager C., Wentzel J., Gijsen F., et al. The role of shear stress in the destabilization of vulnerable plaques and related therapeutic implications. Nat Clin Pract Cardiovasc Med 2005;2(9):456–64. Doi: 10.1038/ncpcardio0298.

138. Lu Y., Cui X., Zhang L., et al. The Functional Role of Lipoproteins in Atherosclerosis: Novel Directions for Diagnosis and Targeting Therapy. Aging Dis 2022:491–520. Doi: 10.14336/AD.2021.0929.

139. Kolovou G., Kolovou V., Mavrogeni S. Lipidomics in vascular health: current perspectives. Vasc Health Risk Manag 2015:333. Doi: 10.2147/VHRM.S54874.

140. Sachdeva A., Cannon CP., Deedwania PC., et al. Lipid levels in patients hospitalized with coronary artery disease: An analysis of 136,905 hospitalizations in Get With The Guidelines. Am Heart J 2009;157(1). Doi: 10.1016/j.ahj.2008.08.010.

141. Zhou S., Jin J., Wang J., et al. miRNAS in cardiovascular diseases: potential biomarkers, therapeutic targets and challenges. Acta Pharmacol Sin 2018;39(7):1073–84. Doi: 10.1038/aps.2018.30.

142. Ibañez B., Badimon JJ., Garcia MJ. Diagnosis of Atherosclerosis by Imaging. American Journal of Medicine 2009;122(1 SUPPL.):S15–25. Doi: 10.1016/j.amjmed.2008.10.014.

143. Soeki T., Sata M. Inflammatory Biomarkers and Atherosclerosis. Int Heart J 2016;57(2):134–9. Doi: 10.1536/ihj.15-346.

144. Nikpay M., Goel A., Won HH., et al. A comprehensive 1000 Genomes-based genome-wide association meta-analysis of coronary artery disease. Nat Genet 2015;47(10):1121–30. Doi: 10.1038/ng.3396.

145. Cason CA., Dolan KT., Sharma G., et al. Plasma microbiome-modulated indole- and phenyl-derived metabolites associate with advanced atherosclerosis and postoperative outcomes. J Vasc Surg 2018;68:1552-1562.e7. Doi: 10.1016/j.jvs.2017.09.029.

146. Rahman MdM., Islam F., -Or-Rashid MdH., et al. The Gut Microbiota (Microbiome) in Cardiovascular Disease and Its Therapeutic Regulation. Front Cell Infect Microbiol 2022;12. Doi: 10.3389/fcimb.2022.903570.

147. Najam O., Ray KK. Familial Hypercholesterolemia: a Review of the Natural History, Diagnosis, and Management. Cardiol Ther 2015;4(1):25–38. Doi: 10.1007/s40119-015-0037-z.

148. Singh S., Bittner V. Familial Hypercholesterolemia—Epidemiology, Diagnosis, and Screening. Curr Atheroscler Rep 2015;17(2). Doi: 10.1007/s11883-014-0482-5.

149. Henderson R., O'Kane M., McGilligan V., Watterson S. The genetics and screening of familial hypercholesterolaemia. J Biomed Sci 2016;23(1):1–12. Doi: 10.1186/s12929-016-0256-1.

150. Brautbar A., Leary E., Rasmussen K., Wilson DP., Steiner RD., Virani S. Genetics of Familial Hypercholesterolemia. Curr Atheroscler Rep 2015;17(4):20. Doi: 10.1007/s11883-015-0491-z.

151. Kaplan RC., Smith NL., Zucker S., Heckbert SR., Rice K., Psaty BM. Matrix metalloproteinase-3 (MMP3) and MMP9 genes and risk of myocardial infarction, ischemic stroke, and hemorrhagic stroke. Atherosclerosis 2008;201(1):130–7. Doi: 10.1016/j.atherosclerosis.2008.01.003.

152. Wang Q., Ding H., Tang JR., et al. C-reactive protein polymorphisms and genetic susceptibility to ischemic stroke and hemorrhagic stroke in the Chinese Han population. Acta Pharmacol Sin 2009;30(3):291–8. Doi: 10.1038/aps.2009.14.

153. Berezin A. Can C-reactive Protein Genetic Variants Identify Patients with Higher and Lower Cardiovascular Risk? J Clin Exp Cardiolog 2018;09(04):9–11. Doi: 10.4172/2155-9880.1000580.

154. Heidari MM., Khatami M., Hadadzadeh M., et al. Polymorphisms in NOS3, MTHFR, APOB and TNF-α Genes and Risk of Coronary Atherosclerotic Lesions in Iranian Patients. Res Cardiovasc Med 2015. Doi: 10.5812/cardiovascmed.29134.

155. Herrera-maya G., Vargas-alarcón G., Pérez-méndez O., et al. The Ser290Asn and thr715pro polymorphisms of the SELP gene are associated with a lower risk of developing acute coronary syndrome and low soluble p-selectin levels in a Mexican population‡. Biomolecules 2020;10(2). Doi: 10.3390/biom10020270.

156. Koenig W., Khuseyinova N., Baumert J., et al. Increased concentrations of C-reactive protein and IL-6 but not IL-18 are independently associated with incident coronary events in middle-aged men and women: Results from the MONICA/KORA Augsburg

case-cohort study, 1984-2002. Arterioscler Thromb Vasc Biol 2006;26(12):2745–51. Doi: 10.1161/01.ATV.0000248096.62495.73.

157. Tuomisto K., Jousilahti P., Sundvall J., Pajunen P., Salomaa V. C-reactive protein, interleukin-6 and tumor necrosis factor alpha as predictors of incident coronary and cardiovascular events and total mortality. Thromb Haemost 2006;95(03):511–8. Doi: 10.1160/TH05-08-0571.

158. Ridker PM., Rifai N., Stampfer MJ., Hennekens CH. Plasma concentration of interleukin-6 and the risk of future myocardial infarction among apparently healthy men. Circulation 2000;101(15):1767–72. Doi: 10.1161/01.CIR.101.15.1767.

159. Johnson BD., Kip KE., Marroquin OC., et al. Serum Amyloid A as a Predictor of Coronary Artery Disease and Cardiovascular Outcome in Women: The National Heart, Lung, and Blood Institute-Sponsored Women's Ischemia Syndrome Evaluation (WISE). Circulation 2004;109(6):726–32. Doi: 10.1161/01.CIR.0000115516.54550.B1.

160. Danesh J. Low grade inflammation and coronary heart disease: prospective study and updated meta-analyses. BMJ 2000;321(7255):199–204. Doi: 10.1136/bmj.321.7255.199.

161. Witting PK., Song C., Hsu K., et al. The acute-phase protein serum amyloid A induces endothelial dysfunction that is inhibited by high-density lipoprotein. Free Radic Biol Med 2011;51(7):1390–8. Doi: 10.1016/j.freeradbiomed.2011.06.031.

162. Thakore AH., Guo CY., Larson MG., et al. Association of Multiple Inflammatory Markers with Carotid Intimal Medial Thickness and Stenosis (from the Framingham

Heart Study). American Journal of Cardiology 2007;99(11):1598–602. Doi: 10.1016/j.amjcard.2007.01.036.

163. Rho YH., Chung CP., Oeser A., et al. Novel cardiovascular risk factors in premature coronary atherosclerosis associated with systemic lupus erythematosus. J Rheumatol 2008;35(9):1789–94.

164. dos Santos JL., de Quadros AS., Weschenfelder C., Garofallo SB., Marcadenti A. Oxidative Stress Biomarkers, Nut-Related Antioxidants, and Cardiovascular Disease. Nutrients 2020;12(3). Doi: 10.3390/NU12030682.

165. Singh U., Jialal I. Oxidative stress and atherosclerosis. Pathophysiology 2006;13(3):129–42. Doi: 10.1016/j.pathophys.2006.05.002.

166. Tangeten C., Boudjeltia KZ., Delporte C., van Antwerpen P., Korpak K. Unexpected Role of MPO-Oxidized LDLs in Atherosclerosis: In between Inflammation and Its Resolution. Antioxidants 2022. Doi: 10.3390/antiox11050874.

167. Baldus S., Heeschen C., Meinertz T., et al. Myeloperoxidase Serum Levels Predict Risk in Patients With Acute Coronary Syndromes. Circulation 2003;108(12):1440–5. Doi: 10.1161/01.CIR.0000090690.67322.51.

168. Brevetti G., Schiano V., Laurenzano E., et al. Myeloperoxidase, but not C-reactive protein, predicts cardiovascular risk in peripheral arterial disease. Eur Heart J 2007;29(2):224–30. Doi: 10.1093/eurheartj/ehm587.

169. Exner M., Minar E., Mlekusch W., et al. Myeloperoxidase Predicts Progression of Carotid Stenosis in States of Low High-Density Lipoprotein Cholesterol. J Am Coll Cardiol 2006;47(11):2212–8. Doi: 10.1016/j.jacc.2006.01.067.

170. Garvin P., Jonasson L., Nilsson L., Falk M., Kristenson M. Plasma Matrix Metalloproteinase-9 Levels Predict First-Time Coronary Heart Disease: An 8-Year Follow-Up of a Community-Based Middle-Aged Population. PLoS One 2015;10(9):e0138290. Doi: 10.1371/journal.pone.0138290.

171. Blankenberg S., Rupprecht HJ., Poirier O., et al. Plasma Concentrations and Genetic Variation of Matrix Metalloproteinase 9 and Prognosis of Patients With Cardiovascular Disease. Circulation 2003;107(12):1579–85. Doi: 10.1161/01.CIR.0000058700.41738.12.

172. ORBE J., MONTERO I., RODRÍGUEZ JA., BELOQUI O., RONCAL C., PÁRAMO JA. Independent association of matrix metalloproteinase-10, cardiovascular risk factors and subclinical atherosclerosis. Journal of Thrombosis and Haemostasis 2007;5(1):91–7. Doi: 10.1111/j.1538-7836.2006.02276.x.

173. Wu TC., Leu HB., Lin WT., Lin CP., Lin SJ., Chen JW. Plasma matrix metalloproteinase-3 level is an independent prognostic factor in stable coronary artery disease. Eur J Clin Invest 2005;35(9):537–45. Doi: 10.1111/j.1365-2362.2005.01548.x.

174. Vickers KC., Palmisano BT., Shoucri BM., Shamburek RD., Remaley AT. MicroRNAs are transported in plasma and delivered to recipient cells by high-density lipoproteins. Nat Cell Biol 2011;13(4):423–33. Doi: 10.1038/ncb2210.

175. de Gonzalo-Calvo D., Cenarro A., Garlaschelli K., et al. Translating the microRNA signature of microvesicles derived from human coronary artery smooth muscle cells in patients with familial hypercholesterolemia and coronary artery disease. J Mol Cell Cardiol 2017;106:55–67. Doi: 10.1016/j.yjmcc.2017.03.005.

176. O'Brien J., Hayder H., Zayed Y., Peng C. Overview of microRNA biogenesis, mechanisms of actions, and circulation. Front Endocrinol (Lausanne) 2018:402. Doi: 10.3389/fendo.2018.00402.

177. Salinas J., Lin H., Aparico HJ., et al. Whole blood microRNA expression associated with stroke: Results from the Framingham Heart Study. PLoS One 2019;14(8). Doi: 10.1371/journal.pone.0219261.

178. Jia QW., Chen ZH., Ding XQ., et al. Predictive Effects of Circulating miR-221, miR-130a and miR-155 for Coronary Heart Disease: A Multi-Ethnic Study in China. Cellular Physiology and Biochemistry 2017;42(2):808–23. Doi: 10.1159/000478071.

179. Yilmaz SG., Isbir S., Kunt AT., Isbir T. Circulating microRNAs as novel biomarkers for atherosclerosis. In Vivo 2018;32(3):561–5. Doi: 10.21873/invivo.11276.

180. Li T., Cao H., Zhuang J., et al. Identification of miR-130a, miR-27b and miR-210 as serum biomarkers for atherosclerosis obliterans. Clinica Chimica Acta 2011;412(1–2):66–70. Doi: 10.1016/j.cca.2010.09.029.

181. Fichtlscherer S., de Rosa S., Fox H., et al. Circulating MicroRNAs in Patients With Coronary Artery Disease. Circ Res 2010;107(5):677–84. Doi: 10.1161/CIRCRESAHA.109.215566.

182. Cipollone F., Felicioni L., Sarzani R., et al. A Unique MicroRNA Signature Associated With Plaque Instability in Humans. Stroke 2011;42(9):2556–63. Doi: 10.1161/STROKEAHA.110.597575.

183. Eken SM., Jin H., Chernogubova E., et al. MicroRNA-210 Enhances Fibrous Cap Stability in Advanced Atherosclerotic Lesions. Circ Res 2017;120(4):633–44. Doi: 10.1161/CIRCRESAHA.116.309318.

184. Vogel B., Keller A., Frese KS., et al. Refining Diagnostic MicroRNA Signatures by Whole-miRNome Kinetic Analysis in Acute Myocardial Infarction. Clin Chem 2013;59(2):410–8. Doi: 10.1373/clinchem.2011.181370.

185. Vogel B., Keller A., Frese KS., et al. Refining Diagnostic MicroRNA Signatures by Whole-miRNome Kinetic Analysis in Acute Myocardial Infarction. Clin Chem 2013;59(2):410–8. Doi: 10.1373/clinchem.2011.181370.

186. Zhao J., Yu H., Yan P., Zhou X., Wang Y., Yao Y. Circulating MicroRNA-499 as a Diagnostic Biomarker for Acute Myocardial Infarction: A Meta-analysis. Dis Markers 2019;2019:1–10. Doi: 10.1155/2019/6121696.

187. Pereira-da-Silva T., Coutinho Cruz M., Carrusca C., Cruz Ferreira R., Napoleão P., Mota Carmo M. Circulating microRNA profiles in different arterial territories of stable atherosclerotic disease: a systematic review. Am J Cardiovasc Dis 2018;8(1):1–13.

188. Uchida Y., Shimoyama E., Hiruta N., Tabata T. Detection of early stage of human coronary atherosclerosis by angioscopic imaging of collagen subtypes. J Cardiol 2021;77(5):452–6. Doi: 10.1016/j.jjcc.2020.09.011.

189. Tang WHW., Kitai T., Hazen SL. Gut Microbiota in Cardiovascular Health and Disease. Circ Res 2017;120(7):1183–96. Doi: 10.1161/CIRCRESAHA.117.309715.

190. Wu CD (jhy., Editor S. Role of Gut Microbiota-Generated Short-Chain Fatty Acids in Metabolic and Cardiovascular Health n.d. Doi: 10.1007/s13668-018-0248-8.

191. Wang Z., Klipfell E., Bennett BJ., et al. Gut flora metabolism of phosphatidylcholine promotes cardiovascular disease. Nature 2011;472(7341):57–63. Doi: 10.1038/nature09922.

192. Reigstad CS., Lundén GÖ., Felin J., Bäckhed F. Regulation of serum amyloid A3 (SAA3) in mouse colonic epithelium and adipose tissue by the intestinal microbiota. PLoS One 2009;4(6). Doi: 10.1371/JOURNAL.PONE.0005842.

193. Garshick MS., Nikain C., Tawil M., et al. Reshaping of the gastrointestinal microbiome alters atherosclerotic plaque inflammation resolution in mice. Sci Rep 2021;11(1):8966. Doi: 10.1038/s41598-021-88479-y.

194. Fang H., Pengal RA., Cao X., et al. Lipopolysaccharide-Induced Macrophage Inflammatory Response Is Regulated by SHIP. The Journal of Immunology 2004;173(1):360–6. Doi: 10.4049/jimmunol.173.1.360.

195. Kenny DJ., Plichta DR., Shungin D., et al. Cholesterol Metabolism by Uncultured Human Gut Bacteria Influences Host Cholesterol Level. Cell Host Microbe 2020;28(2):245-257.e6. Doi: 10.1016/j.chom.2020.05.013.

196. le Roy T., Lécuyer E., Chassaing B., et al. The intestinal microbiota regulates host cholesterol homeostasis. BMC Biol 2019;17(1). Doi: 10.1186/s12915-019-0715-8.

197. Wang D., Xia M., Yan X., et al. Gut Microbiota Metabolism of Anthocyanin Promotes Reverse Cholesterol Transport in Mice Via Repressing miRNA-10b. Circ Res 2012;111(8):967–81. Doi: 10.1161/CIRCRESAHA.112.266502.

198. Serra E Silva Filho W., Casarin RCV., Nicolela EL., Passos HM., Sallum AW., Gonçalves RB. Microbial diversity similarities in periodontal pockets and atheromatous plaques of cardiovascular disease patients. PLoS One 2014;9(10). Doi: 10.1371/journal.pone.0109761.

199. Chhibber-Goel J., Singhal V., Bhowmik D., et al. Linkages between oral commensal bacteria and atherosclerotic plaques in coronary artery disease patients. NPJ Biofilms Microbiomes 2016;2(1):7. Doi: 10.1038/s41522-016-0009-7.

200. Amar J., Lelouvier B., Servant F., et al. Blood Microbiota Modification After Myocardial Infarction Depends Upon Low-Density Lipoprotein Cholesterol Levels. J Am Heart Assoc 2019;8(19). Doi: 10.1161/JAHA.118.011797.

201. Sawicka-smiarowska E., Bondarczuk K., Bauer W., et al. Gut microbiome in chronic coronary syndrome patients. J Clin Med 2021;10(21). Doi: 10.3390/jcm10215074.

202. Matsumoto T., Kojima M., Takayanagi K., Taguchi K., Kobayashi T. Role of S-Equol, Indoxyl Sulfate, and Trimethylamine N-Oxide on Vascular Function. Am J Hypertens 2020;33(9):793–803. Doi: 10.1093/ajh/hpaa053.

203. Kolluru GK., Kevil CG. It's a "Gut Feeling": Association of Microbiota, Trimethylamine N-Oxide and Cardiovascular Outcomes. J Am Heart Assoc 2020;9(10). Doi: 10.1161/JAHA.120.016553.

204. Velmurugan G., Dinakaran V., Rajendhran J., Swaminathan K. Blood Microbiota and Circulating Microbial Metabolites in Diabetes and Cardiovascular Disease. Trends in Endocrinology and Metabolism 2020:835–47. Doi: 10.1016/j.tem.2020.01.013.

205. Nemet I., Saha PP., Gupta N., et al. A Cardiovascular Disease-Linked Gut Microbial Metabolite Acts via Adrenergic Receptors. Cell 2020;180(5):862-877.e22. Doi: 10.1016/j.cell.2020.02.016.

206. Tarkin JM., Dweck MR., Evans NR., et al. Imaging Atherosclerosis. Circ Res 2016;118(4):750–69. Doi: 10.1161/CIRCRESAHA.115.306247.

207. Takx RAP., Partovi S., Ghoshhajra BB. Imaging of atherosclerosis. Int J Cardiovasc Imaging 2016;32(1):5–12. Doi: 10.1007/s10554-015-0730-y.

208. Nasir K., Clouse M. Role of Nonenhanced Multidetector CT Coronary Artery Calcium Testing in Asymptomatic and Symptomatic Individuals. Radiology 2012;264(3):637–49. Doi: 10.1148/radiol.12110810.

209. Wildgruber M., Swirski FK., Zernecke A. Molecular imaging of inflammation in atherosclerosis. Theranostics 2013;3(11):865–84. Doi: 10.7150/thno.5771.

210. Sarwar A., Shaw LJ., Shapiro MD., et al. Diagnostic and Prognostic Value of Absence of Coronary Artery Calcification. JACC Cardiovasc Imaging 2009;2(6):675–88. Doi: 10.1016/j.jcmg.2008.12.031.

211. Greenland P., Bonow RO., Brundage BH., et al. ACCF/AHA 2007 Clinical Expert Consensus Document on Coronary Artery Calcium Scoring By Computed Tomography in Global Cardiovascular Risk Assessment and in Evaluation of Patients With Chest Pain. A Report of the American College of Cardiology Foundation Clinical Expert Consensus Task Force (ACCF/AHA Writing Committee to Update the 2000 Expert Consensus Document on Electron Beam Computed Tomography). J Am Coll Cardiol 2007:378–402. Doi: 10.1016/j.jacc.2006.10.001.

212. Chambless LE., Heiss G., Folsom AR., et al. Association of Coronary Heart Disease Incidence with Carotid Arterial Wall Thickness and Major Risk Factors: The Atherosclerosis Risk in Communities (ARIC) Study, 1987-1993. Am J Epidemiol 1997;146(6):483–94. Doi: 10.1093/oxfordjournals.aje.a009302.

213. Lorenz MW., Markus HS., Bots ML., Rosvall M., Sitzer M. Prediction of Clinical Cardiovascular Events With Carotid Intima-Media Thickness. Circulation 2007;115(4):459–67. Doi: 10.1161/CIRCULATIONAHA.106.628875.

214. Fernández-Alvarez V., Linares Sánchez M., López Alvarez F., et al. Evaluation of Intima-Media Thickness and Arterial Stiffness as Early Ultrasound Biomarkers of Carotid Artery Atherosclerosis. Cardiol Ther 2022;11(2):231–47. Doi: 10.1007/s40119-022-00261-x.

215. Lorenz MW., Polak JF., Kavousi M., et al. Carotid intima-media thickness progression to predict cardiovascular events in the general population (the PROG-IMT collaborative project): a meta-analysis of individual participant data. The Lancet 2012;379(9831):2053–62. Doi: 10.1016/S0140-6736(12)60441-3.

216. Nezu T., Hosomi N., Aoki S., Matsumoto M. Carotid Intima-Media Thickness for Atherosclerosis. J Atheroscler Thromb 2016;23(1):18–31. Doi: 10.5551/jat.31989.

217. Segers P., Rietzschel ER., Chirinos JA. How to Measure Arterial Stiffness in Humans. Arterioscler Thromb Vasc Biol 2020;40:1034–43. Doi: 10.1161/ATVBAHA.119.313132.

218. Palombo C., Kozakova M. Arterial stiffness, atherosclerosis and cardiovascular risk: Pathophysiologic mechanisms and emerging clinical indications. Vasc Pharm 2016, 1-7, 77. Doi: 10.1016/j.vph.2015.05.012.

219. Oberoi S., Schoepf UJ., Meyer M., et al. Progression of arterial stiffness and coronary atherosclerosis: Longitudinal evaluation by cardiac CT. American Journal of Roentgenology 2013;200(4):798–804. Doi: 10.2214/AJR.12.8653.

220. Zureik M., Bureau JM., Temmar M., et al. Echogenic carotid plaques are associated with aortic arterial stiffness in subjects with subclinical carotid atherosclerosis. Hypertension 2003;41(3 I):519–27. Doi: 10.1161/01.HYP.0000054978.86286.92.

221. Tsao CW., Pencina KM., Massaro JM., et al. Cross-sectional relations of arterial stiffness, pressure pulsatility, wave reflection, and arterial calcification. Arterioscler Thromb Vasc Biol 2014;34(11):2495–500. Doi: 10.1161/ATVBAHA.114.303916.

222. van Popele NM., Grobbee DE., Bots ML., et al. Association Between Arterial Stiffness and Atherosclerosis. Stroke 2001;32(2):454–60. Doi: 10.1161/01.STR.32.2.454.

223. Zhao Y., Qu H., Wang Y., Xiao W., Zhang Y., Shi D. Small rodent models of atherosclerosis. Biomedicine and Pharmacotherapy 2020;129(April):110426. Doi: 10.1016/j.biopha.2020.110426.

224. Getz GS., Reardon CA. Animal Models of Atherosclerosis. Arterioscler Thromb Vasc Biol 2012;32(5):1104–15. Doi: 10.1161/ATVBAHA.111.237693.

225. Xu S., Weng J. Familial Hypercholesterolemia and Atherosclerosis: Animal Models and Therapeutic Advances. Trends in Endocrinology and Metabolism 2020;31(5):331–3. Doi: 10.1016/j.tem.2020.02.007.

226. Getz GS., Reardon CA. Animal models of Atherosclerosis. Arterioscler Thromb Vasc Biol 2012;32(5):1104–15. Doi: 10.1161/ATVBAHA.111.237693.

227. Emini Veseli B., Perrotta P., de Meyer GRA., et al. Animal models of atherosclerosis. Eur J Pharmacol 2017;816(December 2016):3–13. Doi: 10.1016/j.ejphar.2017.05.010.

228. Plump AS., Smith JD., Hayek T., et al. Severe hypercholesterolemia and atherosclerosis in apolipoprotein E-deficient mice created by homologous

recombination in ES cells. Cell 1992;71(2):343–53. Doi: 10.1016/0092-8674(92)90362-G.

229. Plump AS., Lum PY. Genomics and Cardiovascular Drug Development. J Am Coll Cardiol 2009;53(13):1089–100. Doi: 10.1016/j.jacc.2008.11.050.

230. Smith JD., Breslow JL. The emergence of mouse models of atherosclerosis and their relevance to clinical research. J Intern Med 1997;242(2):99–109. Doi: 10.1046/j.1365-2796.1997.00197.x.

231. Ishibashi S., Goldstein JL., Brown MS., Herz J., Burns DK. Massive xanthomatosis and atherosclerosis in cholesterol-fed low density lipoprotein receptor-negative mice. Journal of Clinical Investigation 1994;93(5):1885–93. Doi: 10.1172/JCI117179.

232. WATANABE Y. Serial inbreeding of rabbits with hereditary hyperlipidemia (WHHL-rabbit)-Incidence and development of atherosclerosis and xanthoma. Atherosclerosis 1980;36(2):261–8. Doi: 10.1016/0021-9150(80)90234-8.

233. Fan J., Kitajima S., Watanabe T., et al. Rabbit models for the study of human atherosclerosis: From pathophysiological mechanisms to translational medicine. Pharmacol Ther 2015;146:104–19. Doi: 10.1016/j.pharmthera.2014.09.009.

234. Baumgartner C., Brandl J., Münch G., Ungerer M. Rabbit models to study atherosclerosis and its complications – Transgenic vascular protein expression in vivo. Prog Biophys Mol Biol 2016;121(2):131–41. Doi: 10.1016/j.pbiomolbio.2016.05.001.

235. Niimi M., Yang D., Kitajima S., et al. ApoE knockout rabbits: A novel model for the study of human hyperlipidemia. Atherosclerosis 2016;245:187–93. Doi: 10.1016/j.atherosclerosis.2015.12.002.

236. Cefalu WT., Wagner JD. Aging and atherosclerosis in human and nonhuman primates. Age (Omaha) 1997;20(1):15–28. Doi: 10.1007/s11357-997-0002-4.

237. de Nisco G., Chiastra C., Hartman EMJ., et al. Comparison of Swine and Human Computational Hemodynamics Models for the Study of Coronary Atherosclerosis. Front Bioeng Biotechnol 2021;9. Doi: 10.3389/fbioe.2021.731924.

238. Wang D., Xu X., Zhao M., Wang X. Accelerated miniature swine models of advanced atherosclerosis: A review based on morphology. Cardiovascular Pathology 2020;49:107241. Doi: 10.1016/j.carpath.2020.107241.

239. Ishii A., Viñuela F., Murayama Y., et al. Swine model of carotid artery atherosclerosis: experimental induction by surgical partial ligation and dietary hypercholesterolemia. AJNR Am J Neuroradiol 2006;27(9):1893–9.

240. Shi ZS., Feng L., He X., et al. Vulnerable plaque in a swine model of carotid atherosclerosis. American Journal of Neuroradiology 2009;30(3):469–72. Doi: 10.3174/ajnr.A1410.

241. Schomberg DT., Tellez A., Meudt JJ., et al. Miniature Swine for Preclinical Modeling of Complexities of Human Disease for Translational Scientific Discovery and Accelerated Development of Therapies and Medical Devices. Toxicol Pathol 2016;44(3):299–314. Doi: 10.1177/0192623315618292.

242. Miranpuri GS., Schomberg DT., Singh K., Shanmuganayagam D. Reproducible infusions into the Wisconsin Miniature Swine™ spinal cord: A platform for development of therapy delivery devices. Research Article Medical Research and Innovations Med Res Innov 2018;2(3):1–4. Doi: 10.15761/MRI.1000145.

243. Granada JF., Milewski K., Zhao H., et al. Vascular response to zotarolimus-coated balloons in injured superficial femoral arteries of the familial hypercholesterolemic swine. Circ Cardiovasc Interv 2011;4(5):447–55. Doi: 10.1161/CIRCINTERVENTIONS.110.960260.

244. Tellez A., Seifert PS., Donskoy E., et al. Experimental evaluation of efficacy and healing response of everolimus-eluting stents in the familial hypercholesterolemic swine model: A comparative study of bioabsorbable versus durable polymer stent platforms. Coron Artery Dis 2014;25(3):198–207. Doi: 10.1097/MCA.0000000000000099.

245. Schinkel AFL., Krueger CG., Tellez A., et al. Contrast-enhanced ultrasound for imaging vasa vasorum: comparison with histopathology in a swine model of atherosclerosis. European Journal of Echocardiography 2010;11(8):659–64. Doi: 10.1093/ejechocard/jeq048.

246. Hasler-Rapacz J., Ellegren H., Fridolfsson A-K., et al. Identification of a Mutation in the Low Density Lipoprotein Receptor Gene Associated With Recessive Familial Hypercholesterolemia in Swine. J Med Genet 1998;76(June 1997):379–86. Doi: 10.1002/(SICI)1096-8628(19980413)76:53.0.CO;2-I.

247. Al-Mashhadi RH., Sørensen CB., Kragh PM., et al. Familial Hypercholesterolemia and Atherosclerosis in Cloned Minipigs Created by DNA Transposition of a Human *PCSK9* Gain-of-Function Mutant. Sci Transl Med 2013;5(166). Doi: 10.1126/scitranslmed.3004853.

248. Matthan NR., Solano-Aguilar G., Meng H., et al. The Ossabaw Pig Is a Suitable Translational Model to Evaluate Dietary Patterns and Coronary Artery Disease Risk. J Nutr 2018;148(4):542–51. Doi: 10.1093/jn/nxy002.

249. Yuan F., Guo L., Park K., et al. Ossabaw Pigs With a PCSK9 Gain-of-Function Mutation Develop Accelerated Coronary Atherosclerotic Lesions: A Novel Model for Preclinical Studies. J Am Heart Assoc 2018;7(6). Doi: 10.1161/JAHA.117.006207.

250. Hong SN., Gona P., Fontes JD., et al. Atherosclerotic biomarkers and aortic atherosclerosis by cardiovascular magnetic resonance imaging in the Framingham Heart Study. J Am Heart Assoc 2013;2(6):1–8. Doi: 10.1161/JAHA.113.000307.

251. Salinas JI., Lin H., Aparico HJ., et al. Whole blood microRNA expression associated with stroke: Results from the Framingham Heart Study 2019. Doi: 10.1371/journal.pone.0219261.

252. Porras AM., Shanmuganayagam D., Meudt JJ., et al. Development of Aortic Valve Disease in Familial Hypercholesterolemic Swine: Implications for Elucidating Disease Etiology. J Am Heart Assoc 2015;4(10). Doi: 10.1161/JAHA.115.002254.

253. Tan X., Zhang X., Pan L., Tian X., Dong P. Identification of Key Pathways and Genes in Advanced Coronary Atherosclerosis Using Bioinformatics Analysis. Biomed Res Int 2017;2017(5):1–12. Doi: 10.1155/2017/4323496.

254. Li Z., Hao J., Chen K., et al. Identification of key pathways and genes in carotid atherosclerosis through bioinformatics analysis of RNA-seq data. Aging 2021;13(9):12733–47. Doi: 10.18632/aging.202943.

255. Yang R., Yao L., Du C., Wu Y. Identification of key pathways and core genes involved in atherosclerotic plaque progression. Ann Transl Med 2021;9(3):267–267. Doi: 10.21037/atm-21-193.

256. Hasler-Rapacz J., Prescott MF., von Linden-Reed J., Rapacz JM., Hu Z., Rapacz J. Elevated concentrations of plasma lipids and apolipoproteins B, C-III, and E are associated with the progression of coronary artery disease in familial hypercholesterolemic swine. Arterioscler Thromb Vasc Biol 1995;15(5):583–92. Doi: 10.1161/01.ATV.15.5.583/FORMAT/EPUB.

257. Bahls M., Bidwell CA., Hu J., et al. Gene expression differences in healthy brachial and femoral arteries of Rapacz familial hypercholesterolemic swine. Physiol Genomics 2011;43(12):781–8. Doi: 10.1152/physiolgenomics.00151.2010.

258. Bahls M., Bidwell CA., Hu J., et al. Gene expression differences during the heterogeneous progression of peripheral atherosclerosis in familial hypercholesterolemic swine 2013. Doi: 10.1186/1471-2164-14-443.

259. Thim T., Hagensen MK., Drouet L., et al. Familial hypercholesterolaemic downsized pig with human-like coronary atherosclerosis: a model for preclinical studies. EuroIntervention 2010;6(2):261–8. Doi: 10.4244/.

260. Tellez A., Krueger CG., Seifert P., et al. Coronary bare metal stent implantation in homozygous LDL receptor deficient swine induces a neointimal formation pattern similar to humans. Atherosclerosis 2010;213(2):518–24. Doi: 10.1016/j.atherosclerosis.2010.09.021.

261. Tong KL., Zuhdi ASM., Ahmad WAW., et al. Circulating microRNAs in young patients with acute coronary syndrome. Int J Mol Sci 2018;19(5). Doi: 10.3390/ijms19051467.

262. Zhang JY., Gong YL., Li CJ., Qi Q., Zhang QM., Yu DM. Circulating miRNA biomarkers serve as a fingerprint for diabetic atherosclerosis. Am J Transl Res 2016;8(6):2650–8.

263. Vimal J., Himal I., Kannan S. Role of microbial dysbiosis in carcinogenesis & cancer therapies. Indian Journal of Medical Research 2020;152(6):553. Doi: 10.4103/ijmr.IJMR_1026_18.

264. Santana PT., Rosas SLB., Ribeiro BE., Marinho Y., de Souza HSP. Dysbiosis in Inflammatory Bowel Disease: Pathogenic Role and Potential Therapeutic Targets. Int J Mol Sci 2022;23(7):3464. Doi: 10.3390/ijms23073464.

265. Renko J., Lepp PW., Oksala N., Nikkari S., Nikkari ST. Bacterial signatures in atherosclerotic lesions represent human commensals and pathogens. Atherosclerosis 2008;201(1):192–7. Doi: 10.1016/j.atherosclerosis.2008.01.006.

266. Koren O., Spor A., Felin J., et al. Human oral, gut, and plaque microbiota in patients with atherosclerosis. Proceedings of the National Academy of Sciences 2011;108(Supplement_1):4592–8. Doi: 10.1073/pnas.1011383107.

267. Wang F., Jiang H., Shi K., Ren Y., Zhang P., Cheng S. Gut bacterial translocation is associated with microinflammation in end-stage renal disease patients. Nephrology 2012;17(8):733–8. Doi: 10.1111/j.1440-1797.2012.01647.x.

268. Zhang XN., Yu ZL., Chen JY., et al. The crosstalk between NLRP3 inflammasome and gut microbiome in atherosclerosis. Pharmacol Res 2022. Doi: 10.1016/j.phrs.2022.106289.

269. Amar J., Lange C., Payros G., et al. Blood Microbiota Dysbiosis Is Associated with the Onset of Cardiovascular Events in a Large General Population: The D.E.S.I.R. Study. PLoS One 2013;8(1). Doi: 10.1371/journal.pone.0054461.

CHAPTER TWO: HUB-GENES INFLUENCE CELLULAR-MEDIATED RESPONSES AND MYOFIBROBLAST KINETICS IN FIBRO-ATHEROMA DEVELOPMENT IN AN ATHEROSCLEROSIS SWINE MODEL

Submitted to JACC: Basic to Translational Science.

Hadjer Namous, MS,[a] Maria Giuseppina Strillacci DVM, PhD,[b] Camila Urbano Braz, PhD,[a] Dhanu Shanmuganayagam, PhD,[a] Christian Krueger, BS,[a] Athanasios Peppas, MS,[c] William C. Soffregen, DVM, PhD, ACVP,[d] Jess Reed, PhD,[a] Juan F. Granada, MD,[c] Hasan Khatib, PhD [a]

[a]Department of Animal and Dairy Sciences – University of Wisconsin Madison, WI, USA. [b]Department of Medicine Veterinary and Animal Science – University of Milan, Milan, Italy. [c]Skirball Center for Innovation, Cardiovascular Research Foundation, New York, New York, U.S.A. [d]Northstar Preclinical and Pathology Services, LLC and Skirball Center for Innovation, Cardiovascular Research Foundation, New York, New York, U.S.A. **Address for correspondence**

Juan F. Granada: jgranada@crf.org. 1700 Broadway, 9th Floor, New York, NY, USA, 10019. Phone: 845-580-3084

Hasan Khatib: hkhatib@wisc.edu. 1675 Observatory Drive, Madison, WI, USA, 53706. Phone: 608-263-3484

Abstract

Background: The complexity of atherosclerosis pathophysiology and the interplay between different biological pathways rendered identifying specific therapeutic targets a challenging quest. We aimed to identify specific genes and mechanistic pathways associated with the early development of fibro-atheroma in a swine model of atherosclerosis.

Methods: The Wisconsin Miniature Swine™ of Familial Hypercholesterolemia (WMS-FH, n=11) and WMS controls (WMS-N, n=11) of ~12 months of age were used. The infrarenal aorta was harvested from both groups for histopathologic and transcriptomic profiling. Bioinformatic analysis was performed to identify hub genes and pathways central to disease pathophysiology. The expression of ITGB2, the most commonly expressed hub gene, was manipulated in cell culture and the expression of interconnected genes was tested.

Results: Fibro-atheromatous lesions were present in all WMS-FH aortic tissues and displayed internal elastic lamina (IEL) disruption, significant reduction of myofibroblasts and aberrant collagen deposition. No fibro-atheromas were observed in the control group. A total of 266 differentially expressed genes (DEGs) were upregulated in WMS-FH aortic tissues, while 29 genes were downregulated. These DEGs are involved in inflammatory processes and cholesterol metabolism. Identified hub genes included ITGB2, C1QA, LCP2, SPI1, CSF1R, C5AR1, CTSS, MPEG1, C1QC, and CSF2RB. Overexpression of ITGB2 resulted in elevated expression of other interconnected genes expressed in porcine endothelial cells.

Conclusion: In a swine translational model of atherosclerosis, hub gene analysis identified a set of genes involved in fibro-atheroma development that have the potential to become therapeutic targets at this disease stage.

Keywords: Atherosclerosis, gene-expression, pathways, hub-genes, fibro-atheroma

List of abbreviations

C1QA: Complement Component 1, Q subcomponent, A Chain

C1QC : Complement Component 1, Q subcomponent, C Chain

C5AR1: Complement C5a Receptor 1

CSF1R: Colony Stimulating Factor 1 Receptor

CSF2RB: Colony Stimulating Factor 2 Receptor Subunit Beta

CTSS: Cathepsin S

EEL: External Elastic Lamina

IEL: Internal Elastic Lamina

ITGB2: Integrin Subunit Beta 2

KEGG: Kyoto Encyclopedia of Genes and Genomes

SPI1: Hematopoietic Transcription Factor PU.1

WMS-FH: Wisconsin Miniature Swine of Familial Hypercholesterolemia

WMS-N: Wisconsin Miniature Swine Normocholesterolemic/Normal

Introduction

Atherosclerosis is a complex disease that changes in structural and biological makeup as disease progresses. Dysfunctional cellular responses within the three layers of the vascular wall ultimately contribute to the onset and progression of the disease (1–4). Although many advances have been made in elucidating the underlying mechanisms of atherosclerosis development, the interplay between different mechanistic pathways is not fully understood. While advances towards atherosclerosis therapeutics continue to grow (5,6), the complex crosstalk between the various pathways involved in disease onset and progression has made the development of specific therapeutic targets difficult (7–9). Consequently, effective treatments to significantly reverse or slow disease progression are lacking at the present time. Moreover, there is still a need to understand the biological pathways involved in the early phases of atherosclerosis development, particularly in identifying central genes, and pathways at the different stages of the disease, which will significantly improve the development of targeted therapies.

Here, we aimed to characterize early stage atherosclerosis transcriptome and identify key pathways and genes central to the pathophysiology of the disease. We used a swine translational model, the Wisconsin Miniature Swine™ of Familial Hypercholesterolemia (WMS™-FH), a downsized derivative of our "Rapacz swine". The WMS-FH has a homozygous single-point mutation in the ligand region of the low-density lipoprotein receptor (LDLR) that prevents binding and thus clearance of cholesterol from the blood (10,11) and develops human-like complex lesions in different arterial beds (coronary, femoral, and brachial) starting at 12-months (12–15). The natural history of disease progression and response to interventional vascular therapies in this animal model has been previously documented in the literature (16–19). In contrast, the WMS-N do not have the LDLR gene mutation but are otherwise from the same genetic background as the

WMS-FH. We selected animals of ~12 months of age as at which time there is a notable transition phase from pathological intimal thickening into fibro-atheroma development in the model. We examined specific histopathological features and correlated the gene expression differences between diseased and healthy abdominal aortic tissues to identify novel disease-specific genes/pathways involved in the disease progression.

Methods

Study design and experimental model

The animal protocol was approved by the Institutional Animal Care and Use Committees (IACUC) at the University of Wisconsin-Madison in compliance with the *Guide for the Care and Use for Laboratory Animals* (20) and the Animal Welfare (21). Both, WMS with (WMS-FH, *n = 11*) and without LDLR mutation (WMS-N, *n = 11)* were randomly selected from the herd and housed at the University of Wisconsin Swine Research and Teaching Center (Madison, WI). All WMS-FH, homozygous for the LDLR mutation, had elevated cholesterol levels while the WMS-N (control group) displayed normal cholesterol profiles. All animals were housed at the same location and consumed a regular diet, formulated with essential nutrients meeting requirements to ensure normal growth and development of animals (Appendix A. Table 1). The characteristics of the animals used in the study are summarized in Table 1.

Table 1. Characteristics of WMS-FH and normal animal groups: Age, sex, weight, and total cholesterol.

Variable	WMS-FH	WMS-N
Age (months, mean ± SD)	13.18 (± 0.78)	13.73 (± 0.61)
Females (n, %)	8 (72.72)	6 (54.66)
Males (n, %)	3 (27.28)	5 (45)
Weight* (kg, mean ± SD)	63.3 (± 13.07)	75.16 (± 8.71)
Total cholesterol** (mg/dL, mean ± SD)	346.18 (± 74.30)	86.63 (± 19.11)

FH: familial hypercholesterolemia; SD: standard deviation. *: significant difference between groups (p=0.021); **: significant difference between groups (p=4.41E-10).

Tissue collection

Animals at 13.25 ± 0.75 months of age were sacrificed at the University of Wisconsin-Madison Meat Laboratory facility. The abdominal aorta ~2.5 cm above the common iliac artery bifurcation and below the renal arteries was harvested and a 3-cm segment was dissected. This segment was cut into 3 separate 1-cm sections, the center section (segment B) was used for gene expression analyses and the proximal and distal sections (segments A & C, respectively) for histopathology (Figure 1). The collected segments were flushed with cold Krebs solution to remove blood. The segment allocated to RNA extraction was preserved in RNA later (Thermofisher Scientific, DE, USA) and stored at -80°C until needed, while the histopathology segments were placed in 10% formalin.

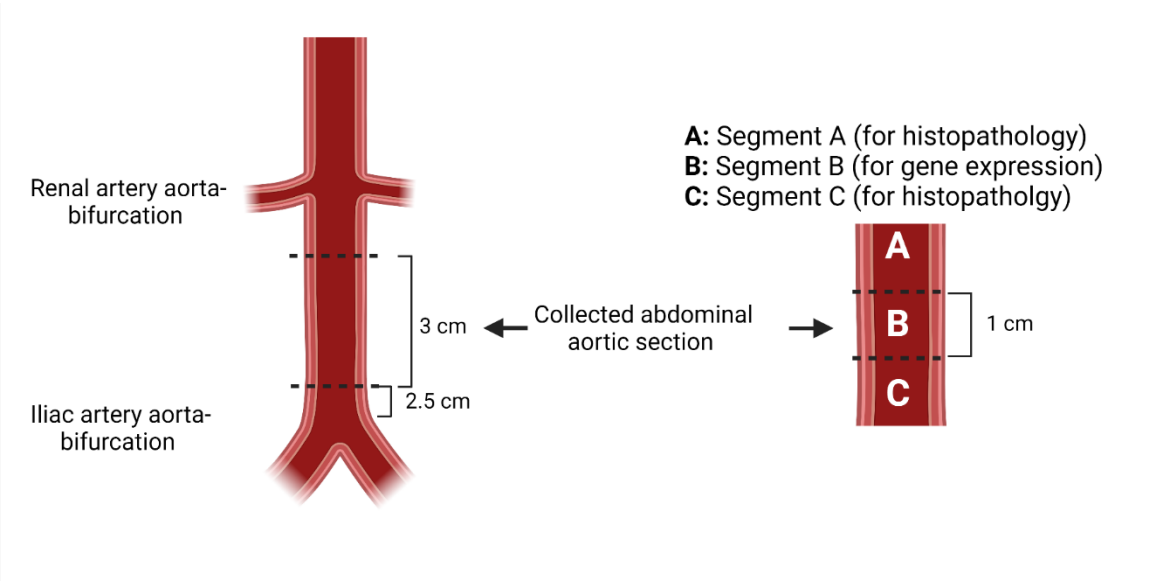

Figure 1. Schematic describing the abdominal (infrarenal) aortic segments used in the study. **A)** Infrarenal upper segment (1cm) used to assess histopathology. **B**) Infrarenal middle segment (1cm) used in gene expression analysis. **C)** infrarenal lower segment also for histopathology assessment. Created with Biorender.com.

RNA extraction

Total RNA was extracted from each tissue using the RNeasy Mini Kit (QIAGEN, Valencia, CA). Briefly, ≤ 3 mg of the tissue sample from each pig was lyophilized and reduced to powder using liquid nitrogen. Then, pulverized tissues were transferred to a QIAshred column to homogenize and reduce sample viscosity. Subsequent steps followed the manufacturer's instructions. Finally, RNA quality and quantity were assessed using NanodropONE (Thermofisher Scientific, DE, USA) and Bioanalyzer 2100 Eukaryote Total RNA Nano (Agilent Technologies, CA, USA).

Histopathology processing

Each animal had two aortic tissue segments except for one WMS-FH animal. A total of 23 WMS-FH and 24 WMS-N aortic segments were submitted for histo-pathological evaluation. Cross-sectional sections (segments A & C) of infrarenal aortic arteries were flushed with Krebs solution. After all the tissue samples were cleared of blood, they were immediately immersed in tubes containing 10% formalin. The arterial cross-sectional sections were trimmed into proximal and distal segments to create one slice for each segment. The resulting slices were processed and sequentially embedded in paraffin in proximal-distal orientation. Blocks were sectioned twice via microtome, mounted to glass slides and stained with hematoxylin and eosin (H&E) and Elastin Trichrome (ET), with two slides per artery segment. Histopathology analysis was performed by a board-certified veterinary pathologist (WCS). A semiquantitative scoring (on a scale of 5 for each parameter, Appendix A. Scored parameters) system was used to quantify the morphological changes seen in all the histological samples.

RNA sequencing and differential expression analysis at gene, isoform, and splice variant levels

RNA sequencing was performed to assess the differential expression between WMS-FH and WMS-N abdominal aortic tissues. An equivalent amount of RNA from each sample was used to construct three pools per group with 1.5 μg per pool. Appendix A. Table 2 summarizes sample distribution across pools and groups. Library preparation and RNA sequencing were performed by LC Sciences (Houston, TX, USA). Upon confirmation of sequencing quality and trimming adapters, obtained reads were mapped to the swine genome (*Sus Scrofa* 10.2) using Bowtie 2 (22). Transcript abundance at the gene and isoform levels were estimated using RSEM(23). Differential expression analysis was performed using the "edgeR" R package (24). To determine differentially expressed splice variants, alternative splicing variant analysis was performed using Multivariate Analysis of Transcript Splicing software for replicates, rMATS (25). Results were reported for five types of alternative splicing events, including skipped exon (SE), alternative 5′ splice site (A5SS), alternative 3′ splice site (A3SS), mutually exclusive exons (MXE), and retained intron (RI). Only significant splice variants at a false discovery rate (FDR) ≤ 0.05 were reported.

Technical validation of differentially expressed genes (DEGs) with quantitative PCR (qPCR)

RNA sequencing was performed in pooled samples; therefore, we opted to validate a set of genes in individual samples. Twelve DEGs, found to be significant in the RNA-Seq pools analysis, were selected for validation in individual RNA samples using real-time quantitative PCR (RT-qPCR). Selection criteria were based on gene function and expression pattern (up/downregulation). Appendix A. Table 3 summarizes the selected genes and their corresponding roles in atherosclerosis if known.

Total RNA was extracted from the twenty-two aortic tissue samples using RNeasy Mini Kit (Qiagen) following the manufacturer's instructions. First, the RNA purity was assessed using NanoDrop™ One (Nanodrop Technologies). Next, 100 ng RNA from each sample was used to produce cDNA using the iScript™ cDNA synthesis Kit (BioRad, Hercules, CA). Gene expression was determined for each sample individually by real-time PCR following the iTaq SYBR Green kit protocol (BioRad). Primers were designed to span introns using NCBI primer-blast (https://www.ncbi.nlm.nih.gov/tools/primer-blast/) (Appendix A. Table 4). The *YWHAZ* gene was selected as a reference control for its stability across all samples. The relative gene expression was evaluated using the $2^{-\Delta\Delta CT}$ method (26) .

Protein-Protein interaction network, pathway enrichment, and hub gene analyses

To identify protein-protein interactions between DEGs, we selected genes with significant differential expression at FDR ≤ 5%. To construct a protein-protein interaction (PPI) network, the Search Tool for the Retrieval of Interacting Genes/Proteins (STRINGdb v10.5) (27) was used. The medium confidence score of the PPI network was set to 0.4. To determine the biological function and relation in which the protein products of DEGs are involved, we performed gene ontology (GO) of biological processes (BP) and Kyoto Encyclopedia of Genes and Genomes (KEGG) pathway enrichment analyses using ClueGO (28) in Cytoscape. ClueGo kappa score (kappa > 0.4) was used to define term-term interrelation and functional groups based on shared genes between terms. Hence, BP and KEGG terms/pathway results were grouped under the most significant term. Determining hub genes within a PPI network allows for identifying central genes to the pathophysiology of the disease and potential therapeutic targets. We used the Cytohubba plug-in (29) in Cytoscape to identify the hub genes. Genes were scored using the Maximal Clique Centrality (MCC) method, and the 10 highest-scoring genes were reported.

ITGB2 gRNA sequences design and plasmid constructs

The integrin subunit β2 (ITGB2) is at the center of most interconnections with other genes within the PPI network; hence, this gene was selected for expression manipulation via epigenome editing. ITGB2 promoter-specific gRNA sequences were designed with CRISPOR (30); ITGB2 gRNA1: 5`TCATACAGTCCGTCTTGTG3` and ITGB2 gRNA2: 5`TGTGCCTGTGTCACGCCCGG 3`. The gRNAs spanned a 494 bp region upstream of the ITGB2 gene. This region was selected based on ITGB2 promoter/enhancer regions in human and mice. The gRNAs oligonucleotides were synthesized by Integrated DNA Technologies (IDT Technologies, IA, USA). ITGB2 gRNA expression plasmids were constructed by ligating annealed gRNA oligonucleotides using T4 ligase (NEB, USA) to psPgRNA vector (Addgene, cat# 47108). The pcDNA-dCas9-p300 plasmid construct was obtained from Addgene (cat#61357). To determine transfection success and efficiency, PL-SIN-EF1α-EGFP plasmid (cat#21320) was used.

Cell culture of porcine aortic endothelial cells (PAECs) and manipulation of ITGB2 expression

ITGB2 was the top hub gene with multiple interactions within the PPI network. The high interconnectivity of ITGB2 with other genes indicates its involvement in multiple pathways, making it an appealing therapeutic target. Thus, to determine whether manipulating ITGB2 expression would affect the expression of interconnecting genes in a similar manner observed in the differential expression and PPI network analyses, we opted to overexpress the gene in porcine aorta endothelial cells (PAECs) obtained from iXCells Biotechnologies (CA, USA). Cells were grown in iXCells Biotechnologies' Endothelial Cell Medium supplemented with Basal medium

and Endothelial Cell Growth Supplement (ECGS). Cells were incubated at 37°C in humidified 5% (v/v) CO_2-containing atmosphere.

For the overexpression of ITGB2, PAEC cells were transfected with pcDNA-dCas9-P300 and ITGB2 gRNAs constructs between the third and seventh passages. Cells were seeded in 6-well plates (1 well per treatment/control), and 24 hours after seeding, they were transfected with lipofectamine 2000 (Life Technologies), 2.25 μg of pc-DNA-dCas9-p300, and 0.75 μg of an equimolar concentration of each ITGB2 gRNA expression vector. Two days post-transfection, cells were harvested, and RNA was extracted using Direct-zol RNA MiniPrep Kit (Zymo Research, CA, USA) following manufacturer's instructions. All transfections were performed in three biological replicates. ITGB2 overexpression was assessed via RT-qPCR, and fold change expression between transfected and nontransfected cells was determined using the $2^{-\Delta\Delta CT}$ method. Genes from the PPI network that connect directly (C3 and FCER1G) or indirectly (S100A4 and CD68) with ITGB2 were selected to assess their expression. The other evaluated genes (MMP9, LCP1, ACTC1, and CNN1) demonstrated no expression in either control or treated cells. Table 4. Appendix A contains the primer sequences. *YWHAZ* (endogenous control) was used for normalization

Statistical analysis

The statistical significance of DEGs was determined using a binomial linear regression model coupled with multiple testing adjustment inherent in the edgeR package. For gene expression validation via RT-qPCR, a two-tail t-test was used to determine the statistical significance of relative gene expression (ΔCT values) between WMS-FH and WMS-N samples. The statistical significance of gene expression in the cell culture experiments was assessed using

paired t-test between normal cells and cells overexpressing ITGB2. Statistical significance was determined when the p-value was < 0.1.

Results

Atherosclerosis stage and disease phenotype

Intimal hyperplasia was observed in 17 of 23 (74%) of the WMS-FH arteries and 17 of 24 (71%) of the WMS-N arteries (Appendix A. Table 5). The severity of intimal hyperplasia was higher in the WMS-FH (mean score = 1.38±0.24; mean percentage of circumference involved = 28.1%±4.3%) compared to the WMS-N mean score = 0.74±0.09; mean percentage of circumference involved = 17.6%±3.2%). Pathological changes consistent with atheromatous changes were seen in all (17/17, 100%) of the WMS-FH arterial segments and none (0/17, 0%) in the WMS-N control group (Figure 2).

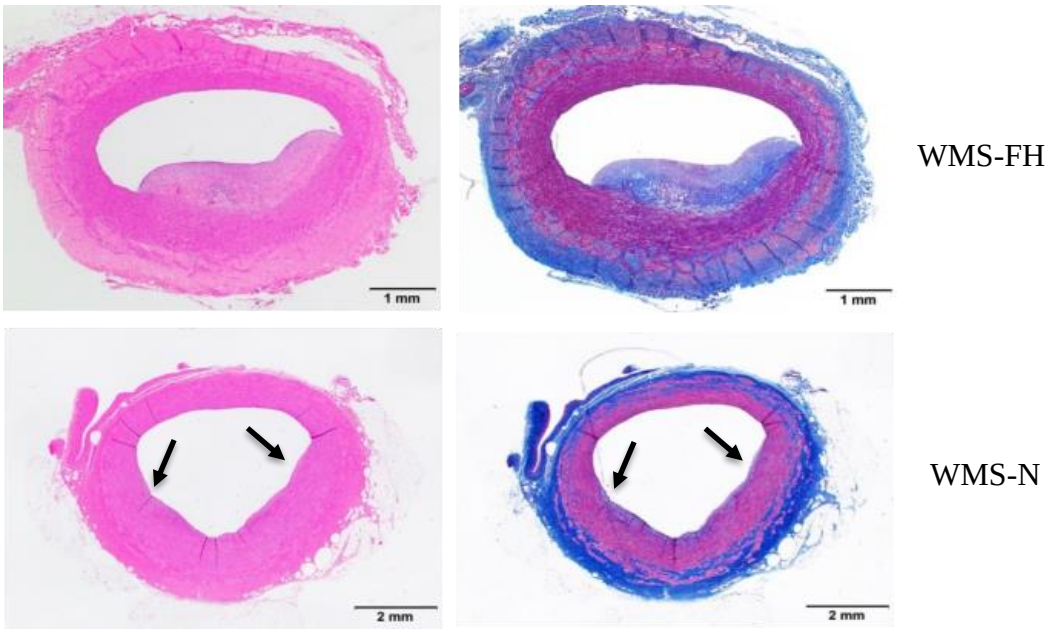

Figure 2. Histopathology of representative animals from WMS-FH and WMS-N.

Photograph in the top row includes representative histopathology images (H&E left, ET right) of an aortic section of the WMS-FH group. There is a segmental area of intimal hyperplasia

consistent with atheromatous change. Lipid and cholesterol clefts are contained within the neointima that also contains a large area of dense collagen with small numbers of myofibroblasts. The lower panels are representative pictures of the aorta in the control WMS group. Segmental region of slight intimal hyperplasia composed of myofibroblasts and associated connective tissue matrix, mostly collagen, are shown (black arrows).

The pathological neointima of the WMS-FH arteries was composed solely of myofibroblasts with associated connective tissue deposition and exhibited variable levels of lipid (17/17, 100%), macrophage infiltration (17/17, 100%), cholesterol clefts (11/17, 65%), and mineralization (3/17, 18%). Overall, there was more than a 50% reduction of myofibroblast presence in the WMS-FH compared to the control group. However, collagen was more abundant but organized differently in the WMS-FH compared to the WMS-N control group. In the WMS-FH arteries, foci of dense collagen unassociated with myofibroblasts were seen in each affected arterial segment, whereas collagen was evenly interspersed between the myofibroblast cells in the WMS-N control group. Vacuolation consistent with lipid infiltration was observed in the tunica media of 12 of 24 (50%) WMS-FH arteries and 0 of 23 (0%) WMS-N arteries. The medial lipid was always subjacent to the segmental region of intimal hyperplasia exhibiting the atheromatous changes in the affected WMS-FH arteries (Figure 3).

Histological alterations consistent with underlying arterial wall injury were more commonly observed in the WMS-FH group and included disruption of the internal elastic lamina (IEL) (WMS-FH = 12 of 24, 50%; WMS-N = 6 of 23, 26%) and adventitial fibrosis (WMS-FH =

14 of 24, 58%; WMS-N = 19 of 23, 83%). When present, the disruption/loss of the IEL was in small focal or multifocal areas subjacent to the intimal hyperplasia.

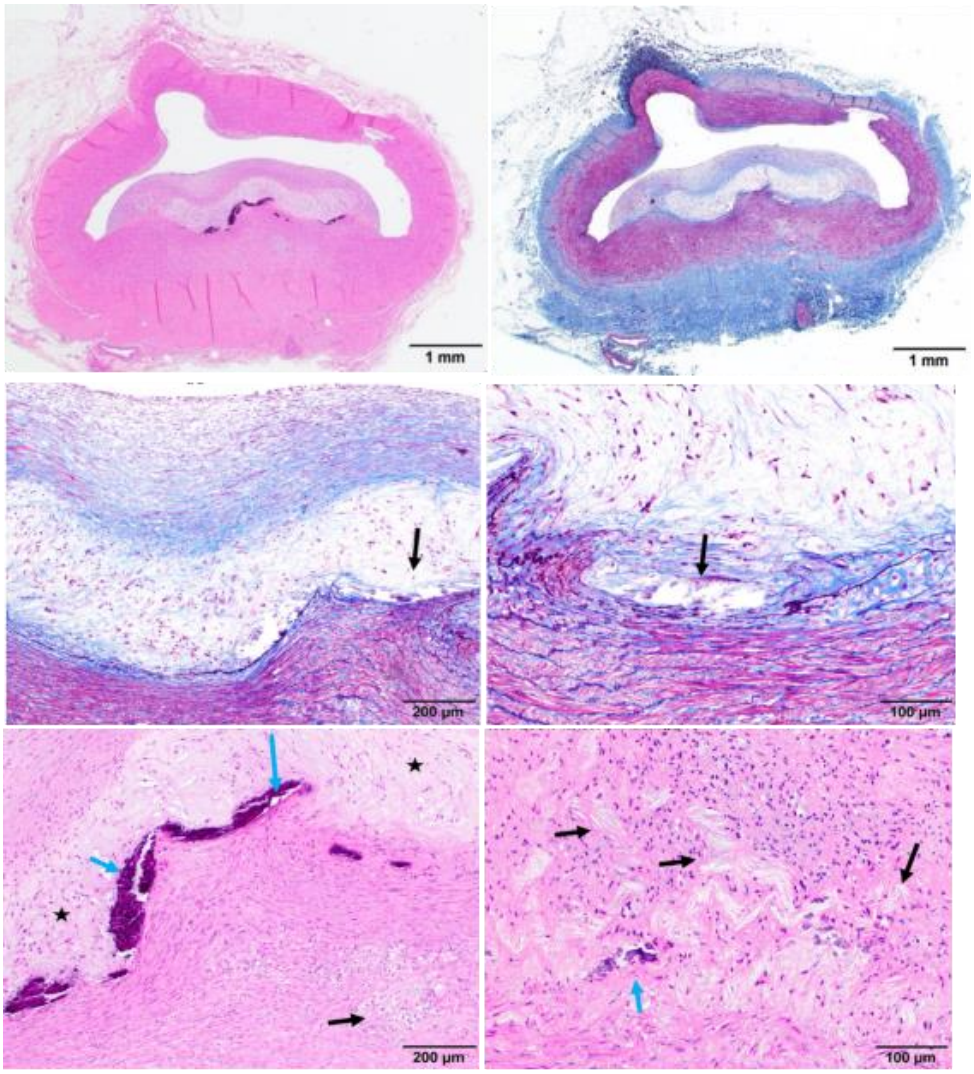

Figure 3. Intimal thickening to the early phases of fibro-atheroma formation in WMS-FH.

Photographs in the top row (left HE, right ET) are representative pictures of the aorta in the WMS-FH group in which is there is a segmental area of intimal hyperplasia consistent with atheromatous changes as well. Clefts of mineralization at the interface of the neointima and IEL. There is additionally a central core of lipid, and an outer region of collagen with small numbers of myofibroblasts. Mid panel displays the interface of the lipid-rich neointima and the tunica media

(left :10X; right: 20X). There are small disruptions of the IEL (arrows). Bottom left panel presents the neointima, which contains a large region of lipid (stars), and the inner media which contains foci of vacuolation/lipid infiltration (black arrow). There are clefts of mineralization at the interface of the neointimal and media (blue arrow). The bottom right panel shows the neointima which contains lipid and cholesterol clefts (black arrows) among collagen and occasional foci of mineralization (blue arrow).

Identification of DEGs

A total of twenty-two abdominal aortic tissue samples from WMS-FH (n = 11)and WMS-N (n = 11) swine were used in this study. Extracted RNA was pooled (n = 3 pools per group) and sequenced. RNA-Seq analysis revealed 295 DEGs between the two groups at 5% FDR. In the WMS-FH group, 266 genes were upregulated and the remaining 29 DEGs were downregulated (Figures 4 B and C, Appendix A. Table 6). Similarly, at 5% FDR, 186 isoforms were differentially expressed (DEIs), with 169 upregulated isoforms and 17 downregulated isoforms (Figures 4 A and C; Appendix A. Table 7). In addition to gene- and isoform-level differential expression, 13 splice variants were captured. These variants belonged to 9 DEGs (Appendix A. Table 8).

Validation of DEGs via RT-qPCR

The present work used a pooling strategy for RNA sequencing to determine DEGs between WMS-FH and WMS-N group. Hence, we selected 12 DEGs for validation in the individual samples used to construct the pools (Appendix A. Figure 2). Differential gene expression results of the mRNA sequencing showed high expression of the CXCL14, APOE, LCP1, ITGB2, AIF1, CD36, TLR4, and TLR6 genes in WMS-FH pools compared to the WMS-N control pools. Similarly, the relative gene expression analysis in individual samples showed significantly higher expression of these genes in WMS-FH compared to WMS-N samples with a fold change (FC) of

11.83 for CXCL14 (P = 0.010), 9.70 for APOE (P = 0.005), 5.01 for LCP1 (P = 0.028), 3.75 for ITGB2 (P = 0.010), and 2.84 for AIF1 (P = 0.031). CD36 showed high expression in WMS-FH; however, no significant differences were observed (FC = 2.00, P = 0.157). Similar to RNA-Seq results, relative gene expression for the TLR4 confirmed the differential expression with an FC= 3.51 (P = 0.029). In contrast, TLR 6 showed a lower expression in WMS-FH (FC = 0.36, P = 0.012).

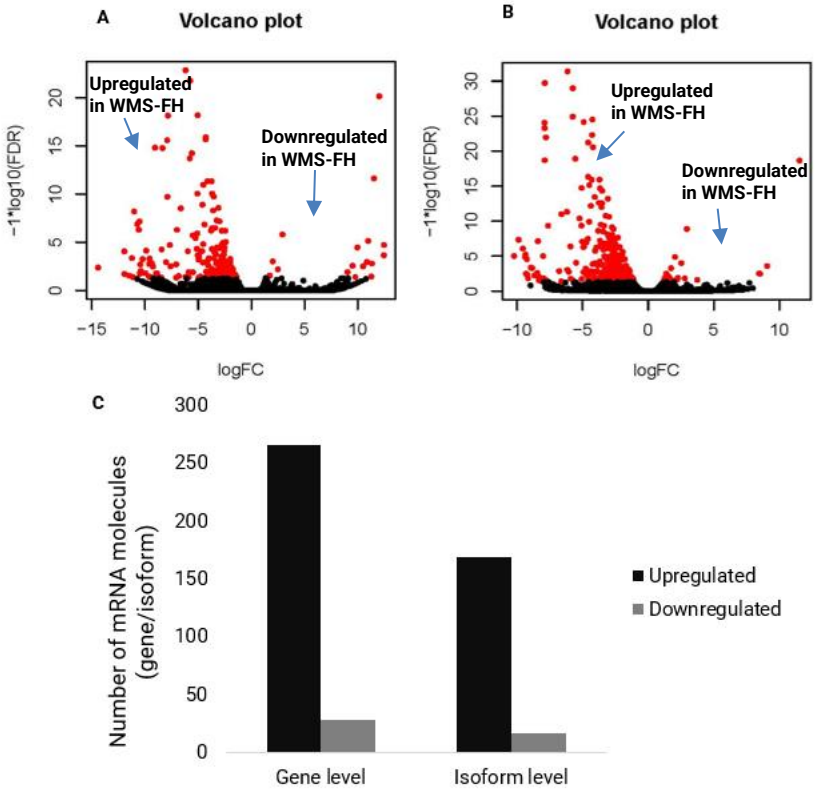

Figure 4. Differential expression between WMS-FH and WMS-N at gene and isoform levels. **A)** Volcano plot for isoform-level differences. **B)** Volcano plot for gene-level differences. A negative logFC indicates upregulation in WMS-FH. **C)** Number of differentially expressed genes and isoforms between abdominal aortic tissues from WMS-FH and WMS normal (5% FDR).

CYP2B22, CILP2, CNN1, and ACTC1 genes were downregulated in WMS-FH pools compared with WMS-N pools. For this set of genes, only CYP2B22 and CILP2 showed a significant relative gene expression between the groups, thus validating the sequencing results. Fold change differences were 16.3 for CYP2B22 (P = 0.009) and 3.79 for CILP2 (P = 0.034). CYP2B22 showed an almost exclusive expression in the WMS-N group. CNN1 (FC = 0.81) and ACTC1 (FC = 0.40) showed no significant differences in relative gene expression between the two groups.

Functional enrichment and hub gene analyses

We carried out a PPI network analysis to predict interactions between the DEGs and identify the involved mechanisms. The constructed PPI network was significantly enriched (P< 1.0e-16) for interactions between the DEGs, indicating that the proteins are biologically connected (Appendix A. Figure 3). Additionally, we performed a pathway enrichment analysis focused on biological processes (BP) and KEGG pathways. Gene ontology of BP analysis suggests that the DEGs primarily function in the immune system and inflammatory responses. Specifically, the regulation of the immune system process was the most enriched BP, followed by phagocytosis, inflammatory response, myeloid cell differentiation, and leukocyte activation. Other significant BPs are listed in Figure 5 B.

KEGG pathway enrichment analysis showed that DEGs are enriched in the phagosome, *staphylococcus aureus* infection, Fc epsilon RI signaling, osteoclast differentiation, lysosome, malaria, cholesterol metabolism, leukocyte transendothelial migration, natural killer cells mediated toxicity, chemokine signaling, and PPAR signaling pathways (Figure 5 A). Given the complexity of networks and the crosstalk between pathways, we analyzed the PPI for hub genes. Hub genes have high interconnectivity levels and central roles in the PPI network and could

become potential therapeutic targets. The 10 highest scored and most significant nodes within the PPI network were selected as hub genes (Table 2). Our findings indicate that ITGB2, C1QA, LCP2, SPI1, CSF1R, CSF2RB, C5AR1, CTSS, MPEG1, and C1QC genes are the most central to the pathophysiology within the DEGs obtained.

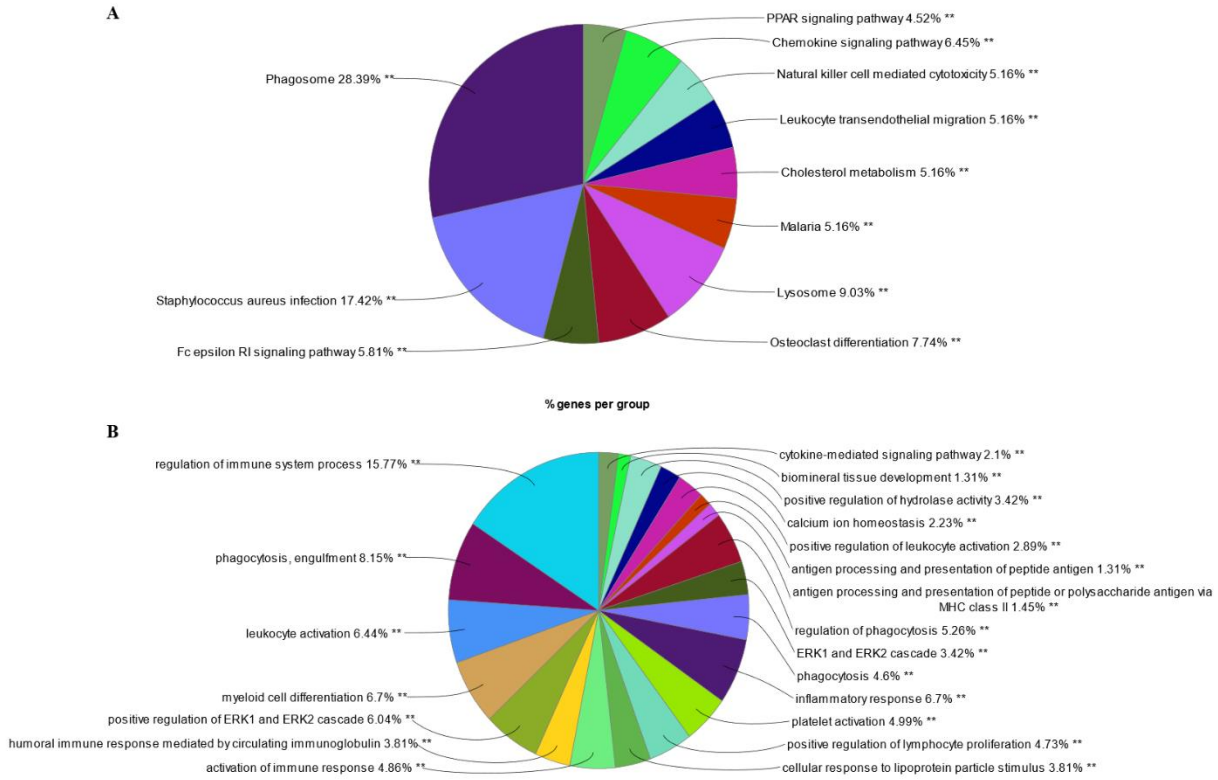

Figure 5. Pie charts of biological processes and KEGG Pathway enrichment analyses were generated using ClueGO in Cytoscape. **A)** KEGG pathways and **B)** Biological processes of differentially expressed genes at 5% FDR. % : represent percentage of DEGs within the pathway (number of DEGs / number of genes within the pathway).

ITGB2 upregulation in PAECs and its effect on interconnecting genes

ITGB2 was the top hub gene with the highest interconnections with other genes within the PPI network. Hence this gene is at the core of interactions and enriched pathways. Indeed, our analysis showed that ITGB2 participates in many KEGG pathways and has interconnections with

other DEGs also enriched in the reported KEGG pathways (Appendix A. Figure 3). Therefore, manipulating the expression of ITGB2 would likely affect the expression of the interconnected genes.

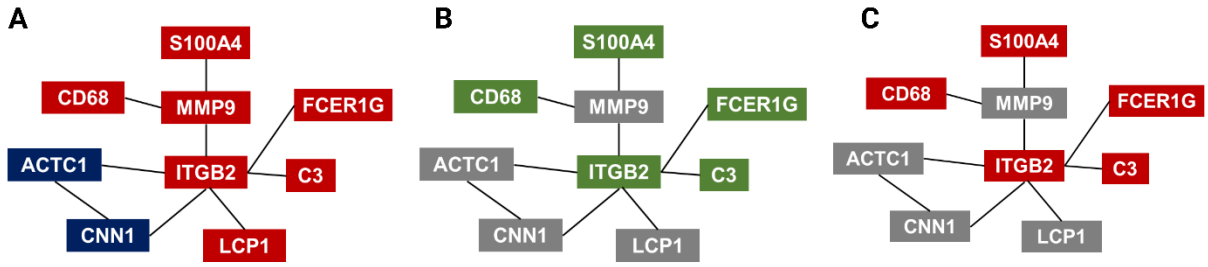

Figure 6. Interaction networks for ITGB2 and tested genes with color coding for expression patterns in WMS-FH. **A)** Differentially expressed genes from RNA sequencing data (red and blue indicate upregulation and downregulation of gene expression in WMS-FH animals, respectively.). **B)** Expression pattern of the same genes in nontreated (not transfected with dCas9-p300 and ITGB2 gRNAs) porcine aortic endothelial cells (Green indicates expression of gene whereas gray indicates no expression). **C)** Changes in expression of genes in treated (transfected with dCas9-p300 and ITGB2 gRNAs; overexpress ITGB2) porcine aortic endothelial cells overexpressing ITGB2 (Red indicates increased expression of gene; gray indicate no expression).

Transfection of PAECs with dCas9-p300, which adds acetyl groups to the ITGB2 promoter region, resulted in a 3.13-fold change of expression (P = 0.032) of ITGB2. Consequently, we measured the expression of C3, FCER1G, S100A4, and CD68, which were selected based on their interconnectivity with ITGB2 within the PPI network (Figure 6).Upon overexpression of ITGB2, the expression of C3, CD68, S100A4, and FCER1G was increased by 2.36 (P = 0.063), 2.75 (P =

0.001), 1.61 (P = 0.076), and 1.67 (P = 0.017) fold changes, respectively (Figure 7). Other tested genes were not expressed in PAECS before or after ITGB2 expression manipulation.

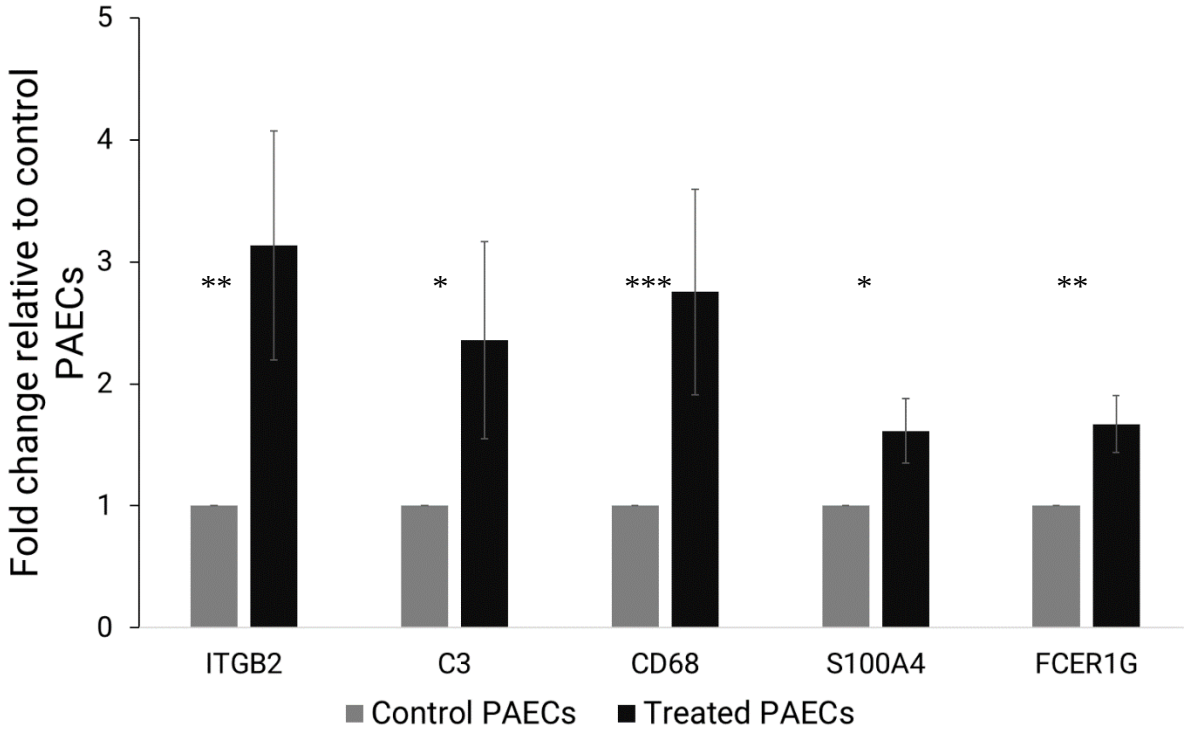

Figure 7. Relative gene expression of ITGB2, C3, FCER1G, S100A4, and CD68 in non-treated and treated PAECs. Treated PAECs overexpress ITGB2. Fold change was calculated using $2^{\wedge-(\Delta CT \text{ of treated PAECs} - \Delta \text{ of control PAECs})}$. Data in the Figure represent three biological replicates. Error bars represent the standard deviation in fold change difference. ***: $p<0.01$, **: $p<0.05$, *: $p<0.1$.

Table 2. Top 10 hub genes within protein-protein interaction network ranked using Cytohubba - MCC method.

Rank	Gene Name	Description	MCC Score	Protein Encoded	Protein Function	Target Cells
1	ITGB2	Integrin Subunit Beta 2	1.0810E+08	CD18	Cellular adhesion to ECM and surface signaling	Leukocytes including T-cells and neutrophils
2	C1QA	Complement C1Q A Chain	1.0808E+08	Complement C1q subcomponent subunit A[3]	Yields the 1st component of the serum complement system	Non-specific
3	LCP2	Lymphocyte Cytosolic Protein 2	1.0798E+08	SLP-76	Signal-transducing adaptor protein	T-cells and myeloid cells
4	SPI1	Hematopoietc Transcription Factor PU.1 SPI1 proto-oncogene	1.0793E+08	SPI1 proto-oncogene	ETS-domain transcription factor that activates gene expression during myeloid and B-lymphoid cell development	Myeloid and B-lymphoid cell
5	CSF1R	Colony Stimulating Factor 1 Receptor	1.0732E+08	Receptor for colony stimulating factor 1	controls the production, differentiation, and function of macrophages	Macrophages
6	CSF2RB	Colony Stimulating Factor 2 Receptor Subunit Beta	1.0603E+08	Common beta chain of the high affinity receptor for IL-3, IL-5 and CSF	TBD	Granulocyte-macrophages
7	C5AR1	Complement C5a Receptor 1	9.8356E+07	CD88	G-protein-coupled receptor for C5a	Granulocytes, Monocytes, Brain Cells
8	CTSS	Cathepsin	9.6714E+07	Cathepsin S	Secreted cathepsin S cleaves some extracellular matrix (ECM) proteins. Cathepsin S may be considered the most potent elastase known.	Macrophages, B-lymphocytes, dendritic cells and microglia
9	MPEG1	Macrophage Expressed 1	9.6209E+07	protein belonging to the Membrane Attack Complex/Perforin (MACPF)	pore-forming protein expressed in macrophages and neutrophils	Macrophages and neutrophils
10	C1QC	Complement C1q C chain	9.5626E+07	Complement C1q subcomponent subunit C	associates with C1r and C1s to yield the first component of the serum complement system	Non-specific

Discussion

Atherosclerosis results from multiple and complex mechanistic interactions influenced by genetic and environmental factors. The disease develops over several decades, and its pathobiological fingerprints and biological mechanisms vary according to its stage of development. Our study investigated the transcriptomic profile and biological mechanisms involved in the early stages of atherosclerosis development using a large translational animal model of atherosclerosis (WMS-FH) and a genetically related control group (WMS-N). After identifying the most commonly differentially expressed genes, a specific group of hub genes was identified based on their specific biological interactions. These hub genes are thought to play a central role in atherosclerosis development and could become specific therapeutic targets for this stage of disease. WMS-FH is a well-characterized model of atherosclerosis (16–19), offering a unique opportunity to study disease development and progression mechanisms in a controlled environment.

The histopathology results of the arteries examined demonstrated the presence of early-stage atherosclerosis development in all arteries in the WMS-FH group and no evidence of the disease in the WMS-N control group. The phenotype of these lesions represents a transition phase from pathological intimal thickening into the early phases of fibro-atheroma formation. This is a critical phase in atherosclerosis development in which disease progression could be modified by targeting specific pathways and genes. Importantly, although most of the biological activity seen in all WMS-FH arterial samples points to well-described lipid or inflammatory-related pathways, a distinct mechanistic feature was the reduced presence of myofibroblasts, and the disorganized presence of collagen deposition observed in each affected arterial segment. Organized collagen deposition is essential for the stability of the fully developed atheroma, and plaque rupture and

instability have been associated with the so-called thin cap fibro-atheroma (31). Therefore, understanding the underlying mechanisms of fibrous cap formations and plaque destabilization is key for developing therapeutic alternatives at the early stages of disease development.

In alignment with the phenotypic features, the RNA-Seq data demonstrated a distinct expression pattern between WMS-FH diseased and normal WMS-N arteries, including expression differences at isoform levels. These phenotypic changes during this stage of atherosclerosis development reflect the alterations in mRNA expression patterns and subsequent cellular responses and correlate positively with histopathology findings. Indeed, transcriptomic studies in human atherosclerotic lesions demonstrated differences in mRNA expression between normal aortic tissues and those with atherosclerotic lesions in different arterial beds and at different stages of the disease (32–38). Moreover, gene isoforms were also shown to associate with cardiovascular disease development (39–42).

Since one goal was to understand mechanistic pathways and related genes participating in this transition phase during atherosclerosis development, we carried out a pathway enrichment analysis. Our results showed that DEGs are involved in several BPs and KEGG pathways related to inflammatory and immune response pathways, cholesterol homeostasis and metabolism. Similar pathways have been described in human studies of aortic lesion transcriptomes (32,34,43). The findings of this work further support the role of such mechanisms/pathways in the early stages of the disease.

When comparing differential expression and pathway analysis results with histopathology findings, we observe gene and biological pathways that are common in the early stage of the disease. For instance, macrophage infiltration and lipid deposition were commonly seen in the aortic lesions of WMS-FH. Indeed, the leukocyte transendothelial migration and chemokine

signaling pathways – enriched in our analysis- are activated during the initial stages of the disease (44,45) allowing monocyte migration and differentiation to macrophages. Subsequently, macrophages become foam cells (46,47) upon phagocytosis of lipids. Formed foam cells in the subintimal space are characterized by dysfunctional lipid-laden lysosomes(48). Thus, enrichment of DEGs in the phagosome and lysosome pathways is expected and indicates that both pathways are active in WMS-FH aortic tissues in response to the presence of lipids and macrophages within the lesions. Also, the observed upregulation of DEGs active in the peroxisome proliferator-activated receptor (PPARs) signaling pathway is likely an adaptation to clear the high blood cholesterol levels and promote macrophage cholesterol efflux in our animal model. PPARγ promotes monocyte differentiation and uptake of oxLDL through the upregulation of CD36 (49).

There is an intimate relationship between lipids and inflammation. Hence, observing mechanisms involving cholesterol metabolism, and immune-inflammatory pathways such as chemokine signaling is anticipated in hypercholesterolemic WMS-FH animal. Lipid uptake induces a shift in vascular smooth muscle cells (VSMCs) phenotype to a macrophage/foam-like proinflammatory phenotype (50,51). Also, VSMCs produce large amounts of extracellular matrix (ECM) proteins such as collagen and metallomatrix proteinases (MMPs) (i.e., MMP9 (Appendix A Table 6), upregulated in WMS-FH) as well as cytokines (52,53); thus, VSMCs potentially regulate neighboring cells and releasing extracellular vesicles to induce calcification (53,54). WMS-FH arteries presented spots with microcalcification. Interestingly, the osteoclasts differentiation pathway is upregulated in WMS-FH. Osteoclasts are cells that resorb calcification and are critical in maintaining healthy tissues such as arteries where calcification is ectopic. Chinetti-Gbaguidi et al. (55) showed that macrophages in lesions exhibit osteoclast-like function, which suggests that the mechanisms for calcification resorption are in place in WMS-FH. Another

observation is that focal disruption of the Internal Elastic Lamina (IEL) subjacent to the intimal hyperplasia was more commonly seen in the WMS-FH arteries. IEL disruption is one of the earliest anomalies observed in human atherosclerosis (56). The progressive loss of the elastic fibers in the lamina suggests an aberrant ability to restore the elastic tissue. Also, increased IEL disruption may trigger cellular proliferation, altering collagen production (57). Subsequently, microscopic mineralization/calcification occurs (56), which was observed in the arteries of our WMS-FH.

WMS-FH histopathology showed a distinct pattern of collagen distribution in the neointima compared to WMS-N, showing foci of dense collagen not associated with myofibroblasts in each atherosclerotic lesion. Myofibroblasts are essential for maintaining the structural integrity of tissue via the secretion of elastin and collagen (58). The origins of myofibroblasts include adventitial fibroblasts, VSMCs (59,60), ECs and macrophages (61). Upon differentiation to myofibroblasts, collagen secretion increases (59). Given the observed aberrant distribution of myofibroblasts in the neointima, it is very likely that the myofibroblasts present resulted from other cells rather than adventitial fibroblasts under the influence of oxLDL and the upregulated immune-inflammatory pathways observed in WMS-FH arteries. Moreover, the presence of less collagen in WMS-FH coupled with its uneven distribution indicates either a lesser production or degradation of collagen. Indeed, our findings showed an increased expression of MMP9, MMP19, and CTSS in WMS-FH (Appendix A. Table 6). These genes are known to degrade ECM proteins including elastin and collagen (62,63). Moreover, a recent study in APOE-/- mice demonstrated that collagen damage occurs in early atherosclerosis stages (64). Furthermore, CNN1, ACTA1, ACTC1, CSRP1, COMP, and DES were found to be downregulated in WMS-FH (Appendix A. Table 6). These genes are associated with healthy VSMCs phenotype and participate in muscle contraction and actinin binding, and the observed downregulation

indicates a change in VSMC phenotype and altered function. Altered functions of VSMCs in the medial layer include vascular calcification and formation of the fibrous cap covering the plaques (65). Recently, studies have shown that VSMCs expand to different cells present in atherosclerosis lesions (38,66,67). Furthermore, a sign of expanding VSMCs is the upregulation of Complement C3, which is highly upregulated in WMS-FH, and its effect on macrophages and VSMCs proliferation (66). These studies further confirm the aberrant phenotype VSMCs are exhibiting within WMS-FH arteries and the observed distribution and amount of myofibroblasts and collagen.

An interesting pathway identified in this study, also noted in human studies, is the *Staphylococcus aureus* infection pathway. *Staphylococcus aureus* is a member of commensal microflora. A recent study using rabbits showed that superantigen (SAg) toxic shock syndrome toxin-1 (TSST -1) produced by *Staphylococcus aureus* stimulates the progression of atherosclerosis by inducing inflammation (68). In contrast, heat-killed *Staphylococcus aureus* prevented the progression of atherosclerosis via reduced VCAM1 and CD68 expression in the aortic tissue of $LDLR^{-/-}$ mice (69). Although microbiota, in general, has been linked to atherosclerosis (70–72), in-depth studies are needed to understand their role in the disease.

Identifying specific pathways relevant to the pathophysiology of the disease presents an excellent opportunity to develop therapeutic targets at the gene level, especially since many DEGs are shared between pathways (Appendix A. Figure 3). Selecting core genes from the constructed PPI network is the likeliest approach to identifying those with therapeutic potential. In the present work we identified hub genes central to the pathology in the early stage of atherosclerosis. Several hub genes have been reported in human transcriptomic atherosclerosis studies. These included ITGB2 (43,73–77), C1QA (78) & C1QC (75,78), CSF1R (74,78), C5AR1 (74), and CTSS (43).

Hub genes have been shown to play a role in atherosclerosis development and progression, suggesting their involvement in disease onset in WMS-FH aortic tissues. For example, ITGB2 is expressed on monocyte surfaces and binds adhesion molecules on endothelial cells upon endothelial dysfunction (4,44,79), thereby participating in monocyte trafficking to the subendothelium. Although the C1q components can modulate the uptake of atherogenic lipoproteins in the early stages of atherosclerosis, they also have a proinflammatory effect that can accelerate the formation of atherosclerosis (80,81). Moreover, C1q regulates collagen-induced platelet activation, reactive oxygen species (ROS) production, and associated leukocyte recruitment during vessel wall injury (82). Whereas CSF1R, CSF2RB, and MPEG1 promote atherosclerosis by regulating macrophage proliferation, differentiation (83), and increased macrophage content in lesions (84,85). Recently, CTSS was shown to mediate phagosomes during atherosclerosis (86). Moreover, CTSS is also involved in collagen degradation (63). Niyonzima et al. (87) showed that C5AR1 mediates signaling to control IL-1β production, altering mitochondrial activity, and increasing reactive oxygen species production. Additionally, the authors showed that the deletion of C5AR1 in myeloid cells in mice reduced the severity of atherosclerosis (87). Hematopoietic Transcription Factor PU.1 (SPI1) is upregulated during myeloid cell differentiation (88). This is consistent with our observation of the significant increase in SPI1 expression in WMS-FH, further suggesting that the activation of myeloid cells contributes to atherosclerosis. Overall, identified hub genes exhibited upregulation in WMS-FH atherosclerotic aortic tissues. Coupled with pathology results, our findings suggest that these key genes are involved in the transition from atheroma to fibro-atheroma by affecting phagocytosis, leukocyte trafficking and differentiation in addition to the complement and coagulation cascades (Appendix A. Figure 3)

and collagen deposition abnormalities. Further work is needed to elucidate their specific roles and the cascade of events that modulate the phenotypic changes in early lesions.

Given that ITGB2 (CD18) is a top-ranked hub gene, we opted to assess the effect of manipulating its expression on interacting genes to validate the observed expression pattern in RNA-Seq data. Indeed, overexpression of ITGB2 in PAECs increased the expression of the tested interconnecting genes. Therefore, ITGB2 could be a target gene for preventing the progression or onset of atherosclerosis because the gene confers binding of leukocytes to ECs and, subsequently their migration. Previous studies demonstrated that depletion or inhibition of ITGB2 reduced lesion sizes and monocyte trafficking (44,89). Thus, our results suggest a potential therapeutic effect of hub genes.

Study limitations

The present work was limited to whole tissue gene expression analysis instead of single-cell RNA sequencing, which would provide a more precise tracking of the expression profile of each cell type. Additionally, the RNA-Seq of pooled samples did not allow us to investigate gene expression variability between individuals and correlate the findings with lesion phenotypes. Also, in the ITGB2 overexpression study, we only used porcine aortic endothelial cells (PAECs). Assessing one hub gene in single cell culture does not mimic the complexity of atherosclerotic disease. Using additional cell lines could provide further insights into other different mechanistic pathways not identified in this study.

Conclusions

In the WMS-FH, the development of fibroatheromas is predominantly driven by immune and inflammatory-related pathways. RNA-Seq results demonstrated unique differential gene expression patterns between abdominal aortic tissue with atherosclerotic lesions (WMS-FH) and

lesion-free tissues (WMS normal), at the gene and isoform levels. Ten hub genes were identified as potential therapeutic targets. The manipulation of ITGB2 expression, a top-ranked hub gene, in PAECs affected the expression of interconnecting genes. Overall, this study identified key pathways and hub genes for atherosclerosis development in WMS-FH. Importantly, we demonstrated that WMS-FH has remarkable similarities to human atherosclerosis at the levels of gene expression and involved pathways allowing the identification of candidate genes with promising therapeutic potential.

Clinical perspectives

Atherosclerosis is a complex multi-factorial disease involving multiple biological pathways that change during the process of disease progression. Although significant progress has been made in the understanding of the different biological mechanisms involved in atherosclerosis development, the specific cellular events responsible for causing the disease are still unclear. Most of the knowledge gathered today has been based on studies involving either small animal models or human tissue. Small animal models lack the vascular architecture or hemodynamic profile seen in humans. In vivo histopathological studies in humans are typically limited to advanced disease and lack of appropriate control groups. The present study studied the transcriptomic profile of early stage fibroatheromas in a large model of atherosclerosis and compared the results with a control group of animals that are genetically related but not affected by the disease. Our findings identified ten hub genes involved in the process of early fibroatheroma development that could become targets for future research in diagnostics and therapeutics. Our approach provides a unique opportunity to study the mechanisms involved in atherosclerosis development in vivo in a

prospective manner by correlating the phenotypic findings with genetic markers in diseased and healthy study groups.

Visual abstract

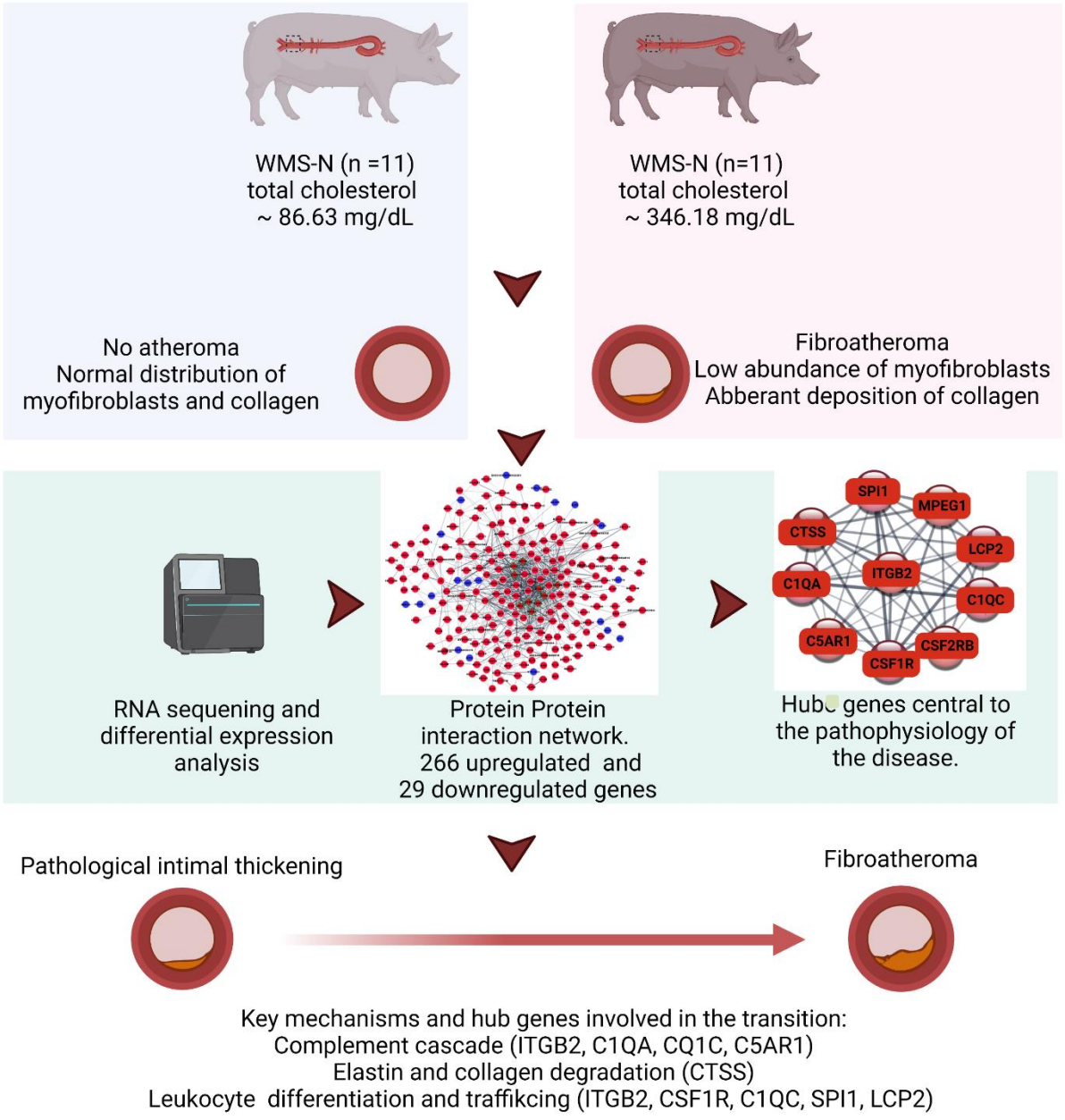

Acknowledgements

We thank the Swine Research Teaching Center staff for their diligent work in caring for the animals and Nell Bekiares for helping with tissue collection and preservation. We also thank Charles Gersbach for donating the dCas9-p300 and psPgRNA plasmids used in this study.

Author Contributions

JG, JR, AP, KG, and HK: Conceived and designed the study. JG, WS, and AP: performed histopathology and data interpretation. HN: performed the experiments, data analysis and interpretations. DS: participated in data interpretation and revised the manuscript. HN, MS, and CB: participated in bioinformatics analysis. HN wrote and revised the manuscript. All the authors contributed to the manuscript and approved the submitted version.

Data availability

https://www.ncbi.nlm.nih.gov/geo/query/acc.cgi?acc=GSE199592

References

1. Mundi S., Massaro M., Scoditti E., et al. Endothelial permeability, LDL deposition, and cardiovascular risk factors-A review. Cardiovasc Res 2018;114(1):35–52. Doi: 10.1093/cvr/cvx226.

2. Tavares JC., Muscará MN. Adhesion Molecules and Endothelium. Endothelium and Cardiovascular Diseases: Vascular Biology and Clinical Syndromes 2018:189–201. Doi: 10.1016/B978-0-12-812348-5.00014-3.

3. Fuhrman B., Partoush A., Volkova N., Aviram M. Ox-LDL induces monocyte-to-macrophage differentiation in vivo: Possible role for the macrophage colony stimulating factor receptor (M-CSF-R). Atherosclerosis 2008;196(2):598–607. Doi: 10.1016/j.atherosclerosis.2007.06.026.

4. Fernando S., Bursill CA., Nicholls SJ., Psaltis PJ. Pathophysiology of atherosclerosis. Mechanisms of Vascular Disease. Springer Nature Switzerland; 2020. p. 19–45.

5. Mohanta SK., Weber C., Yin C., Habenicht AJR. The dawn has come for new therapeutics to treat atherosclerosis: Targeting neuroimmune cardiovascular interfaces in artery brain circuits. Clin Transl Med 2022;12(9). Doi: 10.1002/ctm2.1040.

6. Márquez AB., van der Vorst EPC., Maas SL. Key chemokine pathways in atherosclerosis and their therapeutic potential. J Clin Med 2021. Doi: 10.3390/jcm10173825.

7. Yurdagul A. Crosstalk Between Macrophages and Vascular Smooth Muscle Cells in Atherosclerotic Plaque Stability. Arterioscler Thromb Vasc Biol 2022:ATVBAHA121316233. Doi: 10.1161/ATVBAHA.121.316233.

8. Hetherington I., Totary-Jain H. Anti-atherosclerotic therapies: Milestones, challenges, and emerging innovations. Molecular Therapy 2022;30(10):3106–17. Doi: 10.1016/j.ymthe.2022.08.024.

9. Bäck M., Hansson G. Basic Mechanisms of Atherosclerosis. Chronic Coronary Artery Disease: A Companion to Braunwald's Heart Disease. Elsevier Inc.; 2018. p. 45–54.

10. Hasler-Rapacz J., Ellegren H., Fridolfsson a K., et al. Identification of a mutation in the low density lipoprotein receptor gene associated with recessive familial hypercholesterolemia in swine. Am J Med Genet 1998. Doi: 10.1002/(SICI)1096-8628(19980413)76:5<379::AID-AJMG3>3.0.CO;2-I.

11. Schomberg DT., Tellez A., Meudt JJ., et al. Miniature Swine for Preclinical Modeling of Complexities of Human Disease for Translational Scientific Discovery and Accelerated Development of Therapies and Medical Devices. Toxicol Pathol 2016;44(3):299–314. Doi: 10.1177/0192623315618292.

12. Hasler-Rapacz J., Prescott MF., von Linden-Reed J., Rapacz JM., Hu Z., Rapacz J. Elevated concentrations of plasma lipids and apolipoproteins B, C-III, and E are associated with the progression of coronary artery disease in familial hypercholesterolemic swine. Arterioscler Thromb Vasc Biol 1995;15(5):583–92. Doi: 10.1161/01.ATV.15.5.583/FORMAT/EPUB.

13. Schinkel AFL., Krueger CG., Tellez A., et al. Contrast-enhanced ultrasound for imaging vasa vasorum: comparison with histopathology in a swine model of atherosclerosis. European Journal of Echocardiography 2010;11(8):659–64. Doi: 10.1093/ejechocard/jeq048.

14. Bahls M., Bidwell CA., Hu J., et al. Gene expression differences in healthy brachial and femoral arteries of Rapacz familial hypercholesterolemic swine. Physiol Genomics 2011;43(12):781–8. Doi: 10.1152/physiolgenomics.00151.2010.

15. Bahls M., Bidwell CA., Hu J., et al. Gene expression differences during the heterogeneous progression of peripheral atherosclerosis in familial hypercholesterolemic swine 2013. Doi: 10.1186/1471-2164-14-443.

16. Thim T., Hagensen MK., Drouet L., et al. Familial hypercholesterolaemic downsized pig with human-like coronary atherosclerosis: a model for preclinical studies. EuroIntervention 2010;6(2):261–8. Doi: 10.4244/.

17. Tellez A., Krueger CG., Seifert P., et al. Coronary bare metal stent implantation in homozygous LDL receptor deficient swine induces a neointimal formation pattern similar to humans. Atherosclerosis 2010;213(2):518–24. Doi: 10.1016/j.atherosclerosis.2010.09.021.

18. Tellez A., Seifert PS., Donskoy E., et al. Experimental evaluation of efficacy and healing response of everolimus-eluting stents in the familial hypercholesterolemic swine model: A comparative study of bioabsorbable versus durable polymer stent platforms. Coron Artery Dis 2014;25(3):198–207. Doi: 10.1097/MCA.0000000000000099.

19. Granada JF., Milewski K., Zhao H., et al. Vascular response to zotarolimus-coated balloons in injured superficial femoral arteries of the familial hypercholesterolemic swine. Circ Cardiovasc Interv 2011;4(5):447–55. Doi: 10.1161/CIRCINTERVENTIONS.110.960260.

20. Nih., Od., Oer., Olaw. GUIDE LABORATORY ANIMALS FOR THE CARE AND USE OF Eighth Edition Committee for the Update of the Guide for the Care and Use of Laboratory Animals Institute for Laboratory Animal Research Division on Earth and Life Studies. THE NATIONAL ACADEMIES PRESS 2011:1–209.

21. Animal Welfare Act as Amended. . 7 USC § 2013:2132–59.

22. Langmead B., Salzberg SL. Fast gapped-read alignment with Bowtie 2. Nat Methods 2012;9(4):357–9. Doi: 10.1038/nmeth.1923.

23. Li B., Dewey CN. RSEM: Accurate transcript quantification from RNA-Seq data with or without a reference genome. BMC Bioinformatics 2011;12(1):1–16. Doi: 10.1186/1471-2105-12-323/TABLES/6.

24. Robinson MD., Mccarthy DJ., Smyth GK. edgeR: a Bioconductor package for differential expression analysis of digital gene expression data. BIOINFORMATICS APPLICATIONS NOTE 2010;26(1):139–40. Doi: 10.1093/bioinformatics/btp616.

25. Shen S., Won Park J., Lu Z., et al. rMATS: Robust and flexible detection of differential alternative splicing from replicate RNA-Seq data n.d.;16:2022. Doi: 10.1073/pnas.1419161111.

26. Livak KJ., Schmittgen TD. Analysis of relative gene expression data using real-time quantitative PCR and the 2-ΔΔCT method. Methods 2001;25(4):402–8. Doi: 10.1006/meth.2001.1262.

27. Szklarczyk D., Franceschini A., Wyder S., et al. STRING v10: Protein-protein interaction networks, integrated over the tree of life. Nucleic Acids Res 2015;43(D1):D447–52. Doi: 10.1093/nar/gku1003.

28. Bindea G., Mlecnik B., Hackl H., et al. ClueGO: a Cytoscape plug-in to decipher functionally grouped gene ontology and pathway annotation networks. BIOINFORMATICS APPLICATIONS NOTE 2009;25(8):1091–3. Doi: 10.1093/bioinformatics/btp101.

29. Chin CH., Chen SH., Wu HH., Ho CW., Ko MT., Lin CY. cytoHubba: Identifying hub objects and sub-networks from complex interactome. BMC Syst Biol 2014;8(4). Doi: 10.1186/1752-0509-8-S4-S11.

30. Haeussler M., Schönig K., Eckert H., et al. Evaluation of off-target and on-target scoring algorithms and integration into the guide RNA selection tool CRISPOR. Genome Biol 2016;17(1):1–12. Doi: 10.1186/s13059-016-1012-2.

31. Nadkarni SK., Pierce MC., Park BH., et al. Measurement of Collagen and Smooth Muscle Cell Content in Atherosclerotic Plaques Using Polarization-Sensitive Optical Coherence Tomography. J Am Coll Cardiol 2007;49(13):1474–81. Doi: 10.1016/j.jacc.2006.11.040.

32. Tan X., Zhang X., Pan L., Tian X., Dong P. Identification of Key Pathways and Genes in Advanced Coronary Atherosclerosis Using Bioinformatics Analysis. Biomed Res Int 2017;2017(5):1–12. Doi: 10.1155/2017/4323496.

33. Li Z., Hao J., Chen K., et al. Identification of key pathways and genes in carotid atherosclerosis through bioinformatics analysis of RNA-seq data. Aging 2021;13(9):12733–47. Doi: 10.18632/aging.202943.

34. Yang R., Yao L., Du C., Wu Y. Identification of key pathways and core genes involved in atherosclerotic plaque progression. Ann Transl Med 2021;9(3):267–267. Doi: 10.21037/atm-21-193.

35. Cochain C., Vafadarnejad E., Arampatzi P., et al. Single-cell RNA-seq reveals the transcriptional landscape and heterogeneity of aortic macrophages in murine atherosclerosis. Circ Res 2018;122(12):1661–74. Doi: 10.1161/CIRCRESAHA.117.312509.

36. Fernandez DM., Rahman AH., Fernandez NF., et al. Single-cell immune landscape of human atherosclerotic plaques. Nat Med 2019;25(10):1576–88. Doi: 10.1038/s41591-019-0590-4.

37. Depuydt MAC., Prange KHM., Slenders L., et al. Microanatomy of the Human Atherosclerotic Plaque by Single-Cell Transcriptomics. Circ Res 2020;127(11):1437–55. Doi: 10.1161/CIRCRESAHA.120.316770.

38. Ma WF., Hodonsky CJ., Turner AW., et al. Enhanced single-cell RNA-seq workflow reveals coronary artery disease cellular cross-talk and candidate drug targets. Atherosclerosis 2022;340:12–22. Doi: 10.1016/j.atherosclerosis.2021.11.025.

39. Liao S., Bodmer J., Pietras D., Azhar M., Doetschman T., Schultz JEJ. Biological functions of the low and high molecular weight protein isoforms of fibroblast growth factor-2 in cardiovascular development and disease. Dev Dyn 2009;238(2):249–64. Doi: 10.1002/DVDY.21677.

40. Zhu C., Wu J., Sun H., et al. Single-molecule, full-length transcript isoform sequencing reveals disease-associated RNA isoforms in cardiomyocytes. Nat Commun 2021;12(1). Doi: 10.1038/S41467-021-24484-Z.

41. Lundberg AK., Jonasson L., Hansson GK., Mailer RKW. Activation-induced FOXP3 isoform profile in peripheral CD4+ T cells is associated with coronary artery disease. Atherosclerosis 2017;267:27–33. Doi: 10.1016/J.ATHEROSCLEROSIS.2017.10.026.

42. Wang B., Yang · Xi., Sun X., et al. ATF3 in atherosclerosis: a controversial transcription factor. Journal of Molecular Medicine 2022 2022;1:1–12. Doi: 10.1007/S00109-022-02263-7.

43. Huo T-M., Wang Z-W. Comprehensive Analysis to Identify Key Genes Involved in Advanced Atherosclerosis 2021. Doi: 10.1155/2021/4026604.

44. Schenkel AR., Mamdouh Z., Muller WA. Locomotion of monocytes on endothelium is a critical step during extravasation. Nature Immunology 2004 5:4 2004;5(4):393–400. Doi: 10.1038/ni1051.

45. Olson TS., Ley K. Chemokines and chemokine receptors in leukocyte trafficking. American Journal of Physiology-Regulatory, Integrative and Comparative Physiology 2002;283(1):R7–28. Doi: 10.1152/ajpregu.00738.2001.

46. Rader DJ., Puré E. Lipoproteins, macrophage function, and atherosclerosis: Beyond the foam cell? Cell Metab 2005:223–30. Doi: 10.1016/j.cmet.2005.03.005.

47. Luo Y., Duan H., Qian Y., et al. Macrophagic CD146 promotes foam cell formation and retention during atherosclerosis. Cell Res 2017;27(3):352–72. Doi: 10.1038/cr.2017.8.

48. Marques ARA., Ramos C., Machado-Oliveira G., Vieira O v. Lysosome (Dys)function in Atherosclerosis—A Big Weight on the Shoulders of a Small Organelle. Front Cell Dev Biol 2021. Doi: 10.3389/fcell.2021.658995.

49. Tontonoz P., Nagy L., Alvarez JGA., Thomazy VA., Evans RM. PPARγ promotes monocyte/macrophage differentiation and uptake of oxidized LDL. Cell 1998;93(2):241–52. Doi: 10.1016/S0092-8674(00)81575-5.

50. Li Y., Zhu H., Zhang Q., et al. Smooth muscle-derived macrophage-like cells contribute to multiple cell lineages in the atherosclerotic plaque. Cell Discov 2021. Doi: 10.1038/s41421-021-00328-4.

51. Basatemur GL., Jørgensen HF., Clarke MCH., Bennett MR., Mallat Z. Vascular smooth muscle cells in atherosclerosis. Nat Rev Cardiol 2019;16(12):727–44. Doi: 10.1038/s41569-019-0227-9.

52. Bennett MR., Sinha S., Owens GK. Vascular Smooth Muscle Cells in Atherosclerosis. Circ Res 2016;118(4):692–702. Doi: 10.1161/CIRCRESAHA.115.306361.

53. Grootaert MOJ., Moulis M., Roth L., et al. Vascular smooth muscle cell death, autophagy and senescence in atherosclerosis. Cardiovasc Res 2018;114(4):622–34. Doi: 10.1093/cvr/cvy007.

54. Grootaert MOJ., Bennett MR. Vascular smooth muscle cells in atherosclerosis: Time for a re-assessment. Cardiovasc Res 2021:2326–39. Doi: 10.1093/cvr/cvab046.

55. Chinetti-Gbaguidi G., Daoudi M., Rosa M., et al. Human Alternative Macrophages Populate Calcified Areas of Atherosclerotic Lesions and Display Impaired RANKL-Induced Osteoclastic Bone Resorption Activity. Circ Res 2017;121(1):19–30. Doi: 10.1161/CIRCRESAHA.116.310262.

56. Adeva-Andany MM., Adeva-Contreras L., Fernández-Fernández C., González-Lucán M., Funcasta-Calderón R. Elastic tissue disruption is a major pathogenic factor to human vascular disease. Mol Biol Rep 2021:4865–78. Doi: 10.1007/s11033-021-06478-8.

57. Krishnan P., Purushothaman KR., Purushothaman M., et al. Relation of internal elastic lamellar layer disruption to neointimal cellular proliferation and type III collagen deposition in human peripheral artery restenosis. American Journal of Cardiology 2016;117(7):1173–9. Doi: 10.1016/j.amjcard.2016.01.006.

58. Coen M., Gabbiani G., Bochaton-Piallat ML. Myofibroblast-mediated adventitial remodeling: an underestimated player in arterial pathology. Arterioscler Thromb Vasc Biol 2011;31(11):2391–6. Doi: 10.1161/ATVBAHA.111.231548.

59. Gibb AA., Lazaropoulos MP., Elrod JW. Myofibroblasts and fibrosis: Mitochondrial and metabolic control of cellular differentiation. Circ Res 2020:427–47. Doi: 10.1161/CIRCRESAHA.120.316958.

60. Zhang L., Chen Y., Li G., et al. TGF-β1/FGF-2 signaling mediates the 15-HETE-induced differentiation of adventitial fibroblasts into myofibroblasts. Lipids Health Dis 2016;15(1):1–8. Doi: 10.1186/S12944-015-0174-3/FIGURES/5.

61. Singh., Torzewski. Fibroblasts and Their Pathological Functions in the Fibrosis of Aortic Valve Sclerosis and Atherosclerosis. Biomolecules 2019;9(9):472. Doi: 10.3390/biom9090472.

62. Galis ZS., Sukhova GK., Lark MW., Libby P. Increased expression of matrix metalloproteinases and matrix degrading activity in vulnerable regions of human atherosclerotic plaques. Journal of Clinical Investigation 1994;94(6):2493. Doi: 10.1172/JCI117619.

63. Klaus V., Schmies F., Reeps C., et al. Cathepsin S is associated with degradation of collagen I in abdominal aortic aneurysm. Vasa 2018;47(4):285–93. Doi: 10.1024/0301-1526/a000701.

64. Smith KA., Lin AH., Stevens AH., Yu SM., Weiss JA., Timmins LH. Collagen Molecular Damage is a Hallmark of Early Atherosclerosis Development. J Cardiovasc Transl Res 2022. Doi: 10.1007/s12265-022-10316-y.

65. Misra A., Rehan R., Lin A., Patel S., Fisher EA. Emerging Concepts of Vascular Cell Clonal Expansion in Atherosclerosis. Arterioscler Thromb Vasc Biol 2022:E74–84. Doi: 10.1161/ATVBAHA.121.316093.

66. Wang Y., Nanda V., Direnzo D., et al. Clonally expanding smooth muscle cells promote atherosclerosis by escaping efferocytosis and activating the complement cascade. PNAS 2022;117(27). Doi: 10.1073/pnas.2006348117/-/DCSupplemental.

67. Wirka RC., Wagh D., Paik DT., et al. Atheroprotective roles of smooth muscle cell phenotypic modulation and the TCF21 disease gene as revealed by single-cell analysis. Nat Med 2019;25(8):1280–9. Doi: 10.1038/s41591-019-0512-5.

68. Zhao H., Chen L., He C., et al. Chronic staphylococcus aureus superantigen toxic shock syndrome toxin-1 exposure accelerates the progression of atherosclerosis in rabbits. Acta Cardiol Sin 2020;36(1):24–32. Doi: 10.6515/ACS.202001_36(1).20190611B.

69. Frodermann V., van Duijn J., van Puijvelde GHM., et al. Heat-Killed staphylococcus aureus reduces atherosclerosis by inducing anti-inflammatory macrophages. J Intern Med 2016;279(6):592–605. Doi: 10.1111/joim.12484.

70. Sawicka-smiarowska E., Bondarczuk K., Bauer W., et al. Gut microbiome in chronic coronary syndrome patients. J Clin Med 2021;10(21). Doi: 10.3390/jcm10215074.

71. Xu J., Yang Y. Implications of gut microbiome on coronary artery disease. Cardiovasc Diagn Ther 2020;10(4):869–80. Doi: 10.21037/cdt-20-428.

72. Ahmad AF., Dwivedi G., O'gara F., Caparros-Martin J., Ward NC. The gut microbiome and cardiovascular disease: current knowledge and clinical potential. Am J Physiol Heart Circ Physiol 2019;317:923–38. Doi: 10.1152/ajpheart.00376.2019.-Cardiovascular.

73. Xu J., Yang Y. Potential genes and pathways along with immune cells infiltration in the progression of atherosclerosis identified via microarray gene expression dataset re-analysis. Vascular 2020;28(5):643–54. Doi: 10.1177/1708538120922700.

74. Wan Z., Zhao B., Zhang X., Zhao Y. Drug discovery in cardiovascular disease identified by text mining and data analysis. Ann Cardiothorac Surg 2020;9(5):3089–99. Doi: 10.21037/apm-20-705.

75. Zhao B., Wang D., Liu Y., et al. Six-Gene Signature Associated with Immune Cells in the Progression of Atherosclerosis Discovered by Comprehensive Bioinformatics Analyses. Cardiovasc Ther 2020;2020. Doi: 10.1155/2020/1230513.

76. Shen Y., Xu L rong., Tang X., et al. Identification of potential therapeutic targets for atherosclerosis by analysing the gene signature related to different immune cells and immune regulators in atheromatous plaques. BMC Med Genomics 2021;14(1). Doi: 10.1186/s12920-021-00991-2.

77. Meng Y., Zhang C., Liang L., et al. Identification of Potential Key Genes Involved in the Carotid Atherosclerosis. Clin Interv Aging 2021;16:1071–84. Doi: 10.2147/CIA.S312941.

78. Xu J., Chen C., Yang Y. Identification and Validation of Candidate Gene Module Along With Immune Cells Infiltration Patterns in Atherosclerosis Progression to Plaque Rupture via Transcriptome Analysis. Front Cardiovasc Med 2022;9. Doi: 10.3389/fcvm.2022.894879.

79. Meerschaert J., Furie MB. ligands on endothelium. monocytes and ICAM-1, VCAM-1, and other CD11a/CD18, CD11b/CD18, and VLA-4 on migration across endothelium include The adhesion molecules used by monocytes for. 1995.

80. Bhatia VK., Yun S., Leung V., et al. Complement C1q Reduces Early Atherosclerosis in Low-Density Lipoprotein Receptor-Deficient Mice. Am J Pathol 2007;170(1):416–26. Doi: 10.2353/AJPATH.2007.060406.

81. Speidl WS., Kastl SP., Huber K., Wojta J. Complement in atherosclerosis: friend or foe? Journal of Thrombosis and Haemostasis 2011;9(3):428–40. Doi: 10.1111/J.1538-7836.2010.04172.X.

82. Skoglund C., Wetterö J., Bengtsson T. C1q regulates collagen-dependent production of reactive oxygen species, aggregation and levels of soluble P-selectin in whole blood. Immunol Lett 2012;142(1–2):28–33. Doi: 10.1016/J.IMLET.2011.11.003.

83. Wei Y., Zhu M., Corbalán-Campos J., Heyll K., Weber C., Schober A. Regulation of Csf1r and Bcl6 in macrophages mediates the stage-specific effects of MicroRNA-155 on atherosclerosis. Arterioscler Thromb Vasc Biol 2015;35(4):796–803. Doi: 10.1161/ATVBAHA.114.304723.

84. Wang M., Subramanian M., Abramowicz S., et al. Interleukin-3/granulocyte macrophage colony-stimulating factor receptor promotes stem cell expansion, monocytosis, and atheroma macrophage burden in mice with hematopoietic ApoE deficiency. Arterioscler Thromb Vasc Biol 2014;34(5):976–84. Doi: 10.1161/ATVBAHA.113.303097.

85. Spilsbury K., O'Mara MA., Wu WM., Rowe PB., Symonds G., Takayama Y. Isolation of a novel macrophage-specific gene by differential cDNA analysis. Blood 1995;85(6):1620–9.

86. Wang H., Jiang H., Cheng XW. Cathepsin S are involved in human carotid atherosclerotic disease progression, mainly by mediating phagosomes: bioinformatics and in vivo and vitro experiments. PeerJ 2022;10:e12846. Doi: 10.7717/peerj.12846.

87. Niyonzima N., Rahman J., Kunz N., et al. Mitochondrial C5aR1 activity in macrophages controls IL-1β production underlying sterile inflammation. Sci Immunol 2021;6(66). Doi: 10.1126/sciimmunol.abf2489.

88. Wittwer J., Marti-Jaun J., Hersberger M. Functional polymorphism in ALOX15 results in increased allele-specific transcription in macrophages through binding of the transcription factor SPI1. Hum Mutat 2006;27(1):78–87. Doi: 10.1002/HUMU.20273.

89. Nageh MF., Sandberg ET., Marotti KR., et al. Deficiency of inflammatory cell adhesion molecules protects against atherosclerosis in mice. Arterioscler Thromb Vasc Biol 1997;17(8):1517–20. Doi: 10.1161/01.ATV.17.8.1517/FORMAT/EPUB.

CHAPTER THREE: CIRCULATING MIRNA DYNAMICS IN WISCONSIN MINIATURE SWINE™ OF FAMILIAL HYPERCHOLESTEROLEMIA: POTENTIAL BIOMARKERS FOR EARLY DIAGNOSIS OF CORONARY ARTERY DISEASE

Manuscript in preparation

Hadjer Namous, Christian Kreuger, Athanasios Peppas, Jess Reed, Hasan Khatib, Juan F. Granada.

Corresponding authors
Juan Granada
Hasan Khatib

Abstract

Background: Atherosclerosis is a slowly progressive disease that spans decades, often without a diagnosis until major cardiac events occur (e.g., stroke). In this work, we used the Wisconsin Miniature Swine (WMS) model of atherosclerosis in a longitudinal study to identify circulating miRNA signatures in the early life of animals before the disease is known to be present.

Methods: 18 female pigs were selected, nine were familial hypercholesterolemic (WMS-FH), and nine were normal (WMS-N). Plasma was collected at months 3, 6, and 9 of age. miRNA sequencing was carried out on plasma cell-free RNA. Bioinformatic analysis was performed to identify differentially expressed (DE) miRNAs. DE miRNAs with similar sequences to human-known miRNAs were used to determine mRNA targets and biological processes. Optical Coherence Tomography (OCT) was performed to determine the presence/absence of atherosclerosis in animals. The Receiver Operating Characteristic Curve (ROC) analysis with Area Under the Curve (AUC) was used to assess the discriminatory power of identified miRNAs. RT-qPCR validated DE miRNAs in a new cohort of animals with both sexes.

Results: 20, 19, and 9 miRNAs were significantly differentially expressed between WMS-FH and WMS-N at months 3, 6, and 9, respectively. Gene ontology enrichment showed that DE miRNAs and their target genes are involved in biological processes like cholesterol homeostasis, inflammatory responses, foam cell formation, endothelial dysfunction, smooth muscle cell proliferation and migration, and amyloid beta clearance. OCT results showed the presence of atherosclerosis in seven out of nine WMS-FH in the coronary arteries. WMS-N presented no lesions. The discriminatory power analysis showed that miR-138, miR-152, miR-190a, and miR-196a have significant diagnostic power at 3 months of age, whereas miR-486, miR-126-3p, miR-

335, and miR-423-5p were of significant diagnostic power at month 9. Month 6 DE miRNAs did not show significant discriminatory power for atherosclerosis diagnosis.

Conclusion: As measured by OCT, circulating miRNA dynamics change over time between animals with and without coronary atherosclerosis. Some DE miRNAs showed significant discriminatory power at months 3 and 9. Therefore, these miRNAs are promising biomarkers for early diagnosis of atherosclerosis in the coronary arteries.

Keywords: Atherosclerosis, miRNAs, biomarkers, diagnosis

Introduction

Atherosclerosis is a chronic condition that develops slowly over decades. As a result, the disease often goes undiagnosed until clinical manifestations arise, such as stroke and ischemic heart disease. Stroke and ischemic heart disease contribute to the highest mortality worldwide (1,2). The slow progression of atherosclerosis presents a critical window of time for early detection when the disease is in its early stages. In addition, early detection confers an advantage in mitigating disease development. Thus, diagnostic biomarkers are needed.

Traditionally, lipid biomarkers, such as LDL-cholesterol, were used to assess disease susceptibility. However, these markers could not explain why CVD events occur in individuals with normal cholesterol levels (3). Additionally, although effective in many cases, drugs used to lower cholesterol levels (e.g., statins) do not guarantee protection against the disease (4). They may exert adverse effects, such as promoting atheroma calcification (5–7). Other proposed biomarkers like serum C-reactive protein (CRP), interleukin-6 (IL-6), and tumor necrosis factor-alpha (TNFα) showed promising results in predicting cardiac events (8–10). However, some of these molecules showed a significant correlation in males but not females (8). Moreover, no significant associations were observed between atherosclerosis and other proposed biomarkers (fibrinogen, ICAM1, IL-6, IL-18, MCP-1, lipoprotein-associated phospholipase-A2 (Lp-PLA2), and P-selectin (11). These findings emphasize the current limitations and the need for more studies to validate proposed biomarkers and discover new ones.

MicroRNAs (miRNAs) are also promising biomarkers for atherosclerosis. Ample evidence in the literature reported that miRNAs play a role in CVDs (12–15), making them appealing markers and treatment targets for atherosclerosis. However, human studies of circulating miRNAs assess or identify miRNA biomarkers in cohorts with clinical manifestations of the disease

(12,16,17), which is in later stages. In later stages, atherosclerosis diagnosis limits successful interventions because the arterial wall is altered, and lesion regression will not ensue. Additionally, longitudinal studies aimed at the early characterization of miRNA biomarkers are scarce. Moreover, animal models that have been used to study the disease are mostly small ones. While these animal models have been and continue to be critical in elucidating the mechanisms underlying atherosclerosis, the inherent differences in lipoprotein profile, disease distribution, and complexity limit the interpretation and translational potential of the findings (18–20). As such, larger animal models can be employed to address these shortcomings.

Among large animal models of atherosclerosis, swine models have been utilized in various studies (21–25). In the present work, we used the Wisconsin Miniature Swine™ of Familial hypercholesterolemia (WMS-FH) to study circulating miRNA dynamics in the early life of pigs before atherosclerosis is known to occur. We aimed to identify miRNA signatures that are specific to atherosclerosis and evaluate their diagnostic power. WMS-FH pigs are hypercholesterolemic because the low-density lipoprotein (LDL) pathway is dysregulated. The dysregulation is due to a one-point mutation in the ligand region of the low-density lipoprotein receptor (LDLR) (23,26). The excess levels of LDL in the circulation leads to the development of atherosclerosis in these pigs. WMS-FH develops human-like complex lesions starting at 12 months (27–30). They also exhibit altered gene expression profiles in the aortic tissue as early as 13 days old (29). Atherosclerosis progression and response to interventional vascular treatments have been well documented for this animal model (31–34).

Plasma miRNA levels were assessed at three different time points (3, 6, and 9 months of age). Then, we identified differentially expressed (DE) miRNAs between WMS-FH and WMS-N pigs. Around 12 months old, the presence and location of atherosclerosis was determined using

Optical Coherence Tomography (OCT). Then, we determined the diagnostic power of each miRNA in discriminating between presence and absence of atherosclerosis. Gene ontology (GO) and mRNA targets of DE miRNAs were identified to understand the mechanisms in place during early onset of the disease.

Methods

Ethics statement

The study was approved by the IACUC at the University of Wisconsin-Madison in compliance with the *Guide for the Care and Use for Laboratory Animals* (35) and the Animal Welfare Act (36).

Animals

Two cohorts of the Wisconsin Mini Swine™ of Familial Hypercholesterolemia (WMS-FH) and WMS normal (WMS-N) were selected for this study. WMS-N pigs have the same genetic background as WMS-FH; however, these pigs are normocholesterolemic with a completely functional LDLR. Cohort 1 had nine WMS-FH (females) and nine WMS-N (females). In the second cohort, 15 WMS-FH (females n = 8, males n = 7) and 15 WMS-N(females n= 8, males n = 7) were selected. Animals were randomly selected for the study and were housed with the main herd at the Swine Research and Teaching Center (SRTC) at the University of Wisconsin-Madison throughout the duration of the study. All animals were fed the same diet formulated to meet the nutritional requirements of swine (Appendix A. Table 1). Cohort 1 animals was used to profile plasma cell-free RNAs using small-RNA sequencing and identify DE miRNAs, whereas cohort 2 animals were used for biological validation in RT-qPCR.

Blood collection and plasma processing

Whole blood was collected at 3, 6, and 9 months from each animal in 8 mL K3 EDTA tubes (Covidien, MA, USA). Then, blood tubes were centrifuged at 4 °C for 10 minutes to separate plasma. Next, the collected plasma was centrifuged using the same settings to remove any cellular debris. Samples were then preserved in 1.5 mL tubes at -80 °C until needed.

The three-time points were selected based on previous data showing the progression of atherosclerotic lesions in coronary and aortic arteries and the cholesterol profiles of WMS-FH pigs. Month 3 was selected as an early time point before serum cholesterol levels peak and stabilize. Total cholesterol then peaks around month 6 and stabilizes around month 9.

Optical coherence tomography (OCT) imaging was performed in cohort 1 animals (~ 12 months of age) to determine the presence and location of atherosclerosis.

Hemolysis and total cholesterol measurements

Studies have shown that hemolysis considerably affects the levels of cell-free miRNAs (37). To correct for this effect, we measured hemolysis in plasma samples by assessing absorbance at A414 using NanodropONE spectrophotometry (Thermofisher Scientific, DE, USA). For each sample, the average of at least three measurements was calculated. The A414 absorbance values were used as a covariate in statistical analysis to assess the differential expression of miRNAs.

Total cholesterol levels were measured in plasma samples using ELISA Cholesterol Assay Kit - HDL and LDL/VLDL (Abcam, CA, USA) following the product's manual. Plasma samples from WMS-FH were diluted (2-fold) so that colorimetric readings fell within the range of cholesterol standard curve.

miRNA extraction

Cell-free RNA (cf-RNA) was extracted from plasma samples using Quick-cfRNA Serum & Plasma Kit (Zymo Search, CA, USA). Briefly, plasma samples were centrifuged at 12,000 g for 15 minutes to remove cellular debris, then 400 uL of plasma was digested for 2 hours at 37°C using proteinase K. After digestion, the remaining steps were followed as are described in the manufacturer's manual. To obtain concentrated samples, we eluted the column content in 10 uL of nuclease free water. For biological validation samples used in RT-qPCR (cohort 2 of animals), cel-miR-39 mimic (QIAGEN) was spiked in each sample after 2 hours of digestion to assess extraction efficiency and consistency across samples.

Small RNA sequencing and miRNA differential expression analysis

Small RNA sequencing was performed by RealSeq-Biosciences (CA, USA). Library preparation was carried out using the RealSeq-Biofluids library prep kit (RealSeq Biosciences). Libraries were then sequenced on a NextSeq 500 v2 High-Output with a read length of 75 bp in one direction (single read).

Both raw and trimmed fastq files were obtained from RealSeq-Biosciences. For each file, FastQC (38) was used to assess sequencing quality. We performed bioinformatics analysis using OASIS for small RNA sequencing pipeline (39). Briefly, trimmed reads were aligned to the swine miRNA database and reference genome (Sus Scrofa ssc3), using STAR (40). Next, using DESeq2 (41), the obtained mapped raw reads were normalized, and differential expression was performed following the negative binomial generalized linear regression model. The regression model included hemolysis in plasma samples, weight of animals and grouping (WMS-FH vs WMS-N) for each time point (M3, M6 or M9). Time course analysis to detect changes in miRNA expression within individual animals and between groups included the age of animal as an additional variable

(M3, M6 or M9). Only miRNAs with adjusted p-value < 0.1 were considered significantly differentially expressed between WMS-FH and WMS-N.

miRNA target prediction and Gene Ontology

To assess the biological function of the differentially expressed miRNAs, we predicted the miRNA targets and miRNA functions via Gene Ontology (GO). Swine differentially expressed miRNA sequences were blasted against the human miRNAs using the miRBase database (42), to check for sequence similarity. Human miRNAs that are (>90%) similar in sequence to the swine miRNAs were used to search for mRNA targets available in the database of validated miRNA-target interactions (miRTarBase) (43). GO terms for each miRNA were obtained using miRBase database (42).

Validation of DE miRNAs in a new cohort of animals via RT-qPCR

We selected a subset of DE miRNAs for validation in a new cohort of animals. Selection criteria were based on expression pattern (up/downregulation), early time point of detection (month 3, or 6) and detection at multiple time points (months 3, 6, and 9). A total of 30 samples (cohort 2) were used to validate DE miRNAs. For each plasma sample, 2 uL of extracted cf-RNAs were used in cDNA synthesis with MIRCURY LNA RT kit (QIAGEN, CA, USA). Additionally, each cDNA reaction was spiked in with UniSp6 to assess a consistent cDNA synthesis across all samples. MIRCURY LNA assay primers were obtained from QIAGEN. MIRCURY LNA SYBR Green assay kit (QIAGEN) was used to assess the expression of miRNAs. Also, two miRNA endogenous controls (bta-miR-93 and miR-17-3p) were used to normalize expression results. The endogenous controls were selected based on stability of multiple miRNAs using Normfinder (44). miR-17-3p showed high stability in all sequenced samples.

cf-RNA extraction was repeated for samples showing variability of cel-miR-39 and UniSp6 expression.

The common base method (45) was used to assess differential expression, where each well of the RT-qPCR assay efficiency was incorporated in the final calculation of the ΔΔCT method (46).

Discriminatory power analysis

To determine the diagnostic power of our miRNAs, we performed a discriminatory power analysis using the ROC curves of the pROC R package (47). First, animals were categorized into "healthy" and "with disease" based on OCT imaging. Only significantly differentially expressed miRNAs obtained with DESeq2 from each time point were used in this step. Next, we used normalized sequencing reads for each miRNA to measure the area under the curve (AUC), the confidence interval, and significance level. Due to the small sample size, we determined those miRNAs with AUCs that show a statistical power of 0.95 and 0.8 with $\alpha = 0.05$.

Statistical analysis

For miRNA sequencing data, DE miRNAs and statistical significance were determined using a negative binomial regression model that included the following covariables : hemolysis, weight, and group (WMS-FH vs. WMS-N). For RT-qPCR gene expression, a general linear regression model was used to determine the statistical significance in miRNA differences between WMS-FH and WMS-N with animal weight, plasma hemolysis, and sex of animals as variables using the R programming language (48). Finally, the statistical significance of the AUC was estimated using *power.roc.test* function in pROC package (47).

Results

Characteristics of recruited animals

The characteristics of the animals used for small RNA sequencing are summarized in Table 1. No significant differences were observed between WMS-FH and WMS-N in the weight category. However, total cholesterol levels, across the three-time points, were higher in WMS-FH compared to WMS-N ($p < 0.001$), which is anticipated given that WMS-FH animals harbor a mutation at the LDLR (49) preventing these animals from clearing circulating cholesterol. We also observed high variability in total cholesterol levels between the individuals within the WMS-FH group (Table 1, Figure 1). Total cholesterol levels in WMS-FH increased from 281.75 mg/dL at month 3 to 436,9 mg/dL (month 3 vs. month 6, $p < 0.05$) at month 6 and stabilized at month 9 (month 6 vs. month 9, $p > 0.1$).

Table1. Characteristics of the animal cohort used for miRNA sequencing.

Variables	**WMS-FH**			**WMS-N**		
	Month3	Month6	Month9	Month3	Month6	Month9
Age [ns] (Months, mean ± SD)	03.03± 0.08	6.06± 0.06	9.16± 0.02	2.98± 0.08	5.97± 0.10	9.10± 0.10
Weight[ns] (kg, mean ± SD)	15.16± 2.32	26.73± 5.46	38.67± 9.66	14.48± 3.21	25.19± 4.20	42.27± 8.11
Total cholesterol* ** (mg/dL, mean ± SD)	281.75± 89.86	436.9± 142.95	436.77± 238.99	81.52±2 0.44	96.78±3 5.25	61.73± 12.44

FH: familial hypercholesterolemia; SD: standard deviation. ***: statistically signficant difference between groups ($p<0001$) at three time points (months 3, 6, and 9). ns: no statistical significance between groups ($p > 0.1$).

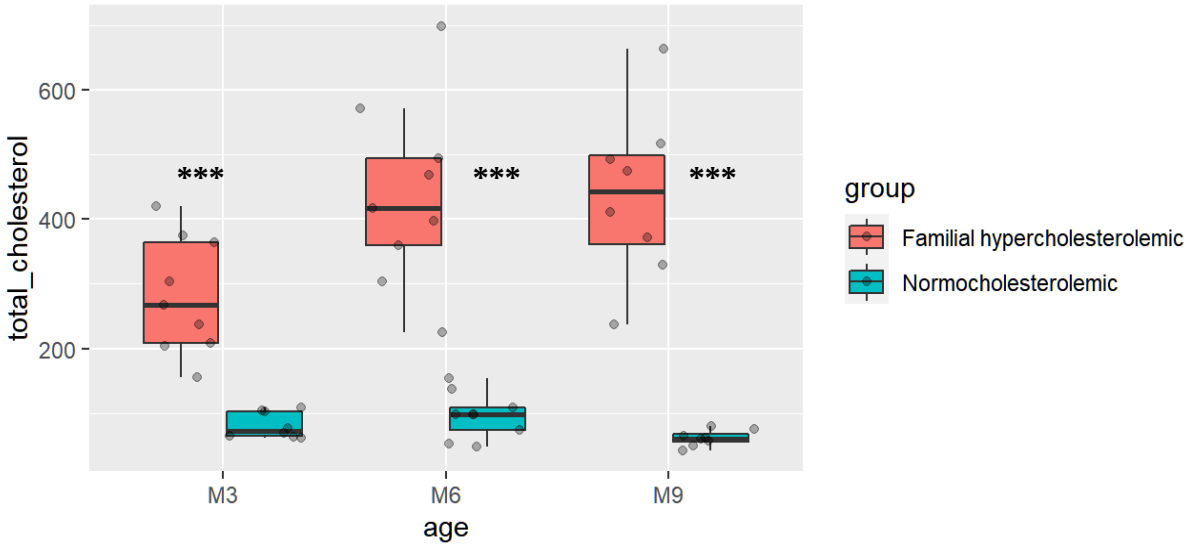

Figure 1. Estimated total cholesterol mg/dL measured using ELISA kit. The boxplots represent total cholesterol levels per group (WMS-FH vs. WMS normal) at each time point (months 3, 6, and 9). The data are for animals recruited in cohort 1. *** : $p < 0.001$.

Differentially expressed miRNAs between WMS-FH and WMS-N

We assessed the differential expression of plasma miRNAs between WMS-FH and WMS-N at months 3, 6, and 9. Table 2 summarizes the significant DE miRNAs with $p < 0.1$. A total of 20, 19, and 9 DE miRNAs were identified for months 3, 6, and 9, respectively. In addition, some DE miRNAs were present in at least two-time points (i.e., 3 and 6 months, 6 and 9 months, 3 and 9 months) (Figure 2). miR-194b-5p was differentially expressed between WMS-FH and WMS-N at all three-time points (months 3, 6, and 9). In contrast, miR-7140-5p, miR-7140-3p, miR-9805-3p, miR-138, and miR-130a were only captured at months 3 and 6. Similarly, miRNAs miR-486 and miR-126-3p were differentially expressed at two-time points (months 6 and 9) only.

Table 2. Significantly differentially expressed miRNAs between WMS-FH and WMS-N at months 3, 6, and 9 ($p < 0.1$).

Age	miRNA	Fold change	Adjusted p-value	Expression
Month 3	miR-7140-3p	3.74	0.048	Upregulated
	miR-7140-5p	6.28	0.048	Upregulated
	miR-194b-5p	3.16	0.085	Upregulated
	miR-7	1.47	0.086	Upregulated
	miR-499-3p	1.88	0.086	Upregulated
	miR-193a-3p	1.34	0.086	Upregulated
	miR-144	1.45	0.090	Upregulated
	miR-9805-3p	2.18	0.090	Upregulated
	miR-183	0.64	0.048	Downregulated
	miR-190a	0.53	0.048	Downregulated
	miR-574	0.58	0.048	Downregulated
	miR-129a-3p	0.66	0.053	Downregulated
	miR-196a	0.55	0.069	Downregulated
	miR-182	0.51	0.070	Downregulated
	miR-138	0.61	0.070	Downregulated
	miR-126-5p	0.69	0.086	Downregulated
	miR-130a	0.78	0.086	Downregulated
	miR-23b	0.70	0.086	Downregulated
	miR-146a-5p	0.74	0.086	Downregulated
	miR-152	0.72	0.090	Downregulated
Month 6	miR-7140-5p	6.27	0.000	Upregulated
	miR-7140-3p	5.13	0.000	Upregulated
	miR-143-3p	1.91	0.037	Upregulated
	miR-9805-3p	3.74	0.041	Upregulated
	miR-194b-5p	5.67	0.041	Upregulated
	miR-1	10.35	0.041	Upregulated
	miR-204	6.20	0.041	Upregulated
	miR-127	2.46	0.050	Upregulated
	miR-486	1.98	0.071	Upregulated
	miR-206	10.72	0.084	Upregulated
	miR-133a-3p	7.52	0.096	Upregulated
	miR-184	3.41	0.098	Upregulated
	miR-133a-5p	5.63	0.098	Upregulated
	miR-138	0.44	0.037	Downregulated
	miR-126-3p	0.61	0.037	Downregulated
	miR-130a	0.68	0.050	Downregulated
	miR-210	0.55	0.054	Downregulated
	miR-24-3p	0.71	0.098	Downregulated

	miR-140-3p	0.57	0.098	Downregulated
Month 9	miR-486	1.81	0.015	Upregulated
	miR-423-5p	1.30	0.015	Upregulated
	miR-335	1.56	0.038	Upregulated
	miR-9858-5p	1.72	0.037	Upregulated
	miR-194b-5p	3.42	0.071	Upregulated
	miR-2483	1.45	0.083	Upregulated
	miR-34c	0.46	0.037	Downregulated
	miR-122	0.43	0.071	Downregulated
	miR-126-3p	0.71	0.083	Downregulated

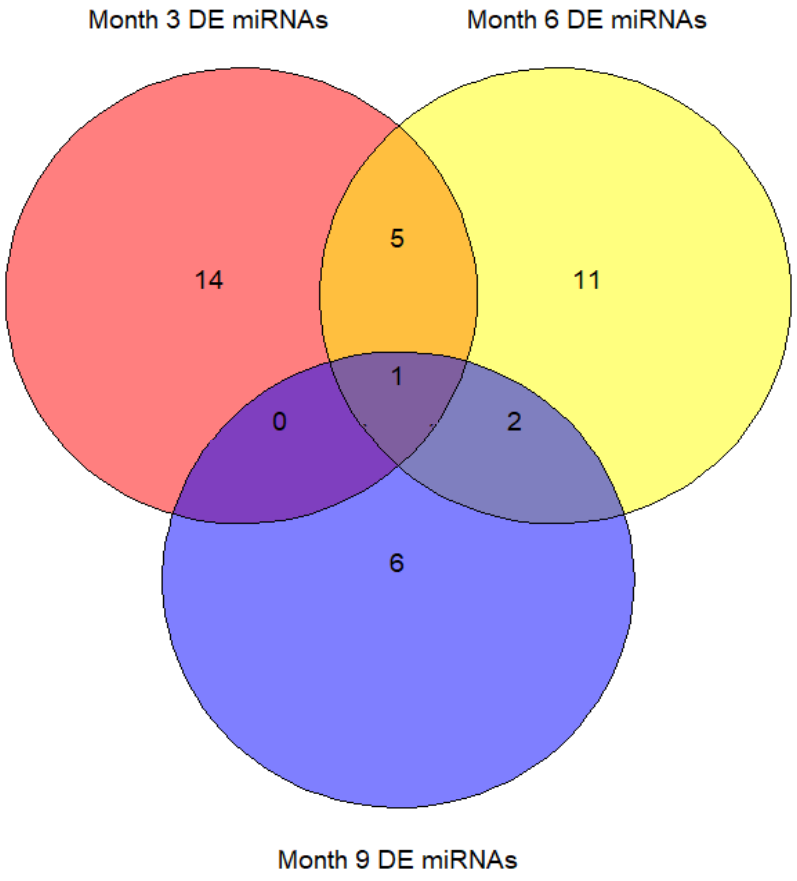

Figure 2. Venn diagram of differentially expressed miRNAs between WMS-FH and WMS-N, at months 3, 6, and 9.

We also performed a time course analysis to identify miRNAs that differ between WMS-FH and WMS-N within individual animals and between groups across the three time-points (3, 6, and 9 months of age). The analysis showed that at a $p < 0.1$ the dynamics of three miRNAs (miR-206, miR-1, and miR-143-3p) change over time in each animal and between groups (Table 3). Expression of all three miRNAs decreases over time in WMS-FH animals.

Table 3. miRNAs with changing expression patterns over time between WMS-FH and WMS-N ($p < 0.1$).

miRNA	Fold Change	Adjusted p-value	Expression in WMS-FH
miR-206	26.34	<0.001	Decreases
miR-1	21.15	<0.001	Decreases
miR-143-3p	1.18	0.069	Decreases

miRNA targets and gene ontology

miRNAs are known regulators of mRNA expression (50). We identified validated mRNA targets for the DE miRNAs that share >90% sequence similarity with human miRNAs (Appendix B. Table 2). Several of the obtained mRNAs are targeted by multiple DE miRNAs. Among the targets we identified chemokines (e.g., CXCL12, CXCL8, CXCR4), cytokines (e.g., CSF1), adhesion molecules (e.g., ICAM1, and VCAM1), growth factors (e.g., VEGFA), integrins (e.g., ITGB1 and 4, ITGA5 and 6), matrix metalloproteinases (MMP13, MMP14, MMP2, MMP7 , MMP9), transcription factors (e.g., PPARG, SOX4, SOX9, SOX2, SP1, and YY1) , calcium binding proteins (S100A1, S100A8, and S100A9) , toll-like receptors (e.g., TLR2, TLR4), and epigenome modifiers (e.g., DNMT1, DNMT3A , SIRT, EP300, MECP2 and SIRT1). The full list of validated targets can be found in Appendix B. Table 3.

The biological relevance of DE miRNAs was assessed via gene ontology search. Several relevant GO terms to hypercholesterolemia and atherosclerosis were enriched in our results such as negative regulation of interleukin-10 production (miR-194b-5p), negative regulation of amyloid beta clearance (miR-7), positive regulation of cell molecule adhesion (miR-144), positive regulation of high-density lipoprotein particle clearance (miR-144), negative regulation of cholesterol storage and IL-6 and IL-8 production (miR-146a-5p), positive regulation of phagocytosis, cholesterol and fatty acid biosynthesis processes (miR-183-5p), and regulation of vascular associated smooth muscle cell proliferation and differentiation (miR-182). Some of the GO terms were represented by more than one miRNA (Table 4). The full data for GO terms per DE miRNA is summarized in Appendix B. Table 4.

Table 4. Representative gene ontology terms shared between at least two DE miRNAs

miRNA ID	Age(months)	Gene Ontology Term
miR-138-5p	3, 6	Negative regulation of cell migration
miR-126-5p	3	
miR-204-5p	6	
miR-126-3p	6, 9	
miR-335-5p	9	
miR-144-3p	3	Cholesterol homeostasis
miR-182-5p	3	
miR-138-5p	3, 6	Negative regulation of inflammatory responses
miR-146a-5p	3	
miR-204	6	
miR-126-3p	6, 9	
miR-146a-5p	3	Negative regulation of interleukin 6 and interleukin 8
miR-204-5p	6	
miR-130a-3p	3, 6	Negative regulation of tumor necrosis factor production
miR-204-5p	6	
miR-182-5p	3	Negative regulation of vascular associated smooth muscle cell proliferation
miR-1-3p	6	
miR-182-5p	3	Positive regulation of NIK/NF Kappa beta signaling
miR-130a-3p	3, 6	
miR-146a-5p	3	Negative regulation of NIK/NF Kappa beta signaling
miR-204	6	
miR-138-5p	3, 6	Negative regulation of cell adhesion
miR-146a-5p	3	

miR-138-5p miR-204-5p miR-335	3, 6 6 9	Negative regulation of cell proliferation
miR-23b-3p miR-196a-5p	3 3	Cellular response to vascular endothelial growth factor stimulus
miR-23b-3p miR-204-5p	3 6	Positive regulation of cardiac muscle cell proliferation
miR-23b-3p miR-24-3p	3 6	Cell growth involved in cardiac muscle cell development
miR-23b-3p miR-126-3p miR-24-3p	3 6, 9 6	Positive regulation of ERK1 and ERK2 cascade
miR-23b-3p miR-126-5p miR-146a-5p miR-126-3p	3 3 3 6, 9	Positive regulation of cell migration involved in sprouting angiogenesis Positive regulation of blood vessel endothelial cell proliferation involved in sprouting angiogenesis
miR-23b-3p miR-7-5p miR-138-5p miR-34c-5p	3 3 3, 6 9	Negative regulation of sprouting angiogenesis
miR-499a-3p miR-143-3p miR-126-3p miR-210-3p	3 6 3 6	Positive regulation of blood vessel endothelial cell migration
miR-499a-3p miR-130a-3p	3 3, 6	Positive regulation of vascular associated smooth muscle cell proliferation
miR-499a-3p miR-143-3p	3 6	Positive regulation of vascular associated smooth muscle cell migration
miR-499-3p miR-126-5p miR-130a-3p	3 3 3, 6	Positive regulation of vascular endothelial cell proliferation
miR-193a-3p miR-196a-5p miR-146a-5p	3 3 3	Negative regulation of cell migration involved in sprouting angiogenesis
miR-193a-3p miR-24-3p	3 6	Negative regulation of blood vessel endothelial cell proliferation involving sprouting angiogenesis
miR-146a-5p miR-152-3p miR-24-3p	3 3 6	Negative regulation of matrix metallopeptidase secretion and activity
miR-146a-5p miR-143-3p miR-24-3p	3 6 6	Negative regulation of angiogenesis
miR-130a-3p miR-143-3p	3, 6 6	Positive regulation of angiogenesis

miR-126-3p	3, 9	
miR-210-3p	6	
miR-152-3p	3	
miR-204-5p	6	Negative regulation of blood vessel endothelial cell migration
miR-24-3p	6	

RT-qPCR validation of DE miRNAs in the second cohort of animals

We validated a subset of DE miRNAs in a new cohort of animals. Among the tested miRNAs, miR-194b-5p was differentially expressed between WMS-FH and WMS-N at 3, 6, and 9 months of age; however, the RT-qPCR showed a significant higher expression in WMS-FH at months 6 and 9 but not at month 3. Also, miR-194b-5p expression increased with age (month 6 : FC = 1.579, p-value = 0.007; month 9: FC= 3.313, p-value = 0.042). Moreover, DE miR-194b-5p showed expression differences between females and males (p-value = 0.036), at month 9, where females exhibit higher expression for this miRNA.

Similar to miRNA sequencing results, upregulated miR-206, downregulated miR-138, and miR-126-3p were also validated at month 6. No statistically significant differences between WMS-FH and WMS-N were found for miR-138 at month 3.

Table 5. Differential expression of miRNAs in WMS-FH (n =15) relative to WMS-N (n=15) in a new cohort of animals via RT-qPCR.

miRNA	**Fold change**			**Linear regression model p-value**		
	Month 3	**Month 6**	**Month 9**	**Month 3**	**Month 6**	**Month 9**
miR-194-5p ↑in WMS-FH	1.42	1.58	3.31	Weight: 0.722 Hemolysis: 0.016 Sex: <0.001 Group: 0.425	0.019 0.007 0.970 **0.007**	0.126 0.126 **0.036** **0.042**
miR-206 ↑in WMS-FH	-	1.82	-	Weight: - Hemolysis: - Sex: - Group: -	0.023 0.204 0.354 **0.032**	- - - -
miR-1	-	0.84	-	Weight: - Hemolysis: -	0.774 0.060	- -

↓ in WMS-FH				Sex: - Group: -	0.340 0.660	- -
miR-138-5p ↓ in WMS-FH	0.70	0.45	-	Weight: 0.082 Hemolysis: 0.001 Sex: 0.008 Group: 0.281	0.368 0.004 0.337 **0.005**	- - - -
miR-126-3p ↓ in WMS-FH	-	0.71	-	Weight: - Hemolysis: - Sex: - Group: -	0.104 0.003 0.494 **0.021**	- - - -

-: Not tested.

Diagnostic power of DE miRNAs

The presence and absence of atherosclerosis in WMS-FH and WMS-N were assessed by OCT. At ~ 12 months of age, seven out of 9 WMS-FH exhibited atherosclerosis lesions in the coronary arteries, while no lesions were observed in other arterial beds. Also, no lesions were observed in WMS-N pigs. The discriminatory power between healthy animals and those with the disease was assessed using the ROC method. Since we have a small number of animals, only miRNAs with an AUC threshold that confers statistical power ≥ 0.8 and $p < 0.05$ were considered powerful enough to distinguish between groups. The estimated AUC threshold was 89.63 %. miRNAs that can discriminate between animals with the disease and healthy ones were found at months 3 and 9 (Table 6 and Figure 3), whereas miRNAs at month 6 showed weak discriminatory power.

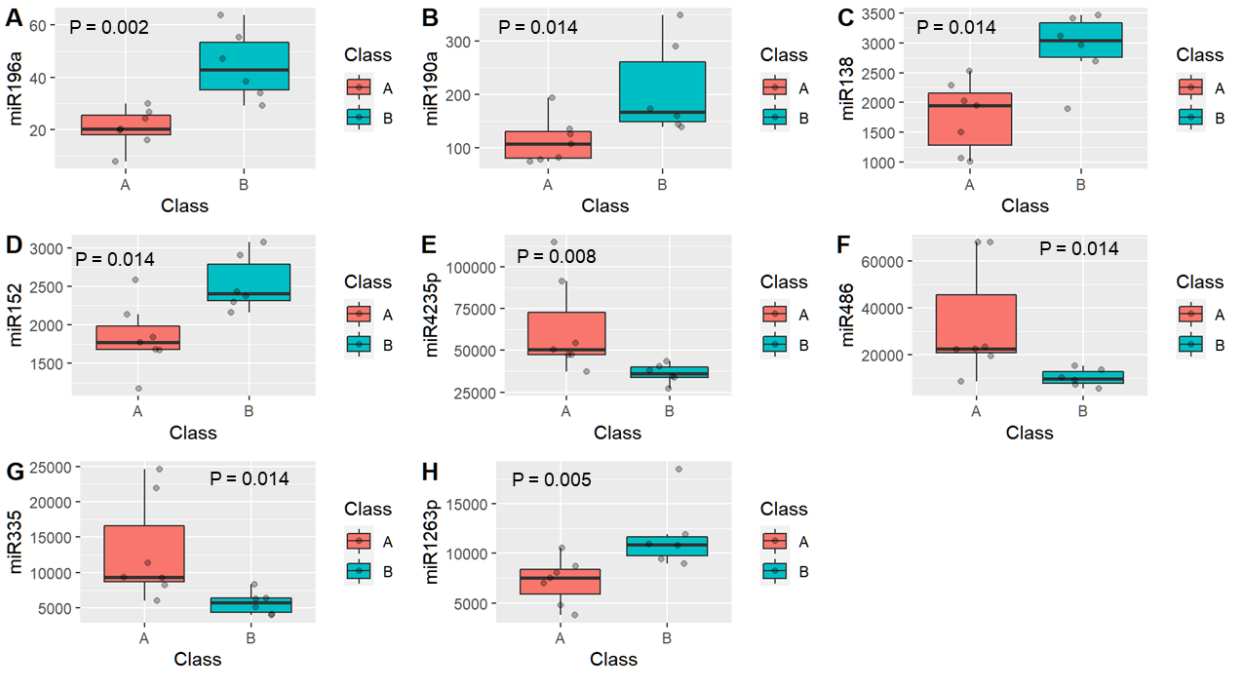

Figure 3. Boxplot of normalized reads for miRNA with discriminatory power between WMS animals with coronary artery disease (Class A) and healthy (Class B).

Table 6. miRNAs with discriminatory power to differentiate case (disease) from control (healthy). P-value < 0.05.

Age	miRNA	AUC (%)	CI 95%
Power = 0.8; AUC threshold = 89.63%			
Month3	miR138	90.48	70.68-100
	miR190a	90.48	70.90-100
	miR152	90.48	70.90-100
	miR196a	97.62	91.02-100
Month9	miR423-5p	92.86	77.52-100
	miR486	90.48	70.90-100
	miR335	90.48	73.65-100
	miR126-3p	95.24	84.19-100
Power = 0.95; AUC threshold = 93.91%			
Month3	miR196a	97.62	91.02-100
Month9	miR126-3p	95.24	84.19-100

Discussion

Early diagnosis of atherosclerosis is critical to risk management of the disease and therapeutic interventions. MicroRNAs can be found circulating in the blood bound to lipoproteins (51) or, encapsulated in exosomes and microvesicles (52). They also regulate gene expression and cell-to-cell communication (50). Furthermore, circulating miRNAs levels have been shown to correlate with atherosclerosis (12,16,17,53); hence, they make very promising biomarkers. In this work, using a swine translational model of atherosclerosis (WMS-FH) in a longitudinal study, we identified miRNA signatures early on in the life of animals. The observed association between atherosclerosis and miRNA signatures suggests that these miRNAs are promising circulating biomarkers for early diagnosis of atherosclerosis. We also identified mRNA targets and biological processes influenced by these miRNAs, thus, explaining the possible biological relevance of these molecules in the context of atherosclerosis.

The present study demonstrated that miRNA profiles differ between WMS-FH and WMS-N at very early stages of life. Specifically, at 3 and 6 months of age, a total of 20 and 19 miRNAs were shown to be differentially expressed between WMS-FH and WMS-N, respectively. However, only 9 miRNAs were differentially expressed at month 9 of age. Furthermore, among the identified DE miRNAs, several were reported in human studies to associate with atherosclerosis and its clinical manifestations. For example, miR-126-5p and miR-126-3p expression levels were shown to distinguish between individuals with and without coronary atherosclerosis (54). Moreover, miR-126 was significantly lower in patients with coronary artery atherosclerosis compared to healthy patients (55). Similarly, miR-126-3p was significantly lower in WMS-FH than WMS-N. This miRNA also demonstrated a strong diagnostic power for coronary artery atherosclerosis in these pigs at month 9. miR-196a was downregulated in WMS-FH. miR-196a was also reported to have

low expression in patients with myocardial infarction (56). miR-196a also showed the strongest diagnostic power at month 3.

In the Framingham Heart Study, miR-574-3p correlates negatively with stroke (57). Likewise, the downregulation of miR-574 in WMS-FH is negatively associated with atherosclerosis in these pigs. Also, similar to their downregulation in WMS-FH, miR-182, and miR-152 expression levels were lower in patients with coronary artery atherosclerosis (58,59). Additionally, downregulated miR-130a in WMS-FH correlated negatively with the presence of atherosclerosis in humans (60). In contrast to the downregulation of miR-130a and miR-210 in WMS-FH, these miRNA levels were higher in the serum of patients with peripheral artery atherosclerosis (61). Since our WMS-FH only demonstrated lesions in the coronary arteries, these contrasting findings could indicate that miR-130a and miR-210 are specific to the disease location. A systematic review showed that circulating miRNA signatures differ based on atherosclerosis location (62). A recent study also demonstrated that some miRNAs are specific to disease location (63). These contrasting reports may also reflect the stage of the disease.

Of note, the studies mentioned earlier profiled circulating miRNAs in patients with an already known disease status, i.e., the presence of atherosclerosis or clinical manifestations of the disease such as stroke, whereas our findings were obtained at earlier time points. Consequently, our results could indicate that DE miRNAs can continue to be dysregulated in the advanced stages of atherosclerosis. These miRNAs may disappear and reappear later on depending on the physiological state of the disease and the involved mechanisms. This is supported by the detection of DE miR-194b-5p at months 3, 6, 9 and other miRNAs that were captured only at one time point.

The dysregulated miRNA fingerprints across the three-time points (months 3, 6, and 9) could reflect the biological processes occurring during each phase of atherosclerosis progression.

GO enrichment of biological processes identified many terms (Appendix B. Tables 4 and 5) related to cholesterol homeostasis, endothelium dysregulation, inflammatory processes, smooth muscle cell proliferation and migration, all of which are well known to participate in atherogenesis (64). The findings of mRNA targets and GO terms are supported by studies that examined miRNAs mechanisms of action in atherosclerosis using *in-vivo* and *ex-vivo* approaches. Reports showed that miRNAs could modulate lipoprotein metabolism (65,66), and atherosclerosis development (13,67). For example, among the DE miRNAs in the present work, miR-7, miR-144, miR-146a-5p, miR-24-3p, and miR-486-5p contribute to foam cell formation, albeit in opposing ways. miR-146-5p appears to have an atheroprotective effect. By adversely affecting foam cell formation through the downregulation of NF-κB and TRAF6 expression (68,69). miR-146a is downregulated in WMS-FH at month 3, suggesting that negative regulation of foam cell formation is lacking in these pigs. In contrast, miR-7, miR-144, and miR-486-5p promote foam cell formation by directly downregulating genes involved in cholesterol efflux (STK11, ABCA1, and TR4) (70,71). Moreover, miR-486-5p was reported to target HAT1, which then downregulates ABCA1, hence, affecting cholesterol efflux (72). Our results showed that miR-7, miR-144, and miR486-5p are upregulated in WMS-FH. Therefore, mechanisms disturbing cholesterol clearance from macrophages are upregulated. Consequently, WMS-FH pigs are more prone to atherosclerosis progression. Other DE miRNAs regulate smooth muscle cell proliferation, such as miR-23b, miR-206, miR-204, miR-1, miR-126-3p, and miR-34c. The expression of miR-23b, miR-126-3p, and miR-34c was shown to tightly regulate SMC proliferation and prevent neointima formation by targeting LRP6 (73), and SCF (74). Moreover, miR-126-3p prevents leukocyte adherence to endothelial cells by reducing VCAM1 expression (75), whereas miR-138 was shown to reduce coronary endothelial cell injury (76). These miRNAs were also downregulated in WMS-FH,

suggesting a lack of mechanisms protecting against atherogenesis. Another downregulated miRNA in WMS-FH is miR-182 which was shown recently to inhibit vascular smooth muscle cell proliferation (58). Similarly, miR-24 was shown to inhibit endothelial cell proliferation (77). Moreover, reduced expression of miR-24 resulted in increased MMP14 expression and lesion size in mice (78). miR-152 exhibited atheroprotection by targeting KLF5 and reducing inflammation in mice (79). Similarly, miR-335-5p inhibits macrophage immune responses by targeting Notch signaling resulting in reduced atherosclerotic vulnerable plaque formation (80).

WMS-FH exhibited an upregulation in miR-194b-5p across the three-time points. This miRNA targets IL-10 (Appendix B. Table 3) and is involved in the negative regulation of IL10 (Appendix B. Table 3). IL-10 has been shown to confer protection against atherosclerosis (81,82). Therefore, the consistent upregulation of this miRNA indicates another lacking mechanism of atheroprotection in WMS-FH that is persistent and spans a long period. Additionally, miR-194b-5p was significantly different between male and female pigs.

In addition to universally known biological processes participating in atherosclerosis, such as foam cell formation and endothelial dysfunction, GO terms in our study showed that miR-7, upregulated in WMS-FH, is involved in the negative regulation of amyloid beta clearance (Appendix B. Table 4). Aberrant deposition and clearance of amyloid from the subintima have been linked to inflammation and the promotion of atherosclerosis (83). In our data, cellular response to DNA damage was another GO term found to be targeted by miR193-3p. DNA damage responses are induced by oxidative stress, cell death, and osteogenic differentiation in the vasculature (84). In addition, DNA damage accelerates vascular calcification (84).

Several DE miRNAs were found to target epigenetic modifiers such as DNMT1, DNMT3A, and EP300 (Appendix B. Table 3), suggesting the presence of alterations in epigenetics

mechanisms between WMS-FH and WMS-N. Alterations in epigenetic marks result in aberrant gene expression and phenotypes (85). Furthermore, aberrations in epigenetic marks have been linked to atherogenesis (85–88).

Some of the miRNAs we found in this study include miR-7140-3p, miR-7140-5p, miR-9805-3p, miR-9858-5p, and miR-2483. These miRNAs did not share similarities with any known miRNA human, mice, rat, rabbits, or non-human primate sequences currently available in miRBase. The uniqueness of these miRNAs suggests that they are swine specific. However, these miRNAs are possibly novel ones. Further investigations are needed to assess the functionality of these miRNAs in atherosclerosis

Study limitations

One limitation of the present work is that GO search was carried out for those miRNAs similar in sequence to human miRNAs. Another limitation was the absence of live imaging in animals at each studied time point to confirm the absence of the disease in early life. However, WMS-FH swine develop lesions in the arteries around 1-year-old when the animals are fed the normal diet used in this work.

Conclusion

The findings above demonstrate that circulating miRNAs expression differ between WMS-FH and WMS-N. Also, these differences can be identified in animals' early life before the manifestation of atherosclerosis. Additionally, these miRNAs are involved in mechanisms governing the pathophysiology of the disease, further supporting the evidence of early onset before disease manifestation; hence, these miRNAs are promising biomarkers for early detection.

Specifically, in WMS-FH, atherosclerosis can be detected at 3 months of age using miR-138, miR-152, miR-190a, and miR-196a. While miRNAs miR486, miR-126-3p, miR-335, and miR-423-5p can detect the disease at month 9 of age.

References

1. Benjamin EJ., Muntner P., Alonso A., et al. Heart Disease and Stroke Statistics-2019 Update: A Report From the American Heart Association. Circ 2019. vol. 139 :e56-e528. Doi: 10.1161/CIR.0000000000000659.

2. Benjamin EJ., Virani SS., Callaway CW., et al. Heart Disease and Stroke Statistics—2018 Update: A Report From the American Heart Association. Circ 2018. Doi: 10.1161/CIR.0000000000000558.

3. Sachdeva A., Cannon CP., Deedwania PC., et al. Lipid levels in patients hospitalized with coronary artery disease: An analysis of 136,905 hospitalizations in Get With The Guidelines. Am Heart J 2009;157(1). Doi: 10.1016/j.ahj.2008.08.010.

4. Glass CK., Witztum JL. Atherosclerosis: The road ahead. Cell 2001;104(4):503–16. Doi: 10.1016/S0092-8674(01)00238-0.

5. Puri R., Nicholls SJ., Shao M., et al. Impact of statins on serial coronary calcification during atheroma progression and regression. J Am Coll Cardiol 2015;65(13):1273–82. Doi: 10.1016/j.jacc.2015.01.036.

6. Banach M., Serban C., Sahebkar A., et al. Impact of statin therapy on coronary plaque composition: A systematic review and meta-analysis of virtual histology intravascular ultrasound studies. BMC Med 2015;13(1). Doi: 10.1186/s12916-015-0459-4.

7. Okuyama H., Langsjoen PH., Hamazaki T., et al. Statins stimulate atherosclerosis and heart failure: Pharmacological mechanisms. Expert Rev Clin Pharmacol 2015;8(2):189–99. Doi: 10.1586/17512433.2015.1011125.

8. Tuomisto K., Jousilahti P., Sundvall J., Pajunen P., Salomaa V. C-reactive protein, interleukin-6 and tumor necrosis factor alpha as predictors of incident coronary and cardiovascular events and total mortality. Thromb Haemost 2006;95(03):511–8. Doi: 10.1160/TH05-08-0571.

9. Koenig W., Khuseyinova N., Baumert J., et al. Increased concentrations of C-reactive protein and IL-6 but not IL-18 are independently associated with incident coronary events in middle-aged men and women: Results from the MONICA/KORA Augsburg case-cohort study, 1984-2002. Arterioscler Thromb Vasc Biol 2006;26(12):2745–51. Doi: 10.1161/01.ATV.0000248096.62495.73.

10. Ridker PM., Rifai N., Stampfer MJ., Hennekens CH. Plasma concentration of interleukin-6 and the risk of future myocardial infarction among apparently healthy men. Circulation 2000;101(15):1767–72. Doi: 10.1161/01.CIR.101.15.1767.

11. Hong SN., Gona P., Fontes JD., et al. Atherosclerotic biomarkers and aortic atherosclerosis by cardiovascular magnetic resonance imaging in the Framingham Heart Study. J Am Heart Assoc 2013;2(6):1–8. Doi: 10.1161/JAHA.113.000307.

12. Yilmaz SG., Isbir S., Kunt AT., Isbir T. Circulating microRNAs as novel biomarkers for atherosclerosis. In Vivo (Brooklyn) 2018;32(3):561–5. Doi: 10.21873/invivo.11276.

13. Andreou I., Sun X., Stone PH., Edelman ER., Feinberg MW. miRNAs in atherosclerotic plaque initiation, progression, and rupture. Trends Mol Med 2015;21:307–18. Doi: 10.1016/j.molmed.2015.02.003.

14. Gonzalo-Calvo D., Vilades D., Martínez-Camblor P., et al. Circulating microRNAs in suspected stable coronary artery disease: A coronary computed tomography angiography study. J Intern Med 2019;286(3):341–55. Doi: 10.1111/joim.12921.

15. de Gonzalo-Calvo D., Cenarro A., Garlaschelli K., et al. Translating the microRNA signature of microvesicles derived from human coronary artery smooth muscle cells in patients with familial hypercholesterolemia and coronary artery disease. J Mol Cell Cardiol 2017;106:55–67. Doi: 10.1016/j.yjmcc.2017.03.005.

16. Salinas J., Lin H., Aparico HJ., et al. Whole blood microRNA expression associated with stroke: Results from the Framingham Heart Study. PLoS One 2019;14(8). Doi: 10.1371/journal.pone.0219261.

17. Zhang JY., Gong YL., Li CJ., Qi Q., Zhang QM., Yu DM. Circulating miRNA biomarkers serve as a fingerprint for diabetic atherosclerosis. Am J Transl Res 2016;8(6):2650–8.

18. Getz GS., Reardon CA. Animal Models of Atherosclerosis. Animal Models for the Study of Human Disease: Second Edition 2017;816(December 2016):205–17. Doi: 10.1016/B978-0-12-809468-6.00008-5.

19. Zhao Y., Qu H., Wang Y., Xiao W., Zhang Y., Shi D. Small rodent models of atherosclerosis. Biomedicine and Pharmacotherapy 2020;129(April):110426. Doi: 10.1016/j.biopha.2020.110426.

20. Johnston JM., Francis SE., Kiss-Toth E. Experimental models of murine atherosclerosis: Does perception match reality? Cardiovasc Res 2018;114(14):1845–7. Doi: 10.1093/cvr/cvy140.

21. Shi ZS., Feng L., He X., et al. Vulnerable plaque in a swine model of carotid atherosclerosis. American Journal of Neuroradiology 2009;30(3):469–72. Doi: 10.3174/ajnr.A1410.

22. Wang D., Xu X., Zhao M., Wang X. Accelerated miniature swine models of advanced atherosclerosis: A review based on morphology. Cardiovascular Pathology 2020;49:107241. Doi: 10.1016/j.carpath.2020.107241.

23. Schomberg DT., Tellez A., Meudt JJ., et al. Miniature Swine for Preclinical Modeling of Complexities of Human Disease for Translational Scientific Discovery and Accelerated Development of Therapies and Medical Devices. Toxicol Pathol 2016;44(3):299–314. Doi: 10.1177/0192623315618292.

24. Ishii A., Viñuela F., Murayama Y., et al. Swine model of carotid artery atherosclerosis: experimental induction by surgical partial ligation and dietary hypercholesterolemia. AJNR Am J Neuroradiol 2006;27(9):1893–9.

25. Yuan F., Guo L., Park K., et al. Ossabaw Pigs With a PCSK9 Gain-of-Function Mutation Develop Accelerated Coronary Atherosclerotic Lesions: A Novel Model for Preclinical Studies. J Am Heart Assoc 2018;7(6). Doi: 10.1161/JAHA.117.006207.

26. Hasler-Rapacz J., Ellegren H., Fridolfsson a K., et al. Identification of a mutation in the low density lipoprotein receptor gene associated with recessive familial hypercholesterolemia in swine. Am J Med Genet 1998. Doi: 10.1002/(SICI)1096-8628(19980413)76:5<379::AID-AJMG3>3.0.CO;2-I.

27. Hasler-Rapacz J., Prescott MF., von Linden-Reed J., Rapacz JM., Hu Z., Rapacz J. Elevated concentrations of plasma lipids and apolipoproteins B, C-III, and E are associated with the progression of coronary artery disease in familial hypercholesterolemic swine. Arterioscler Thromb Vasc Biol 1995;15(5):583–92. Doi: 10.1161/01.ATV.15.5.583/FORMAT/EPUB.

28. Schinkel AFL., Krueger CG., Tellez A., et al. Contrast-enhanced ultrasound for imaging vasa vasorum: comparison with histopathology in a swine model of atherosclerosis. European Journal of Echocardiography 2010;11(8):659–64. Doi: 10.1093/ejechocard/jeq048.

29. Bahls M., Bidwell CA., Hu J., et al. Gene expression differences in healthy brachial and femoral arteries of Rapacz familial hypercholesterolemic swine. Physiol Genomics 2011;43(12):781–8. Doi: 10.1152/physiolgenomics.00151.2010.

30. Bahls M., Bidwell CA., Hu J., et al. Gene expression differences during the heterogeneous progression of peripheral atherosclerosis in familial hypercholesterolemic swine 2013. Doi: 10.1186/1471-2164-14-443.

31. Thim T., Hagensen MK., Drouet L., et al. Familial hypercholesterolaemic downsized pig with human-like coronary atherosclerosis: a model for preclinical studies. EuroIntervention 2010;6(2):261–8. Doi: 10.4244/.

32. Tellez A., Krueger CG., Seifert P., et al. Coronary bare metal stent implantation in homozygous LDL receptor deficient swine induces a neointimal formation pattern similar to humans. Atherosclerosis 2010;213(2):518–24. Doi: 10.1016/j.atherosclerosis.2010.09.021.

33. Tellez A., Seifert PS., Donskoy E., et al. Experimental evaluation of efficacy and healing response of everolimus-eluting stents in the familial hypercholesterolemic swine model: A comparative study of bioabsorbable versus durable polymer stent platforms. Coron Artery Dis 2014;25(3):198–207. Doi: 10.1097/MCA.0000000000000099.

34. Granada JF., Milewski K., Zhao H., et al. Vascular response to zotarolimus-coated balloons in injured superficial femoral arteries of the familial hypercholesterolemic swine. Circ Cardiovasc Interv 2011;4(5):447–55. Doi: 10.1161/CIRCINTERVENTIONS.110.960260.

35. Nih., Od., Oer., Olaw. GUIDE LABORATORY ANIMALS FOR THE CARE AND USE OF Eighth Edition Committee for the Update of the Guide for the Care and Use of Laboratory Animals Institute for Laboratory Animal Research Division on Earth and Life Studies. THE NATIONAL ACADEMIES PRESS 2011:1–209.

36. Animal Welfare Act as Amended. . 7 USC § 2013:2132–59.

37. Kirschner MB., Edelman JJB., Kao SCH., Vallely MP., Van Zandwijk N., Reid G. The impact of hemolysis on cell-free microRNA biomarkers. Front Genet 2013;4(MAY). Doi: 10.3389/fgene.2013.00094.

38. Simon Andrews. FastQC: A Quality Control Tool for High Throughput Sequence Data. Available Online at: Http://WwwBioinformaticsBabrahamAcUk/Projects/Fastqc/ 2010.

39. Rahman R-U., Gautam A., Bethune J., et al. Oasis 2: improved online analysis of small RNA-seq data n.d. Doi: 10.1186/s12859-018-2047-z.

40. Dobin A., Davis CA., Schlesinger F., et al. STAR: ultrafast universal RNA-seq aligner. Bioinformatics 2013;29(1):15–21. Doi: 10.1093/bioinformatics/bts635.

41. Love MI., Huber W., Anders S. Moderated estimation of fold change and dispersion for RNA-seq data with DESeq2. Genome Biol 2014;15:550. Doi: 10.1186/s13059-014-0550-8.

42. Kozomara A., Birgaoanu M., Griffiths-Jones S. miRBase: from microRNA sequences to function. Nucleic Acids Res 2018;47:155–62. Doi: 10.1093/nar/gky1141.

43. Huang H-Y., Lin Y-C-D., Li J., et al. miRTarBase 2020: updates to the experimentally validated microRNA-target interaction database. Nucleic Acids Res 2020;48. Doi: 10.1093/nar/gkz896.

44. Cancer C., Sets D. Documentation for running Normfinder in R The Normfinder algorithm 2013:1–7.

45. Ganger MT., Dietz GD., Ewing SJ. A common base method for analysis of qPCR data and the application of simple blocking in qPCR experiments n.d. Doi: 10.1186/s12859-017-1949-5.

46. Livak KJ., Schmittgen TD. Analysis of relative gene expression data using real-time quantitative PCR and the 2-ΔΔCT method. Methods 2001;25(4):402–8. Doi: 10.1006/meth.2001.1262.

47. Robin X., Turck N., Hainard A., et al. pROC: an open-source package for R and S+ to analyze and compare ROC curves. BMC Bioinformatics 2011;12(1):77. Doi: 10.1186/1471-2105-12-77.

48. Peng RD. R Programming for Data Science. The R Project; R Foundation 2015:132. Doi: 10.1073/pnas.0703993104.

49. Hasler-Rapacz J., Ellegren H. Identification of a mutation in the low density lipoprotein receptor gene associated with recessive familial hypercholesterolemia in swine. Am J Med Genetics 1999;76(February 1997):379–86.

50. O'Brien J., Hayder H., Zayed Y., Peng C. Overview of microRNA biogenesis, mechanisms of actions, and circulation. Front Endocrinol (Lausanne) 2018:402. Doi: 10.3389/fendo.2018.00402.

51. Vickers KC., Palmisano BT., Shoucri BM., Shamburek RD., Remaley AT. MicroRNAs are Transported in Plasma and Delivered to Recipient Cells by High-Density Lipoproteins n.d. Doi: 10.1038/ncb2210.

52. de Gonzalo-Calvo D., Cenarro A., Garlaschelli K., et al. Translating the microRNA signature of microvesicles derived from human coronary artery smooth muscle cells in patients with familial hypercholesterolemia and coronary artery disease. J Mol Cell Cardiol 2017;106:55–67. Doi: 10.1016/j.yjmcc.2017.03.005.

53. Mao Z., Wu F., Shan Y. Identification of key genes and miRNAs associated with carotid atherosclerosis based on mRNA-seq data. Medicine (United States) 2018;97(13). Doi: 10.1097/MD.0000000000009832.

54. Ormseth MJ., Solus JF., Sheng Q., et al. Plasma miRNAs improve the prediction of coronary atherosclerosis in patients with rheumatoid arthritis 2021. Doi: 10.1007/s10067-020-05573-8/Published.

55. Fichtlscherer S., de Rosa S., Fox H., et al. Circulating MicroRNAs in Patients With Coronary Artery Disease. Circ Res 2010;107(5):677–84. Doi: 10.1161/CIRCRESAHA.109.215566.

56. Karacorlu OF., Cetin M., Yumrutas O., Bozgeyik I., Dumlupinar E., Bagis H. Circulating miR-196a-5p miR-373-3p and miR-375: Novel candidate biomarkers for diagnosis of acute coronary syndrome. Meta Gene 2018;17:1–8. Doi: 10.1016/j.mgene.2018.03.013.

57. Salinas JI., Lin H., Aparico HJ., et al. Whole blood microRNA expression associated with stroke: Results from the Framingham Heart Study 2019. Doi: 10.1371/journal.pone.0219261.

58. Jin C., Gao S., Li D., et al. MiR-182-5p inhibits the proliferation of vascular smooth muscle cells induced by ox-LDL through targeting PAPPA. Int Heart J 2020;61(4):822–30. Doi: 10.1536/ihj.19-708.

59. Wu Y., Huang A., Li T., et al. MiR-152 reduces human umbilical vein endothelial cell proliferation and migration by targeting ADAM17. FEBS Lett 2014;588(12):2063–9. Doi: 10.1016/j.febslet.2014.04.037.

60. Jia QW., Chen ZH., Ding XQ., et al. Predictive Effects of Circulating miR-221, miR-130a and miR-155 for Coronary Heart Disease: A Multi-Ethnic Study in China. Cellular Physiology and Biochemistry 2017;42(2):808–23. Doi: 10.1159/000478071.

61. Li T., Cao H., Zhuang J., et al. Identification of miR-130a, miR-27b and miR-210 as serum biomarkers for atherosclerosis obliterans. Clinica Chimica Acta 2011;412(1–2):66–70. Doi: 10.1016/j.cca.2010.09.029.

62. Pereira-da-Silva T., Coutinho Cruz M., Carrusca C., Cruz Ferreira R., Napoleão P., Mota Carmo M. Circulating microRNA profiles in different arterial territories of stable atherosclerotic disease: a systematic review. Am J Cardiovasc Dis 2018;8(1):1–13.

63. Hildebrandt A., Kirchner B., Meidert AS., et al. Detection of Atherosclerosis by Small RNA-Sequencing Analysis of Extracellular Vesicle Enriched Serum Samples. Front Cell Dev Biol 2021;9. Doi: 10.3389/fcell.2021.729061.

64. Fernando S., Bursill CA., Nicholls SJ., Psaltis PJ. Pathophysiology of atherosclerosis. Mechanisms of Vascular Disease. Springer Nature Switzerland; 2020. p. 19–45.

65. Rotllan N., Price N., Pati P., Goedeke L., Fernández-Hernando C. microRNAs in lipoprotein metabolism and cardiometabolic disorders. Atherosclerosis 2016:352–60. Doi: 10.1016/j.atherosclerosis.2016.01.025.

66. Goedeke L., Wagschal A., Fernández-Hernando C., Näär AM. miRNA regulation of LDL-cholesterol metabolism. Biochim Biophys Acta Mol Cell Biol Lipids 2016;1861(12):2047–52. Doi: 10.1016/j.bbalip.2016.03.007.

67. Feinberg MW., Moore KJ. MicroRNA Regulation of Atherosclerosis. Circ Res 2016;118(4):703–20. Doi: 10.1161/CIRCRESAHA.115.306300.

68. Lin N., An Y. Blockade of 146b-5p promotes inflammation in atherosclerosis-associated foam cell formation by targeting TRAF6. Exp Ther Med 2017:5087–92. Doi: 10.3892/etm.2017.5121.

69. Li K., Ching D., Luk FS., Raffai RL. Apolipoprotein e Enhances MicroRNA-146a in Monocytes and Macrophages to Suppress Nuclear Factor-κB-Driven Inflammation and Atherosclerosis. Circ Res 2015;117(1):e1–11. Doi: 10.1161/CIRCRESAHA.117.305844.

70. Li C hui., Gong D., Chen L yan., et al. Puerarin promotes ABCA1-mediated cholesterol efflux and decreases cellular lipid accumulation in THP-1 macrophages. Eur J Pharmacol 2017;811(November 2016):74–86. Doi: 10.1016/j.ejphar.2017.05.055.

71. Ramírez CM., Rotllan N., Vlassov A v., et al. Control of cholesterol metabolism and plasma high-density lipoprotein levels by microRNA-144. Circ Res 2013;112(12):1592–601. Doi: 10.1161/CIRCRESAHA.112.300626.

72. Liu D., Zhang M., Xie W., et al. MiR-486 regulates cholesterol efflux by targeting HAT1. Biochem Biophys Res Commun 2016;472(3):418–24. Doi: 10.1016/j.bbrc.2015.11.128.

73. Jansen F., Stumpf T., Proebsting S., et al. Intercellular transfer of miR-126-3p by endothelial microparticles reduces vascular smooth muscle cell proliferation and limits neointima formation by inhibiting LRP6. J Mol Cell Cardiol 2017;104:43–52. Doi: 10.1016/j.yjmcc.2016.12.005.

74. Choe N., Kwon JS., Kim YS., et al. The microRNA miR-34c inhibits vascular smooth muscle cell proliferation and neointimal hyperplasia by targeting stem cell factor. Cell Signal 2015;27(6):1056–65. Doi: 10.1016/j.cellsig.2014.12.022.

75. Harris TA., Yamakuchi M., Ferlito M., Mendell JT., Lowenstein CJ. MicroRNA-126 regulates endothelial expression of vascular cell adhesion molecule 1. 2008.

76. Li JB., Wang HY., Yao Y., et al. Overexpression of microRNA-138 alleviates human coronary artery endothelial cell injury and inflammatory response by inhibiting the PI3K/Akt/eNOS pathway. J Cell Mol Med 2017;21(8):1482–91. Doi: 10.1111/jcmm.13074.

77. Zheng Y., Li Y., Liu G., Qi X., Cao X. MicroRNA-24 inhibits the proliferation and migration of endothelial cells in patients with atherosclerosis by targeting importin-α3 and regulating inflammatory responses. Exp Ther Med 2017. Doi: 10.3892/etm.2017.5355.

78. di Gregoli K., Jenkins N., Salter R., White S., Newby AC., Johnson JL. MicroRNA-24 regulates macrophage behavior and retards atherosclerosis. Arterioscler Thromb Vasc Biol 2014;34(9):1990–2000. Doi: 10.1161/ATVBAHA.114.304088.

79. Wang W., Zhang Y., Wang L., et al. mircroRNA-152 prevents the malignant progression of atherosclerosis via down-regulation of KLF5. Biomedicine & Pharmacotherapy 2019;109:2409–14. Doi: 10.1016/j.biopha.2018.08.014.

80. Sun D., Ma T., Zhang Y., Zhang F., Cui B. Overexpressed miR-335-5p reduces atherosclerotic vulnerable plaque formation in acute coronary syndrome. J Clin Lab Anal 2021;35(2). Doi: 10.1002/jcla.23608.

81. Mallat Z., Besnard S., Duriez M., et al. Protective Role of Interleukin-10 in Atherosclerosis. 1999.

82. Han X., Boisvert WA. Interleukin-10 protects against atherosclerosis by modulating multiple atherogenic macrophage function. Thromb Haemost 2015;113(3):505–12. Doi: 10.1160/TH14-06-0509/ID/JR0509-6.

83. Howlett GJ., Moore KJ., Williams L. Untangling the role of amyloid in atherosclerosis. vol. 17. 2006.

84. Duer M., Cobb AM., Shanahan CM. DNA Damage Response. Arterioscler Thromb Vasc Biol 2020;40:E193–202. Doi: 10.1161/ATVBAHA.120.313792.

85. Aavik E., Turunen MP., Ylä-Herttuala S. Epigenetics and atherosclerosis. Patho-Epigenetics of Disease, vol. 9781461433. 2012. p. 397–418.

86. Gregersen I., Halvorsen B. Epigenetics and Atherosclerosis – Challenges and Potential Epigenetic mechanisms. JSM Atheroscler 2016;1(2):14–6.

87. Wierda RJ., Geutskens SB., Jukema JW., Quax PHA. Epigenetics in atherosclerosis and inflammation 2010;14(6):1225–40. Doi: 10.1111/j.1582-4934.2010.01022.x.

88. Khyzha N., Alizada A., Wilson MD., Fish JE. Epigenetics of Atherosclerosis: Emerging Mechanisms and Methods. Trends Mol Med 2017. Doi: 10.1016/j.molmed.2017.02.004.

CHAPTER FOUR: PLASMA MICROBIOME SIGNATURES IN FAMILIAL HYPERCHOLESTEROLEMIC WISCONSIN MINIATURE SWINE™ MODEL OF ATHEROSCLEROSIS

Manuscript in preparation

Hadjer Namous, Hasan Khatib

Corresponding author:

Hasan Khatib

Abstract

Background: Microbiome dysbiosis is linked to cardiovascular diseases; however, there are no reports of circulating microbiome profiles associated with atherosclerosis. The objective of the present study was to identify circulating microbiome signatures as potential diagnostic biomarkers for atherosclerosis using the Wisconsin Miniature Swine™ of Familial Hypercholesterolemia (WMS-FH), a swine model for the disease.

Methods: Eighteen pigs were used (WMS-FH n =9; WMS-N n = 9). Full-length 16S rRNA gene sequencing was performed to identify differentially abundant (DU) taxa between both groups. ROC analysis with the AUC were employed to determine the diagnostic power of DU taxa. Correlation analysis was carried out to determine those taxa that associate with total cholesterol.

Results: 16S bacterial DNA levels were lower in WMS-FH compared to WMS-N. Significant DU taxa were captured at months 6 and 9 but not 3. *Bacteroidetes* phylum at month 9 exhibited a strong diagnostic power with AUC = 0.97 at a statistical power of 0.99.

Conclusion: Circulating microbiome signatures associated with atherosclerosis in WMS-FH. Specifically, *Bacteroidetes* phylum showed a significantly powerful diagnostic power and represents a promising biomarker for atherosclerosis.

Keywords: Plasma, microbiome, 16S, biomarker, atherosclerosis

Introduction

The microbiome is recognized as an essential player in human health. It is present in different locations within the host system, including the gut, oral cavity, respiratory tract, wounds, and circulation (1,2).

Microbiome dysbiosis has been associated with cancer, inflammatory bowel disease, and cardiovascular diseases (CVDs) (3–8). Although mechanisms by which the microbiome contributes to disease onset or prevention are unclear, current knowledge suggests that the host microbiome, specifically in the gut, regulates the host immune system and metabolism (3,9,10). For instance, lipopolysaccharides (LPS) produced by bacteria stimulate macrophages' pro-inflammatory (M1) state (11) via Toll-Like Receptors (TLRs), leading to cytokine production and the promotion of atherosclerosis (12,13). Also, the gut microbiome modulates cholesterol homeostasis (14) by regulating the expression of genes involved in cholesterol efflux, such as ABCA1/ABCG1(15). Recently, Kenny et al. also reported gut bacteria that metabolize cholesterol leading to a decrease in its serum levels (16). Also, trimethylamine N-oxide (TMOA) synthesis by gut microbes is connected to an increased risk of cardiovascular diseases (17).

Blood microbiome comes from different sources: gut, oral cavity, respiratory tract, skin, and injuries (18, 19). Disturbances of the circulating microbiome were also associated with cancer, diabetes, and cardiovascular diseases (20–27). For instance, low levels of circulating bacterial DNA for all phyla except for *Proteobacteria* were detected in patients with cardiovascular complications (25). In a subsequent study, the authors showed that patients with myocardial infarction exhibited low levels of bacterial DNA in the blood for *Norcardiaceae, Aerococcaceae, Gordonia, Propionibacterium, Chryseobacterium,*and *Rhodococcus,* which are cholesterol-

degrading bacteria (24). Whether circulating microbiome has a role in driving the disease or is present in the circulation due to weakened intestinal barriers and wounds is yet to be determined.

To the best of our knowledge, the present work is the first to report the circulating microbiome dynamics within the context of atherosclerosis, the underlying condition causing CVDs. Previous reports confirmed the presence of bacterial DNA within atherosclerosis plaque (28–31), but not in circulation. Herein, we used a large animal model that develops atherosclerosis spontaneously, the Wisconsin Miniature Swine™ of Familial Hypercholesterolemia (WMS™-FH), in a longitudinal study to identify microbiome signatures in circulation during early stages of the disease. We analyzed plasma bacterial DNA using PacBio 16S rRNA gene full-length sequencing and determined differences in taxa abundance between WMS-FH animals and their counterparts WMS-N. We also conducted a discriminatory power analysis to determine taxa with strong diagnosis power.

Material and Methods

Ethics statement

The University of Wisconsin-Madison Institutional Animal Care and Use Committee (IACUC) approved the animal protocol following the Guide for the Care and Use for Laboratory Animals (32) and the Animal Welfare Act (33).

Experimental model and animal care

The Wisconsin Mini Swine™ (WMS) is a breed of pigs developed at the University of Wisconsin-Madison. There are two distinct groups within the WMS herd, familial hypercholesterolemic (WMS-FH) and normocholesterolemic WMS (WMS-N). The WMS-FH are homozygous for a single point mutation at the low-density lipoprotein receptor gene (LDLR)

(34,35). The LDLR mutation is present at the protein's ligand region and affects the binding of cholesterol-laden particles, hindering cholesterol clearance from the bloodstream. As a result, WMS-FH develops human-like complex lesions in different arterial beds and display necrotic core, calcification, neovascularization, and neointimal formation (36–40). The WMS-N animals have the same genetic background as the WMS-FH, except these animals do not have the LDLR mutation.

This study recruited nine WMS-FH and nine WMS-N females. Animals were housed under the same conditions at the Swine Research and Teaching Center (SRTC), University of Wisconsin- Madison. The diet was formulated to meet the swine requirements for essential nutrients (Appendix A. Table 1).

Plasma collection and total cholesterol measurement

We collected blood samples from each animal to identify circulating microbiome taxa differences between WMS-FH and WMS-N. Blood was collected at three time points (3, 6, and 9 months of age) in 10 mL EDTA tubes and then processed to collect plasma. Under aseptic conditions, EDTA tubes were centrifuged at 3000 rpm for 15 minutes at 4° C. Separated plasma was then transferred to 15 mL sterile tubes and centrifuged again using the same conditions to remove residual cells and cell debris. Plasma was stored in sterile, RNase/DNase-free 1.5 mL tubes in separate aliquots at -80°C until needed. All supplies used were sterile.

Total cholesterol levels were measured in plasma samples using ELISA Cholesterol Assay Kit - HDL and LDL/VLDL (Abcam, CA, USA) following the product manual. Plasma samples from WMS-FH were diluted (2-fold) so that colorimetric readings fell within the range of the cholesterol standard curve.

DNA extraction

Microbial DNA was extracted from 400 uL plasma following the Cador Pathogen 96 QIAcube HT-an automated purification process of bacterial DNA from animal blood, serum, plasma, and other biofluids (QIAGEN, MD, USA). DNA extraction was carried out following manufacturer instructions with minor modifications. Briefly, nuclease-free water was used instead of the internal control provided by the kit. Additionally, DNA was eluted in nuclease-free water instead of the AVE buffer. All samples (n = 54) were extracted at the same time.

16S rRNA gene amplification, library preparation, and sequencing

The variable region of the 16S rRNA gene was sequenced to assess differences in taxa levels between WMS-FH and WMS-N. For each sample, full-length 16S rRNA genes (V1_V9) were amplified using two universal PCR primers: forward primer - 5'AGRGTTYGATYMTGGCTCAG3' and reverse primer – 5' RGYTACCTTGTTACGACTT3'. Both primers were tailed with sample-specific PacBio barcode sequencing to allow for multiplex sequencing and reduce chimera formation. Amplification PCR was performed using PacBio Amplification of bacterial full-length 16S gene with barcoded primers (Pacific Biosciences, CA, USA).

SMRTbell libraries were prepared from the PCR amplicons via blunt-ligations using SMRTbell prep kit 3.0 according to PacBio protocol for preparing multiplexed amplicon libraries. In addition, purified libraries were sequenced on a single PacBio Sequel II cell using S/P5-C2/5.0 sequencing chemistry. Detailed protocols can be found at: Procedure & checklist - Amplification of bacterial full-length 16S rRNA gene with barcoded primers (pacb.com); Procedure & checklist - Preparing multiplexed amplicon libraries using SMRTbell prep kit 3.0 (pacb.com).

Data processing and taxonomy assignment

Circular consensus sequence (CCS) reads were generated from raw PacBio sequencing data using standard tools provided by the manufacturer (Pacific Biosciences). Raw reads were demultiplexed using the lima application of the PacBio platform (Biotechnology Center, the University of Wisconsin-Madison).

Obtained bam files were converted to fastq files for each sample. Fastq files were then checked for sequence quality using FASTQC (41) . Next, fastq files were processed using DADA2 (42). First, primers were removed from reads using *removePrimers(max.mismatch =3, orient = TRUE)*. Then, after checking for read distribution across samples, reads with 100bp to 1600 bp were retained using the function *FilterAndTrim(minLen=100, maxLen=1600)*. Another FASTQC analysis was performed after trimming and filtering to ensure the good quality of the reads. Next, a dereplication step followed the filtering step to remove duplicate sequences and simplify analysis using *derepFastq(qualityType= "FastqQuality")*. Error learning was assessed using *learnErrors(errorEstimationFunction = PacBioErrFun, BAND_SIZE= 32, qualityType="FastqQuality")*. Generated Amplicon Sequence variants (ASVs) were then mapped to the Silva database (Silva_nr_v128_train_set.fa.gz) to assign taxonomy at phylum, class, order, family, and genus levels. Taxonomy assignment was carried out using the *assignTaxonomy* function in DADA2.

Differential abundance analysis

Using the data containing the counts, taxa, metadata, and tables, we generated a Phyloseq object using Phyloseq (43). Non-bacterial sequences were removed from the dataset. Relative abundance, alpha- and beta-diversities were calculated. To determine the differential abundance of taxa between WMS-FH and WMS-N, we used the DESeq2 package in R (44). Differential

abundance (DU) was determined separately for each time point (Months 3, 6, and 9). Differential abundance was carried out at the five taxonomic levels (phylum, order, class, family, and genus) with and without *Cyanobacteria*. Taxa with adjusted p-values < 0.1 were considered statistically significant.

Discriminatory power analysis of DU taxa

To determine the diagnostic power of DU taxa, we performed a discriminatory power analysis using the ROC curves via the pROC R package (45). Animals were previously categorized into "Disease" versus "healthy" groups based on Optical Coherence Tomography (OCT) around ~12 months of age (Chapter 3). Then, for each DU taxa, normalized sequencing reads were used to measure the AUC, and its statistical power at a significance level < 0.05.

Statistical analysis

Statistical analysis on total cholesterol, weight, alpha diversity, and differential abundance was conducted using PhyloSeq in the R environment version 4.1.3. WMS-FH and WMS-N main features were compared using a two-tailed t-test. Statistical difference in alpha diversity was assessed using the Wilcoxon test. Statistical difference in alpha- diversity (shannon) was assessed using the Wilcoxon test, whereas statistical difference in beta-diversity (Bray-Curtis) was assessed using a multivariate homogeneity of groups dispersions (variance) using the *betadisper* function in Vegan R package. Differential abundance analysis was carried out using the negative binomial regression model in DESeq2 with adjustment for the collection date of plasma in the model.

Results

Characteristics of the animals

The characteristics of the animal groups used in the study are summarized in Table 1. Our animal groups did not exhibit significant differences in weight at all three-time points. However, significant differences were observed in total cholesterol levels between the groups at months 3, 6, and 9. We also observed significant differences in total cholesterol within the WMS-FH group between months 3 and 6 and months 6 and 9. WMS-FH levels of total cholesterol increased from 281.75 mg/dL at month 3 (M3) to 436.98 mg/dL at month 6 (M6) (M3 vs. M6, $p = 0.014$) and stabilized at an average of 436.77mg/dL at month 9 (M9) (M6 vs. M9 $p = 0.99$). Additionally, WMS-FH showed high variability in total cholesterol levels within animals at the same age (months 3, 6, and 9) (Figure 1).

Table 1. Characteristics of the animal cohort used for 16S rRNA gene full-length sequencing.

Variables	**Age** [ns] (Months, mean ± SD)	**Weight** [ns] (kg, mean ± SD)	**Total cholesterol***** (mg/dL, mean ± SD)
WMS-FH			
Month 3	3.03±0.08	15.16±2.32	281.75±89.86
Month 6	6.06±0.06	26.73±5.46	436.98±142.95
Month 9	9.16±0.02	38.67±9.66	436.77±238.99
WMS-N			
Month 3	2.98±0.08	14.48±3.21	81.52±20.44
Month 6	5.97±0.10	25.19±4.20	96.78±35.25
Month 9	9.10±0.10	42.27±8.11	61.73±12.44

FH: familial hypercholesterolemia; SD: standard deviation. ***: statistically significant difference between groups ($p<0.001$) at three-time points (months 3, 6, and 9). ns: no statistical significance between groups ($p>0.1$).

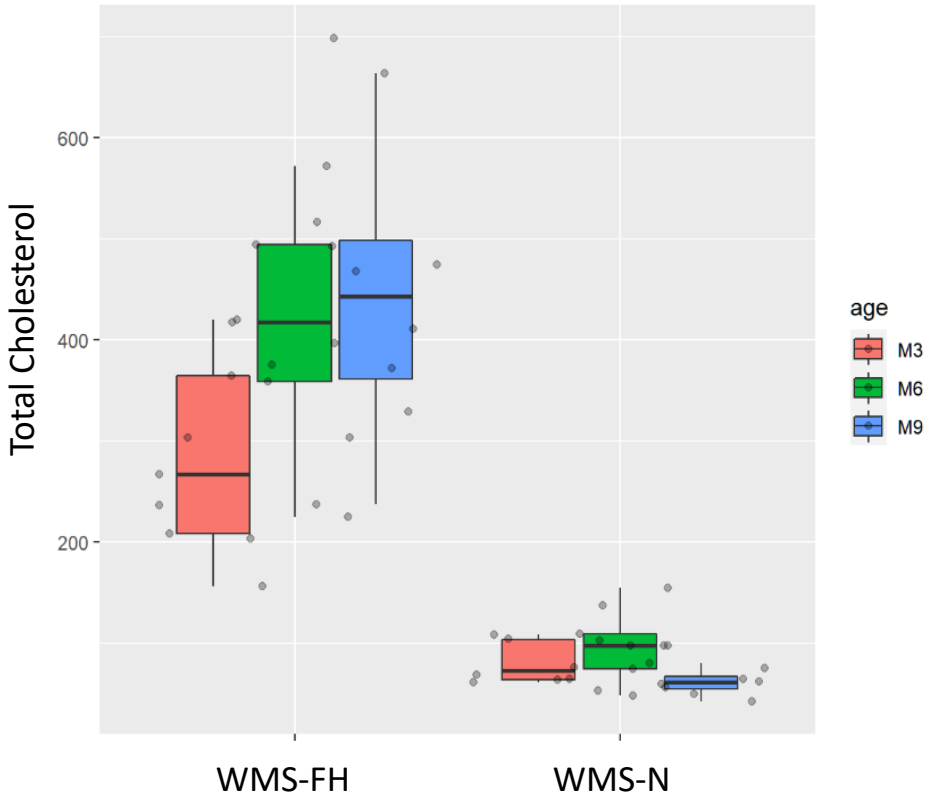

Figure 1. Total cholesterol (mg/dl) levels in WMS-FH vs. WMS-N at three-time points of plasma collection (months 3, 6, and 9).

16S rDNA sequences and microbial composition

A total of 54 plasma samples were profiled for 16S rRNA gene sequences. The overall number of sequences varied between samples (Figure 2). However, WMS-N animals had a higher number of reads compared to WMS-FH when the animals were nine months of age ($p < 0.01$) (Figure 2). We also observed two peaks in the distribution of reads, around 500 bp and 1500 bp, respectively (Figure 3**)**.

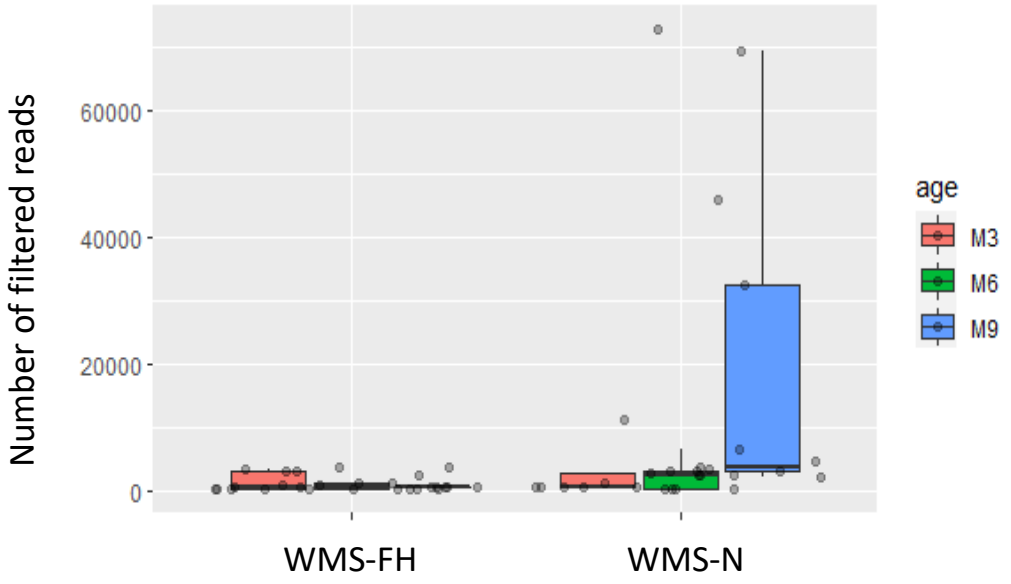

Figure 2. Boxplots of filtered reads (16S rRNA gene sequences) in WMS-FH and WMS-N at months 3, 6 , and 9.

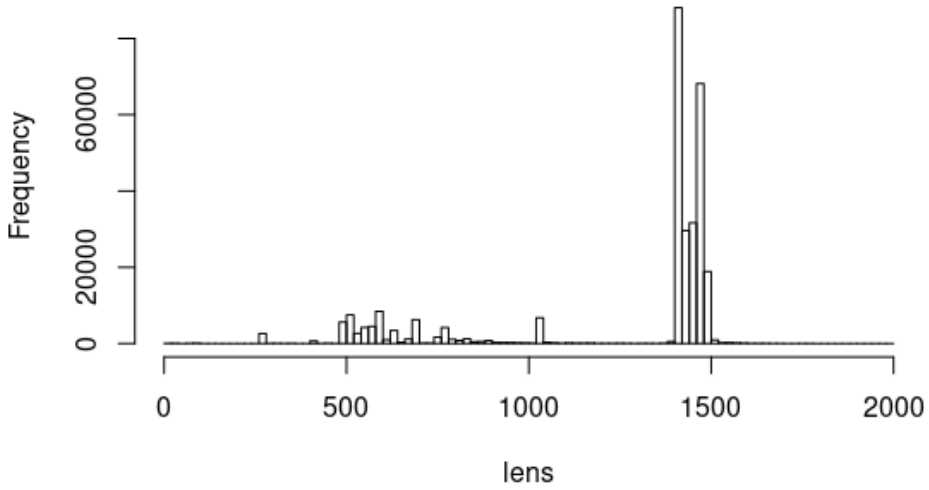

Figure 3. Histogram plot for reads length distribution across all samples (n=54) after removal of primers.

When assessing read length distribution at each sample, we noted the presence of either smaller reads (~200 bp) or, longer ones (~1500 bp); hence, to cover more sequences, we retained

reads between 100 bp to 1600 bp for further analysis. The 16S rRNA gene sequences analysis resulted in 234,715 amplicon sequence variants (ASVs) across all 54 samples. The minimum and maximum lengths of ASVs were 502 bp and 1600 bp, respectively, which correspond to the regular range in length of V1-V9 16S rRNA gene. Also, reads above 1600 bp exhibit low sequence quality.

Next, we investigated taxonomic diversity. The alpha- and beta-diversities were not statistically different, suggesting no difference in the structure and richness between WMS-FH and WMS-N at the Phylum level. However, at month 9, the beta diversity at the family level was significantly different between WMS-FH and WMS-N ($p = 0.049$). We then performed taxonomic assignment of the ASVs sequences present in the plasma of both groups. As shown in Figure 4, plasma bacterial DNA sequences belonged mainly to the *Firmicutes*, *Actinobacteria*, *Proteobacteria*, and *Cyanobacteria* for the three-time points (months 3, 6, and 9). Other phyla were grouped under <1%.

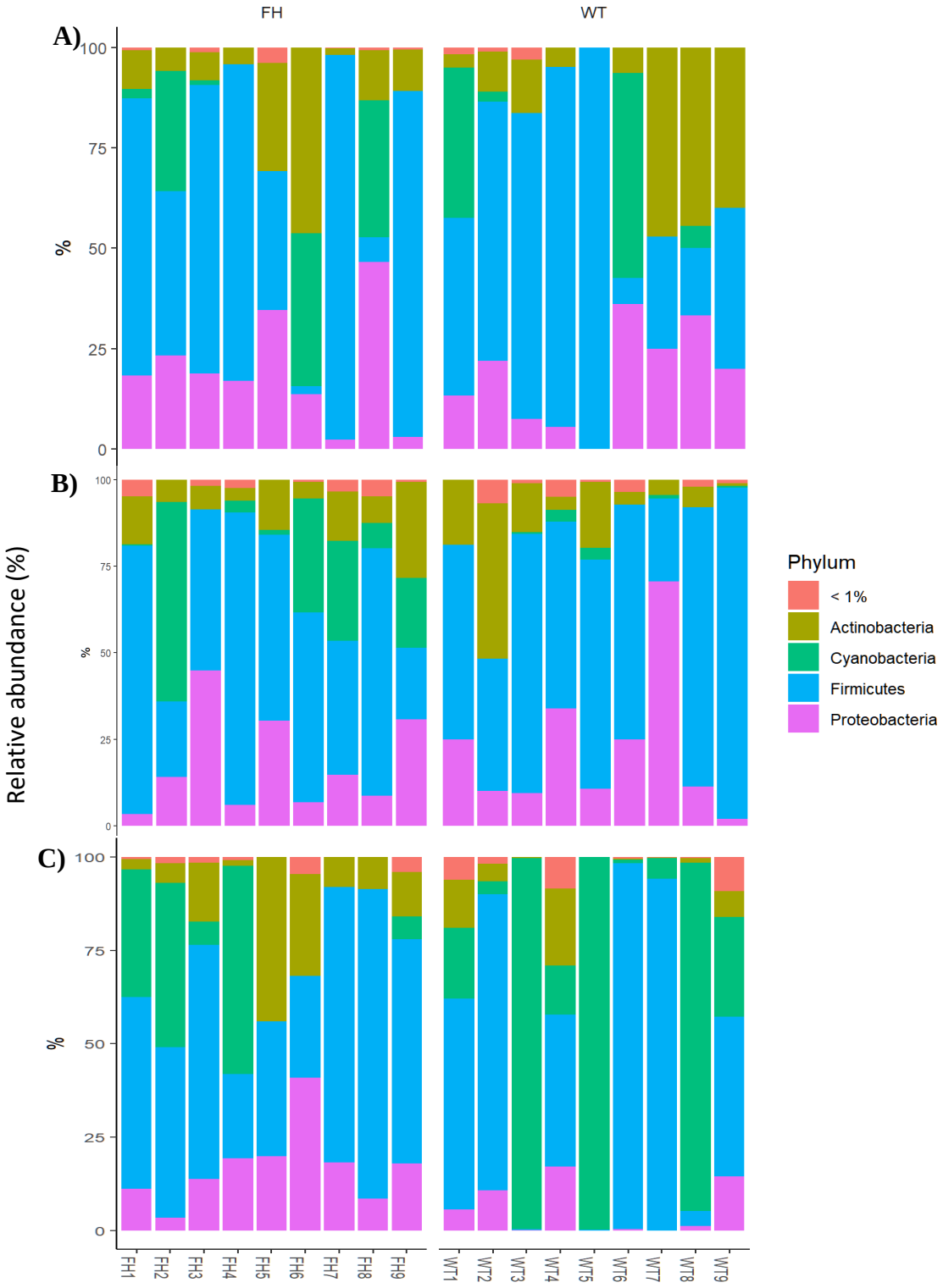

Figure 4. Most abundant phyla in plasma of WMS animals at months 3 (A), 6 (B), and 9 (C). FH = WMS-FH ; WT = WMS-N.

Differential abundance of different taxa levels and correlation with total cholesterol levels

To determine differentially abundant taxa between WMS-FH and WMS-N, we used the raw count reads obtained from DADA2 and normalized them to account for the differences in sequencing depth for each sample. Tables 2 and 3 summarize the DU results at different taxonomic levels with and without Cyanobacteria, respectively.

Table 2. Differential abundance of taxa between WMS-FH and WMS-N at months 3, 6, and 9 before removing *Cyanobacteria*.

Time	Taxa level	Fold change	Adjusted p-value	Abundance
Month 3	NS		NS	NS
Month 6	**Phylum**:			
	Cyanobacteria	11.11	0.028	↑ in WMS-FH
	Class:			↓ in WM-N
	Chloroplast	14.28	0.009	
Month 9	**Phylum**:			
	Bacteroidetes	5.98	0.027	
	Cyanobacteria	49.5	0.002	
	Class:			
	Bacteroidia	13.86	0.016	
	Chloroplast	34.09	0.019	↑ in WMS-N
	Order:			↓ in WM-FH
	Bacteroidales	17.67	0.019	
	Choloroplast|Unknown	40.06	0.050	
	Family:			
	Prevotellaceae	22.66	0.068	
	Choloroplast|Unknown|Unknow	40.50	0.068	

↑: upregulation; ↓: downregulation; NS: no significance

At the age of 3 months, no statistically significant differences were found between WMS-FH and WMS-N when DU analysis was carried with and without *Cyanobacteria*.

At month 6 of age, only one phylum showed significant differences, *Cyanobacteria*, between WMS-FH and WMS-N. However, *Cyanobacteria* was higher in WMS-FH with an FC of 11.11 (adjusted p-value =0.028). We also found that WMS-FH (FC = 14.28, adjusted p-value =

0.009) have higher levels of the *Chloroplast* class from the *Cyanobacteria* phylum than WMS-N. When *Cyanobacteria* was removed from the data, no significant difference were observed between WMS-FH and WMS-N.

Similarly, *Cyanobacteria* and class of *Chloroplast* were differentially abundant at 9 months of age, although these taxa were more abundant in WMS-N than in WMS-FH (*Cyanobacteria* FC = 49.5 and adj. p = 0.002; *Chloroplast* FC = 34.09 and adj. p= 0.019). Moreover, differences at the order and family levels within *Cyanobacteria* | *Chloroplast* were observed; however, these taxa were of an unknown assignment. *Bacteroidetes*, another phylum with a lesser relative abundance in our samples, was shown to be differentially abundant with higher levels in WMS-N animals (FC = 5.98; adj. p= 0.027). Similarly, differences at other taxa levels within the *Bacteroidetes* were higher in WMS-N. These were: class of *Bacteroidia* (FC = 13.86 adj. p = 0.016), order of *Bacteroidales* (FC = 17.67, adj. p = 0.019), and family of *Prevotellaceae* (FC = 22.66, adj. p = 0.068).

Table 3. Differential abundance of taxa between WMS-FH and WMS-N at months 3, 6, and 9 after removing *Cyanobacteria*.

Time	Taxa level	Fold change	Adjusted p-value	Abundance
Month 3	NS	-	NS	NS
Month 6	NS	-	NS	NS
Month 9	**Phylum**: *Bacteroidetes*	7.73	0.032	↑ in WMS-N ↓ in WM-FH
	Class: *Bacteroidia*	12.91	0.035	
	Order: *Bacteroidales*	17.51	0.018	
	Family: Prevotellaceae	23.25	0.006	

↑: upregulation; ↓: downregulation; NS: No significance

Bacteroidetes (FC = 7.73, adj. p = 0.032), *Bacteroidia (FC* = 12.91, adj. p = 0.035), *Bacteroidales* (FC = 17.51, adj. p = 0.018), and *Prevotellaceae* (FC = 23.26, adj. p = 0.006) were the only DU taxa when the analysis was carried on raw data after removing *Cyanobacteria*. Interestingly, the *Prevotellaceae* family is almost exclusively present in WMS-N animals (Figure 5).

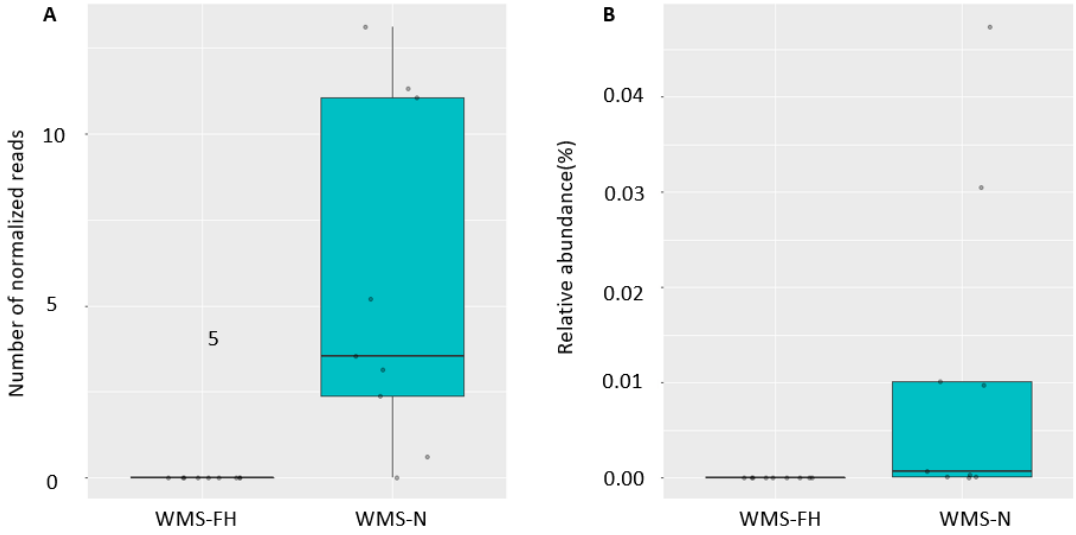

Figure 5. Prevotellaceae family almost exclusively expressed in WMS-N. A) Normalized reads of the family obtained using DESeq2, B) Relative abundance of the family in each group.

Diagnostic power of DU taxa

Discriminatory power analysis was performed to assess whether the DU taxa obtained with DESeq2 are powerful in diagnosing atherosclerosis. OCT imaging confirmed the presence of atherosclerosis in the coronary arteries in 7 out of 9 WMS-FH. No lesions were present in WMS-N. Table 4 summarizes the results of ROC analysis with the AUC and the statistical power as indicators of the diagnostic power of the DU.

Among the DU taxa, month 6 taxa *Cyanobacteria* (AUC = 0.678 and power = 0.197) and the class *Chloroplast* (AUC = 0.738 and power = 0.317) demonstrated weak statistical power. Similarly, *Cyanobacteria* and *Chloroplast* exhibited weak diagnostic power at month 9. In contrast, *Bacteroidetes* showed a strong discriminatory power with an AUC = 0.97 and a statistical power of 0.99. Under this phylum level, the class "*Bacteroidia*," order "*Bacteroidales*," and family "*Prevotellaceae*" did not have a strong diagnostic power but performed better than *Cyanobacteria* and *Chloroplast*.

Table 4. The discriminatory power of DU taxa using ROC analysis.

Age and Taxa	**AUC**	**Statistical Power at alpha = 0.05**
Month 6		
Phylum:		
Cyanobacteria	0.678	0.197
Class:		
Chloroplast	0.738	0.317
Month 9		
Phylum:		
Bacteroidetes	0.97	0.99
Cyanobacteria	0.722	0.243
Class:		
Bacteroidia	0.819	0.597
Chloroplast	0.695	0.194
Order:		
Bacteroidales	0.810	0.510
Choloroplast|*Unknown*	0.726	0.29
Family:		
Prevotellaceae	0.833	0.582
Choloroplast|Unknown|Unknown	0.726	0.290

Discussion

Microbiome alterations have been linked to several diseases, including atherosclerosis (26, 46–50). Inflammation and dyslipidemia are key risk factors in atherosclerosis development, and both can be modulated by the host microbiome (12, 13, 14, 15, 51). Our study aimed to identify the plasma microbiome signatures associated with atherosclerosis using a swine model.

The 16S rRNA full-length sequencing data showed that both WMS-FH and WMS-N harbor bacterial DNA in the plasma, most likely due to bacterial translocation from the gut and/or the oral cavity (19). These findings are consistent with previous studies that have demonstrated that bacteria and their DNA were found in the blood of healthy individuals (18). Studies have also shown that bacterial signatures differed between healthy and patients with other diseases, including diabetes and cardiovascular diseases (22–25,52,53). Although few studies reported the presence of bacterial DNA in atherosclerosis plaque (28–31), no studies addressed the relationship between atherosclerosis and the circulating microbiome.

In the present study, we observed differences in bacterial DNA (16S rRNA gene) between WMS-FH and WMS-N at different taxa levels. Although we did not assess the gut and oral cavity microbiome, the observed 16S rRNA gene DNA likely originate from the gut due to bacterial translocation, the oral cavity, or even minor injuries. We also observed that WMS-FH pigs have lower levels of bacterial DNA in the plasma compared to WMS-N. Similar findings by Amar et al. noted lower levels of bacterial DNA in the blood of patients with CVDs (25). Conversely, the level of bacteria DNA was higher in patients with myocardial infarction compared to healthy people (24). Other studies also found increased levels of bacterial DNA in unhealthy individuals, often associated with increased inflammation (54, 55). So, it is unclear why such differences in bacterial DNA levels vary, and further investigations are needed to determine the cause.

The most abundant phyla in our samples were *Firmicutes, Actinobacteria, Proteobacteria,* and *Cyanobacteria*. Similar to our results, studies based on the 16S rRNA gene showed that the blood microbiome is predominantly made of *Proteobacteria, Actinobacteria, Firmicutes, and Bacteroidetes* (25, 56, 57,58). *Proteobacteria* was also higher in CVD patients (25, 24). However, despite the higher levels of *Proteobacteria* in WMS-FH, this phylum was not statistically different from WMS-N.

We found that *Firmicutes* is the most abundant phylum in the blood in plasma samples. Firmicutes did not show significant differences between WMS-FH and WMS-N, although, some of WMS-N animals harbored higher levels of this phylum (Appendix C. Table 1). *Firmicutes* is a dominant phylum in the gut (59). A study showed that *Firmicutes* levels were lower in the gut of type 2 diabetes patients (60). Similarly, patients with inflammatory thoracic aorta aneurysms exhibited lower levels of *Firmicutes* in the aortic tissue compared to healthy individuals (61). The authors also noted that the genus *Prevotella* is less abundant in the disease group (61). The *Prevotella* genus belongs to the *Prevotellaceae* family and *Bacteroidetes* phylum. Our data demonstrated that *Bacteroidetes* were significantly different between the groups showing a higher level in WMS-N, although the abundance was low in plasma samples. A recent study found low levels of *Bacteroides* of the *Bacteroidetes* phylum in the blood of patients with a high risk for CVD mortality (26). We also found the *Prevotellaceae* family to have an exclusive presence in WMS-N group, albeit at low levels.

Little is known about the mechanisms by which the microbiome contributes to atherosclerosis, although current evidence suggests a role in inflammation modulation and cholesterol metabolism (12- 16). The abundance of the *Prevotella* genus of the *Prevotellaceae* family has been associated with lower levels of inflammatory cytokines (e.g., TNF-alpha) (62).

Moreover, *Prevotellaceae* family members are known to produce butyrate (63), a short fatty acid with anti-inflammatory activities and anti-atherogenic properties (59). Butyrate reduces the risk of atherosclerosis development via the regulation of monocyte-endothelial interactions and the accumulation of lipids in macrophages (59,64). These findings suggest that WMS-FH lack the atheroprotective effect of butyrate that is conferred to WMS-N by the *Prevotellaceae* from the *Bacteroidetes* phylum.

Gut microbiota regulates host cholesterol homeostasis (14,65–67). Among the DU taxa, *Bacteroidetes* possess the cholesterol oxidases (Chox) genes which oxidize cholesterol and subsequently lower total cholesterol levels in the circulation (68). This enzymatic activity of *Bacteroidetes* suggests that WMS-N animals have another mechanism to lower cholesterol levels that WMS-FH do not possess. Additionally, the high diagnostic power of *Bacteroidetes* coupled with its role in cholesterol metabolism suggests that this phylum is a promising diagnostic biomarker for atherosclerosis. However, due to the low number of animals recruited in this study, additional studies with a larger sample size are needed to confirm the current findings. Further research is needed to understand why *Bacteroidetes* is present at low levels in animals with atherosclerosis, as well as how this taxon affects the disease.

Conclusion

In conclusion, our findings showed that bacterial DNA is present in the plasma of WMS animals. In addition, we observed differences in the abundance of taxa between WMS-FH and WMS-N. Specifically, *Bacteroidetes*, a phylum with a protective effect against hyperlipidemia and atherogenesis were significantly lower in WMS-FH. At a higher resolution of taxa, *Prevotellaceae* was almost exclusively present in WMS-N. Also, *Bacteroidetes* exhibited a strong diagnostic

power for atherosclerosis in the coronary arteries. Whether the observed differences have an impact on dyslipidemia and atherosclerosis development remains to be explored. Nonetheless, these findings suggest that the variation of specific taxa in plasma represents potential predictive/diagnostic biomarkers for atherosclerosis.

Acknowledgements

We thank SRTC staff for their diligent work caring for the animals used in the study. We also thank professor Hilario Mantovani and Professor Joseph Francis Pierre for their help and guidance with the 16S rRNA gene analysis.

Author's contribution

HN and HK: Conceived and designed the study. HN: Carried the experiments, bioinformatics analysis, and data interpretation. HN: wrote and revised the manuscript. All authors read and approved the submitted version of the manuscript.

References

1. Kowarsky M., Camunas-Soler J., Kertesz M., et al. Numerous uncharacterized and highly divergent microbes which colonize humans are revealed by circulating cell-free DNA. Proceedings of the National Academy of Sciences 2017;114(36):9623–8. Doi: 10.1073/pnas.1707009114.

2. Lloyd-Price J., Abu-Ali G., Huttenhower C. The healthy human microbiome. Genome Med 2016;8(1):51. Doi: 10.1186/s13073-016-0307-y.

3. Tang WHW., Kitai T., Hazen SL. Gut Microbiota in Cardiovascular Health and Disease. Circ Res 2017;120(7):1183–96. Doi: 10.1161/CIRCRESAHA.117.309715.

4. Carding S., Verbeke K., Vipond DT., Corfe BM., Owen LJ. Dysbiosis of the gut microbiota in disease. Microb Ecol Health Dis 2015;26(0). Doi: 10.3402/mehd.v26.26191.

5. Vimal J., Himal I., Kannan S. Role of microbial dysbiosis in carcinogenesis & cancer therapies. Indian Journal of Medical Research 2020;152(6):553. Doi: 10.4103/ijmr.IJMR_1026_18.

6. Santana PT., Rosas SLB., Ribeiro BE., Marinho Y., de Souza HSP. Dysbiosis in Inflammatory Bowel Disease: Pathogenic Role and Potential Therapeutic Targets. Int J Mol Sci 2022;23(7):3464. Doi: 10.3390/ijms23073464.

7. Kumar D., Mukherjee SS., Chakraborty R., et al. The emerging role of gut microbiota in cardiovascular diseases. Indian Heart J 2021:264–72. Doi: 10.1016/j.ihj.2021.04.008.

8. Montagnana M., Degli Studi Di Verona U., Yan R., Li H., Ma J. The Role of Gut Microbiota in Atherosclerosis and Hypertension 2018. Doi: 10.3389/fphar.2018.01082.

9. Wang Z., Klipfell E., Bennett BJ., et al. Gut flora metabolism of phosphatidylcholine promotes cardiovascular disease. Nature 2011;472(7341):57–63. Doi: 10.1038/nature09922.

10. Zhang XN., Yu ZL., Chen JY., et al. The crosstalk between NLRP3 inflammasome and gut microbiome in atherosclerosis. Pharmacol Res 2022. Doi: 10.1016/j.phrs.2022.106289.

11. Reigstad CS., Lundén GÖ., Felin J., Bäckhed F. Regulation of serum amyloid A3 (SAA3) in mouse colonic epithelium and adipose tissue by the intestinal microbiota. PLoS One 2009;4(6). Doi: 10.1371/JOURNAL.PONE.0005842.

12. Garshick MS., Nikain C., Tawil M., et al. Reshaping of the gastrointestinal microbiome alters atherosclerotic plaque inflammation resolution in mice. Scientific Reports | 2021;11(8966):1–9. Doi: 10.1038/s41598-021-88479-y.

13. Fang H., Pengal RA., Cao X., et al. Lipopolysaccharide-Induced Macrophage Inflammatory Response Is Regulated by SHIP. The Journal of Immunology 2004;173(1):360–6. Doi: 10.4049/jimmunol.173.1.360.

14. le Roy T., Lécuyer E., Chassaing B., et al. The intestinal microbiota regulates host cholesterol homeostasis. BMC Biol 2019;17(1). Doi: 10.1186/s12915-019-0715-8.

15. Wang D., Xia M., Yan X., et al. Gut Microbiota Metabolism of Anthocyanin Promotes Reverse Cholesterol Transport in Mice Via Repressing miRNA-10b. Circ Res 2012;111(8):967–81. Doi: 10.1161/CIRCRESAHA.112.266502.

16. Kenny DJ., Plichta DR., Shungin D., et al. Cholesterol Metabolism by Uncultured Human Gut Bacteria Influences Host Cholesterol Level. Cell Host Microbe 2020;28(2):245-257.e6. Doi: 10.1016/j.chom.2020.05.013.

17. Rahman MdM., Islam F., -Or-Rashid MdH., et al. The Gut Microbiota (Microbiome) in Cardiovascular Disease and Its Therapeutic Regulation. Front Cell Infect Microbiol 2022;12. Doi: 10.3389/fcimb.2022.903570.

18. Castillo DJ., Rifkin RF., Cowan DA., Potgieter M. The Healthy Human Blood Microbiome: Fact or Fiction? Front Cell Infect Microbiol 2019;9(MAY):148. Doi: 10.3389/FCIMB.2019.00148.

19. Velmurugan G., Dinakaran V., Rajendhran J., Swaminathan K. Blood Microbiota and Circulating Microbial Metabolites in Diabetes and Cardiovascular Disease. Trends in Endocrinology and Metabolism 2020:835–47. Doi: 10.1016/j.tem.2020.01.013.

20. Schierwagen R., Alvarez-Silva C., Madsen MSA., et al. Circulating microbiome in blood of different circulatory compartments. Gut 2019;68(3):578–80. Doi: 10.1136/gutjnl-2018-316227.

21. Kwan BC-H., Chow K-M., Leung C-B., et al. Circulating bacterial-derived DNA fragments as a marker * of systemic inflammation in peritoneal dialysis. Nephrology Dialysis Transplantation 2013;28(8):2139–45. Doi: 10.1093/ndt/gft100.

22. Chen H., Ma Y., Liu Z., et al. Circulating microbiome DNA: An emerging paradigm for cancer liquid biopsy. Cancer Lett 2021;521:82–7. Doi: 10.1016/j.canlet.2021.08.036.

23. Gedgaudas R., Bajaj JS., Skieceviciene J., et al. Circulating microbiome in patients with portal hypertension. Gut Microbes 2022;14(1). Doi: 10.1080/19490976.2022.2029674.

24. Amar J., Lelouvier B., Servant F., et al. Blood Microbiota Modification After Myocardial Infarction Depends Upon Low-Density Lipoprotein Cholesterol Levels. J Am Heart Assoc 2019;8(19). Doi: 10.1161/JAHA.118.011797.

25. Amar J., Lange C., Payros G., et al. Blood Microbiota Dysbiosis Is Associated with the Onset of Cardiovascular Events in a Large General Population: The D.E.S.I.R. Study. PLoS One 2013;8(1). Doi: 10.1371/journal.pone.0054461.

26. Lawrence G., Midtervoll I., Samuelsen SO., Kristoffersen AK., Enersen M., Håheim LL. The blood microbiome and its association to cardiovascular disease mortality: case-cohort study. BMC Cardiovasc Disord 2022;22(1). Doi: 10.1186/s12872-022-02791-7.

27. Qiu J., Zhou H., Jing Y., Dong C. Association between blood microbiome and type 2 diabetes mellitus: A nested case-control study. J Clin Lab Anal 2019;33(4):e22842. Doi: 10.1002/jcla.22842.

28. Renko J., Lepp PW., Oksala N., Nikkari S., Nikkari ST. Bacterial signatures in atherosclerotic lesions represent human commensals and pathogens. Atherosclerosis 2008;201(1):192–7. Doi: 10.1016/j.atherosclerosis.2008.01.006.

29. Koren O., Spor A., Felin J., et al. Human oral, gut, and plaque microbiota in patients with atherosclerosis. Proceedings of the National Academy of Sciences 2011;108(Supplement_1):4592–8. Doi: 10.1073/pnas.1011383107.

30. Serra E Silva Filho W., Casarin RCV., Nicolela EL., Passos HM., Sallum AW., Gonçalves RB. Microbial diversity similarities in periodontal pockets and atheromatous plaques of cardiovascular disease patients. PLoS One 2014;9(10). Doi: 10.1371/journal.pone.0109761.

31. Chhibber-Goel J., Singhal V., Bhowmik D., et al. Linkages between oral commensal bacteria and atherosclerotic plaques in coronary artery disease patients. NPJ Biofilms Microbiomes 2016;2(1):7. Doi: 10.1038/s41522-016-0009-7.

32. Nih., Od., Oer., Olaw. GUIDE LABORATORY ANIMALS FOR THE CARE AND USE OF Eighth Edition Committee for the Update of the Guide for the Care and Use of Laboratory Animals Institute for Laboratory Animal Research Division on Earth and Life Studies. THE NATIONAL ACADEMIES PRESS 2011:1–209.

33. Animal Welfare Act as Amended. . 7 USC § 2013:2132–59.

34. Hasler-Rapacz J., Ellegren H., Fridolfsson a K., et al. Identification of a mutation in the low density lipoprotein receptor gene associated with recessive familial hypercholesterolemia in swine. Am J Med Genet 1998. Doi: 10.1002/(SICI)1096-8628(19980413)76:5<379::AID-AJMG3>3.0.CO;2-I.

35. Schomberg DT., Tellez A., Meudt JJ., et al. Miniature Swine for Preclinical Modeling of Complexities of Human Disease for Translational Scientific Discovery and Accelerated

Development of Therapies and Medical Devices. Toxicol Pathol 2016;44(3):299–314. Doi: 10.1177/0192623315618292.

36. Hasler-Rapacz J., Prescott MF., von Linden-Reed J., Rapacz JM., Hu Z., Rapacz J. Elevated concentrations of plasma lipids and apolipoproteins B, C-III, and E are associated with the progression of coronary artery disease in familial hypercholesterolemic swine. Arterioscler Thromb Vasc Biol 1995;15(5):583–92. Doi: 10.1161/01.ATV.15.5.583/FORMAT/EPUB.

37. Schinkel AFL., Krueger CG., Tellez A., et al. Contrast-enhanced ultrasound for imaging vasa vasorum: comparison with histopathology in a swine model of atherosclerosis. European Journal of Echocardiography 2010;11(8):659–64. Doi: 10.1093/ejechocard/jeq048.

38. Bahls M., Bidwell CA., Hu J., et al. Gene expression differences in healthy brachial and femoral arteries of Rapacz familial hypercholesterolemic swine. Physiol Genomics 2011;43(12):781–8. Doi: 10.1152/physiolgenomics.00151.2010.

39. Bahls M., Bidwell CA., Hu J., et al. Gene expression differences during the heterogeneous progression of peripheral atherosclerosis in familial hypercholesterolemic swine 2013. Doi: 10.1186/1471-2164-14-443.

40. Tellez A., Krueger CG., Seifert P., et al. Coronary bare metal stent implantation in homozygous LDL receptor deficient swine induces a neointimal formation pattern similar to humans. Atherosclerosis 2010;213(2):518–24. Doi: 10.1016/J.ATHEROSCLEROSIS.2010.09.021.

41. Simon Andrews. FastQC: A Quality Control Tool for High Throughput Sequence Data. Available Online at: Http://WwwBioinformaticsBabrahamAcUk/Projects/Fastqc/ 2010.

42. Callahan BJ., McMurdie PJ., Rosen MJ., Han AW., Johnson AJA., Holmes SP. DADA2: High-resolution sample inference from Illumina amplicon data. Nature Methods 2016 13:7 2016;13(7):581–3. Doi: 10.1038/nmeth.3869.

43. McMurdie PJ., Holmes S. phyloseq: an R package for reproducible interactive analysis and graphics of microbiome census data. PLoS One 2013;8(4). Doi: 10.1371/JOURNAL.PONE.0061217.

44. Love MI., Huber W., Anders S. Moderated estimation of fold change and dispersion for RNA-seq data with DESeq2. Genome Biol 2014;15:550. Doi: 10.1186/s13059-014-0550-8.

45. Robin X., Turck N., Hainard A., et al. pROC: an open-source package for R and S+ to analyze and compare ROC curves. BMC Bioinformatics 2011;12(1):77. Doi: 10.1186/1471-2105-12-77.

46. Cason CA., Dolan KT., Sharma G., et al. Plasma microbiome-modulated indole- and phenyl-derived metabolites associate with advanced atherosclerosis and postoperative outcomes. J Vasc Surg 2018;68:1552-1562.e7. Doi: 10.1016/j.jvs.2017.09.029.

47. Zeisel SH., Warrier M. Trimethylamine N -Oxide, the Microbiome, and Heart and Kidney Disease . Annu Rev Nutr 2017;37(1):157–81. Doi: 10.1146/annurev-nutr-071816-064732.

48. Jovanovich A., Isakova T., Stubbs J. Microbiome and Cardiovascular Disease in CKD. Clinical Journal of the American Society of Nephrology 2018;13(10):1598–604. Doi: 10.2215/CJN.12691117.

49. Sawicka-smiarowska E., Bondarczuk K., Bauer W., et al. Gut microbiome in chronic coronary syndrome patients. J Clin Med 2021;10(21). Doi: 10.3390/jcm10215074.

50. Jie Z., Xia H., Zhong S-L., et al. The gut microbiome in atherosclerotic cardiovascular disease n.d. Doi: 10.1038/s41467-017-00900-1.

51. Chistiakov DA., Bobryshev Y v., Kozarov E., Sobenin IA., Orekhov AN. Role of gut microbiota in the modulation of atherosclerosis-associated immune response. Front Microbiol 2015;6(JUN):671. Doi: 10.3389/FMICB.2015.00671/BIBTEX.

52. Liu Y., Xiao F., Zhang R., Zhang X. Alterations of Plasma Microbiome: A Potentially New Perspective to the Dysbiosis in Systemic Lupus Erythematosus? Journal of Rheumatology 2022:549–51. Doi: 10.3899/jrheum.220023.

53. Rajendhran J., Shankar M., Dinakaran V., Rathinavel A., Gunasekaran P. Contrasting circulating microbiome in cardiovascular disease patients and healthy individuals. Int J Cardiol 2013;168(5):5118–20. Doi: 10.1016/j.ijcard.2013.07.232.

54. Szeto C-C., Kwan BC-H., Chow K-M., et al. Circulating Bacterial-Derived DNA Fragment Level Is a Strong Predictor of Cardiovascular Disease in Peritoneal Dialysis Patients. PLoS One 2015;10(5):e0125162. Doi: 10.1371/journal.pone.0125162.

55. Lunjani N., Albrich WC., Suh N., et al. Higher levels of bacterial DNA in serum associate with severe and fatal COVID-19. Allergy 2022;77(4):1312–4. Doi: 10.1111/all.15218.

56. Dinakaran V., Rathinavel A., Pushpanathan M., Sivakumar R., Gunasekaran P., Rajendhran J. Elevated levels of circulating DNA in cardiovascular disease patients: Metagenomic profiling of microbiome in the circulation. PLoS One 2014;9(8). Doi: 10.1371/journal.pone.0105221.

57. Whittle E., Leonard MO., Harrison R., Gant TW., Tonge DP. Multi-Method Characterization of the Human Circulating Microbiome. Front Microbiol 2019;9. Doi: 10.3389/fmicb.2018.03266.

58. Gosiewski T., Ludwig-Galezowska AH., Huminska K., et al. Comprehensive detection and identification of bacterial DNA in the blood of patients with sepsis and healthy volunteers using

next-generation sequencing method - the observation of DNAemia. European Journal of Clinical Microbiology & Infectious Diseases 2017;36(2):329–36. Doi: 10.1007/s10096-016-2805-7.

59. Magne F., Gotteland M., Gauthier L., et al. The firmicutes/bacteroidetes ratio: A relevant marker of gut dysbiosis in obese patients? Nutrients 2020;12(5). Doi: 10.3390/NU12051474.

60. Demirci M., Bahar Tokman H., Taner Z., et al. Bacteroidetes and Firmicutes levels in gut microbiota and effects of hosts TLR2/TLR4 gene expression levels in adult type 1 diabetes patients in Istanbul, Turkey. J Diabetes Complications 2020;34(2):107449. Doi: 10.1016/j.jdiacomp.2019.107449.

61. Ted Getz AM., Hoffman GS., Padmanabhan R., et al. Microbiomes of Inflammatory Thoracic Aortic Aneurysms Due to Giant Cell Arteritis and Clinically Isolated Aortitis Differ From Those of Non-Inflammatory Aneurysms. Pathog Immun 2019;4(1). Doi: 10.20411/pai.v4i1.269.

62. Larsen JM., Musavian HS., Butt TM., Ingvorsen C., Thysen AH., Brix S. Chronic obstructive pulmonary disease and asthma-associated Proteobacteria, but not commensal *Prevotella* spp., promote Toll-like receptor 2-independent lung inflammation and pathology. Immunology 2015;144(2):333–42. Doi: 10.1111/imm.12376.

63. Chen Y., Liu Y., Wang Y., et al. Prevotellaceae produces butyrate to alleviate PD-1/PD-L1 inhibitor-related cardiotoxicity via PPARα-CYP4X1 axis in colonic macrophages. Journal of Experimental and Clinical Cancer Research 2022;41(1). Doi: 10.1186/s13046-021-02201-4.

64. Xiao Y., Guo Z., Li Z., Ling H., Song C. Role and mechanism of action of butyrate in atherosclerotic diseases: a review. J Appl Microbiol 2021:543–52. Doi: 10.1111/jam.14906.

65. Yun KE., Kim J., Kim MH., et al. Major lipids, apolipoproteins, and alterations of gut microbiota. J Clin Med 2020;9(5). Doi: 10.3390/jcm9051589.

66. López-Montoya P., Cerqueda-García D., Rodríguez-Flores M., et al. Association of Gut Microbiota with Atherogenic Dyslipidemia, and Its Impact on Serum Lipid Levels after Bariatric Surgery. Nutrients 2022;14(17). Doi: 10.3390/nu14173545.

67. Guo L., Wang YY., Wang JH., et al. Associations of gut microbiota with dyslipidemia based on sex differences in subjects from Northwestern China. World J Gastroenterol 2022;28(27):3455–75. Doi: 10.3748/wjg.v28.i27.3455.

68. Molinero N., Ruiz L., Sánchez B., Margolles A., Delgado S. Intestinal bacteria interplay with bile and cholesterol metabolism: Implications on host physiology. Front Physiol 2019;10(MAR). Doi: 10.3389/fphys.2019.00185.

CHAPTER FIVE: CONCLUSION AND FUTURE DIRECTIONS

Atherosclerosis progresses silently over decades without diagnosis until the disease is clinically overt (e.g., stroke, ischemic heart disease); hence, identifying biomarkers for early diagnosis of the disease is critical to effective treatment strategies and cardiovascular risk management.

The present work demonstrated that circulating biomarkers for early diagnosis of atherosclerosis using a translational swine model of the disease (WMS-FH) can be detected in early life before disease onset and progression.

WMS-FH model of atherosclerosis displays similar phenotypic features of atherosclerosis to humans. In chapter 2, we demonstrated that gene expression profiles and mechanistic pathways involved in fibroatheroma are similar to those identified in human lesions. These findings further strengthen the suitability of the WMS-FH model to study the disease. Of particular interest are the hub genes identified in this work that are central to the mechanisms taking place in fibroatheroma. Fibroatheroma is characterized by a thick fibrous cap. Thinning of this cap is detrimental to an individual's health since prone to rupture and leads to the release of the necrotic core content into the bloodstream, eventually leading to thrombosis. Therefore, maintaining the integrity of the fibrous cap is critical to preventing such events. The identified hub genes present promising therapeutic targets to achieve such a goal, especially with the current area of targeted gene therapy. However, the therapeutic potential of these genes needs extensive mechanistic and functional investigations, both ex-vivo and in-vivo, using proper models that mimic the disease environment and complexity. To this end, and given the complexity of the aortic tissue, future studies should

focus on investigating the transcriptome of fibroatheroma at the single-cell level, which will provide further insights into the different cell populations and their contributions to the transcriptomic profile. Such an approach will allow a better targeting efficiency of any genetic and epigenetic therapeutic approaches.

The presence of fatty streaks reflects the earliest manifestation of atherosclerosis. However, not all fatty streaks progress to fibroatheroma. Fatty streaks can regress, although the exact mechanisms are unknown. Early diagnosis of atherosclerosis will provide adequate time for interventions to reduce further progression of the disease. In chapter 3, we identified circulating miRNA biomarkers in the early life of WMS-FH before atherosclerosis onset and progression. By profiling plasma miRNA signatures at early time points in the life of the animals before disease development, we found several miRNAs with strong discriminatory power. The longitudinal approach demonstrated that miRNA dynamics change over time and correlate with disease onset later in life. Although the identified miRNAs were reported to correlate with atherosclerosis in human studies, future studies should also assess the presence of these miRNAs in early life in people and not only focus on end-point analysis. Furthermore, understanding the array of mechanisms in which these miRNAs are participating would add more information regarding the use of these molecules as therapeutic targets or agents in atherosclerosis. Additionally, the identified miRNAs target genes and participate in biological processes not previously described to be related to the disease. Therefore, they are interesting to investigate in future studies as they will provide insights into new atherosclerosis mechanisms. The novel miRNAs captured here also necessitate further mechanistic investigation.

A novel category of circulating biomarkers was also investigated in this work. In chapter 4, we demonstrated for the first time that circulating microbiome (i.e., 16S bacterial DNA) signatures in young WMS-FH are associated with atherosclerosis development when the pigs are older. Specific taxa showed a significantly powerful diagnostic power for atherosclerosis and represent promising biomarkers. Future studies should focus on determining whether there are live and functional bacteria in the circulation participating in atherosclerosis development and the subsequent mechanisms involved. Additionally, using a metagenomics approach will yield better profiling of taxa with more genetic material as well as profiling other microorganisms (viruses and fungi). It is equally important to study lesions, gut, and oral cavity microbiomes concomitantly to better understand the mechanisms by which host microbes contribute to the disease.

Overall, this dissertation focused on discovering biomarkers for early diagnosis of atherosclerosis using a longitudinal approach. Ultimately, we identified circulating miRNA and microbiome biomarkers that showed potential in diagnosing atherosclerosis in WMS-FH as early as 3 and 9 months old. Using the current swine model facilitates the translation of findings to humans. However, future studies should focus on replicating the current work in human plasma samples and studying the mechanisms of these molecules and their potential as therapeutic agents and targets.

APPENDICES

APPENDIX A : CHAPTER 2

Table 1. Composition of the pellet diet fed to WMS FH and WMS normal pigs used in the study.

Ingredients	Amount (%)
Corn grain	75.51
Soybean meal	21.25
Monocalcium phosphate (21%)	0.67
Calcium Carbonate (limestone)	1.09
I-lysine mHCL	0.12
Sodium chloride (Iodized)	0.35
UW VTM G[1]	1.00
Total	**100**

1. UW VTM G w/o D is a custom-mixed vitamin trace mineral premixes formulated to provide target levels of the following supplemental nutrients per kilogram of diet: vitamin A, 4,200 IU; vitamin D, 280 IU; vitamin E, 21 IU; vitamin K, 1.12 IU; niacin, 33 mg; pantothenic acid, 18 mg; riboflavin, 12 mg; vitamin B12, 50 µg; Cu (from copper sulfate), 2.25 mg; I (from ethylenediamine dihydroiodide), 0.45 mg; Fe (from ferrous sulfate), 57 mg; Se (from sodium selenite), 0.30 mg; and Zn (from zinc oxide), 135 mg.

The amount of feed was limited for both WMS-FH and WMS-N pigs to prevent excessive body fat accumulation. The amounts were estimated from body weight as 150 kCal * Body Weight ^ 0.75. Adjustments in the amount of feed provided was adjusted as the pigs grew.

Table 2. RNA sample distribution across pools.

WMS FH group			WMS N group		
Pool1	**Pool2**	**Pool3**	**Pool4**	**Pool5**	**Pool6**
G0068[a]	G0070[a]	G0069[a]	B0033[d]	B0031[d]	B0035[d]
G0065[a]	G0066[a]	G0067[a]	B0044[e]	B0041[e]	B0040[e]
G0047[b]	G0052[b]	G0046[b]	B0048[f]	B0050[f]	B0049[f]
G0061[c]	G0043[c]			B0042[j]	B0036[j]

*Letters assigned to group siblings

Table 3. Selected genes for validation by RT-qPCR. Up/downregulation in WMS FH and gene function.

Gene	up/downregulation	function
CXCL14	upregulated	Involved in immunoregulatory and inflammatory processes (1). Promotes atherogenesis (2).
APOE	upregulated	Involved in the stimulation of cholesterol efflux from macrophage foam cells in the atherosclerotic lesion, and the regulation of immune and inflammatory responses (3)
ITGB2	upregulated	Participates in the regulation of leukocyte trafficking across the vessel wall (4)
AIF1	upregulated	Involved in inflammatory processes (5) Promotes vascular smooth muscle cell migration and uptake of oxLDL (6,7)
CD36	upregulated	Interacts with oxidized low-density lipoprotein (oxLDL), which triggers signaling cascades for inflammatory responses (8,9)
TLR4	upregulated	Deficiency of TLR4 protects macrophages from lipid accumulation during atherosclerosis (10) Enhances and sustains the innate immune and inflammatory responses(11)
TLR6	upregulated	Heterodimerizes with Toll-Like Receptor-4 (TRL4) and CD36 inside cells in response to oxidized LDL (12)
LCP1	upregulated	Involved in inflammatory responses, cell migration, and proliferation (13)
CILP2	downregulated	Stimulates oxLDL uptake by macrophages (14)
CNN1	downregulated	No known role in atherosclerosis/CVDs
CYP2B22	downregulated	The cytochrome P450 (P450) family is known for regulating cholesterol balance and preventing or regressing atherosclerosis(15)
ACTC1	downregulated	No known role in atherosclerosis/CVDs

References

1. Lu J., Chatterjee M., Schmid H., Beck S., Gawaz M. CXCL14 as an emerging immune and inflammatory modulator 2015. Doi: 10.1186/s12950-015-0109-9.

2. Tong W., Duan Y., Yang R., et al. Foam Cell-Derived CXCL14 Muti-Functionally Promotes Atherogenesis and Is a Potent Therapeutic Target in Atherosclerosis. J Cardiovasc Transl Res 2020;(13):215–224. Doi: https://doi.org/10.1007/s12265-019-09915-z.

3. Greenow Kirsty., Pearce NJ., Ramji DP. The key role of apolipoprotein e in atherosclerosis. J Mol Med 2005:329–42. Doi: 10.1007/s00109-004-0631-3.

4. Galkina E., Ley K. Vascular Adhesion Molecules in Atherosclerosis. Arterioscler Thromb Vasc Biol 2007;27(11):2292–301. Doi: 10.1161/ATVBAHA.107.149179.

5. Zhao YY., Yan DJ., Chen ZW. Role of AIF-1 in the regulation of inflammatory activation and diverse disease processes. Cell Immunol 2013:75–83. Doi: 10.1016/j.cellimm.2013.07.008.
6. Autieri M v., Kelemen SE., Wendt KW. AIF-1 is an actin-polymerizing and Rac1-activating protein that promotes vascular smooth muscle cell migration. Circ Res 2003;92(10):1107–14. Doi: 10.1161/01.RES.0000074000.03562.CC.
7. Sommerville LJ., Kelemen SE., Ellison SP., England RN., Autieri M v. Increased atherosclerosis and vascular smooth muscle cell activation in AIF-1 transgenic mice fed a high-fat diet. Atherosclerosis 2011;220:45–52. Doi: 10.1016/j.atherosclerosis.2011.07.095.
8. Park YM. CD36, a scavenger receptor implicated in atherosclerosis. Exp Mol Med 2014;46(6):e99–e99. Doi: 10.1038/emm.2014.38.
9. Tian K., Xu Y., Sahebkar A., Xu S. CD36 in Atherosclerosis: Pathophysiological Mechanisms and Therapeutic Implications. Curr Atheroscler Rep 2020;22(10):59. Doi: 10.1007/s11883-020-00870-8.
10. Singh RK., Haka AS., Asmal A., et al. TLR4 (Toll-Like Receptor 4)-Dependent Signaling Drives Extracellular Catabolism of LDL (Low-Density Lipoprotein) Aggregates. Arterioscler Thromb Vasc Biol 2020;40(1):86–102. Doi: 10.1161/ATVBAHA.119.313200.
11. Xu XH., Shah PK., Faure E., et al. Toll-Like Receptor-4 Is Expressed by Macrophages in Murine and Human Lipid-Rich Atherosclerotic Plaques and Upregulated by Oxidized LDL. Circulation 2001;104(25):3103–8. Doi: 10.1161/HC5001.100631.
12. Stewart CR., Stuart LM., Wilkinson K., et al. CD36 ligands promote sterile inflammation through assembly of a Toll-like receptor 4 and 6 heterodimer. Nat Immunol 2010;11(2):155–61. Doi: 10.1038/ni.1836.
13. Vega FM., Gautier V., Fernandez-Ponce CM., et al. The atheroma plaque secretome stimulates the mobilization of endothelial progenitor cells ex vivo. J Mol Cell Cardiol 2017;105:12–23. Doi: 10.1016/j.yjmcc.2017.02.001.
14. Hu W., Li K., Han H., et al. Circulating Levels of CILP2 Are Elevated in Coronary Heart Disease and Associated with Atherosclerosis. Oxid Med Cell Longev 2020;2020. Doi: 10.1155/2020/1871984.
15. Luoma P v. Cytochrome P450 — physiological key factor against cholesterol accumulation and the atherosclerotic vascular process. Ann Med 2007;39(5):359–70. Doi: 10.1080/07853890701379767.

Table 4. Real-time quantitative PCR primers

Gene	Primer sequence 5'- 3'	Amplicon size (bp)
APOE	Forward: TGCTTTGGTGGTAACCCTCC Reverse: GTCAGACAGGGACTGCACC	169
CXCL14	Forward: CAGCATGAGGCTCCTGACG Reverse: AACCATCTTCTCCTCGCAGTG	172
CD36	Forward: TCCTTGGCCTGGTAGAAATCATC Reverse: TATTAAGAAAGGTCCTGACGTAGC	156
TRL4	Forward: GACAGCAATAGCTTCTCCAGC Reverse: AAAGGCTCCCAGGGCTAAAC	159
TRL6	Forward: GAAATCTTGAATTTGGATGCCTAGC Reverse: AGGGTTCCCCATACTAAGGTCA	152
CYP2B22	Forward: ACCACTTTCTGGATGCCACT Reverse: AGGAATAATTCGGTGCGGGC	112
CILP2	Forward: CTCCAACTACCACGTGCGC Reverse: ATGCATCTCCAGCGGAGC	140
LCP1	Forward: CTGGGGGGCAACATGAAGAA Reverse: ACCAAGGCCAGTGTTAAGGT	137
CNN1	Forward: CCTCTGCTCACTTCAACCGA Reverse: CGTCCATGAAGTTGTTGCCG	153
ACTC1	Forward: ATGAGATGGCTACAGCTGCTT Reverse: GTTTCATGGATGCCAGCAGA	157
AIF1	Forward: ACCCTGGATTTACAGGGAGG Reverse: GAAGGCTTCCAGTTTGGAGGA	141
ITGB2	Forward: CCATCCTGACCCCCAATGAC Reverse: TTGCTTTCGGCCAGTTTGTG	115
C3	Forward: AGGCATCGTATCCTCTGGGA Reverse: ACATGGTCACCACCGACAAG	121
CD68	Forward: GCAGAAACGCAAGCATCATT Reverse: GGCCAAGGAAAATCAGTCCA	168
S100A4	Forward: TACTCAGGCAAGGAGGGTGA Reverse: TGGAAAGCAGCTTCATCCGT	113
FCER1G	Forward: GCATTGTCCTCACCCTCCTC Reverse: TAAGTCTCCTGGTTCCGGGT	121
YWHAZ	Forward: GCATCCCACAGACTATTTCC Reverse: GCAAAGACAATGACAGACCA	120

Table 5. Incidence and descriptive statistics of histological changes and composition of the neointima by treatment group

		Intimal Hyperplasia and Composition of Neointima											
Group	**Descriptive Statistic**	**Intimal Hyperplasia**	**% Circumference Containing NI**	**Cholesterol Clefts**	**Lipid**	**Macrophages, Mononuclear inflammatory cells**	**Mineralization**	**Collagen**	**Myofibroblasts and associated CT**	**Medial Vacuolation/Lipid**	**IEL Disruption**	**EEL Disruption**	**Adventitial Fibrosis**
WT (n=23)	Median	1	15	0	0	0	0	2	3	0	0	4	2
	Mean	0.74	17.61	0.00	0.00	0.00	0.00	1.94	3.65	0.00	0.26	3.61	1.74
	SD	0.44	15.59	0.00	0.00	0.00	0.00	0.64	0.76	0.00	0.44	1.01	1.07
	SEM	0.09	3.25	0.00	0.00	0.00	0.00	0.13	0.16	0.00	0.09	0.21	0.22
	Min	0	0	0	0	0	0	1	3	0	0	0	0
	Max	1	60	0	0	0	0	3	5	0	1	4	3
	Incidence	17	17	0	0	0	0	17	17	0	6	22	19
FH (n=24)	Median	1	35	1	2	2	0	3	1	0.5	0.5	4	1
	Mean	1.38	28.13	0.88	2.18	1.71	0.24	2.65	1.53	0.71	0.50	3.50	0.83
	SD	1.18	21.40	0.76	0.86	0.67	0.55	0.76	0.61	0.79	0.50	1.04	0.80
	SEM	0.24	4.37	0.15	0.17	0.14	0.11	0.16	0.12	0.16	0.10	0.21	0.16
	Min	0	0	0	1	1	0	1	1	0	0	0	0
	Max	4	60	2	4	3	2	4	3	2	1	4	2
	Incidence	17	17	11	17	17	3	17	17	12	12	23	14

Scored Parameters

Intimal Hyperplasia

0 No intimal hyperplasia present

1 Intimal hyperplasia in a minimal amount either segmentally or circumferentially. The amount of intimal hyperplasia would result in stenosis of less than 20%

2 Intimal hyperplasia in a mild amount either segmentally or circumferentially. The amount of intimal hyperplasia would result in stenosis of 20-40%

3 Intimal hyperplasia in a moderate amount either segmentally or circumferentially. The amount of intimal hyperplasia would result in stenosis of 40-60%

4 Intimal hyperplasia in a moderate to marked amount either segmentally or circumferentially. The amount of intimal hyperplasia would result in stenosis of 60-80%

5 Intimal hyperplasia in a moderate to marked amount either segmentally or circumferentially. The amount of intimal hyperplasia would result in stenosis of >80%

Components of Neointima/Media (Cholesterol Clefts, Lipid, Macrophages, Collagen, Myofibroblasts, Medial Lipid/Vacuolation)

0 The component is not present

1 The component occupies ≤5% of the area of the neointima/media.

2 The component occupies ~5-25% of the area of the neointima/media.

3 The component occupies ~25-50% of the area of the neointima/media.

4 The component occupies ~50-75% of the area of the neointima/media.

5 The component occupies >75% of the area of the neointima/media.

IEL Disruption

0 No disruption of the IEL/intima; 100% of the circumference has intact IEL/intima.

1 Disruption of approximately < 25% of the circumference of the vessel.

2 Disruption of approximately 25-50% of the circumference of the vessel.

3 Disruption of approximately 51-75% of the circumference of the vessel.

4 Disruption of approximately >75% of the circumference of the vessel.

EEL Disruption

0 No disruption of the EEL; 100% of the circumference has intact EEL.

1 Disruption of approximately < 25% of the circumference of the vessel.

2 Disruption of approximately 25-50% of the circumference of the vessel.

3 Disruption of approximately 51-75% of the circumference of the vessel.

4 Disruption of approximately >75% of the circumference of the vessel.

Adventitial Fibrosis

0 None

1 Approximately <25% of area affected.

2 Approximately 25-50% of the area affected.

3 Approximately 51-75% of the area affected.

4 Approximately >75% of the area affected.

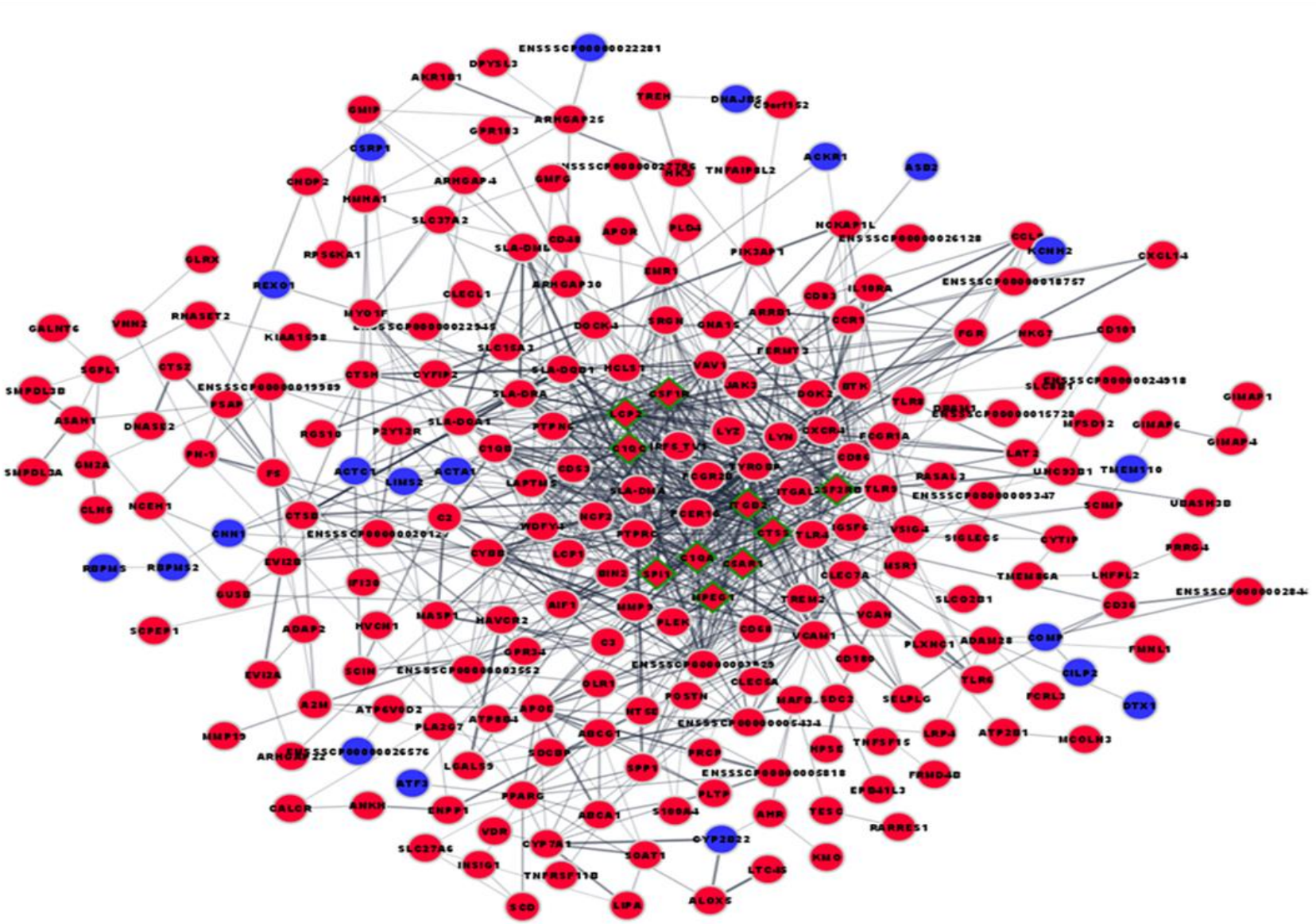
ENSSSCP00000022281
DPYSL3
AKR1B1
TREH
DNAJB6
C9orf152
GMIP
ARHGAP25
GPR183
CSRP1
ACKR1
ASB2
CNDP2
ARHGAP4
GMFG
THEMIS2
HMHA1
SLC37A2
NCKAP1L
ENSSSCP00000026128
CCL4
RPS6KA1
SLA-DMB
CD48
APOR
PLD4
PIK3AP1
KCNH2
CXCL14
GLRX
REXO1
EMR1
ARHGAP30
ENSSSCP00000018757
CLECL1
IL10RA
CD83
MYO1F
ARRB1
CCR1
GALNT6
VNN1
RNASET2
DOCK4
IRGM
GNA15
FGR
NKG7
CD101
KIAA1598
SLC15A3
FERMT3
SGPL1
CTSZ
CTSH
CYFIP2
HCLS1
VAV1
SLA-DQB1
JAK3
DOK2
BTK
SLC8B1
ENSSSCP00000024918
SMPDL3B
ENSSSCP00000019589
SLA-DRA
TLR8
GIMAP1
PSAP
ASAH1
DNASE2
SLA-DQA1
PTPN6
LCP2
LYZ
LYN
CXCR4
FCGR1A
MFSD12
GIMAP6
GIMAP4
RGS10
P2Y13R
C1QB
C1QC
RPS6KB1
CD84
LAT2
PHF1
SMPDL3A
GNZA
FS
ACTC1
LIMS2
ACTA1
CDS1
FCGR3B
TYROBP
RASAL2
UNC93B1
TMEM110
LAPTM5
SLA-DMA
ITGAL
ITGB2
TLR3
NCEH1
CLNS
CTSB
C2
NCF2
FCER1G
ENSSSCP00000009347
SCIMP
UBASH3B
CHN1
ENSSSCP00000020127
MDFVL
PTPRC
CTSS
TLR4
IGSF6
VSIG4
SIGLEC5
CYTIP
RRM2
RBPMS
RBPMS2
CYBB
LCP1
C1QA
CSAR1
MSR1
CLEC7A
TMEM86A
LHFPL2
EVI2B
PI3D
BIN2
SPI1
MPEG1
TREM2
SLCO2B1
ENSSSCP00000028
GUSB
CD36
SCPEP1
ADAP2
MASP1
HAVCR2
AIF1
MMP9
PLEK
VCAM1
VCAN
ADAM28
COMP
HVCN1
C3
CD68
PLXNC1
FMNL1
GPR34
CD180
EVI2A
SCIN
ENSSSCP00000003552
OLR1
CLEC5A
CILP2
TLR6
A2M
POSTN
MAFB
SDC2
SELPLG
FCRL2
DTX1
ATP6V0D2
APOE
ATP8B4
MTSS
PLA2G7
ENSSSCP00000005434
LRP4
ATP2B1
MMP19
ABCG1
TNFSF15
MCOLN3
ARHGAP22
ENSSSCP00000026576
SDCBP
PRCP
HPSE
LGALS9
SPP1
ENSSSCP00000005818
FRMD4B
ATF3
PLTP
EPB41L3
CALCR
ANKH
ENPP1
PPARG
ABCA1
S100A4
AHR
TESC
RARRES1
VDR
CYP27B1
CYP2D22
SLC27A6
SOAT1
XMO
INSIG1
TNFRSF11B
LTC4S
SCD
LIPA
ALOX5

Figure 1. Protein-Protein Interaction network of differentially expressed genes (5% FDR). Genes highlighted in Red are upregulated in WMS FH. Genes highlighted in blue are downregulated in WMS FH.

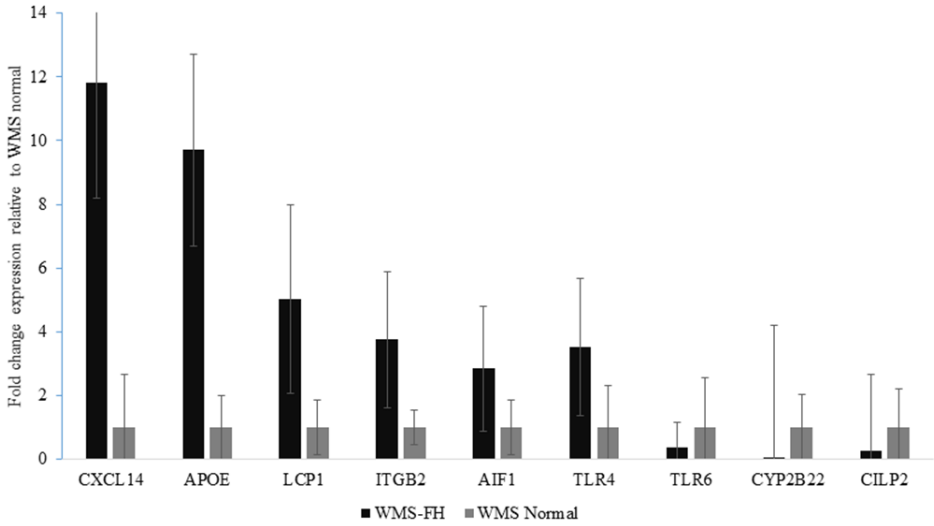

Figure 2. Relative gene expression of DEGs tested with RT-qPCR. Fold change was calculated using $2^{\wedge -(\text{avg } \Delta CT \text{ of WMS FH} - \text{avg } \Delta CT \text{ WMS normal})}$. Error bars represent ΔCT standard deviation. Only genes with significant ($p < 0.05$) differential expression are represented in this figure.

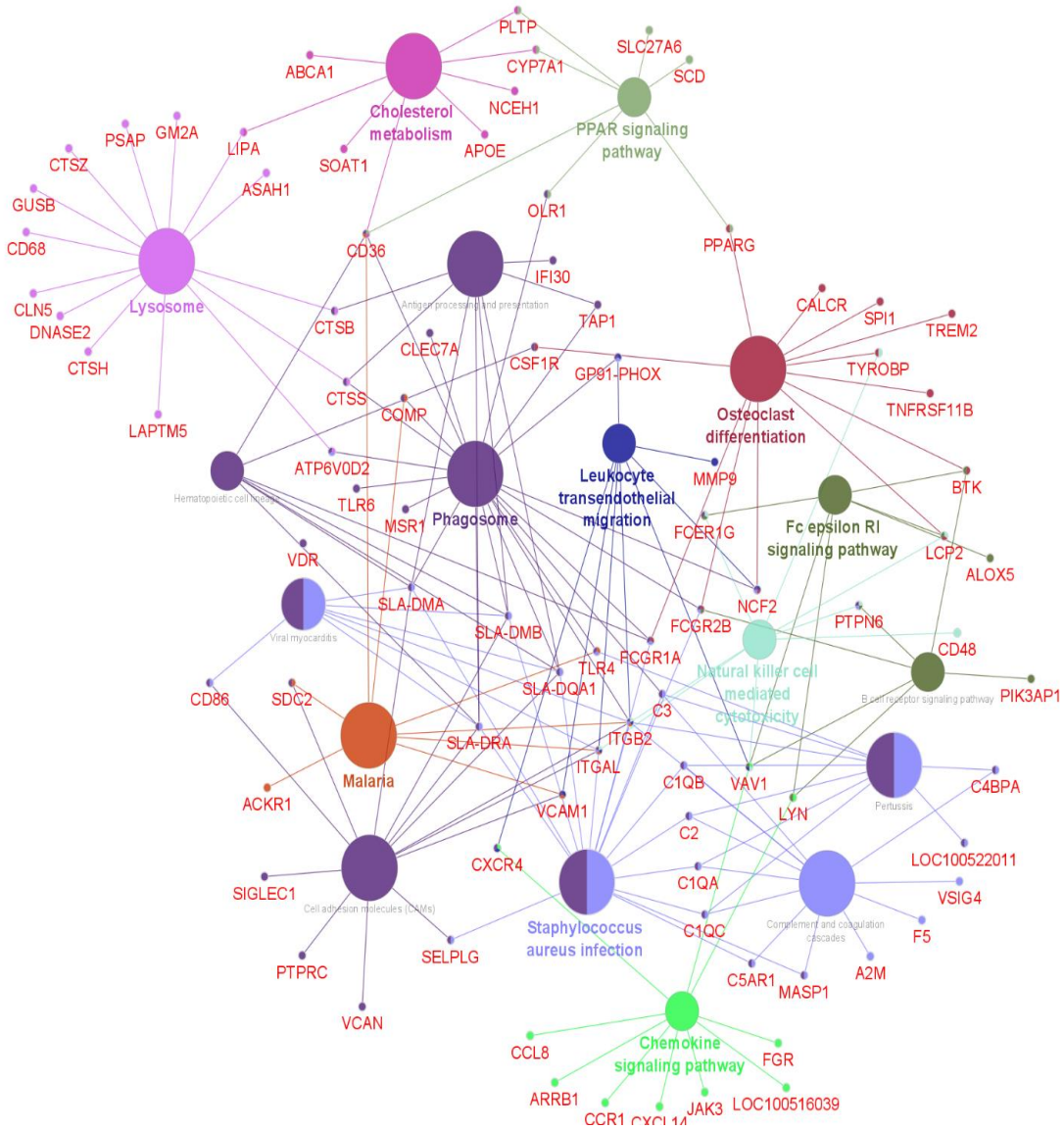

Figure 3. Enriched KEGG pathways and participating differentially expressed genes. Edges correspond to interactions between DEGs, pathways, and DEGs and pathways. Pathways with the same color indicate that they are related. For examples, cholesterol and metaboblims involves transportation and porcessing of LDL-cholesterol particles via lyzosomes.

Table 6. List of differentially expressed genes between WMS-FH and WMS-N. Results of RNA sequencing analysis at gene level. (P1-P3: Pools)

gene symbol	log2-fold-changes	FDR	WMS-FH P1	WMS-FH P2	WMS-FH P3	WMS-N P1	WMS-N P2	WMS-N P3
CXCL14	-6.18	4.0E-32	3,293	3,078	5,037	63	67	39
AMBN	-7.91	1.9E-30	286	531	711	4	0	2
APOE	-5.78	1.0E-29	12,365	33,005	54,173	812	349	562
HAVCR2	-5.79	1.2E-25	422	605	601	9	9	13
LCP1	-4.28	3.1E-25	955	1,627	2,245	91	67	92
S100A4	-4.94	7.2E-25	1,219	2,603	4,632	123	60	82
LYZ	-7.94	9.0E-25	5,714	2,253	10,369	22	42	17
CH242-305H5.1	-7.93	5.3E-24	534	471	1,975	6	0	6
C3	-4.31	5.0E-23	4,324	5,568	9,184	258	394	331
SPP1	-7.82	1.1E-22	9,961	6,126	4,339	16	36	63
MSR1	-4.60	6.2E-22	1,061	1,245	1,359	70	54	39
CYBB	-4.24	2.8E-21	492	814	1,122	46	45	38
RNF128	-5.58	1.2E-19	2,242	1,440	1,576	32	57	42
CLEC7A	-7.92	2.0E-19	254	270	474	4	0	0
REXO1	11.51	2.2E-19	0	0	0	697	202	201
SELPLG	-4.61	4.6E-17	256	528	984	27	15	28
C3 precursor	-3.74	1.2E-16	8,831	13,872	16,336	1,490	848	658
LGALS3	-4.33	1.3E-16	1,589	1,467	2,336	155	66	74
CTSS	-4.52	7.0E-16	2,804	2,246	3,128	219	74	118
PLTP	-5.10	1.8E-15	705	820	1,591	62	11	22
FCER1G	-3.70	2.0E-15	1,345	1,708	3,377	221	158	120
ITGB2	-3.54	4.8E-15	1,165	1,370	2,404	188	136	115

CD68	-4.10	3.5E-14	879	1,443	4,066	163	105	87
MPEG1	-3.10	6.5E-14	1,488	1,936	3,026	311	224	245
MYO1F	-3.79	2.6E-13	235	566	650	45	29	28
AIF1	-3.55	2.8E-13	450	731	721	82	44	42
SCIN	-4.40	6.6E-13	446	416	709	44	22	14
C5AR1	-3.58	1.0E-12	1,267	925	1,678	144	112	106
SMPDL3A	-6.22	4.7E-12	1,104	561	949	32	8	2
MMP9	-6.65	1.1E-11	1,387	868	2,952	36	0	21
BASP1	-3.27	1.7E-11	644	902	2,293	108	127	154
C1QC	-3.01	2.4E-11	3,803	4,181	6,168	848	558	469
ADAM28	-5.27	4.3E-11	229	542	418	23	1	7
OLR1	-4.53	1.2E-10	167	237	435	10	15	11
WDFY4	-3.64	3.2E-10	226	331	534	30	33	25
PLXNC1	-5.12	4.5E-10	612	694	747	23	1	43
P2Y12R	-7.66	4.7E-10	106	170	181	0	0	2
LIPA	-3.39	4.8E-10	1,441	897	1,302	138	106	170
C1QB	-2.79	7.7E-10	1,628	2,296	4,742	489	430	324
CYP2B22	2.93	1.3E-09	403	642	372	5,640	2,911	3,118
DMB	-2.68	1.4E-09	549	817	1,112	168	117	111
CH242-168I5.2	-3.83	2.5E-09	309	367	472	50	19	17
TRPV2	-3.46	3.2E-09	208	370	406	30	35	25
DRAM1	-3.11	8.0E-09	365	439	420	57	49	48
HCLS1	-2.77	1.0E-08	486	712	1,006	156	99	76
C2	-3.02	2.2E-08	530	629	1,092	157	54	80
CTSH	-2.33	2.4E-08	3,000	4,009	5,403	1,096	657	846

SLC27A6	-4.63	3.5E-08	318	214	185	16	11	8
IFI30	-2.77	3.5E-08	1,055	907	1,239	230	121	183
GM2A	-2.66	3.9E-08	1,319	1,481	2,956	432	189	331
HMHA1	-2.84	4.4E-08	206	513	676	77	55	55
TREM2	-9.91	4.7E-08	43	108	235	0	0	0
CD36	-3.70	6.4E-08	739	510	446	26	67	64
CYTIP	-8.43	7.6E-08	172	52	156	0	0	1
PLTP	-5.05	8.8E-08	160	243	640	17	0	14
F5	-4.75	1.1E-07	185	113	662	6	17	12
LAPTM5	-3.08	1.5E-07	271	805	1,883	146	70	106
CD32	-3.36	1.5E-07	545	319	611	83	37	48
APOR	-2.54	1.5E-07	1,662	2,280	2,119	527	352	228
ABCA1	-2.73	1.8E-07	1,149	1,161	900	158	224	166
SNX10	-3.49	3.6E-07	340	214	348	29	30	34
NKG7	-4.93	3.9E-07	276	205	616	21	0	18
LAT2	-3.71	4.0E-07	436	1,061	1,330	129	11	74
CHIA	-5.95	4.2E-07	471	301	417	1	20	0
RARRES1	-3.06	5.1E-07	278	279	452	33	38	60
ENSSSCG00000027868	-3.22	5.2E-07	316	2,070	1,508	47	141	186
RNASET2	-2.19	5.2E-07	355	822	829	159	112	165
KIAA1598	-4.96	5.2E-07	269	209	304	18	0	11
CD48	-3.99	6.3E-07	286	160	431	35	11	16
IL10RA	-2.39	6.4E-07	357	542	662	83	109	114
GIMAP4	-3.10	7.6E-07	124	408	389	30	31	41
PIK3AP1	-2.59	8.3E-07	491	544	660	89	132	79

TYROBP	-2.85	8.3E-07	421	622	1,125	169	44	93
C1QA	-2.56	8.3E-07	2,133	2,316	3,840	759	437	287
GALNT6	-9.58	8.5E-07	69	69	133	0	0	0
LAIR1	-2.80	1.2E-06	231	487	717	94	31	79
SRGN	-3.44	1.2E-06	1,249	719	936	201	58	68
VSIG4	-4.06	1.5E-06	286	119	401	27	10	19
VDR	-4.07	1.8E-06	73	281	272	12	14	8
DNASE2	-2.76	1.9E-06	429	388	803	128	52	78
MAFB	-1.98	2.6E-06	1,275	1,819	2,164	570	392	437
ENSSSCG00000003528	-2.62	3.2E-06	1,969	2,442	3,200	795	264	264
CSF1R	-2.02	4.9E-06	392	887	1,160	188	161	241
TCN1	-9.38	6.1E-06	59	65	113	0	0	0
PLD4	-2.44	6.2E-06	307	389	471	85	77	65
HVCN1	-2.63	9.5E-06	259	373	465	90	34	62
TREH	-8.04	9.8E-06	61	26	287	0	1	0
CYP7A1	-10.25	9.9E-06	35	12	463	0	0	0
PTPRC	-3.37	1.0E-05	688	403	503	94	68	22
GMFG	-2.88	1.1E-05	406	371	719	69	108	34
EVI2B	-3.30	1.1E-05	253	198	724	37	60	22
POSTN	-2.17	1.2E-05	4,956	3,787	6,483	1,282	1,043	1,513
CD53	-2.84	1.2E-05	562	612	568	166	56	50
JAK3	-3.12	1.2E-05	225	220	305	20	36	38
GIMAP6	-2.40	1.2E-05	314	349	573	78	92	75
FCRL3	-9.42	1.3E-05	75	40	112	0	0	0
CHI3L1	-3.36	1.3E-05	978	698	5,076	329	180	119

ENSSSCG00000011452	2.01	1.4E-05	1,282	4,447	5,039	18,059	9,725	12,962
PTPN6	-2.38	1.6E-05	212	427	550	97	70	57
FOLR1	-1.99	1.8E-05	1,471	2,013	3,097	803	444	459
C16orf54	-9.27	2.7E-05	50	44	130	0	0	0
SAT1	-1.81	2.9E-05	1,659	2,216	2,238	703	560	604
ENSSSCG00000028536	-2.01	3.3E-05	666	919	804	223	141	282
ARHGAP30	-3.11	3.7E-05	224	365	585	89	14	35
RGS10	-3.15	3.8E-05	276	282	330	69	18	24
PLEK	-3.08	4.6E-05	143	285	292	19	17	51
GPR34	-3.72	5.9E-05	327	203	306	36	4	37
VCAM1	-2.47	6.2E-05	1,529	1,201	740	251	221	296
TMEM86A	-2.90	7.4E-05	177	200	313	40	33	24
CSF2RB	-2.70	7.6E-05	517	453	967	201	51	69
CA4	-5.52	9.3E-05	45	85	329	7	0	2
NT5E	-3.03	9.5E-05	380	295	491	93	15	55
CLECL1	-3.07	9.8E-05	286	308	592	93	38	15
ENSSSCG00000017749	-4.07	1.0E-04	97	121	148	9	6	8
CILP2	2.50	1.0E-04	36	301	89	695	586	909
FMNL1	-2.40	1.3E-04	159	343	410	55	68	45
ASAH1	-2.24	1.4E-04	1,058	918	1,408	337	116	359
BIN2	-4.25	1.4E-04	271	186	325	27	0	21
GPR183	-3.52	1.8E-04	109	208	224	27	5	16
CALCR	-3.58	1.8E-04	238	122	214	16	29	11
CD86	-3.87	2.0E-04	208	105	283	10	5	33
SPI1	-2.31	2.1E-04	264	627	1,148	216	95	77

ENSSSCG00000027124	-1.73	2.3E-04	725	1,410	2,210	433	479	354
FERMT3	-2.41	2.3E-04	126	355	501	79	46	50
UBASH3B	-2.36	2.6E-04	197	337	283	62	58	44
GIMAP1	-2.65	2.7E-04	87	538	475	75	32	52
ENSSSCG00000028793	9.04	2.7E-04	0	0	0	29	115	46
ENSSSCG00000012893	-1.83	3.3E-04	248	563	644	125	106	173
VCAN	-1.94	3.3E-04	1,940	1,985	3,539	408	665	1,010
MFSD12	-1.79	4.3E-04	362	516	826	200	134	171
ATP6V0D2	-8.96	4.5E-04	12	62	137	0	0	0
PADI2	-2.88	4.6E-04	268	248	470	35	16	98
PAF-AH	-3.21	4.7E-04	245	239	505	55	48	6
FGR	-2.65	4.8E-04	161	192	320	46	22	45
SCD	-1.70	5.2E-04	1,658	2,067	3,018	505	689	988
CLEC5A	-8.88	5.3E-04	59	36	54	0	0	0
ACTA1	1.72	5.3E-04	118	284	412	829	613	1,175
HPSE	-4.79	5.9E-04	30	162	117	4	1	5
MFSD7	-1.78	6.8E-04	289	610	1,013	153	202	176
GUSB	-1.52	8.0E-04	1,025	1,493	1,720	514	422	617
ENSSSCG00000005423	-2.36	8.7E-04	162	486	347	28	71	89
SMPDL3B	-3.36	8.9E-04	136	112	239	7	19	25
ENSSSCG00000017754	-1.96	9.3E-04	222	706	1,282	222	124	181
LY64	-6.19	9.4E-04	80	60	69	3	0	0
SLA-DMA	-1.92	9.4E-04	313	357	674	156	85	130
B3GNT3	-2.25	1.4E-03	218	420	500	110	27	108
SAMSN1	-6.81	1.4E-03	116	27	46	0	0	2

TESC	-4.62	1.4E-03	119	194	247	0	1	23
CTSZ	-1.43	1.4E-03	1,829	5,205	5,281	1,717	1,164	1,519
CXCR4	-3.93	1.4E-03	170	71	171	8	19	4
WDR63	-4.39	1.5E-03	113	165	102	0	12	7
CH242-51E15.1	-2.27	1.6E-03	330	221	363	61	58	102
PigE-108A11.6	-4.24	1.7E-03	74	146	197	14	0	8
SCIMP	-6.08	1.8E-03	38	54	134	0	0	3
SLA-DQB*G07	-1.56	1.8E-03	447	1,368	1,386	464	259	311
INSIG1	-1.97	1.9E-03	356	294	519	84	108	136
CCL23	-2.65	1.9E-03	291	325	180	85	29	33
VNN2	-4.96	2.0E-03	73	28	339	7	0	7
NCF2	-3.08	2.0E-03	134	303	237	7	50	20
ENSSSCG00000021158	-2.92	2.1E-03	173	177	168	16	39	20
ENSSSCG00000000295	-3.45	2.1E-03	77	94	207	16	8	11
MBNL3	-2.34	2.2E-03	241	209	274	61	33	69
ABRACL	-3.67	2.4E-03	191	139	142	32	8	4
AKR1B1	-1.48	2.5E-03	1,048	1,388	1,726	550	559	455
BTK	-4.14	2.6E-03	136	104	155	13	0	13
TNFSF15	-8.49	2.6E-03	35	33	56	0	0	0
ARRB1	-1.65	2.7E-03	239	533	445	134	130	123
SLA-DQA1	-1.55	2.8E-03	2,143	2,376	3,955	1,348	802	925
ENSSSCG00000026855	8.44	3.1E-03	0	0	0	35	59	33
SGPL1	-1.65	3.1E-03	744	720	841	220	291	306
FCGR1A	-4.33	3.1E-03	99	151	222	21	0	3
CNN1	1.35	3.3E-03	14,996	43,498	45,994	86,379	73,719	95,072

ENSSSCG00000028407	-9.34	3.4E-03	0	147	147	0	0	0
5_8S_rRNA	-2.40	3.4E-03	624	434	641	128	34	224
ENSSSCG00000024080	8.50	3.4E-03	0	0	0	17	63	53
ARHGAP4	-2.15	3.5E-03	164	275	370	50	86	44
TLR4	-2.70	3.7E-03	277	201	175	32	61	25
KMO	-3.46	3.8E-03	138	99	167	26	4	12
FGD2	-2.80	3.9E-03	220	229	288	65	7	47
PPARG	-4.65	4.0E-03	78	88	87	8	0	3
C9orf152	-4.73	4.3E-03	46	53	122	1	4	3
SOAT1	-2.46	4.3E-03	222	187	233	55	21	59
TAP	-9.24	4.8E-03	0	111	163	0	0	0
ADAP2	-2.09	5.1E-03	190	219	294	76	45	56
SLCO2B1	-2.05	5.1E-03	211	369	436	72	126	43
RBPMS	1.44	5.8E-03	459	1,457	2,037	3,014	3,477	3,474
KIAA1551	-1.70	5.9E-03	244	355	402	95	114	112
TLR6	-8.70	6.2E-03	73	21	15	0	0	0
RPS6KA1	-2.62	6.7E-03	78	239	302	25	14	58
ENSSSCG00000016237	-2.51	7.0E-03	147	207	310	64	12	46
SDCBP	-1.39	7.2E-03	2,535	3,074	2,795	1,213	1,084	1,224
IRF5	-3.12	7.2E-03	185	217	289	66	4	16
GNA15	-3.00	7.5E-03	123	121	159	32	13	10
VAV1	-3.44	8.9E-03	315	420	536	87	0	40
ENSSSCG00000020913	-8.37	9.0E-03	37	13	59	0	0	0
TTYH2	-2.26	9.4E-03	183	219	289	87	25	43
ENSSSCG00000025840	-2.23	9.9E-03	150	164	267	37	51	42

CLEC14A	-1.30	9.9E-03	472	1,301	1,339	448	316	465
RASAL3	-4.62	1.0E-02	42	80	107	0	3	6
HK3	-3.67	1.0E-02	121	113	397	32	0	19
MYOC	1.56	1.0E-02	98	478	242	885	502	898
DES	1.30	1.1E-02	16,807	63,627	59,920	109,135	101,879	111,487
EPB41L3	-2.66	1.1E-02	108	136	204	13	33	27
SLC15A3	-1.56	1.1E-02	395	481	1,009	268	218	161
ARHGAP25	-2.03	1.1E-02	137	206	293	46	58	54
IGSF6	-4.13	1.2E-02	89	70	72	1	7	7
ACTC1	2.24	1.3E-02	10	120	187	448	328	527
ST14	-4.11	1.4E-02	35	100	196	8	0	10
UNC5A	-8.03	1.5E-02	11	49	46	0	0	0
RBPMS2	1.23	1.5E-02	942	2,545	3,261	4,939	4,582	5,624
ENSSSCG00000005304	-9.18	1.5E-02	97	60	0	0	0	0
PSAP	-1.19	1.5E-02	14,411	23,603	27,179	9,930	8,208	11,371
PRCP	-1.82	1.6E-02	317	452	617	209	47	160
SLC8B1	-2.72	1.6E-02	182	227	301	53	4	61
ATF3	2.76	1.6E-02	94	136	337	94	1,647	1,997
ITGAL	-1.65	1.6E-02	210	285	371	104	80	105
ENSSSCG00000004870	-1.22	1.6E-02	637	1,157	1,245	494	352	489
PN-1	-1.39	1.6E-02	846	971	1,112	513	376	323
TLR9	-2.61	1.6E-02	107	111	311	28	42	15
ENSSSCG00000016648	-2.25	1.7E-02	126	149	226	34	27	51
DNAJB5	1.32	1.7E-02	306	1,280	1,289	2,144	2,020	2,461
FRMD4B	-1.73	1.7E-02	304	398	313	128	61	152

MASP1	-5.93	1.7E-02	28	32	80	0	0	2
SLA-DRA1	-1.33	1.7E-02	1,986	3,233	5,605	1,893	1,244	1,117
IVNS1ABP	-1.26	1.7E-02	429	727	733	279	232	307
CCR1	-3.02	1.8E-02	173	66	227	16	38	10
PRRG4	-2.18	1.9E-02	181	158	253	61	24	61
ZC3H12D	-5.10	1.9E-02	115	90	16	7	1	0
ARAP3	-1.65	1.9E-02	266	398	361	75	101	174
SCPEP1	-1.25	1.9E-02	1,014	1,389	2,221	744	520	739
LTC4S	-2.00	2.0E-02	112	203	379	76	48	45
CTSB	-1.17	2.1E-02	7,211	12,301	13,642	5,844	3,851	5,492
ENSSSCG00000027499	2.20	2.1E-02	33	42	34	149	177	218
CLN5	-1.65	2.1E-02	245	299	300	94	85	114
ATP2B1	-2.17	2.2E-02	316	367	263	22	84	131
CD101	-4.20	2.2E-02	37	65	165	5	0	9
SLC37A2	-1.30	2.2E-02	287	572	686	191	217	211
GMIP	-1.46	2.2E-02	203	420	537	156	97	166
A2M	-1.28	2.3E-02	13,908	21,692	39,695	8,631	8,709	13,833
ENSSSCG00000025078	1.35	2.4E-02	216	769	1,048	1,882	1,531	1,363
MCOLN3	-8.11	2.4E-02	26	8	62	0	0	0
DARC	1.74	2.4E-02	32	125	86	276	254	235
CSRP1	1.38	2.5E-02	16,410	68,789	89,123	169,934	114,097	129,115
ENSSSCG00000025889	-7.86	2.5E-02	9	44	42	0	0	0
LRP3	1.36	2.5E-02	91	284	373	682	586	525
DTX1	3.71	2.6E-02	0	13	10	106	67	95
GLRX	-2.07	2.7E-02	144	159	292	60	55	31

ENPP1	-1.88	2.8E-02	498	271	355	175	103	96
TNFRSF11B	-3.31	2.8E-02	291	155	317	41	0	53
DOK2	-3.41	2.8E-02	50	217	267	25	0	22
GL	-1.45	2.8E-02	558	543	558	267	222	194
ASB2	1.20	2.8E-02	163	352	402	608	709	765
ST18	-8.37	2.8E-02	61	14	8	0	0	0
SDC2	-1.30	2.8E-02	2,028	1,975	2,761	1,157	742	1,145
SIGLEC5	-3.99	2.9E-02	107	91	112	3	0	20
RGS1	-1.62	3.0E-02	173	410	251	105	64	107
TLR8	-8.02	3.0E-02	3	65	46	0	0	0
LCP2	-1.99	3.0E-02	84	252	257	55	50	36
CYFIP2	-2.64	3.0E-02	127	124	181	17	10	51
MMP19	-1.67	3.2E-02	194	235	684	134	84	131
CCL8	-5.74	3.3E-02	74	33	23	0	0	3
SLAMF6	-7.84	3.3E-02	26	15	34	0	0	0
ABCB10	-1.84	3.3E-02	489	212	447	103	149	132
VASH1	-1.56	3.3E-02	234	249	473	103	96	143
GLIS1	-7.78	3.3E-02	17	18	45	0	0	0
COMP	1.40	3.4E-02	713	2,021	661	2,419	2,859	3,814
ENSSSCG00000027264	-4.58	3.4E-02	192	29	28	8	0	8
ANKH	-1.37	3.4E-02	260	604	434	119	169	216
CD83	-2.42	3.4E-02	84	129	166	29	16	28
EMR1	-4.44	3.4E-02	26	47	112	5	0	3
SIGLEC1	-2.67	3.5E-02	104	77	145	21	15	21
FAM20A	-1.97	3.6E-02	163	271	161	41	72	47

ABCG1	-4.25	3.6E-02	126	67	32	8	7	0
ATP8B4	-4.17	3.6E-02	94	50	66	0	6	8
LRP4	-2.66	3.7E-02	56	165	153	22	8	28
LYN	-1.58	3.7E-02	461	404	441	245	119	137
NCEH1	-2.07	3.7E-02	86	201	193	44	37	31
DTX4	-2.04	3.8E-02	206	160	246	39	39	93
PYCARD	-3.49	3.8E-02	83	96	208	23	0	13
ENSSSCG00000025704	-3.15	3.8E-02	58	57	150	14	10	6
ENSSSCG00000030484	-2.11	3.8E-02	294	180	262	43	108	45
ACVRL1	-1.19	3.9E-02	326	935	1,030	295	335	324
FAM111A	-2.16	3.9E-02	183	362	264	18	112	49
KCNH2	1.33	4.0E-02	105	526	418	985	584	863
ENSSSCG00000023930	-6.66	4.0E-02	66	10	17	0	0	1
ssc-mir-21	-1.35	4.1E-02	481	535	616	316	183	201
ENSSSCG00000027404	-8.11	4.2E-02	42	4	33	0	0	0
ENSSSCG00000024047	-2.15	4.4E-02	145	305	101	29	53	48
HOXA7	1.38	4.4E-02	73	258	302	692	433	408
LIMS2	1.14	4.5E-02	2,882	7,975	10,365	17,102	12,457	14,797
TNFAIP8L2	-4.40	4.7E-02	59	82	131	13	0	0
STEAP3	-2.02	4.9E-02	167	144	172	43	40	52
UBALD1	1.31	4.9E-02	146	517	810	1,344	1,034	979
ALOX5	-2.34	4.9E-02	206	181	99	62	20	35
ENSSSCG00000022199	1.21	5.0E-02	171	302	479	908	536	745

Table 7. List of differentially expressed isoforms between WMS-FH and WMS-N.

transcript id	gene symbol	log2-fold-changes	FDR	WMS-FH P1	WMS-FH P2	WMS-FH P3	WMS-N P1	WMS-N P2	WMS-N P3
ENSSSCT00000015634	CXCL14-001	-6.21	1.4E-23	3,293	3,078	5,037	63	67	39
ENSSSCT00000003426	APOE-201	-5.79	1.7E-22	12,365	33,005	54,173	812	349	562
ENSSSCT00000034964	MAPK1-001	12.00	7.1E-21	0	0	0	455	503	594
ENSSSCT00000007206	S100A4-201	-5.07	6.7E-19	1,180	2,260	4,455	93	55	82
ENSSSCT00000010091	SPP1-001	-7.87	7.3E-19	9,961	6,126	4,339	16	36	63
ENSSSCT00000010313	LCP1-201	-4.31	1.3E-16	955	1,627	2,245	91	67	92
ENSSSCT00000014800	GPR108-201	-4.34	2.1E-16	4,324	5,568	9,184	258	394	331
ENSSSCT00000009789	AMBN-201	-7.93	2.6E-16	286	531	711	4	0	2
ENSSSCT00000000530	LYZ-001	-9.07	1.6E-15	5,714	2,253	10,369	22	0	17
ENSSSCT00000009594	CH242-305H5.1-001	-8.38	1.7E-15	534	410	996	6	0	0
ENSSSCT00000013723	RNF128-001	-5.62	5.7E-15	2,240	1,440	1,559	32	57	42
ENSSSCT00000026943	HAVCR2-201	-5.82	2.1E-14	422	605	601	9	9	13
ENSSSCT00000014685	ONECUT3-201	11.51	2.5E-12	0	0	0	697	202	201
ENSSSCT00000019540	CD68-001	-4.13	4.6E-12	879	1,443	3,567	133	105	87
ENSSSCT00000023681	VAV1-201	-3.76	4.8E-12	8,831	13,872	16,336	1,490	848	658
ENSSSCT00000007284	CTSS-201	-4.54	1.1E-11	2,804	2,246	3,128	219	74	118
ENSSSCT00000012307	EPM2AIP1-201	-5.11	9.1E-11	705	820	1,591	62	11	22
ENSSSCT00000006966	FCER1G-001	-3.71	9.1E-11	1,285	1,685	3,296	215	158	116
ENSSSCT00000029647	ITGB2-201	-3.57	1.8E-10	1,165	1,370	2,404	188	136	115
ENSSSCT00000033700	CLEC7A-002	-7.93	1.9E-10	254	270	464	4	0	0
ENSSSCT00000027398	SELPLG-201	-4.62	1.2E-09	256	528	984	27	15	28
ENSSSCT00000014364	MPEG1-201	-3.12	2.8E-09	1,488	1,936	3,026	311	224	245

ENSSSCT0000 0008139	MMP9-201	-6.66	3.1E-09	1,387	868	2,952	36	0	21
ENSSSCT0000 0027942	C5AR1-201	-3.61	5.1E-09	1,267	925	1,678	144	112	106
ENSSSCT0000 0030246	CCDC66-202	-11.05	6.7E-09	293	129	203	0	0	0
ENSSSCT0000 0018284	U6.450-201	-3.30	5.6E-08	644	902	2,293	108	127	154
ENSSSCT0000 0003916	C1QC-201	-3.03	6.8E-08	3,803	4,181	6,168	848	558	469
ENSSSCT0000 0022983	ERBB2IP-201	-10.54	7.1E-08	108	179	266	0	0	0
ENSSSCT0000 0006051	TLR4-001	-10.75	1.3E-07	222	201	104	0	0	0
ENSSSCT0000 0016727	SCIN-201	-4.42	1.4E-07	446	416	709	44	22	14
ENSSSCT0000 0011436	LIPA-201	-3.42	3.4E-07	1,441	897	1,302	138	106	170
ENSSSCT0000 0001539	AIF1-001	-3.73	3.7E-07	406	542	678	56	44	30
ENSSSCT0000 0032962	ABCA1-002	-10.61	5.0E-07	182	243	76	0	0	0
ENSSSCT0000 0004678	SMPDL3A-001	-7.02	5.1E-07	1,104	501	925	23	0	1
ENSSSCT0000 0014859	MYO1F-201	-3.80	6.4E-07	235	566	650	45	29	28
ENSSSCT0000 0003917	C1QC-201	-2.81	6.4E-07	1,628	2,296	4,742	489	430	324
ENSSSCT0000 0001983	CTSH-001	-2.49	6.5E-07	2,513	4,009	5,403	697	657	846
ENSSSCT0000 0000991	PLXNC1-201	-5.11	1.2E-06	593	694	724	23	1	43
ENSSSCT0000 0003339	CYP2B22-201	2.90	1.6E-06	403	642	372	5,640	2,911	3,118
ENSSSCT0000 0007644	MSR1-001	-5.53	2.0E-06	879	835	837	42	0	23
ENSSSCT0000 0010572	ADAM28-201	-5.28	3.8E-06	229	542	418	23	1	7
ENSSSCT0000 0018465	ERBB2IP-201	10.96	7.4E-06	0	0	0	11	253	504
ENSSSCT0000 0011253	PSAP-201	-2.44	9.4E-06	13,079	13,967	21,125	2,669	3,727	3,285
ENSSSCT0000 0001633	DMB-001	-2.70	1.2E-05	549	817	1,112	168	117	111
ENSSSCT0000 0018603	GM2A-201	-2.68	1.3E-05	1,319	1,481	2,956	432	189	331
ENSSSCT0000 0000698	OLR1-001	-4.55	1.6E-05	167	237	435	10	15	11
ENSSSCT0000 0015187	IFI30-201	-2.79	1.8E-05	1,055	907	1,239	230	121	183

ENSSSCT0000 0012823	P2Y12R-201	-7.69	1.9E-05	106	170	181	0	0	2
ENSSSCT0000 0035739	CD90-001	12.46	1.9E-05	0	0	0	1,054	993	0
ENSSSCT0000 0022465	POSTN-202	-2.60	2.5E-05	4,093	3,204	5,614	915	558	975
ENSSSCT0000 0015759	PPP2R2B-201	-3.25	3.4E-05	316	2,070	1,508	47	141	186
ENSSSCT0000 0017061	C4BPA-201	-2.57	3.5E-05	1,662	2,280	2,119	527	352	228
ENSSSCT0000 0026637	CCDC66-201	9.94	3.5E-05	0	0	0	150	121	98
ENSSSCT0000 0013000	HCLS1-201	-2.79	3.7E-05	486	712	1,006	156	99	76
ENSSSCT0000 0026814	LAPTM5-201	-3.09	4.4E-05	271	805	1,883	146	70	106
ENSSSCT0000 0035918	MSR1-003	-5.15	4.8E-05	182	335	522	0	13	16
ENSSSCT0000 0028458	LAT2-201	-3.72	4.9E-05	436	1,061	1,330	129	11	74
ENSSSCT0000 0031016	CYTIP-201	-8.47	5.7E-05	172	52	156	0	0	1
ENSSSCT0000 0025862	SRGN-201	-3.46	6.0E-05	1,249	719	936	201	58	68
ENSSSCT0000 0001794	TREM2-001	-9.91	7.6E-05	43	108	235	0	0	0
ENSSSCT0000 0003915	C1QA-201	-2.58	7.8E-05	2,133	2,316	3,840	759	437	287
ENSSSCT0000 0015578	SLC27A6-201	-4.66	8.4E-05	318	214	185	16	11	8
ENSSSCT0000 0006892	F5-201	-4.77	8.6E-05	185	113	662	6	17	12
ENSSSCT0000 0000913	ALDH1L2-201	-11.97	8.9E-05	669	381	0	0	0	0
ENSSSCT0000 0007441	CEPT1-201	-6.00	8.9E-05	471	301	417	1	20	0
ENSSSCT0000 0019627	TRPV2-201	-3.48	1.1E-04	208	370	406	30	35	25
ENSSSCT0000 0016859	CHI3L1-001	-3.37	1.7E-04	978	698	5,076	329	180	119
ENSSSCT0000 0003919	C1QC-201	-2.63	2.0E-04	1,969	2,442	3,200	795	264	264
ENSSSCT0000 0008138	PLTP-201	-5.06	2.3E-04	160	243	640	17	0	14
ENSSSCT0000 0031855	SUPT5H-202	12.44	2.3E-04	0	0	0	2,001	0	92
ENSSSCT0000 0003590	NKG7-001	-4.94	2.9E-04	276	205	616	21	0	18
ENSSSCT0000 0003224	TYROBP-201	-2.86	3.2E-04	421	622	1,125	169	44	93

ENSSSCT0000 0034589	ABCA1-001	-2.70	3.2E-04	967	918	824	158	224	99
ENSSSCT0000 0031323	HMHA1-201	-2.86	4.2E-04	206	513	676	77	55	55
ENSSSCT0000 0000204	KMT2D-202	-11.25	4.4E-04	365	319	0	0	0	0
ENSSSCT0000 0006990	CD48-001	-4.01	4.5E-04	286	160	428	35	11	16
ENSSSCT0000 0018190	SNX10-201	-3.53	4.7E-04	340	214	348	29	30	34
ENSSSCT0000 0024702	DAZAP2-201	-9.60	5.0E-04	69	69	133	0	0	0
ENSSSCT0000 0033106	MAFB-001	-2.00	5.3E-04	1,275	1,819	2,164	570	392	437
ENSSSCT0000 0006836	CYP7A1-201	-10.25	5.6E-04	35	12	463	0	0	0
ENSSSCT0000 0011499	PIK3AP1-201	-2.63	6.5E-04	491	544	660	89	132	79
ENSSSCT0000 0011666	KIAA1598-201	-4.98	6.6E-04	269	209	304	18	0	11
ENSSSCT0000 0013521	MSN-002	-4.08	6.6E-04	286	119	401	27	10	19
ENSSSCT0000 0015005	DNASE2-201	-2.77	9.3E-04	429	388	803	128	52	78
ENSSSCT0000 0012533	ITIH3-201	1.99	9.6E-04	1,282	4,447	5,039	18,059	9,725	12,962
ENSSSCT0000 0004450	FGFR1OP-201	-2.21	9.9E-04	355	822	829	159	112	165
ENSSSCT0000 0023744	RARRES1-201	-3.09	1.1E-03	278	279	452	33	38	60
ENSSSCT0000 0013315	SAT1-001	-2.02	1.1E-03	1,124	1,376	1,764	470	361	306
ENSSSCT0000 0022595	TTYH1-202	-2.86	1.1E-03	231	451	650	86	31	68
ENSSSCT0000 0029102	SENP2-203	10.86	1.1E-03	0	0	0	313	0	413
ENSSSCT0000 0027894	KMT2A-201	-8.05	1.2E-03	61	26	287	0	1	0
ENSSSCT0000 0026292	FOLR1-202	-2.01	1.2E-03	1,471	2,013	3,097	803	444	459
ENSSSCT0000 0001563	C2-001	-4.57	1.3E-03	426	598	861	0	16	70
ENSSSCT0000 0007515	VCAM1-001	-2.52	1.4E-03	1,529	1,201	740	248	220	296
ENSSSCT0000 0014336	TCN1-001	-9.39	1.5E-03	59	65	113	0	0	0
ENSSSCT0000 0029273	TACC2-201	11.32	1.6E-03	0	0	0	43	859	0
ENSSSCT0000 0019319	EVI2B-201	-3.32	1.6E-03	253	198	724	37	60	22

ENSSSCT0000 0030064	SLC25A36-202	-9.64	1.7E-03	122	29	70	0	0	0
ENSSSCT0000 0015787	CSF1R-201	-2.04	1.9E-03	392	887	1,160	188	161	241
ENSSSCT0000 0007074	FCRL3-201	-9.43	1.9E-03	75	40	112	0	0	0
ENSSSCT0000 0009133	GFAT1-202	-10.47	2.0E-03	0	266	375	0	0	0
ENSSSCT0000 0013662	BTK-001	-7.10	2.0E-03	70	90	141	0	0	2
ENSSSCT0000 0026032	GIMAP4-201	-3.12	2.0E-03	124	408	389	30	31	41
ENSSSCT0000 0032274	VDR-201	-4.09	2.5E-03	73	281	272	12	14	8
ENSSSCT0000 0032939	FBXO3-001	9.50	2.8E-03	0	0	0	150	99	17
ENSSSCT0000 0027454	SH2D6-203	-7.62	3.2E-03	40	152	82	0	0	1
ENSSSCT0000 0027376	KDM3A-202	10.49	3.2E-03	0	0	0	311	214	0
ENSSSCT0000 0031601	C16orf54-201	-9.28	3.4E-03	50	44	130	0	0	0
ENSSSCT0000 0007660	ASAH1-201	-2.26	3.5E-03	1,058	918	1,408	337	116	359
ENSSSCT0000 0000142	CSF2RB-201	-2.72	3.7E-03	517	453	967	201	51	69
ENSSSCT0000 0027783	AP3B1-201	-2.04	3.8E-03	666	919	804	223	141	282
ENSSSCT0000 0036681	IL10RA-001	-2.44	4.1E-03	315	384	562	83	72	95
ENSSSCT0000 0000408	MYL6-203	-14.44	4.3E-03	0	10,052	0	0	0	0
ENSSSCT0000 0011546	SCD-001	-1.82	4.8E-03	1,658	2,024	2,794	484	582	924
ENSSSCT0000 0011366	WDFY4-201	-3.77	5.4E-03	106	197	333	14	22	9
ENSSSCT0000 0002839	PLD4-201	-2.47	5.4E-03	307	389	471	85	77	65
ENSSSCT0000 0006982	ARHGAP30-201	-3.12	5.4E-03	224	365	585	89	14	35
ENSSSCT0000 0010770	HVCN1-201	-2.65	5.7E-03	259	373	465	90	34	62
ENSSSCT0000 0031757	GIMAP6-201	-2.43	6.3E-03	314	349	573	78	92	75
ENSSSCT0000 0011685	RGS10-201	-3.17	6.5E-03	276	282	330	69	18	24
ENSSSCT0000 0028880	SELPLG-201	-1.76	6.6E-03	725	1,410	2,210	433	479	354
ENSSSCT0000 0015220	CILP2-201	2.47	6.6E-03	36	301	89	695	586	909

ENSSSCT0000 0000710	CLECL1-001	-3.09	6.8E-03	286	308	592	93	38	15
ENSSSCT0000 0005572	LGALS3-201	-3.43	8.6E-03	110	992	1,864	155	13	74
ENSSSCT0000 0031587	PTPN6-201	-2.40	8.8E-03	212	427	550	97	70	57
ENSSSCT0000 0029793	WASF2-202	-10.42	9.8E-03	265	50	0	0	0	0
ENSSSCT0000 0000240	BIN2-201	-4.27	1.2E-02	271	186	325	27	0	21
ENSSSCT0000 0013375	CYBB-201	-4.19	1.2E-02	6	814	1,121	25	29	35
ENSSSCT0000 0032888	LGALS3-001	-5.91	1.3E-02	1,479	475	472	0	53	0
ENSSSCT0000 0028053	OVCH2-201	9.02	1.3E-02	0	0	0	29	115	46
ENSSSCT0000 0032087	CA4-201	-5.52	1.3E-02	45	85	329	7	0	2
ENSSSCT0000 0032588	VCAN-001	-2.11	1.5E-02	1,865	1,600	3,115	215	657	823
ENSSSCT0000 0016693	CALCR-201	-3.61	1.6E-02	238	122	214	16	29	11
ENSSSCT0000 0009142	PLEK-201	-3.11	1.6E-02	143	285	292	19	17	51
ENSSSCT0000 0033832	CD32-005	-10.00	1.6E-02	164	110	0	0	0	0
ENSSSCT0000 0006731	ATP6V0D2-201	-8.96	1.6E-02	12	62	137	0	0	0
ENSSSCT0000 0036692	SLC50A1-001	-8.91	1.7E-02	40	102	29	0	0	0
ENSSSCT0000 0002510	NR2F2-201	-10.51	1.8E-02	301	0	12	0	0	0
ENSSSCT0000 0034797	CH242-168I5.2-001	-4.17	1.8E-02	181	367	470	47	0	10
ENSSSCT0000 0032344	WDFY4-203	-3.71	1.8E-02	120	134	197	16	11	10
ENSSSCT0000 0001927	PAF-AH-201	-3.23	1.9E-02	245	239	505	55	48	6
ENSSSCT0000 0007406	HIPK1-202	-11.95	2.0E-02	836	0	0	0	0	0
ENSSSCT0000 0019318	NF1-202	-4.09	2.1E-02	97	121	148	9	6	8
ENSSSCT0000 0034423	PTPRC-001	-3.29	2.1E-02	688	218	308	94	59	14
ENSSSCT0000 0027772	PADI2-201	-2.90	2.1E-02	268	248	470	35	16	98
ENSSSCT0000 0014591	TMEM86A-201	-2.92	2.1E-02	177	200	313	40	33	24
ENSSSCT0000 0008484	GUSB-201	-1.55	2.2E-02	1,025	1,493	1,720	514	422	617

ENSSSCT0000 0017914	GIMAP1-201	-2.66	2.5E-02	87	538	475	75	32	52
ENSSSCT0000 0011711	GMFG-201	-2.68	2.6E-02	250	331	554	48	108	23
ENSSSCT0000 0029042	U6.681-201	-11.52	2.9E-02	617	0	0	0	0	0
ENSSSCT0000 0011156	ACTA1-201	1.71	2.9E-02	118	284	412	829	613	1,175
ENSSSCT0000 0010435	GPR183-201	-3.54	3.0E-02	109	208	224	27	5	16
ENSSSCT0000 0019323	KSR1-201	-1.97	3.0E-02	222	706	1,282	222	124	181
ENSSSCT0000 0034552	CD36-003	-3.96	3.2E-02	739	477	306	0	67	59
ENSSSCT0000 0013139	SAMSN1-201	-6.86	3.2E-02	116	27	46	0	0	2
ENSSSCT0000 0008249	CTSZ-001	-1.45	3.3E-02	1,829	5,205	5,281	1,717	1,164	1,519
ENSSSCT0000 0026976	MFSD7-201	-1.81	3.5E-02	289	610	1,013	153	202	176
ENSSSCT0000 0003911	CDC42-202	-9.64	3.5E-02	73	203	0	0	0	0
ENSSSCT0000 0034348	HBA-004	-9.66	3.6E-02	116	117	0	0	0	0
ENSSSCT0000 0014254	FERMT3-201	-2.42	3.6E-02	126	355	501	79	46	50
ENSSSCT0000 0010116	HPSE-201	-4.82	3.6E-02	30	162	117	4	1	5
ENSSSCT0000 0035430	PIGA-002	-8.80	3.6E-02	65	20	42	0	0	0
ENSSSCT0000 0001616	SLA-DQA1-001	-1.57	3.7E-02	2,143	2,376	3,955	1,348	802	925
ENSSSCT0000 0021744	5_8S_rRNA.2-201	-2.43	3.7E-02	624	434	641	128	34	224
ENSSSCT0000 0000074	EP300-202	11.25	3.7E-02	0	0	0	918	0	0
ENSSSCT0000 0029858	MFSD12-201	-1.81	3.8E-02	362	516	826	200	134	171
ENSSSCT0000 0018009	AKR1B1-201	-1.50	3.9E-02	1,048	1,388	1,726	550	559	455
ENSSSCT0000 0018466	LY64-001	-6.21	4.1E-02	80	60	69	3	0	0
ENSSSCT0000 0001617	SLA-DQB*G07-001	-1.58	4.1E-02	447	1,368	1,386	464	259	311
ENSSSCT0000 0025492	LPR1-201	9.76	4.1E-02	0	0	0	33	273	0
ENSSSCT0000 0034803	CYBB-001	-11.17	4.1E-02	486	0	0	0	0	0
ENSSSCT0000 0017088	CXCR4-001	-3.96	4.1E-02	170	71	171	8	19	4

ENSSSCT0000			4.5E-						
0036359	BRCC3-001	-9.53	02	104	0	112	0	0	0
ENSSSCT0000			4.5E-		13,40	16,83			
0000716	A2M-201	-1.41	02	7,680	7	8	4,673	3,529	6,647
ENSSSCT0000	5S_rRNA.2		4.6E-						
0027421	8-201	-9.35	02	0	147	147	0	0	0
ENSSSCT0000	TNFSF15-		4.6E-						
0024202	201	-8.50	02	35	33	56	0	0	0
ENSSSCT0000	RASGRP4-		4.6E-						
0033758	001	-5.92	02	47	95	110	0	0	4
ENSSSCT0000			4.6E-						
0004618	VNN2-201	-4.96	02	73	28	339	7	0	7
ENSSSCT0000			4.6E-						
0010807	TESC-201	-4.65	02	119	194	247	0	1	23
ENSSSCT0000	UBASH3B-		4.6E-						
0016502	201	-2.39	02	197	337	283	62	58	44
	SLA-								
ENSSSCT0000	DRB*K07G		4.6E-						
0001612	-001	-2.14	02	307	937	488	167	166	52
ENSSSCT0000	ALDH3B1-		4.6E-						
0014095	201	-1.86	02	248	563	644	125	106	173
	CH242-								
ENSSSCT0000	305H5.1-		4.8E-						
0034680	007	-7.09	02	0	61	934	0	0	6
ENSSSCT0000			4.8E-						
0011246	SGPL1-201	-1.68	02	744	720	841	220	291	306
ENSSSCT0000	NIPSNAP3		4.9E-						
0005966	A-201	-2.39	02	162	486	347	28	71	89
ENSSSCT0000	SMPDL3B-		4.9E-						
0003977	201	-3.39	02	136	112	239	7	19	25

Table 8. Differentially expressed splice variants between WMS FH and WMS normal aortic tissues WMS FH and WMS normal

GeneID	Chr	FC	logFC	FDR_DE	IncLevelDifference	FDR_DS	Event
CLEC2D	5	0.341	-1.549	4.55e-02	0.319	0.0001	A5SS
DAB2	16	0.460	-1.118	2.46e-03	-0.397	0.0145	MXE
EPB41L2	1	0.428	-1.223	3.62e-04	0.514	0.0001	SE
PDLIM7	2	2.014	1.010	1.69e-02	-0.434	0.0001	RI
PDLIM7	2	2.014	1.010	1.69e-02	-0.224	0.0368	MXE
PDLIM7	2	2.014	1.010	1.69e-02	-0.434	0.0406	A5SS
PLD3	6	0.451	-1.146	4.65e-04	-0.68	0	A5SS
PLD3	6	0.451	-1.146	4.65e-04	-0.704	0	SE
POSTN	11	0.178	-2.488	6.68e-09	0.2	0.0224	SE
POSTN	11	0.178	-2.488	6.68e-09	0.256	<0.0001	SE
PSAP	14	0.381	-1.391	2.66e-05	0.374	<0.0001	SE
RBPMS2	1	2.344	1.229	8.29e-04	0.376	0.0261	A5SS
TNFRSF12A	3	2.080	1.057	4.72e-02	0.395	0.0341	SE

Chr: chromosome; FC: fold change; FDR: false discovery rate.

APPENDIX B : CHAPTER 3

Table 1. Composition of the pellet diet fed to recruited animals for this study is the same presented in Appendix A. Table1.

Table 2. DE swine miRNA sequences and the corresponding human miRNA ID and sequence.

Swine miRNA ID	Swine seq	Human miRNA ID	Human Seq
ssc-miR-7140-3p	augaugccccuuagaguugagc	NA	na
ssc-miR-7140-5p	caacucaaggggcaucauuca	NA	na
ssc-miR-194b-5p	uguaacagcgacuccaugugga	hsa-miR-194-5p	uguaacagcaacuccaugugga
ssc-miR-7	uggaagacuagugauuuuguuguu	hsa-miR-7-5p	uggaagacuagugauuuuguuguu
ssc-miR-499-3p	aacaucacagcaagucugugcu	hsa-miR-499a-3p	aacaucacagcaagucugugcu
ssc-miR-193a-3p	aacuggccuacaaagucccagu	hsa-miR-193a-3p	aacuggccuacaaagucccagu
ssc-miR-144	uacaguauagaugauguac	hsa-miR-144-3p	uacaguauagaugauguacu
ssc-miR-9805-3p	cccagggucugucggaugucu	NA	Na
ssc-miR-183	uauggcacugguagaauucacug	hsa-miR-183-5p	uauggcacugguagaauucacu
ssc-miR-190a	ugauauguuugauauauuagg	hsa-miR-190a-5p	ugauauguuugauauauuagg
ssc-miR-574	cacgcucaugcacacacccaca	hsa-miR-574-3p	cacgcucaugcacacacccaca
ssc-miR-129a-3p	aagcccuuaccccaaaaagcau	hsa-miR-129-2-3p	aagcccuuaccccaaaaagcau
ssc-miR-196a	uagguaguuucauguuguuggg	hsa-miR-196a-5p	uagguaguuucauguuguuggg
ssc-miR-182	uuuggcaaugguagaacucacacu	hsa-miR-182-5p	uuuggcaaugguagaacucacacu
ssc-miR-138	agcugguguugugaaucaggc	hsa-miR-138-5p	agcugguguugugaaucaggc cg
ssc-miR-126-5p	cauuauuacuuuugguacgcg	hsa-miR-126-5p	cauuauuacuuuugguacgcg
ssc-miR-130a	cagugcaauguuaaaagggcau	hsa-miR-130a-3p	cagugcaauguuaaaagggcau
ssc-miR-23b	aucacauugccagggauuacca	hsa-miR-23b-3p	aucacauugccagggauuacca c
ssc-miR-146a-5p	ugagaacugaauuccauggguu	hsa-miR-146a-5p	ugagaacugaauuccauggguu
ssc-miR-152	ucagugcaugacagaacuugg	hsa-miR-152-3p	ucagugcaugacagaacuugg
ssc-miR-7140-5p	augaugccccuuagaguugagc	NA	na
ssc-miR-7140-3p	caacucaaggggcaucauuca	NA	na
ssc-miR-143-3p	ugagaugaagcacuguagcuc	hsa-miR-143-3p	ugagaugaagcacuguagcuc
ssc-miR-9805-3p	cccagggucugucggaugucu	NA	na
ssc-miR-194b-5p	uguaacagcgacuccaugugga	hsa-miR-194-5p	uguaacagcaacuccaugugga
ssc-miR-1	uggaauguaaagaaguaugua	hsa-miR-1-3p	uggaauguaaagaaguaugua u
ssc-miR-204	uucccuuugucauccuaugccu	hsa-miR-204-5p	uucccuuugucauccuaugccu
ssc-miR-127	ucggauccgucugagcuuggcu	hsa-miR-127-3p	ucggauccgucugagcuuggcu
ssc-miR-486	uccuguacugagcugccccgag	hsa-miR-486-5p	uccuguacugagcugccccgag
ssc-miR-206	uggaauguaaggaaguguguga	hsa-miR-206	uggaauguaaggaaguguguggg
ssc-miR-133a-3p	uuggucccuucaaccagcug	hsa-miR-133a-3p	u uuggucccuucaaccagcug
ssc-miR-184	uggacggagaacugauaagggu	hsa-miR-184	uggacggagaacugauaagggu
ssc-miR-133a-5p	agcugguaaaauggaaccaaau	hsa-miR-133a-5p	agcugguaaaauggaaccaaau

ssc-miR-138	agcugguguugugaaucaggc	hsa-miR-138-5p	agcugguguugugaaucaggc cg
ssc-miR-126-3p	ucguaccgugaguaauaaugcg	hsa-miR-126-3p	ucguaccgugaguaauaaugcg
ssc-miR-130a	cagugcaauguuaaaagggcau	hsa-miR-130a-3p	cagugcaauguuaaaagggcau
ssc-miR-210	cugugcgugugacagcggcuga	hsa-miR-210-3p	cugugcgugugacagcggcuga
ssc-miR-24-3p	uggcucaguucagcaggaacag	hsa-miR-24-3p	uggcucaguucagcaggaacag
ssc-miR-140-3p	uaccacaggguagaaccacggac	hsa-miR-140-3p	uaccacaggguagaaccacgg minus ac
ssc-miR-486	uccuguacugagcugccccgag	hsa-miR-486-5p	uccuguacugagcugccccgag
ssc-miR-423-5p	ugaggggcagagagcgagacuuu	hsa-miR-423-5p	ugaggggcagagagcgagacuuu
ssc-miR-335	ucaagagcaauaacgaaaaaug	hsa-miR-335-5p	ucaagagcaauaacgaaaaaug u
ssc-miR-9858-5p	uuccugagucggacugggcu	NA	na
ssc-miR-194b-5p	uguaacagcgacuccaugugga	hsa-miR-194-5p	uguaacagcaacuccaugugga
ssc-miR-2483	aaacaucugguugguugagaga	NA	na
ssc-miR-34c	aggcaguguaguuagcugauugc	hsa-miR-34c-5p	aggcaguguaguuagcugauugc
ssc-miR-122	uggagugugacaaugguguuugu	hsa-miR-122-5p	uggagugugacaaugguguuug minus u
ssc-miR-126-3p	ucguaccgugaguaauaaugcg	hsa-miR-126-3p	ucguaccgugaguaauaaugcg

Table 3. Validated mRNA targets of DE miRNAs obtained from miRTarBase.

miRNA	Target	miRNA	Target	miRNA	Target
hsa-miR-122-5p	AACS	hsa-miR-122-5p	AKT3	hsa-miR-193a-3p	AURKA
hsa-miR-183-5p	AANAT	hsa-miR-122-5p		hsa-miR-24-3p	AURKB
hsa-miR-1-3p	ABCB1	hsa-miR-152-3p	ALCAM	hsa-miR-122-5p	AXL
hsa-miR-24-3p	ABCB9	hsa-miR-210-3p	ALDH5A1	hsa-miR-34c-5p	
hsa-miR-7-5p	ABCC1	hsa-miR-122-5p	ALDOA	hsa-miR-196a-5p	BACH1
hsa-miR-193a-3p	ABI2	hsa-miR-193a-3p	ALKBH5	hsa-miR-138-5p	BAG1
hsa-miR-206	ACTL6A	hsa-miR-204-5p	ALPL	hsa-miR-143-3p	BAG3
hsa-miR-193a-3p	ACTN4	hsa-miR-122-5p	ANK2	hsa-miR-1-3p	BAG4
hsa-miR-130a-3p	Acvr1	hsa-miR-193a-3p	ANKFY1	hsa-miR-127-3p	BAG5
hsa-miR-130a-3p	Acvr1	hsa-miR-204-5p	ANKRD13A	hsa-miR-182-5p	BARD1
hsa-miR-24-3p	ACVR1B	hsa-miR-196a-5p	ANXA1	hsa-miR-122-5p	BAX
hsa-miR-122-5p	ACVR1C	hsa-miR-122-5p	ANXA11	hsa-miR-7-5p	
hsa-miR-194-5p	ACVR2B	hsa-miR-1-3p	ANXA2	hsa-miR-193a-3p	BAZ2A
hsa-miR-122-5p	ADAM10	hsa-miR-206		hsa-miR-24-3p	BCAR1
hsa-miR-122-5p	ADAM17	hsa-miR-204-5p	AP1S2	hsa-miR-138-5p	BCL11A
hsa-miR-152-3p		hsa-miR-122-5p	AP3M2	hsa-miR-126-3p	BCL2
hsa-miR-126-3p	ADAM9	hsa-miR-1-3p	API5	hsa-miR-143-3p	
hsa-miR-126-5p		hsa-miR-130a-3p	APP	hsa-miR-182-5p	
hsa-miR-144-3p	Adamts1	hsa-miR-144-3p		hsa-miR-184	
hsa-miR-1-3p	ADAR	hsa-miR-24-3p	ARHGAP19	hsa-miR-204-5p	
hsa-miR-182-5p	ADCY6	hsa-miR-486-5p	ARHGAP5	hsa-miR-34c-5p	
hsa-miR-138-5p	ADGRA2	hsa-miR-138-5p	ARHGEF3	hsa-miR-7-5p	
hsa-miR-126-3p	ADGRE5	hsa-miR-193a-3p	ARMC1	hsa-miR-122-5p	BCL2L1
hsa-miR-126-3p	ADM	hsa-miR-335-5p	ARPC5L	hsa-miR-24-3p	BCL2L11
hsa-miR-1-3p	AGO1	hsa-miR-182-5p	ARRDC3	hsa-miR-122-5p	BCL2L2
hsa-miR-184	AGO2	hsa-miR-193a-3p	ASB3	hsa-miR-129-2-3p	
hsa-miR-24-3p	AGPAT2	hsa-miR-1-3p	ASPH	hsa-miR-204-5p	
hsa-miR-210-3p	AIFM3	hsa-miR-182-5p	ATF1	hsa-miR-335-5p	
hsa-miR-210-3p	AIFM3	hsa-miR-23b-3p	ATG12	hsa-miR-335-5p	
hsa-miR-193a-3p	AK2	hsa-miR-152-3p	ATG14	hsa-miR-127-3p	BCL6
hsa-miR-183-5p	AKAP12	hsa-miR-130a-3p	ATG2B	hsa-miR-146a-5p	BCLAF1
hsa-miR-126-3p	AKT1	hsa-miR-24-3p	ATG4A	hsa-miR-194-5p	
hsa-miR-138-5p		hsa-miR-210-3p	ATG7	hsa-miR-1-3p	BDNF
hsa-miR-143-3p		hsa-miR-122-5p	ATP1A2	hsa-miR-182-5p	
hsa-miR-184		hsa-miR-140-3p	ATP6AP2	hsa-miR-204-5p	
hsa-miR-206		hsa-miR-1-3p	ATP6V1B2	hsa-miR-210-3p	
hsa-miR-143-3p	AKT2	hsa-miR-140-3p	ATP8A1	hsa-miR-184	BIN3

hsa-miR-184		hsa-miR-130a-3p	ATXN1	hsa-miR-204-5p	BIRC2
hsa-miR-335-5p	BIRC5	hsa-miR-138-5p	CCND3	hsa-miR-23b-3p	CHUK
hsa-miR-138-5p	BLCAP	hsa-miR-7-5p	CCNE1	hsa-miR-193a-3p	CIAO1
hsa-miR-34c-5p	BMF	hsa-miR-126-3p	CCNE2	hsa-miR-486-5p	CIT
hsa-miR-183-5p	BMI1	hsa-miR-34c-5p		hsa-miR-486-5p	CLDN10
hsa-miR-194-5p		hsa-miR-122-5p	CCNG1	hsa-miR-122-5p	CLIC4
hsa-miR-210-3p	BNIP3	hsa-miR-23b-3p	CCNG1	hsa-miR-182-5p	CLOCK
hsa-miR-143-3p	BRAF	hsa-miR-129-2-3p	CCP110	hsa-miR-193a-3p	CLPB
hsa-miR-146a-5p	BRCA1	hsa-miR-152-3p	CD151	hsa-miR-574-3p	CLTC
hsa-miR-24-3p		hsa-miR-138-5p	CD274	hsa-miR-1-3p	CNN3
hsa-miR-335-5p		hsa-miR-152-3p		hsa-miR-146a-5p	CNOT6L
hsa-miR-146a-5p	BRCA2	hsa-miR-140-3p	CD38	hsa-miR-143-3p	COL1A1
hsa-miR-210-3p	BTK	hsa-miR-146a-5p	CD40LG	hsa-miR-143-3p	COL3A1
hsa-miR-183-5p	BTRC	hsa-miR-143-3p	CD44	hsa-miR-140-3p	COL4A1
hsa-miR-193a-3p	BUB1	hsa-miR-146a-5p	CD80	hsa-miR-210-3p	COL4A2
hsa-miR-193a-3p	C1QBP	hsa-miR-204-5p	CDC42	hsa-miR-24-3p	COPS5
hsa-miR-193a-3p	C5orf22	hsa-miR-138-5p	CDH1	hsa-miR-146a-5p	COPS8
hsa-miR-193a-3p	C6orf106	hsa-miR-204-5p		hsa-miR-193a-3p	COQ7
hsa-miR-193a-3p	C6orf47	hsa-miR-194-5p	CDH2	hsa-miR-24-3p	CORO1A
hsa-miR-23b-3p	CA2	hsa-miR-24-3p	CDK1	hsa-miR-1-3p	COX1
hsa-miR-193a-3p	CACFD1	hsa-miR-193a-3p	CDK12	hsa-miR-146a-5p	COX2
hsa-miR-126-3p	CADM1	hsa-miR-122-5p	CDK4	hsa-miR-210-3p	CPEB2
hsa-miR-182-5p		hsa-miR-1-3p		hsa-miR-146a-5p	CPM
hsa-miR-1-3p	CALM3	hsa-miR-206		hsa-miR-193a-3p	CPSF2
hsa-miR-1-3p	CAND1	hsa-miR-24-3p		hsa-miR-122-5p	CREB1
hsa-miR-146a-5p	CARD10	hsa-miR-34c-5p		hsa-miR-182-5p	
hsa-miR-24-3p		hsa-miR-486-5p		hsa-miR-204-5p	CREB1
hsa-miR-138-5p	CASP3	hsa-miR-129-2-3p	CDK6	hsa-miR-182-5p	CREB5
hsa-miR-146a-5p	CASP7	hsa-miR-34c-5p		hsa-miR-204-5p	
hsa-miR-210-3p	CASP8AP2	hsa-miR-146a-5p	CDKN1A	hsa-miR-126-3p	CRK
hsa-miR-193a-3p	CCDC8	hsa-miR-182-5p		hsa-miR-126-5p	
hsa-miR-152-3p	CCKBR	hsa-miR-196a-5p		hsa-miR-126-3p	CRKL
hsa-miR-1-3p	CCL2	hsa-miR-182-5p	CDKN1B	hsa-miR-335-5p	CRKL
hsa-miR-206		hsa-miR-190a-5p		hsa-miR-130a-3p	CSF1
hsa-miR-146a-5p	CCL5	hsa-miR-194-5p		hsa-miR-152-3p	CSF1
hsa-miR-146a-5p	CCNA2	hsa-miR-196a-5p		hsa-miR-193a-3p	CTC1
hsa-miR-24-3p	CCNA2	hsa-miR-24-3p		hsa-miR-122-5p	CTDNEP1
hsa-miR-138-5p	CCND1	hsa-miR-24-3p	CDKN2A	hsa-miR-143-3p	CTGF
hsa-miR-1-3p		hsa-miR-146a-5p	CDKN3	hsa-miR-574-3p	CUL2
hsa-miR-146a-5p		hsa-miR-204-5p	CDX2	hsa-miR-7-5p	CUL5

hsa-miR-152-3p	CCND1	hsa-miR-1-3p	CEBPA	hsa-miR-126-3p	CXCL12
hsa-miR-193a-3p		hsa-miR-193a-3p	CEP89	hsa-miR-126-5p	
hsa-miR-206		hsa-miR-146a-5p	CFH	hsa-miR-1-3p	
hsa-miR-24-3p		hsa-miR-144-3p	CFTR	hsa-miR-146a-5p	
hsa-miR-34c-5p		hsa-miR-194-5p	CHD1	hsa-miR-146a-5p	CXCL8
hsa-miR-146a-5p	CCND2	hsa-miR-24-3p	CHEK1	hsa-miR-126-3p	CXCR4
hsa-miR-182-5p		hsa-miR-182-5p	CHEK2	hsa-miR-146a-5p	
hsa-miR-206		hsa-miR-182-5p	CHL1	hsa-miR-204-5p	
hsa-miR-204-5p	CYBB	hsa-miR-24-3p	CYP11B2	hsa-miR-335-5p	
hsa-miR-143-3p	DDX6	hsa-miR-183-5p	DKK3	hsa-miR-126-5p	CYLD
hsa-miR-24-3p	DEDD	hsa-miR-130a-3p	DLL4	hsa-miR-182-5p	
hsa-miR-24-3p	DHFR	hsa-miR-193a-3p	DNAJB9	hsa-miR-143-3p	CYP2C9
hsa-miR-24-3p	DHFRP1	hsa-miR-24-3p	DND1	hsa-miR-122-5p	CYP7A1
hsa-miR-130a-3p	DICER1	hsa-miR-126-3p	DNMT1	hsa-miR-138-5p	CYTOR
hsa-miR-210-3p	DIMT1	hsa-miR-152-3p		hsa-miR-335-5p	DAAM2
hsa-miR-152-3p	DKK1	hsa-miR-143-3p	DNMT3A	hsa-miR-193a-3p	DCAF7
hsa-miR-335-5p		hsa-miR-194-5p		hsa-miR-193a-3p	DCTN5
hsa-miR-486-5p	DOCK3	hsa-miR-122-5p	EGFR	hsa-miR-193a-3p	DDAH1
hsa-miR-122-5p	DSTYK	hsa-miR-133a-5p		hsa-miR-210-3p	
hsa-miR-143-3p	DTNB	hsa-miR-146a-5p		hsa-miR-130a-3p	ESR1
hsa-miR-146a-5p	DUSP1	hsa-miR-574-3p		hsa-miR-206	
hsa-miR-122-5p	DUSP2	hsa-miR-7-5p		hsa-miR-1-3p	ETS1
hsa-miR-204-5p	DVL3	hsa-miR-122-5p	EGLN3	hsa-miR-144-3p	
hsa-miR-193a-3p	DYRK2	hsa-miR-183-5p	EGR1	hsa-miR-23b-3p	
hsa-miR-24-3p		hsa-miR-210-3p	EHD2	hsa-miR-126-3p	EZH2
hsa-miR-193a-3p	E2F1	hsa-miR-138-5p	EID1	hsa-miR-138-5p	
hsa-miR-24-3p	E2F2	hsa-miR-24-3p	EIF2S3	hsa-miR-138-5p	
hsa-miR-210-3p	E2F3	hsa-miR-138-5p	EIF4EBP1	hsa-miR-144-3p	
hsa-miR-34c-5p		hsa-miR-146a-5p	ELAVL1	hsa-miR-183-5p	EZR
hsa-miR-193a-3p	E2F6	hsa-miR-193a-3p	ELMO2	hsa-miR-184	
hsa-miR-193a-3p	EBAG9	hsa-miR-196a-5p	ELOVL1	hsa-miR-204-5p	
hsa-miR-204-5p	EDEM1	hsa-miR-204-5p	ELOVL6	hsa-miR-1-3p	FABP3
hsa-miR-1-3p	EDN1	hsa-miR-122-5p	ENTPD4	hsa-miR-146a-5p	FADD
hsa-miR-138-5p	EED	hsa-miR-574-3p	EP300	hsa-miR-146a-5p	FAF1
hsa-miR-210-3p	EFNA3	hsa-miR-335-5p	EPN2	hsa-miR-24-3p	
hsa-miR-204-5p	EFNB2	hsa-miR-193a-3p	ERBB2	hsa-miR-122-5p	FAM117B
hsa-miR-126-3p	EGFL7	hsa-miR-146a-5p	ERBB4	hsa-miR-193a-3p	FAM221B
hsa-miR-143-3p	FAM83F	hsa-miR-193a-3p		hsa-miR-423-5p	FAM3A
hsa-miR-146a-5p	FANCM	hsa-miR-144-3p	FGB	hsa-miR-210-3p	Fgfrl1

hsa-miR-146a-5p	FAS	hsa-miR-24-3p	FGF11	hsa-miR-144-3p	FGG
hsa-miR-1-3p	FASN	hsa-miR-152-3p	FGF2	hsa-miR-143-3p	FHIT
hsa-miR-486-5p	FBN1	hsa-miR-182-5p	FGF9	hsa-miR-182-5p	FLOT1
hsa-miR-182-5p	FBXW7	hsa-miR-152-3p	FGFR3	hsa-miR-335-5p	FMN2
hsa-miR-24-3p		hsa-miR-24-3p		hsa-miR-335-5p	FMNL3
hsa-miR-24-3p	FEN1	hsa-miR-210-3p	FGFRL1	hsa-miR-138-5p	FERMT2
hsa-miR-144-3p	FGA				

Table 4. Gene ontology terms for each miRNA. Not all miRNAs have associated GO terms

miRNA	Gene Ontology Terms							
miR-194b-5p	negative regulation of interleukin-10 production							
miR-7	negative regulation of amyloid-beta clearance		negative regulation of insulin receptor signaling pathway		negative regulation of sprouting angiogenesis			
miR-499	positive regulation of blood vessel endothelial cell migration		positive regulation of vascular associated smooth muscle cell proliferation		positive regulation of vascular associated smooth muscle cell migration		positive regulation of vascular endothelial cell proliferation	
miR-193a	cellular response to DNA damage stimulus		negative regulation of cell migration involved in sprouting angiogenesis		negative regulation of blood vessel endothelial cell proliferation involved in sprouting angiogenesis		negative regulation of G1/S transition of mitotic cell cycle	
miR-144	negative regulation of glycoprotein biosynthetic process	negative regulation of epithelial to mesenchymal transition	positive regulation of mitochondrion organization	positive regulation of cell adhesion molecule production	positive regulation of cholesterol storage	positive regulation of high-density lipoprotein particle clearance		positive regulation of interleukin-1 beta production
miR-144	positive regulation of interleukin-6 production	positive regulation of tumor necrosis factor production	cholesterol homeostasis	negative regulation of amyloid precursor protein biosynthetic process	positive regulation of inflammatory response	regulation of high-density lipoprotein particle assembly	negative regulation of cholesterol efflux	negative regulation of reverse cholesterol transport
miR-183	negative regulation of cell-substrate adhesion		positive regulation of phagocytosis		transforming growth factor beta receptor signaling pathway			
miR-196a	negative regulation of lamellipodium assembly	cellular response to vascular endothelial growth factor stimulus	negative regulation of cell migration involved in sprouting angiogenesis	negative regulation of histone deacetylase activity	negative regulation of epithelial cell apoptotic process	negative regulation of vascular associated smooth muscle cell proliferation	negative regulation of vascular associated smooth muscle cell migration	negative regulation of vascular associated smooth muscle cell dedifferentiation

miR-182	positive regulation of cytokine production	positive regulation of cell migration	cholesterol homeostasis	positive regulation of cholesterol biosynthetic process	positive regulation of fatty acid biosynthetic process	positive regulation of lipoprotein lipase activity	cellular response to cholesterol	positive regulation of NIK/NF-kappaB signaling
miR-182	negative regulation of stress fiber assembly	positive regulation of protein kinase B signaling	negative regulation of response to cytokine stimulus	negative regulation of protein K63-linked ubiquitination	negative regulation of sprouting angiogenesis		negative regulation of vascular associated smooth muscle cell apoptotic process	
miR-138	negative regulation of cell adhesion	negative regulation of cell population proliferation	negative regulation of cell migration	negative regulation of NF-kappaB transcription factor activity	negative regulation of osteoblast proliferation	negative regulation of osteoblast differentiation	negative regulation of inflammatory response	negative regulation of nitric-oxide synthase activity
miR-126-5p	negative regulation of cell migration	negative regulation of proteolysis	positive regulation of Notch signaling pathway	cellular response to laminar fluid shear stress	positive regulation of cell migration involved in sprouting angiogenesis	positive regulation of blood vessel endothelial cell proliferation involved in sprouting angiogenesis	positive regulation of vascular endothelial cell proliferation	positive regulation of vascular endothelial cell proliferation

miR-130a	negative regulation of tumor necrosis factor production	NIK/NF-kappaB signaling	negative regulation of macrophage activation	positive regulation of angiogenesis	cellular response to transforming growth factor beta stimulus	cellular response to virus	regulation of viral life cycle	positive regulation of vascular associated smooth muscle cell proliferation	
miR-130a	positive regulation of blood vessel endothelial cell proliferation involved in sprouting angiogenesis			negative regulation of sprouting angiogenesis					
miR-23b	negative regulation of signaling receptor activity	negative regulation of interleukin-11 production	cellular response to vascular endothelial growth factor stimulus	positive regulation of vascular permeability	positive regulation of cardiac muscle cell proliferation	cell growth involved in cardiac muscle cell development	positive regulation of ERK1 and ERK2 cascade	positive regulation of cell migration involved in sprouting angiogenesis	
miR-23b	negative regulation of intracellular signal transduction	negative regulation of matrix metallopeptidase secretion	negative regulation of membrane permeability	negative regulation of chemokine (C-X-C motif) ligand 2 production	negative regulation of endothelial cell proliferation	negative regulation of angiogenesis	regulation of toll-like receptor signaling pathway	negative regulation of toll-like receptor 4 signaling pathway	NIK/NF-kappaB signaling
miR-146a	negative regulation of cellular extravasation	negative regulation of cholesterol storage	negative regulation of interleukin-6 production	negative regulation of interleukin-8 production	negative regulation of dephosphorylation	positive regulation of apoptotic process	negative regulation of inflammatory response	negative regulation of protein kinase B signaling	
miR-152	negative regulation of tumor necrosis factor-mediated signaling pathway	negative regulation of blood vessel endothelial cell migration		negative regulation of fibroblast growth factor production		negative regulation of metalloendopeptidase activity		negative regulation of vascular endothelial cell proliferation	

Table 4. Gene ontology terms for each miRNA. Continued

miRNA	Gene Ontology Terms								
miR-143-3p	regulation of smooth muscle contraction								
miR-143-3p	negative regulation of smooth muscle cell proliferation	negative regulation of angiogenesis	actin cytoskeleton organization	activation of protein kinase B activity	angiotensin-activated signaling pathway	positive regulation of blood vessel endothelial cell migration	establishment or maintenance of cell type involved in phenotypic switching	positive regulation of angiogenesis	negative regulation of glucose import
miR-1	negative regulation of xenobiotic detoxification by transmembrane export across the plasma membrane		positive regulation of protein kinase B signaling	aorta smooth muscle tissue morphogenesis	regulation of phenotypic switching	positive regulation of vascular associated smooth muscle cell migration		positive regulation of pulmonary blood vessel remodeling	
miR-1	negative regulation of insulin-like growth factor receptor signaling pathway		positive regulation of cell fate commitment	positive regulation of heart rate	negative regulation of cardiac muscle hypertrophy	positive regulation of myotube differentiation	regulation of release of sequestered calcium ion into cytosol by sarcoplasmic reticulum		regulation of cardiac muscle contraction by regulation of the release of sequestered calcium ion
miR-1	negative regulation of canonical Wnt signaling pathway		negative regulation of endothelial cell differentiation	negative regulation of cardiac muscle cell proliferation	positive regulation of sarcomere organization	regulation of ventricular cardiac muscle cell membrane depolarization	ventricular septum morphogenesis	positive regulation of cardiac muscle contraction	cell migration involved in coronary vasculogenesis

miR-1	positive regulation of vascular associated smooth muscle cell apoptotic process	negative regulation of delayed rectifier potassium channel activity	positive regulation of sprouting angiogenesis	positive regulation of voltage-gated potassium channel activity involved in ventricular cardiac muscle cell action potential repolarization		negative regulation of cardiac conduction	negative regulation of vascular associated smooth muscle cell proliferation	positive regulation of calcium ion transmembrane transport via high voltage-gated calcium channel	negative regulation of membrane repolarization during cardiac muscle cell action potential
miR-204	negative regulation of interleukin-6 production	positive regulation of mesoderm formation	negative regulation of calcium ion export across plasma membrane	positive regulation of cardiac vascular smooth muscle cell differentiation	positive regulation of cardiac muscle cell differentiation	negative regulation of myoblast proliferation	positive regulation of skeletal muscle cell differentiation	positive regulation of ryanodine-sensitive calcium-release channel activity by adrenergic receptor signaling pathway involved in positive regulation of cardiac muscle contraction	
miR-204	negative regulation of blood vessel endothelial cell migration	negative regulation of interleukin-8 production	negative regulation of tumor necrosis factor production	negative regulation of NIK/NF-kappaB signaling	negative regulation of cell population proliferation	negative regulation of cell migration	negative regulation of prostaglandin biosynthetic process	negative regulation of interleukin-1 beta production	positive regulation of apoptotic process
miR-126-3p	negative regulation of cell migration	negative regulation of inflammatory response		positive regulation of cardiac muscle cell proliferation		negative regulation of cardiac muscle myoblast proliferation		positive regulation of cardiac muscle cell differentiation	

miR-126-3p	positive regulation of ERK1 and ERK2 cascade	negative regulation of proteolysis	positive regulation of phosphatidylinositol 3-kinase signaling	positive regulation of MAPK cascade	positive regulation of blood vessel endothelial cell migration	positive regulation of angiogenesis	negative regulation of inflammatory response	positive regulation of inflammatory response	positive regulation of protein kinase B signaling
miR-210	negative regulation of neuron projection development	positive regulation of cell migration involved in sprouting angiogenesis		positive regulation of sprouting angiogenesis	positive regulation of vasculature development	negative regulation of vascular endothelial cell proliferation	negative regulation of endothelial cell apoptotic process	positive regulation of blood vessel endothelial cell proliferation involved in sprouting angiogenesis	
miR-210	positive regulation of glucose catabolic process to lactate via pyruvate	positive regulation of cell migration	tube formation	positive regulation of blood vessel endothelial cell migration	positive regulation of osteoblast differentiation	positive regulation of angiogenesis	hypoxia-inducible factor-1alpha signaling pathway	regulation of cellular response to hypoxia	negative regulation of mitochondrial electron transport, NADH to ubiquinone
miR-24-3p	negative regulation of interferon-gamma production	negative regulation of aconitate hydratase activity	positive regulation of iron ion import across plasma membrane		negative regulation of apoptotic signaling pathway	positive regulation of apoptotic signaling pathway		negative regulation of vascular associated smooth muscle cell apoptotic process	

miR-24-3p	positive regulation of reactive oxygen species biosynthetic process	negative regulation of amyloid-beta formation	negative regulation of cardiac muscle cell apoptotic process	negative regulation of tumor necrosis factor-mediated signaling pathway	negative regulation of angiogenesis	negative regulation of blood vessel endothelial cell migration	cell growth involved in cardiac muscle cell development	positive regulation of ERK1 and ERK2 cascade	negative regulation of protein serine/threonine kinase activity

Table 4. Gene ontology terms for each miRNA. Continued

miRNA	Gene Ontology Terms		
miR-335	negative regulation of cell population proliferation	negative regulation of cell migration	
miR-34c	negative regulation of protein kinase B signaling	positive regulation of cardiac muscle hypertrophy in response to stress	negative regulation of sprouting angiogenesis

Table 5. Global terms grouping Gene Ontology terms obtained for DE miRNAs

Gene Ontology Term	Global term	Month
regulation of reverse cholesterol transport	Cholesterol homeostasis	Upregulated at Month 3
cholesterol homeostasis		
regulation of cholesterol efflux		
regulation of cholesterol storage		
regulation of high-density lipoprotein particle assembly		
regulation of high-density lipoprotein particle clearance		
regulation of blood vessel endothelial cell migration	Endothelial cells proliferation/migration	
regulation of blood vessel endothelial cell proliferation involved in sprouting angiogenesis		
regulation of vascular endothelial cell proliferation		
regulation of tumor necrosis factor production	Inflammatory processes	
regulation of cell adhesion molecule production		
regulation of inflammatory response		
regulation of interleukin-1 beta production	Interleukin production	
regulation of interleukin-6 production		
regulation of interleukin-10 production		
regulation of amyloid-beta clearance	Other	
regulation of insulin receptor signaling pathway		
regulation of mitochondrion organization		
regulation of epithelial to mesenchymal transition		
regulation of G1/S transition of mitotic cell cycle		
regulation of glycoprotein biosynthetic process		
regulation of amyloid precursor protein biosynthetic process		

regulation of cell migration involved in sprouting angiogenesis	Sprouting and angiogenesis	
regulation of sprouting angiogenesis		
regulation of vascular associated smooth muscle cell proliferation	VSMC proliferation/migration	
regulation of vascular associated smooth muscle cell migration		
cellular response to cholesterol	Cholesterol homeostasis	Downregulated at Month 3
regulation of cholesterol biosynthetic process		
regulation of cholesterol storage		
regulation of fatty acid biosynthetic process		
cellular response to oxidised low-density lipoprotein particle stimulus		
regulation of lipoprotein lipase activity		
cholesterol homeostasis		
regulation of vascular endothelial cell proliferation	Endothelial cells proliferation/migration	
regulation of blood vessel endothelial cell proliferation involved in sprouting angiogenesis		
regulation of endothelial cell proliferation		
regulation of blood vessel endothelial cell migration		
regulation of histone deacetylase activity	Epigenetic regulation	
NIK/NF-kappaB signaling	Inflammatory processes	
regulation of protein kinase B signaling		
regulation of inflammatory response		
cellular response to vascular endothelial growth factor stimulus		
regulation of cellular extravasation		
regulation of response to cytokine stimulus		

regulation of cellular senescence		
regulation of chemokine (C-X-C motif) ligand 2 production		
regulation of tumor necrosis factor production		
regulation of vascular endothelial growth factor production		
regulation of cytokine production		
regulation of cytokine production involved in inflammatory response		
regulation of osteoblast differentiation		
regulation of apoptotic process in bone marrow cell		
regulation of epithelial cell apoptotic process		
regulation of tyrosine phosphorylation of STAT protein		
regulation of ERK1 and ERK2 cascade		
regulation of Notch signaling pathway		
regulation of apoptotic process		
regulation of toll-like receptor 4 signaling pathway		
regulation of tumor necrosis factor-mediated signaling pathway		
regulation of leukocyte adhesion to vascular endothelial cell		
regulation of macrophage activation		
cellular response to cytokine stimulus		
regulation of cell adhesion		
cellular response to lipopolysaccharide		
cellular response to transforming growth factor beta stimulus		
regulation of cell adhesion molecule production		
regulation of nitric-oxide synthase activity		
regulation of matrix metallopeptidase secretion		
interleukin-1-mediated signaling pathway		
regulation of metalloendopeptidase activity		
regulation of toll-like receptor signaling pathway		
transforming growth factor beta receptor signaling pathway		
regulation of NF-kappaB transcription factor activity		
regulation of NIK/NF-kappaB signaling		

regulation of interleukin-11 production		
regulation of interleukin-6 production		
regulation of interleukin-8 production		
regulation of cell migration		
cellular response to virus		
regulation of phagocytosis		
cellular response to laminar fluid shear stress		
regulation of dephosphorylation		
regulation of cell population proliferation		
cell growth involved in cardiac muscle cell development		
regulation of fibroblast growth factor production		
cellular response to glucose stimulus		
regulation of fibroblast growth factor receptor signaling pathway		
regulation of glial cell proliferation		
regulation of osteoblast proliferation		
regulation of protein K63-linked ubiquitination		
regulation of proteolysis		
regulation of signaling receptor activity		
regulation of intracellular signal transduction		
regulation of lamellipodium assembly		
regulation of cell-substrate adhesion		
regulation of vascular permeability		
regulation of cardiac muscle cell proliferation		
cellular response to amyloid-beta		
cellular response to hypoxia		
regulation of stem cell differentiation		
regulation of viral life cycle		
regulation of membrane permeability		
plasma membrane raft assembly		

regulation of neuron differentiation		
regulation of cell migration involved in sprouting angiogenesis	Sprouting and angiogenesis	
regulation of angiogenesis		
regulation of sprouting angiogenesis		
regulation of vascular associated smooth muscle cell proliferation	VSMC proliferation/migration	
regulation of vascular associated smooth muscle cell dedifferentiation		
regulation of vascular associated smooth muscle cell apoptotic process		
regulation of vascular associated smooth muscle cell migration		
positive regulation of blood vessel endothelial cell migration	Endothelial cells proliferation/migration	Upregulated at Month 6
negative regulation of blood vessel endothelial cell migration		
negative regulation of endothelial cell differentiation		
angiotensin-activated signaling pathway	Inflammatory processes	
negative regulation of canonical Wnt signaling pathway		
negative regulation of fibroblast growth factor receptor signaling pathway		
negative regulation of inflammatory response		
negative regulation of insulin-like growth factor receptor signaling pathway		
negative regulation of NIK/NF-kappaB signaling		
negative regulation of tumor necrosis factor production		
negative regulation of interleukin-1 beta production	Interleukin production	
negative regulation of interleukin-10 production		
negative regulation of interleukin-6 production		
negative regulation of interleukin-8 production		
positive regulation of ryanodine-sensitive calcium-release channel activity by adrenergic receptor signaling pathway involved in positive regulation of cardiac muscle contraction	Muscle contraction	
regulation of smooth muscle contraction		
actin cytoskeleton organization		
positive regulation of cardiac muscle contraction		
positive regulation of sarcomere organization		

negative regulation of membrane repolarization during cardiac muscle cell action potential		
regulation of cardiac muscle contraction by regulation of the release of sequestered calcium ion		
regulation of ventricular cardiac muscle cell membrane depolarization		
positive regulation of cardiac muscle cell differentiation	Other	
aorta smooth muscle tissue morphogenesis		
cell migration involved in coronary vasculogenesis		
positive regulation of myotube differentiation		
negative regulation of calcium ion export across plasma membrane		
positive regulation of cardiac muscle cell proliferation		
positive regulation of heart rate		
negative regulation of cardiac conduction		
positive regulation of protein phosphorylation		
negative regulation of cardiac muscle cell proliferation		
negative regulation of cardiac muscle hypertrophy		
positive regulation of voltage-gated potassium channel activity involved in ventricular cardiac muscle cell action potential repolarization		
negative regulation of cardiac muscle myoblast proliferation		
negative regulation of cell migration		
negative regulation of cell population proliferation		
negative regulation of xenobiotic detoxification by transmembrane export across the plasma membrane		
negative regulation of delayed rectifier potassium channel activity		
positive regulation of apoptotic process		
activation of protein kinase B activity		
positive regulation of calcium ion transmembrane transport via high voltage-gated calcium channel		
negative regulation of glucose import		
positive regulation of cell fate commitment		
positive regulation of mesoderm formation		

positive regulation of protein kinase B signaling		
positive regulation of pulmonary blood vessel remodeling		
negative regulation of myoblast proliferation		
regulation of release of sequestered calcium ion into cytosol by sarcoplasmic reticulum		
negative regulation of prostaglandin biosynthetic process		
ventricular septum morphogenesis		
negative regulation of angiogenesis	Sprouting and angiogenesis	
positive regulation of angiogenesis		
positive regulation of sprouting angiogenesis		
negative regulation of vascular associated smooth muscle cell proliferation	VSMCs proliferation/migration	
positive regulation of cardiac vascular smooth muscle cell differentiation		
regulation of phenotypic switching		
establishment or maintenance of cell type involved in phenotypic switching		
positive regulation of vascular associated smooth muscle cell apoptotic process		
positive regulation of skeletal muscle cell differentiation		
positive regulation of vascular associated smooth muscle cell migration		
negative regulation of smooth muscle cell proliferation		
negative regulation of blood vessel endothelial cell migration	Endothelial cell proliferation/migration	Downregulated at Month 6
negative regulation of endothelial cell apoptotic process		
negative regulation of blood vessel endothelial cell proliferation involved in sprouting angiogenesis		
negative regulation of vascular endothelial cell proliferation		
positive regulation of blood vessel endothelial cell migration		
positive regulation of blood vessel endothelial cell proliferation involved in sprouting angiogenesis		
positive regulation of ERK1 and ERK2 cascade	Inflammatory processes	
negative regulation of tumor necrosis factor-mediated signaling pathway		
positive regulation of MAPK cascade		

negative regulation of cell adhesion		
positive regulation of apoptotic signaling pathway		
negative regulation of fibroblast apoptotic process		
hypoxia-inducible factor-1alpha signaling pathway		
positive regulation of inflammatory response		
negative regulation of interferon-gamma production		
negative regulation of macrophage migration		
negative regulation of metalloendopeptidase activity		
negative regulation of NF-kappaB transcription factor activity		
negative regulation of apoptotic signaling pathway		
negative regulation of nitric-oxide synthase activity		
positive regulation of endothelial cell apoptotic process		
positive regulation of phosphatidylinositol 3-kinase signaling		
positive regulation of reactive oxygen species biosynthetic process		
negative regulation of response to cytokine stimulus		
negative regulation of inflammatory response		
negative regulation of cell migration	Other	
positive regulation of protein kinase B signaling		
negative regulation of cardiac muscle cell apoptotic process		
plasma membrane raft assembly		
negative regulation of sodium ion import across plasma membrane		
negative regulation of cell population proliferation		
negative regulation of amyloid-beta formation		
negative regulation of aconitate hydratase activity		
negative regulation of mitochondrial electron transport, NADH to ubiquinone		
negative regulation of voltage-gated sodium channel activity		
negative regulation of neuron projection development		
positive regulation of cell migration		
negative regulation of osteoblast differentiation		
positive regulation of glucose catabolic process to lactate via pyruvate		

positive regulation of iron ion import across plasma membrane		
positive regulation of osteoblast differentiation		
regulation of cellular response to hypoxia		
cell growth involved in cardiac muscle cell development		
negative regulation of osteoblast proliferation		
negative regulation of protein K63-linked ubiquitination		
positive regulation of vasculature development		
negative regulation of protein serine/threonine kinase activity		
tube formation		
negative regulation of proteolysis		
positive regulation of angiogenesis	Sprouting and angiogenesis	
positive regulation of cell migration involved in sprouting angiogenesis		
negative regulation of sprouting angiogenesis		
negative regulation of angiogenesis		
positive regulation of sprouting angiogenesis		
negative regulation of vascular associated smooth muscle cell apoptotic process	VSMCs proliferation/migration	
positive regulation of vascular associated smooth muscle cell apoptotic process		
regulation of interleukin-10 production	Interleukin production	Upregulated at Month 9
regulation of cell migration	Other	
regulation of cell population proliferation		
regulation of blood vessel endothelial cell proliferation involved in sprouting angiogenesis	Endothelial cells proliferation/migration	Downregulated at Month 9
regulation of blood vessel endothelial cell migration		
regulation of vascular endothelial cell proliferation		
regulation of endothelial cell apoptotic process		

regulation of inflammatory response	Inflammatory processes	
regulation of MAPK cascade		
regulation of ERK1 and ERK2 cascade		
regulation of protein kinase B signaling	Other	
regulation of cell migration		
regulation of phosphatidylinositol 3-kinase signaling		
regulation of proteolysis		
regulation of cardiac muscle hypertrophy in response to stress		
regulation of connective tissue replacement		
regulation of vasculature development		
regulation of sprouting angiogenesis	Sprouting and angiogenesis	
regulation of angiogenesis		
regulation of cell migration involved in sprouting angiogenesis		

APPENDIX C : CHAPTER 4

Table 1. Normalized reads of firmicutes in WMS-FH and WMS-N at months 3, 6, and 9.

Animal	Age	Firmicutes	Group
FH1	M3	93.918	Familial hypercholesterolemic
FH2	M3	93.918	Familial hypercholesterolemic
FH3	M3	93.918	Familial hypercholesterolemic
FH4	M3	104.651	Familial hypercholesterolemic
FH5	M3	22.627	Familial hypercholesterolemic
FH6	M3	3.085	Familial hypercholesterolemic
FH7	M3	866.199	Familial hypercholesterolemic
FH8	M3	7.730	Familial hypercholesterolemic
FH9	M3	131.205	Familial hypercholesterolemic
WT1	M3	93.918	Normocholesterolemic
WT2	M3	93.918	Normocholesterolemic
WT3	M3	93.918	Normocholesterolemic
WT4	M3	287.100	Normocholesterolemic
WT5	M3	37254.481	Normocholesterolemic
WT6	M3	15.459	Normocholesterolemic
WT7	M3	25.290	Normocholesterolemic
WT8	M3	11.314	Normocholesterolemic
WT9	M3	45.254	Normocholesterolemic
FH1	M6	93.917	Familial hypercholesterolemic
FH2	M6	52.561	Familial hypercholesterolemic
FH3	M6	93.918	Familial hypercholesterolemic
FH4	M6	317.780	Familial hypercholesterolemic
FH5	M6	57.200	Familial hypercholesterolemic
FH6	M6	178.885	Familial hypercholesterolemic
FH7	M6	59.179	Familial hypercholesterolemic
FH8	M6	144.286	Familial hypercholesterolemic

FH9	M6	15.230	Familial hypercholesterolemic
WT1	M6	50.911	Normocholesterolemic
WT2	M6	85.481	Normocholesterolemic
WT3	M6	93.918	Normocholesterolemic
WT4	M6	93.918	Normocholesterolemic
WT5	M6	93.918	Normocholesterolemic
WT6	M6	93.918	Normocholesterolemic
WT7	M6	85.026	Normocholesterolemic
WT8	M6	160.358	Normocholesterolemic
WT9	M6	1071.337	Normocholesterolemic
FH1	M9	104.085	Familial hypercholesterolemic
FH2	M9	133.980	Familial hypercholesterolemic
FH3	M9	93.918	Familial hypercholesterolemic
FH4	M9	93.918	Familial hypercholesterolemic
FH5	M9	40.730	Familial hypercholesterolemic
FH6	M9	15.460	Familial hypercholesterolemic
FH7	M9	93.918	Familial hypercholesterolemic
FH8	M9	148.408	Familial hypercholesterolemic
FH9	M9	77.296	Familial hypercholesterolemic
WT1	M9	93.918	Normocholesterolemic
WT2	M9	164.920	Normocholesterolemic
WT3	M9	26.768	Normocholesterolemic
WT4	M9	53.241	Normocholesterolemic
WT5	M9	89.188	Normocholesterolemic
WT6	M9	5525.289	Normocholesterolemic
WT7	M9	8440.810	Normocholesterolemic
WT8	M9	72.910	Normocholesterolemic
WT9	M9	93.917	Normocholesterolemic